Magnetic anomalies and plate tectonic history of the Caribbean plate and the Gulf of Mexico

Andreina Garcia-Reyes

▶ **To cite this version:**

Andreina Garcia-Reyes. Magnetic anomalies and plate tectonic history of the Caribbean plate and the Gulf of Mexico. Geophysics [physics.geo-ph]. Université Sorbonne Paris Cité, 2018. English. NNT : . tel-02496674

HAL Id: tel-02496674

https://theses.hal.science/tel-02496674

Submitted on 3 Mar 2020

HAL is a multi-disciplinary open access archive for the deposit and dissemination of scientific research documents, whether they are published or not. The documents may come from teaching and research institutions in France or abroad, or from public or private research centers.

L'archive ouverte pluridisciplinaire **HAL**, est destinée au dépôt et à la diffusion de documents scientifiques de niveau recherche, publiés ou non, émanant des établissements d'enseignement et de recherche français ou étrangers, des laboratoires publics ou privés.

UNIVERSITÉ SORBONNE PARIS CITÉ

Thèse préparée

à l'INSTITUT DE PHYSIQUE DU GLOBE DE PARIS

Ecole doctorale STEP'UP – ED N° 560

IPGP – Equipe de Géosciences Marines

Magnetic anomalies and plate tectonic history of the Caribbean plate and the Gulf of Mexico

par

Andreína García-Reyes

présentée et soutenue publiquement le

10 septembre 2018

Thèse de doctorat de Sciences de la Terre et de l'environnement

dirigée par Jérôme DYMENT

-

devant un jury composé de :

Alejandro ESCALONA Directeur de Recherche - Univ. de Stavanger	Rapporteur
Walter ROEST Chercheur - IFREMER Brest	Rapporteur
Jean BESSE Physicien - IPGP	President
Manuel PUBELLIER Directeur de Recherche - CNRS	Examinateur
Nuris ORIHUELA Chercheuse - Univ. Centrale du Venezuela	Examinateur
Jérôme DYMENT Directeur de Recherche - CNRS	Directeur de thèse

Dedication

I dedicate this work to: two women who marked my life, my Mother, Cruz Elena Reyes de García, who passed away early, but not without leaving me the clear message that every woman should be independent, and that there is no way to achieve it except through disciplined study. To my grandmother Carmen Dolores Eizaga de Reyes, an example of honesty, strength and rectitude.

To my children.

To Caracas, to the Central University of Venezuela, to my Avila mountain; and finally, to all those who think that the past or that the present conditions of life are an impediment to transform reality into what we dream of.

Dedicatoria

Dedico este trabajo: a dos mujeres que marcaron mi vida, a mi Mamá, Cruz Elena Reyes de García, quien partió temprano, pero no sin dejarme el claro mensaje de que toda mujer debe ser independiente, y de que no hay forma de lograrlo sino a través del estudio disciplinado; a mi Abuela Carmen Dolores Eizaga de Reyes, por ser ejemplo de honestidad, fortaleza y rectitud.

A mis hijos.

A Caracas, a la Universidad Central de Venezuela, a mi Avila; y por último, a todos aquellos que piensan que el pasado o que las condiciones presentes de vida son un impedimento para transformar la realidad en aquello que soñamos.

Magnetic anomalies and plate tectonic history of the Caribbean plate and the Gulf of Mexico

Abstract

The origin of the Caribbean plate - Pacific or intra-American - is still under debate. We produced a magnetic map from our compilation of marine magnetic data in the Caribbean plate and the Gulf of Mexico (GoM) in order to perform a magnetic interpretation which could contribute to the debate. In the GoM, we relate a set of fan-like long-wavelength magnetic anomalies with seafloor spreading. We interpret these anomalies by comparing them to filtered polarity time scales and identify the fossil ridge axis. We then carry out plate tectonic reconstruction to establish the initial tectonic framework and evolution of the GoM. The GoM opened asymmetrically in two stages, starting during the Kimmeridgian and ceasing in the Berriasian. We interpret the strong magnetic anomalies and neighboring smoothed magnetic anomalies extending from South to North in the Colombian Basin as Chrons 33 and 33r and the younger part of the CQZ. Comparing the width of magnetic anomalies 33 and 33r in the Colombia Basin, Atlantic and Pacific Oceans shows a similarity between those in the Colombian Basin and the Pacific Ocean. Forward modelling in the Colombian Basin allowed to propose a paleo-latitude of $\sim$10°S and a spreading rate of $\sim$3.6 cm/yr. The crust in the Venezuela Basin shows North-South fracture zones and stronger magnetic variations that would be older, belonging to the middle part of the CQZ. The Caribbean plate more likely formed on the Pacific-Farallón spreading center.

Keywords: Caribbean Plate, Gulf of Mexico, magnetic anomalies, Colombia Basin, CLIP, Venezuela Basin.

Anomalies magnétiques et tectonique des plaques de la plaque Caraïbe et du golfe du Mexique

Résumé

L'origine Pacifique ou intra-Américaine de la plaque Caraïbe est toujours en débat. Nous avons produit une carte magnétique à partir de la compilation des données magnétiques marines de la plaque Caraïbes et du golfe du Mexique (GoM) afin de contribuer au débat. Dans le GoM, nous interprétons un ensemble d'anomalies magnétiques en éventail de grande longueur d'onde comme liées à l'expansion des fonds océaniques. Nous les identifions par comparaison avec de versions filtrées de l'échelle des inversions de polarité magnétique et localisons l'axe d'expansion fossile. Nous effectuons des reconstructions paléogéographiques pour établir le cadre tectonique initial et l'évolution du GoM, ouvert asymétriquement entre le Kimmeridgien et le Berriasien. Nous interprétons les fortes anomalies magnétiques et puis celles, plus lisses, observées du Sud au Nord dans le bassin de Colombie comme les Chrons 33 et 33r et la partie la plus récente de la Période Magnétique Calme du Crétacé (CQZ). Nous comparons la largeur des anomalies magnétiques 33 et 33r du bassin de Colombie et des océans Atlantique et Pacifique pour remarquer une similitude entre bassin de Colombie et océan Pacifique. La modélisation directe dans le bassin de Colombie conduit à une paléolatitude de $\sim$10°S et un taux d'expansion de $\sim$3,6 cm/an. Le bassin du Venezuela présente des zones de fracture Nord-Sud et des variations magnétiques de plus forte amplitude qui serait plus anciennes, reflétant la partie médiane du CQZ. La plaque Caraïbe s'est formée au centre d'expansion Pacifique-Farallón, et la province magmatique Caraibe (CLIP) serait liée au point chaud des Galápagos.

Mots-clés : Plaque Caraïbes, golfe du Mexique, bassin du Colombie, bassin du Venezuela, anomalies magnétiques, CLIP

Anomalías magnéticas e historia de la tectónica de placas en la placa Caribe y el Golfo de México

Resumen

El origin de la placa Caribe - Pacífico o intra-América - está todavía dentro de debate. En esta investigación se produjo un mapa magnético a partir de nuestra compilación de datos magnéticos marinos en la placa Caribe y el Golfo de México (GoM) con el objetivo de realizar una interpretación magnética que sirva de contribución al debate. En el Golfo de México, relacionamos al conjunto de anomalías en abanico y de longitud de onda larga con la expansión del piso oceánico. La interpretación de estas anomalías se realizó mediante su comparación con diferentes escalas de tiempo de la polaridad geomagnética filtradas y mediante la posterior identificación de la cresta de la dorsal fósil. A partir de esos resultados, realizamos la reconstrucción de placas tectónicas para establecer el marco tectónico inicial y la evolución del GoM. El piso oceánico del GoM se expandió asimétricamente en dos estadios de rotación, comenzando durante el Kimmeridgiense y cesando en el Berriasiense. Desde el Sur al Norte de la cuenca de Colombia, son observadas una secuencia de anomalías fuertes y otra secuencia de anomalías suaves las cuales son interpretadas como los Cronos 33 y 33r y parte del Cretácico Quieto Temprano. La comparación del ancho de las anomalías magnéticas 33 y 33r en la cuenca de Colombia con anomalías en los océanos Pacífico y Atlántico permitió establecer la similaridad entre las mismas con las anomalías en el Océano Pacífico. El modelado directo en la cuenca de Colombia permitió proponer una paleo-latitud de $\sim$10°S y una velocidad de expansión de $\sim$3.6 cm/yr. La corteza en la cuenca de Venezuela presente zonas de fractura en dirección Norte-Sur y variaciones magnéticas fuertes que podrían ser más antiguas, siendo su edad correspondiente al período intermedio del Cretácico Quieto. La placa Caribe podría haberse formado sobre el centro de expansión Pacífico-Farallón.

Palabras claves: placa Caribe, Golfo de México, anomalías magnéticas, cuenca de Colombia, CLIP, cuenca de Venezuela.

Contents

Contents x

List of Figures xiv

List of Tables xx

1 Introduction 1

1.1 Problem statement . . . 1

1.2 Latest research . . . 2

1.2.1 Caribbean plate boundaries . . . 4

1.2.2 Geological history of the Caribbean plate . . . 6

1.2.2.1 Spreading events . . . 6

1.2.2.2 Cretaceous-Eocene history . . . 7

1.2.3 Models of origin of the Caribbean plate . . . 7

1.2.3.1 Arguments supporting the Pacific origin of the Caribbean plate . . . 9

1.2.3.2 Arguments supporting the Intra-Americas origin of the Caribbean plate . . . 11

1.2.4 Inner Caribbean plate . . . 11

1.2.4.1 Yucatán basin . . . 12

1.2.4.2 Cayman Trough . . . 12

1.2.4.3 Colombian Basin . . . 13

1.2.4.4 Nicaragua Rise . . . 14

1.2.4.5 Venezuelan Basin . . . 15

1.2.4.6 Beata Ridge . . . 15

1.2.4.7 Aves Ridge . . . 17

1.2.5 Caribbean volcanic province . . . 18

1.2.5.1 Origin . . . 18

1.2.6 Island Arcs of the Caribbean . . . 19

1.2.6.1 Greater Antilles . . . 19

1.2.6.2 Lesser Antilles . . . 20

1.3 References . . . 22

2 Marine magnetic anomaly map of the Caribbean and the Gulf of Mexico 30
2.1 Introduction . . . 31
2.2 Objectives . . . 33
2.3 Theory . . . 33
2.3.1 Main internal magnetic field . . . 34
2.3.2 Magnetic anomalies . . . 35
2.3.3 Source of errors . . . 36
2.3.3.1 Heading effect . . . 37
2.3.4 Spectral analysis . . . 37
2.3.5 Principal component analysis . . . 38
2.4 Data and methods . . . 38
2.4.1 Aeromagnetic . . . 39
2.4.1.1 Data . . . 39
2.4.1.2 Method . . . 40
2.4.2 Marine data . . . 40
2.4.2.1 Data . . . 40
2.4.2.2 Method . . . 41
2.4.3 Main internal magnetic field removal . . . 42
2.4.4 Preprocessing of marine magnetic anomalies . . . 42
2.4.4.1 Detecting outlying surveys . . . 42
2.4.4.2 Detecting erroneous acquisition time . . . 47
2.4.4.3 Evaluation of the magnetic heading effect . . . 49
2.4.5 Levelling . . . 49
2.4.5.1 Detection of internal and external crossovers . . . 49
2.4.5.2 Internal levelling . . . 52
2.4.5.3 External levelling . . . 53
2.4.5.3.1 Unshifting: . . . 53
2.4.5.3.2 Distribution of the crossovers data using x2sys: 53
2.4.6 Frequency analysis and band-pass filtering . . . 53
2.4.7 Statistical validation of the maps: Principal component analysis on the magnetic anomalies and error ellipses. . . . 54
2.5 Results . . . 57
2.5.1 Aeromagnetic data . . . 57
2.5.1.1 Long wavelength magnetic anomaly map . . . 57
2.5.1.2 Short wavelength magnetic anomaly map . . . 60
2.5.1.3 Frequency histogram analysis . . . 61
2.5.2 Compiled database . . . 62
2.5.3 Marine magnetic anomalies . . . 63
2.5.3.1 Caribbean domain and surroundings . . . 63
2.5.4 Comparison of the long wavelength map with previous works . . . 68

2.5.5 Comparison of the short wavelength map with previous works . . . 70
2.5.5.1 Short-wavelengths on the Yucatán Basin 70
2.5.5.2 Short-wavelengths on the Eastern Caribbean plate 70
2.5.5.3 Short-wavelengths on the Nicaragua Rise 71
2.5.6 Validation of the dataset 71
2.5.6.1 Power spectrum of the magnetic anomalies 71
2.5.6.2 Statistical validation: Principal component analysis on the magnetic anomalies and error ellipses. 79
2.6 Conclusions 85
2.7 References 85

3 Plate tectonics on the Gulf of Mexico from gravity and magnetic data 93
3.1 Introduction 94
3.2 Problem statement 95
3.3 Aim 98
3.3.1 Limitations from potential field data 99
3.4 Geological background 101
3.4.1 Margins 101
3.4.2 Models of opening of the GoM 102
3.4.2.1 Principal tectonic events that occurred from 200 to 164 Ma 102
3.4.2.2 Single mantle plume model 103
3.4.3 Regional geological structures 103
3.4.3.1 Western Main Transform Fault 103
3.4.3.2 Sabine Block 103
3.4.3.3 Yucatán Block 103
3.4.3.4 Florida Block 105
3.4.4 Crust in the GoM 106
3.4.4.1 Stratigraphy 106
3.4.4.2 Thickness 107
3.4.4.3 Physical properties 107
3.4.4.4 Ages 107
3.4.5 Evolution models 108
3.4.5.1 Implications (from Van Avendonk et al., 2015) 108
3.4.6 Salt migration and deposition 109
3.5 Data 111
3.6 Methodology 112
3.6.1 Mapping and interpretation of the magnetic and gravity fabric . . . 112
3.6.1.1 Determination of the trial Euler poles from FZs 113
3.6.1.2 Identification of magnetic isochrons 115
3.7 Results and interpretation 117

3.7.1 Mapping and interpretation of the magnetic and gravity fabric . . . 117
3.7.1.1 Surroundings of the Gulf of Mexico . . . 117
3.7.1.2 Interior of the Gulf of Mexico . . . 117
3.7.1.3 Synthesis of the maps interpretation . . . 118
3.7.2 Trial Euler poles . . . 120
3.7.2.1 Laying the foundations for the plate tectonic reconstruction in the GoM . . . 120
3.7.3 Closure . . . 124
3.7.4 Stage poles of rotation and spreading asymmetry . . . 125
3.7.5 Magnetic isochrons and Spreading rates on the GoM . . . 131
3.8 Discussion . . . 138
3.9 Conclusion . . . 143
3.10 References . . . 144

4 Magnetic anomalies in the Colombia and Venezuela Basins 152
4.1 Introduction . . . 152
4.2 Method and results . . . 157
4.3 Magnetic anomalies in the Venezuela and Colombia basins . . . 157
4.3.1 The Colombia Basin . . . 157
4.3.2 The Venezuela Basin . . . 158
4.3.3 Origin of the Caribbean plate . . . 160
4.3.4 Discussion . . . 165
4.4 Conclusion . . . 170
4.5 References . . . 171

5 General conclusions and Perspectives 174
5.1 General conclusions . . . 174
5.2 Perspectives . . . 176
5.3 References . . . 177

6 Conclusions générales et Perspectives 178
6.1 Conclusions générales . . . 178
6.2 Perspectives . . . 180
6.3 References . . . 181

A Carte Structurale des Caraïbes 182
A.1 Le projet et ma contribution . . . 182

B References 184
B.1 References . . . 185

List of Figures

1.1 Simplified geology of the Caribbean domain (from internal reports of the Commission for the Geological Map of the World (CCGM, (Bouysse et al., 2016))) . . . 3
1.2 Caribbean domain and main features . . . 5
1.3 Diachronous eastward displacement of the Caribbean plate relative to the North and South American plates. Black solid lines represent: 1 = ∼80 Ma, 2 = ∼60 Ma, 3 = ∼44 Ma, 4 = ∼30 Ma, 5 = ∼14 Ma, 6 = ∼5 Ma, 7 = Recent. Contours filled with yellow represent foreland basins produced by diachronous oblique convergence between the Caribbean, North American and South American plates. Abbreviations: SB= Sinu Belt, WC = Western Cordillera, SJB = San Jacinto Belt, SNM = Santa Marta Massif, CC = Central Cordillera, EC = Eastern Cordillera, SM = Santander Massif, MA = Merida Andes, LN = Lara Nappes, CCO = Cordillera de la Costa, APP = Araya-Paria Peninsula, SI = Serrania del Interior, and NR = Northern Range of Trinidad (from (Escalona and Mann, 2011)) . . . 6
1.4 Opening of the South Atlantic (model from (Pérez-Díaz and Eagles, 2014, 2017)) . . . 8
1.5 Comparison of time span between different models about the origin of the Caribbean plate . . . 9
1.6 Coincidence of the Galapagos hotspot (red) and the Caribbean Plateau-polygon at 94 Ma Nerlich et al. (2014) . . . 10
1.7 Map of the extent of the Caribbean LIP and eastern Cayman Trough passive margin in the Jamaica passage (Corbeau et al., 2016) . . . 13
1.8 Unmigrated stacked seismic section on the Beata Ridge (Diebold, 2009) . . . 16
1.9 Conceptual plate boundary configurations illustrating the origin of the Caribbean lithosphere at 200 Ma. Proto-Caribbean/Atlantic origin (a), Panthalassa origin (b) (from Boschman et al., 2014) . . . 19
1.10 Three-dimensional model for the lithosphere in the northern Caribbean. Fabric (red) has a vertical foliation and horizontal lineation and is localized at borders of microplates, whereas the interior of microplates has no fabric (from Benford, 2012) . . . 21

2.1 Main geographical features on the Caribbean region 32
2.2 Histogram of surveys per year 33
2.3 Total magnetic field intensity IGRF12 (http://www.gfz-potsdam.de) 34
2.4 Marine magnetic anomalies (From Burger et al. (2006)) 35
2.5 Aeromagnetic tracklines location (Legend: Red circles indicate Syledis navigation stations location, blue triangles indicate ground magnetometer location) (MENEVEN, 1983) 39
2.6 Marine and aerial tracks location 41
2.7 Plot of marine magnetic anomalies located between 55°W and 52.5°W showing outliers 43
2.8 Plot of marine magnetic anomalies located between 65°W and 62.5°W showing outliers 44
2.9 Plot of marine magnetic anomalies located between 65°W and 67.5°W showing outliers 45
2.10 Plot of marine magnetic anomalies located between 17.5°N and 20°N showing outliers 46
2.11 Magnetic anomalies versus decimal year showing erroneous registered acquisition time (Labels "a", "b", and "c" exhibit errors whilst "d" has a correct time, red boxes indicating identified erroneous time) 47
2.12 Accumulated distance vs. ship velocity 48
2.13 Accumulated distance vs. Ship velocity (featuring negative velocities) . . . 48
2.14 Magnetic anomaly vs. magnetic heading on the survey LWI932010 49
2.15 Heading effect and correction on magnetic anomalies 50
2.16 First criterion used to determine the parameters for the internal cross-overs detection 51
2.17 Amplitude of the external crossovers for the marine tracklines 51
2.18 Internal levelling and correction curve 52
2.19 DLDR01HO survey before and after the unshifting step 54
2.20 Example of the frequency analysis used 56
2.21 Aeromagnetic maps over Venezuela from processed magnetic anomalies (Legend: (a) Long wavelength map, (b) Short wavelength map, (c) Total magnetic anomaly map); Acronyms: FB=Falcón Basin, AMG= Apure-Mantecal Basin, EG= Espino Graben, CB=Cariaco Basin, EBM= El Baúl Massif, GR= Lake Guri) 59
2.22 Frequency histogram from aeromagnetic data 62
2.23 Frequency histogram of magnetic anomalies before and after processing . . 63
2.24 Total magnetic anomaly map 66
2.25 Short-wavelength magnetic anomaly map 67
2.26 Long wavelength magnetic anomaly maps (a: Reprocessed magnetic anomalies, b: WDMAM, c: MF7, d: GRIMM-L) 69

2.27 Short wavelength magnetic anomaly maps. (a: Reprocessed magnetic anomalies, b: Processed by NGDC, c: NAMAM, d: WDMAM) 72
2.28 Short wavelength magnetic anomaly map of Yucatán Basin. (a: Reprocessed magnetic anomalies, b: NAMAM, c: WDMAM) 73
2.29 Short wavelength magnetic anomaly map of Eastern Caribbean plate. (a: Reprocessed magnetic anomalies, b: NAMAM, c: WDMAM) 74
2.30 Crust type in the Aves Ridge interpreted from potential field data 75
2.31 Short wavelength magnetic anomaly map of Nicaragua rise. (a: Reprocessed magnetic anomalies, b: NAMAM, c: WDMAM) 76
2.32 Crust type in the Nicaragua Rise interpreted from potential field data 77
2.33 Radially averaged spectrum of the magnetic anomalies for long wavelengths over the Caribbean region and the Gulf of Mexico 77
2.34 Radially averaged spectrum of the magnetic anomalies for short wavelenghts over the Caribbean region and the Gulf of Mexico 78
2.35 Plain and tridimensional view of the bivariate frequency calculated from the magnetic anomalies of the GRIMM-L, WDMAM and MF7 datasets and the magnetic anomalies from this study in the Caribbean region and the Gulf of Mexico 80
2.36 Bivariate frequency from long wavelength datasets. (Using: MF7 (a), WDMAM (b) and GRIMM-L (c)) 81
2.37 Bivariate frequency from short wavelength datasets. (Using: NAMAG (a) and WDMAM (b) 81
2.38 Location of the discrepancies between previous datasets and the processed magnetic anomaly for long wavelengths (Using: MF7 (a), WDMAM (b) and GRIMM-L (c)) 83
2.39 Location of the discrepancies between previous datasets and the processed magnetic anomaly for short wavelengths (Using: NAMAG (a) and WDMAM (b) 84

3.1 Simplified geology of the Gulf of Mexico (from Bouysse et al., 2015) . . . 96
3.2 COB estimations from different authors (Eagles et al., 2015) 97
3.3 Plate tectonic reconstruction in the GoM at 200 Ma (from (Pindell, 1994)) . 97
3.4 Base maps of this study: Vertical gradient of gravity (Sandwell et al., 2014) (a) and marine magnetic anomalies (b) 100
3.5 Previously interpreted fracture zones over Eastern North America (from (Thomas et al., 2006)) 101
3.6 Structural interpretation of the GoM from magnetic anomalies (from Tectonic Analysis) 104
3.7 Map showing Gondwana terranes along the Atlantic and GoM (From (Mueller et al., 2014)) 106

3.8 Tectonic map and location of salt domes in the GoM (from (Worrall and Snelson, 1989)) 110
3.9 Location of the magnetic profiles used individually in this study 111
3.10 Estimation of the Euler pole produced by our Matlab algorithm. Great circles passing perpendicular to the simulated FZ and by the Euler pole (a); detail of the different great circles calculated in the GoM (b) and, global view showing the two set of solutions for the location of the Euler poles, bars represent the statistical frequency of the crossings between the great circles (c) 115
3.11 Parameters that we used to apply the oblique Mercator projection (a) and an example of the use of the Oblique Mercator projection for the Central Atlantic (b) 116
3.12 Three fan-like magnetic anomalies on each flank. Central anomalies are marked by 1, 2 and 3; outer anomalies '*'; dashed black lines represent the boundaries of the Yucatán Block and Florida Block respectively 120
3.13 Focus on the Pangea reconstruction from magnetic and gravity data respectively. Pangea reconstruction based in magnetic data from WDMAM 2.0 (a), focus in the Southern North American continent-Northern South American-Western African continent fit 200 Ma ago, observed amplitude of the magnetic anomalies in the North American continent is stronger than those observed over the South American continent and the African continent (b), similar reconstruction were performed using vertical gradients of gravity (c and d) 121
3.14 View of the Pangea reconstruction from gravity (b), topographical (c) and magnetic data (d) centred in the Atlantic Ocean 123
3.15 Tectonic reconstruction of the Gulf of Mexico from magnetic anomaly . . . 124
3.16 Adopted tectonic model from VGG (a) and magnetic anomaly data (b). Dashed yellow lines represent the correlation that we observe between magnetic anomalies highs of the Yucatán Block and the Florida Block respectively. Dashed fuchsia line represents the respective correlation for the magnetic anomalies lows 125
3.17 Extended view of the adopted tectonic model from VGG and magnetic anomaly data 126
3.18 Magnetic and gravity maps in polar projection, using the Total Euler pole as pole of the projection 127
3.19 Interpretation of the conjugated magnetic anomalies in the GoM. Colors represent different stages of rotation: Light violet represents a younger rotation stage than darker violet (outer magnetic anomalies) 128
3.20 Flow lines showing the different stages of rotation in the GoM 129

3.21 Sketch of the location of the Yucatán Block at different stages of rotation. Legend: Points pattern represent the distribution of the salt provinces over the GoM; flowlines indicate the path followed by the Yucatán Block during the rotation; each color line represent a half-stage of rotation 130
3.22 Percentage of asymmetry along the different stages of rotation 131
3.23 Marine magnetic anomalies from west to east of the GoM as estimate from our grid. We plotted the profiles centered in the ridge axis 133
3.24 Magnetic wiggles from the previously extracted profiles 134
3.25 Filtered geomagnetic time scale (normal polarity). In the background, vertical lines in colours represent the geomagnetic polarity time scales before filtering 135
3.26 Filtered geomagnetic time scale (inverse polarity). In the background, vertical lines in colours represent the geomagnetic polarity time scales before filtering 135
3.27 Identified isochrons in the GoM. 'd1' represent the ridge axis whereas 'd2' represent the inner conjugated magnetic anomalies, associated to the isochron M24n 136
3.28 Identified magnetic isochrons in the GoM with previously identified isochrons in the Central Atlantic (Isochrons from (Seton et al., 2014) database updated on July-2018) 139
3.29 In the figure, our proposed GoM reconstruction is showed together with models suggested by other authors (Lundin and Doré, 2017; Nguyen and Mann, 2016; Pindell et al., 2016) 140
3.30 Position of the Yucatán Block at 245 Ma as an implication of our proposed model 141
3.31 Crustal terrains with our COB interpretation in the GoM (zoom in to the Structural Map of the Caribbean - see Appendix A) 142

4.1 Global distribution of large igneous provinces (Bouysse, 2009). Colors represent crustal ages and are according to the Commission for the Geological Map of the World, excepting orange color which represents oceanic plateaus 154
4.2 Interpretation of thickened oceanic crust in the Caribbean domain from seismic data (Meschede and Frisch, 1998) 155
4.3 Magnetic profiles previously interpreted over the Venezuela Basin, the Aves Ridge and the Grenada Basin (Donnelly, 1973; Ghosh et al., 1984) 156
4.4 N-S profiles used to evaluate the magnetic anomalies in the Colombia Basin. The grid of Vertical Gradient of Gravity is in the background. Color scale from blue to red, represents negative to positive VGG respectively. The Colombian Basin exhibits the minimum averaged VGG of this area 158

4.5 Extracted magnetic anomaly from tracks in the Colombia Basin. Solid black lines: Profile 1-CB extracted from the northern segment of the basin (a) and profiles 1, 2, 3 and 4 extracted in NS direction from the southern segment of the basin (b) 159
4.6 Profiles used to evaluate the magnetic anomalies in the Venezuela Basin. The grid of Vertical Gradient of Gravity is in the background. Color scale from blue to red, represents negative to positive VGG respectively. Solid black lines represent the direction of the extracted profiles whereas dashed black lines represent our tentative fracture zones ('a' and 'b') 161
4.7 Approximately N-S trending magnetic profiles selected in the Venezuela Basin 162
4.8 Magnetic interpretation over the Venezuela Basin from marine data. Black dashed lines represent second order fracture zones, thick solid lines are the limit of a major fracture zone interpreted in the NS direction 163
4.9 Magnetic interpretation from marine data superimposed on satellite magnetic data (satellite magnetic data from (Olsen et al., 2017)) 164
4.10 Magnetic anomaly map (from (Dyment et al., 2015)) used to compare the wavelengths of magnetic anomalies obtained in the Colombia Basin with other marine magnetic wavelengths (In the Caribbean region, we replaced data with the database obtained in this study). Green boxes represent identified compatible areas in the Pacific Ocean and Colombia Basin respectively 166
4.11 Close up on the evaluated area in the Pacific Ocean. We selected magnetic data from available marine tracklines (a) and plotted the magnetic wiggles on those selected tracks (b) 167
4.12 Sub-group of magnetic profiles in the Pacific Ocean used for the magnetic modelling and comparison 168
4.13 Forward modelling of the selected Pacific Ocean and Colombia Basin magnetic anomalies 168
4.14 Magnetic anomalies on the Cretaceous Normal Superchron (Granot et al., 2012) 169
4.15 Sediments thickness in the Caribbean region (from (Whittaker et al., 2013) database) 170

List of Tables

2.1 Description of track lines and total magnetic field measurements 40
2.2 Statistics of the magnetic anomalies before and after the internal levelling . 55
2.3 Basic statistics of magnetic anomalies before and after their reprocessing . . 63
2.4 Statistics before and after the bivariate frequency analysis 82

3.1 Stage poles for each rotation stage in the GoM respect to our interpreted ridge axis 125
3.2 Percentage of seafloor spreading symmetry from our proposed model for each stage of rotation 132
3.3 Average half-spreading rates for the youngest stage of rotation from the three different GPTS used in this study 137

Chapter 1

Introduction

- In lak ‘ ech, - hala ken.
- I am another you, - you are another me.

— MAYAN GREETING

1.1 Problem statement

For many years, several authors noted the difficulty of interpreting magnetic anomalies within the Caribbean plate. Aside of the magnetic isochrons identified in the Colombia Basin (Christofferson, 1973) and along the Cayman Ridge (e.g., Leroy et al., 2000), seafloor spreading structures in the Caribbean plate remain unrevealed. The complexities in the interpretation of the marine magnetic anomalies in the Caribbean plate are mostly due to: longitudinal magnetic anomalies with an amplitude smaller than 10 nT which can be in the same order of the cultural noise (if the plate formed near the Equator); the presence of electro-jets currents which are also part of the cultural noise (these currents can produce peaks or outliers in the magnetic compilation with no geological meaning); very old magnetic profiles with problems of quality, large navigational uncertainties and instrumental calibration; large span in time of the marine magnetic tracks which can also be responsible of artifacts and large amplitude crossovers; magnetic anomalies produced by the volcanic layer which may mask the original magnetic anomalies in area of oceanic crust (the volcanic layer extends along the Venezuelan Basin, Colombia Basin, partially over the Nicaragua Rise and the south of the Hispaniola Island); in particular cases, inaccessibility to the documentation related to the acquisition and pre-processing of the marine tracks and, the lack of magnetic observatories in the Caribbean region, in general, which make infeasible to validate the magnetic measurements and correct them from variations of the external magnetic field. Usually, the use of global geomagnetic reference models (e.g., Sabaka et al., 2004) allows to remove most of the variation of the external magnetic field from the measurements.

The above mentioned reasons explain, first, the low confidence given to the marine

magnetic data in the Caribbean area, and second, that data other than those of magnetic anomalies makes up most of the plate reconstruction models of the Caribbean area (e.g., Boschman et al., 2014; Calais et al., 1989; Giunta and Orioli, 2011; Meschede and Frisch, 1998; Pindell and Dewey, 1982). However marine magnetic anomalies remain a suitable data to address the still-pending issues in the Caribbean plate, ie. to interpret oceanic structures in the Caribbean seafloor, to identify the magnetic signature of the Caribbean Large Igneous Province (CLIP) and to determine where and when the CLIP and the Caribbean plate originated.

In this work we aim to revisit the marine magnetic anomalies in the Caribbean region in order to shed light on the magnetic provinces and contribute to the questions exposed above. We included the Gulf of Mexico (GoM) in our investigation because the Gulf constitutes a temporal and spatial reference for the plate tectonic reconstruction of the Caribbean plate.

1.2 Latest research

The three crustal provinces identified in the Caribbean are (see Fig. 1.1): (1) Precambrian crustal blocks underlain by pre-Mesozoic basement rocks; (2) continental crust formed during the Mesozoic and Cenozoic; and (3) a thickened oceanic crust of a plateau basalt set up in the Middle Cretaceous (e.g., Bouysse et al., 2016; Meschede and Frisch, 1998). Pre-Mesozoic basement occurs in the pre-existent parts of the North and South American plates and the north of the Central American land bridge including southern Guatemala, Honduras, Nicaragua and the Nicaraguan shelf. A primitive Mesozoic and evolved Cenozoic magmatic arc forms the south-eastern part of the Central American land bridge in Costa Rica and Panama, built on top of Caribbean oceanic crust (Meschede and Frisch, 1998). Marine Triassic is not known in the Caribbean region (e.g., Woodring, 1928).

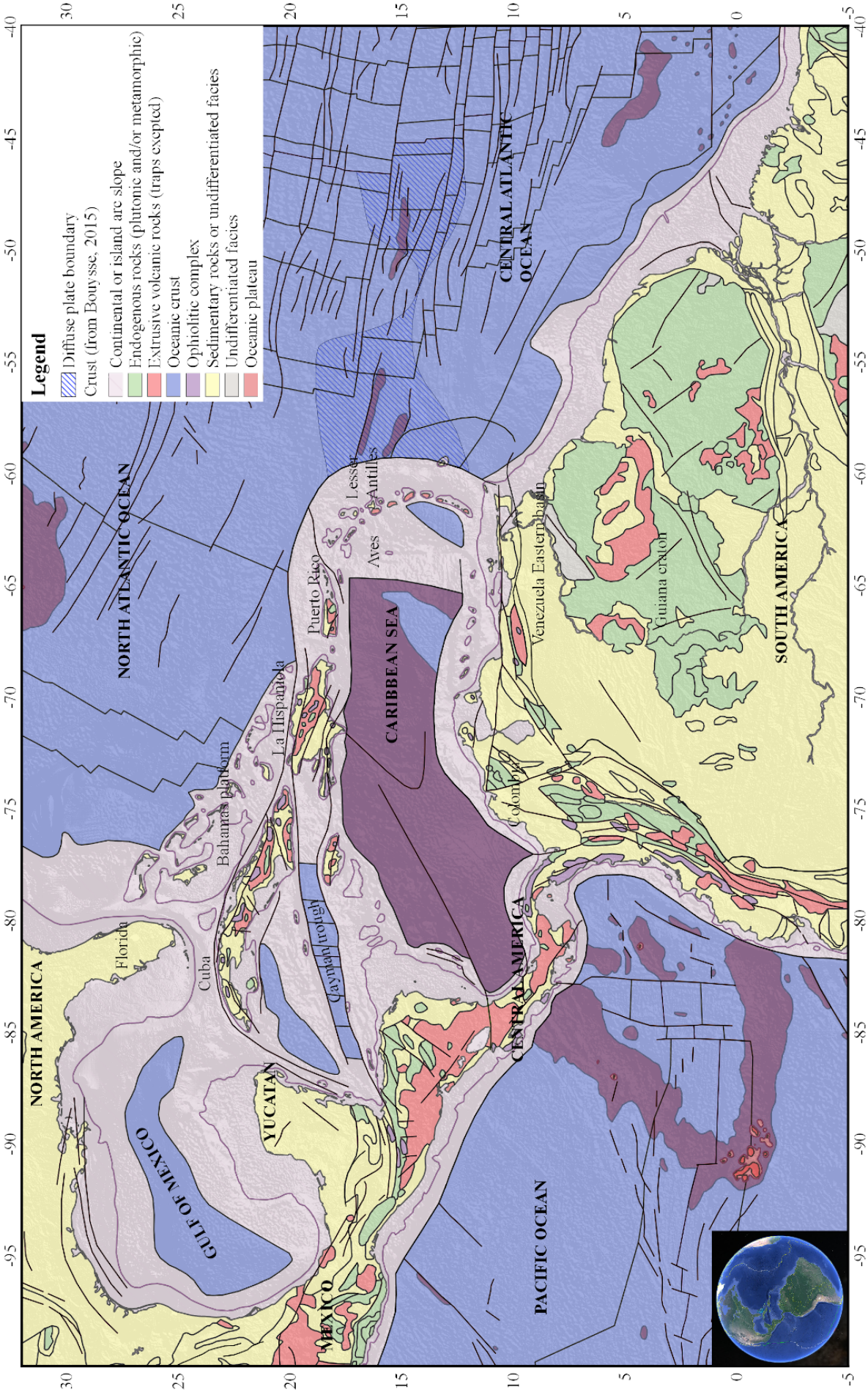

Figure 1.1 – Simplified geology of the Caribbean domain (from internal reports of the Commission for the Geological Map of the World (CCGM, (Bouysse et al., 2016)))

1.2.1 Caribbean plate boundaries

A 100-250 km wide seismic zone defines the convergent boundary between the Caribbean and North America tectonic plates. This zone consists mainly of left-lateral strike-slip deformation extending over 2000 km along the northern edge of the Caribbean Sea (e.g., Leroy et al., 2000; Mann et al., 1995) (see Fig. 1.1). Leroy et al. (2000) and Rosencrantz (1990) proposed that the location of the north-western edge of this boundary by a convergent domain defined along the Cayman Trough. Rosencrantz (1990) interpreted this boundary edge as a younger boundary that dissects and overprints the older convergent one; hence, it may preserve in its interior the record of the concurrent history of the Caribbean. Timing records of the spreading age in the Cayman Trough may also be present in this boundary. Towards the north-east, a transition from this convergent margin in La Hispaniola evolves to an extensional margin up to Puerto Rico, where a subduction system takes place (see Fig. 1.2).

First, the oblique convergence of the Atlantic oceanic lithosphere and second, the subduction of that oceanic lithosphere beneath the lithosphere of the Greater Antilles dominate the W-E variations of the Caribbean-North American margin (e.g., Symithe et al., 2015). The north-eastern edge of this margin exhibits three types of subduction systems: an oblique subduction/collision with strain partitioning in Hispaniola; an oblique subduction with no strain partitioning in Puerto Rico and, an along-strike transition to a plate boundary-normal subduction farther east in the Lesser Antilles (Calais et al., 2016). Escalona and Mann (2011) proposed seven families of faults related to the diachronous eastward displacement of the Caribbean plate relative to the North and South American plates. Calais et al. (1989) and Symithe et al. (2015) identified an intra-arc strike-slip faults family related to the eastward motion of the Caribbean plate in relation to North America and a family of faults linked to the North American plate compression over the Caribbean. (Fig. 1.3).

Profound foreland basins, with sediment thickness ranging from 4 km to 18 km, with ages ranging from the Eocene to present and which become progressively younger to the east characterise the Southern boundary of the Caribbean plate (Audemard, 2009; Escalona and Mann, 2011). Diachronous and oblique collision between the Caribbean arc and the passive margin of South America produced this boundary (Lugo and Mann, 1995; Mann et al., 2006; Pindell and Barrett, 1990), which represents one of the most prolific hydrocarbon regions in the world and comparable in reserves with those of the Middle East (Escalona and Mann, 2011). The Cayman Spreading Center (CSC) marks the western boundary of the Caribbean plate. Leroy et al. (2000) proposed that the CSC activated from the early Eocene (49 Ma). However, based on inherited rotated fault-structure ten Brink et al. (2002) proposed 36 Ma for the initiation of the spreading. Ridge propagation allowed the formation of basins and established the Walton-Enriquillo fault system. The parallel magnetic lineations observed for north and south of the Cayman Ridge delimit those basins. A first phase of compression deformed and folded those basins at about 20 Ma (Corbeau et al., 2016). The Lesser Antilles

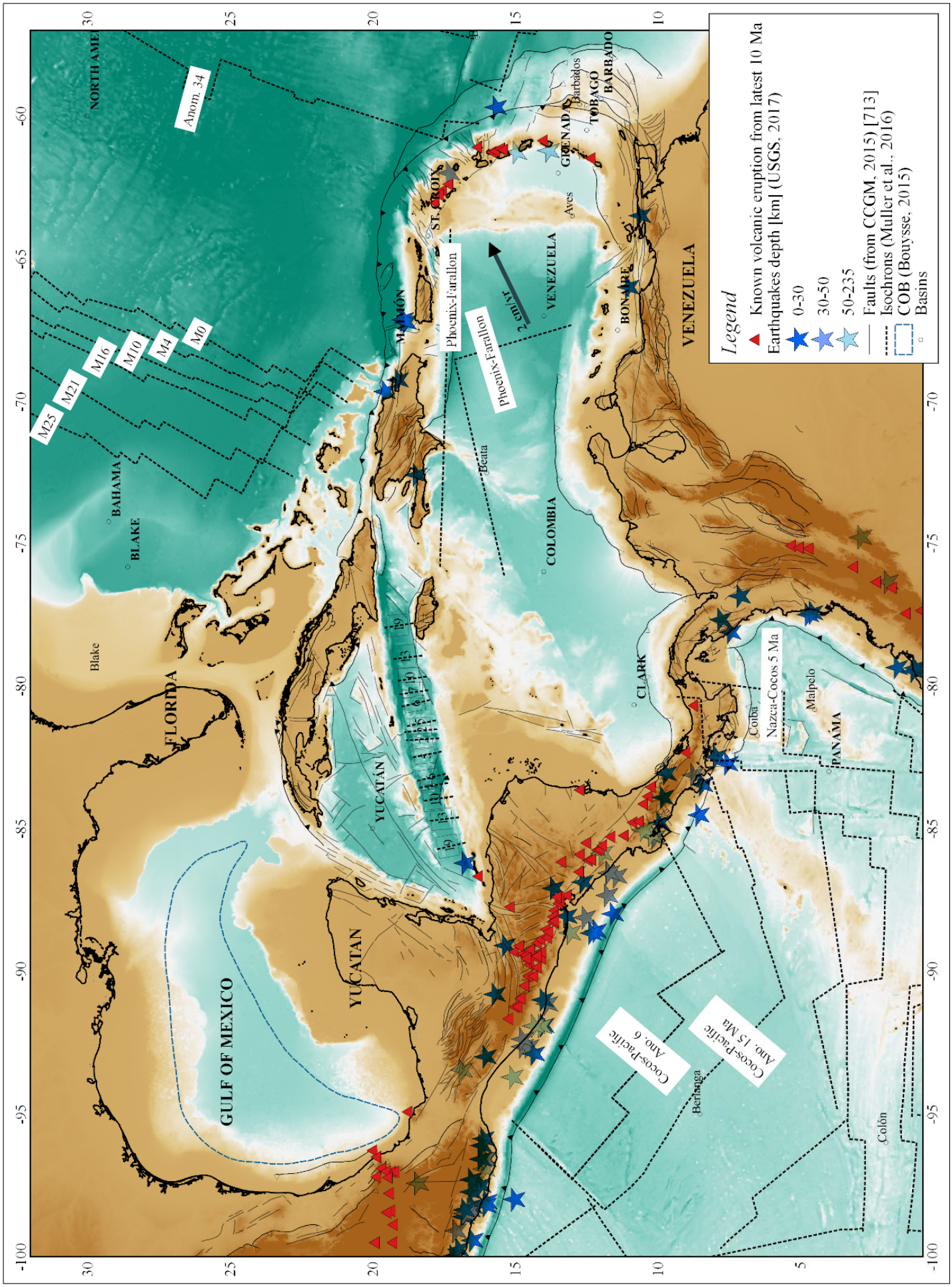

Figure 1.2 – Caribbean domain and main features

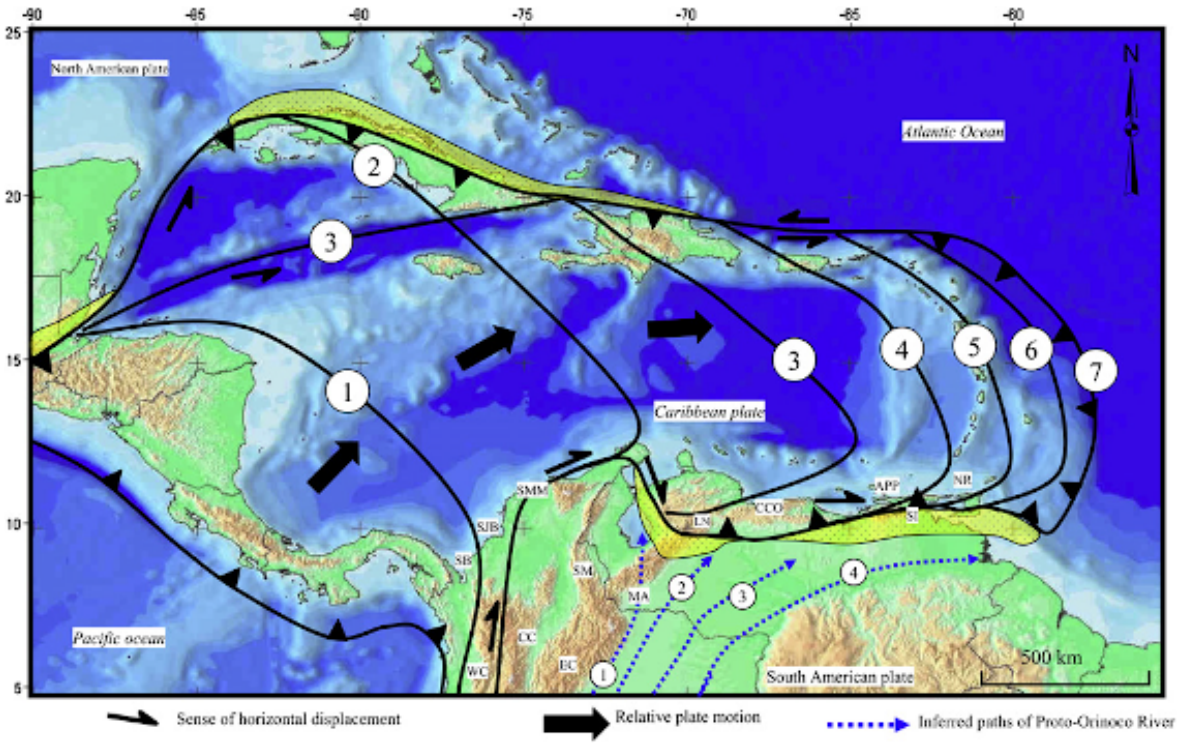

Figure 1.3 – Diachronous eastward displacement of the Caribbean plate relative to the North and South American plates. Black solid lines represent: 1 = ∼80 Ma, 2 = ∼60 Ma, 3 = ∼44 Ma, 4 = ∼30 Ma, 5 = ∼14 Ma, 6 = ∼5 Ma, 7 = Recent. Contours filled with yellow represent foreland basins produced by diachronous oblique convergence between the Caribbean, North American and South American plates. Abbreviations: SB= Sinu Belt, WC = Western Cordillera, SJB = San Jacinto Belt, SNM = Santa Marta Massif, CC = Central Cordillera, EC = Eastern Cordillera, SM = Santander Massif, MA = Merida Andes, LN = Lara Nappes, CCO = Cordillera de la Costa, APP = Araya-Paria Peninsula, SI = Serrania del Interior, and NR = Northern Range of Trinidad (from (Escalona and Mann, 2011))

Arc is the eastern boundary of the Caribbean plate. A chain of volcanic islands form the arc and north-south extend from Anguilla and Saba up to the Grenada volcanic island (e.g., Schlaphorst et al., 2017). The Grenada Basin and the Aves Ridge form the western limit of the arc. The Tobago Basin neighbours the arc on its southeast edge (e.g., Christeson et al., 2008). The arc originated from the relatively slow subduction (∼2 cm/yr; (DeMets et al., 2000)) of the North and South American plates beneath the eastern Caribbean plate.

1.2.2 Geological history of the Caribbean plate

1.2.2.1 Spreading events

Among the most important seafloor spreading events known within the Caribbean region in chronological order are:

1. Spreading in the Central Atlantic Ocean from the Lower Callovian to the present (from 166 Ma);
2. Opening of the Caribbean part of Tethys from the Oxfordian to Middle Cretaceous

(from 164 Ma to 100 Ma);

3. Spreading in the Gulf of Mexico from the Upper Jurassic until the Neocomian (from approx. 140 Ma to 131 Ma);
4. Opening of the southern part of the South Atlantic Ocean from the Aptian (see Fig. 1.4);
5. Opening of the northern part of the South Atlantic Ocean from the Albian (see Fig. 1.4);
6. the spreading of the still active Cayman Trough from the Middle Eocene (Calais et al., 1989, and references therein).

1.2.2.2 Cretaceous-Eocene history

Cretaceous: Stéphan et al. (1990) considered the Campanian magmatic arcs reported in North America, South America, Mexico, and Colombia as first order geotectonic elements and related them to folding, thrusting and metamorphism (e.g., Calais et al., 1989). Iturralde-Vinent et al. (2016) reported the coexistence of these arcs with Proto-Caribbean fragments of oceanic crust (of Atlantic affinity) and, oceanic lithosphere of Pacific origin in Cuba.

Eocene: Transpressive intense tectonics and the transpression active since 57-48 Ma along the northern and southern boundaries of the Caribbean plate, resulted in different families of major strike-slip faults and deformations zones. Both faulting and deformation zones passed through several stages. Those stages gave birth to the main structural basins and ranges of this area (e.g., Calais et al., 1989; Escalona and Mann, 2011; Stéphan et al., 1990). Baquero et al. (2015) reported a rifting event related with the post-Great Arc of the Caribbean. This event could affect the Falcon basin in western Venezuela from 34 Ma to 15.4 Ma.

1.2.3 Models of origin of the Caribbean plate

Proposed models about the origin of the Caribbean plate and the Gulf of Mexico (GoM) span from different geological times (Fig. 1.5) and are mostly based on geological observations and paleomagnetic results, but the latter data are available only in a few locations (e.g., Boschman et al., 2014; Calais et al., 1989; Giunta and Orioli, 2011; Meschede and Frisch, 1998; Pindell and Dewey, 1982).

The large sediment thickness, the absence of clearly identified magnetic anomalies associated with seafloor spreading dates and the absence of deep penetrating drills or deep seismic prevented to conclude on the age and nature of the Caribbean ash and to make plate tectonic reconstruction models other than speculative ones. Although most of the models agree on the fact that the Caribbean plate was in place at least during the Early Paleocene

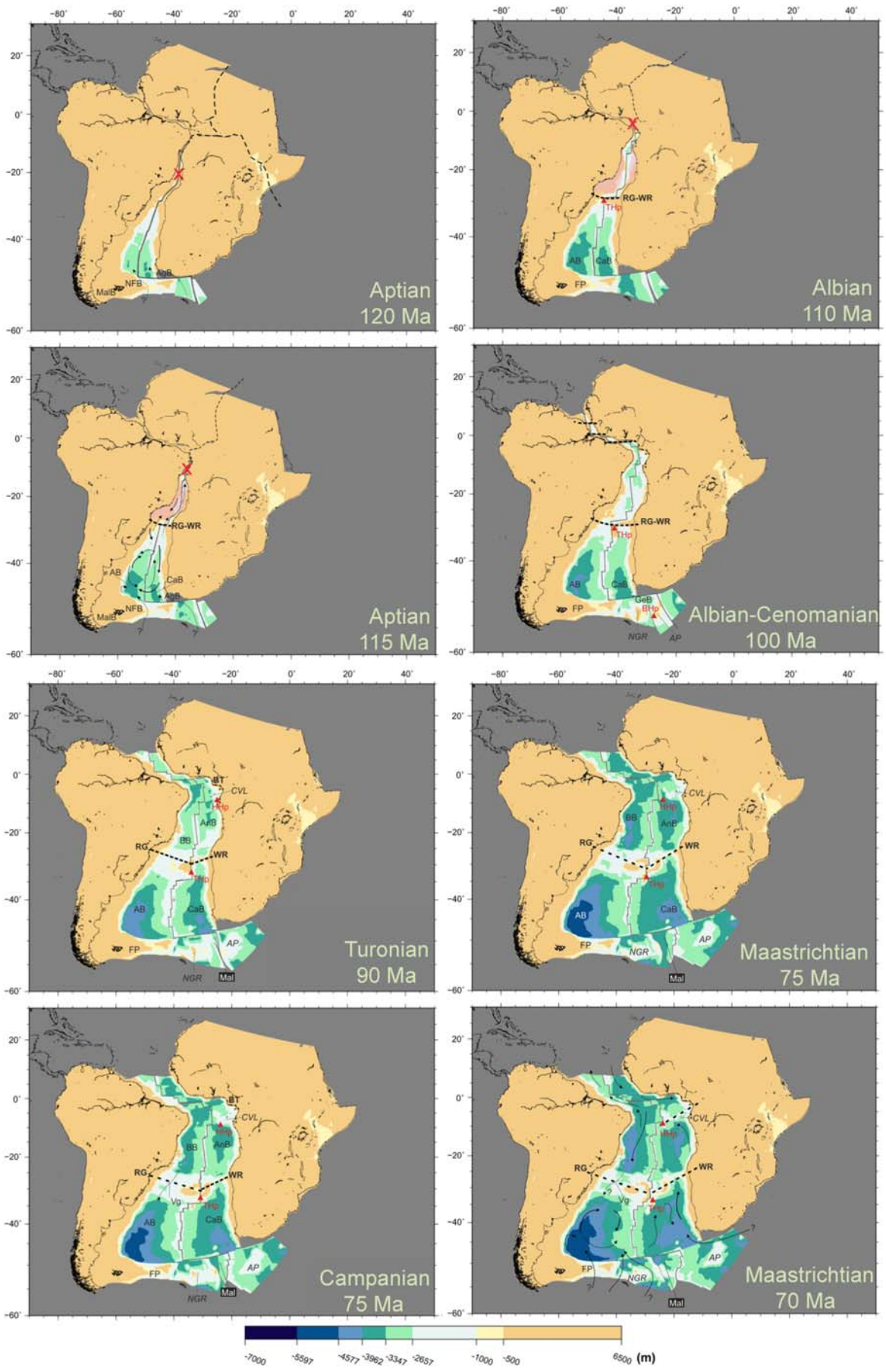

Figure 1.4 – Opening of the South Atlantic (model from (Pérez-Díaz and Eagles, 2014, 2017))

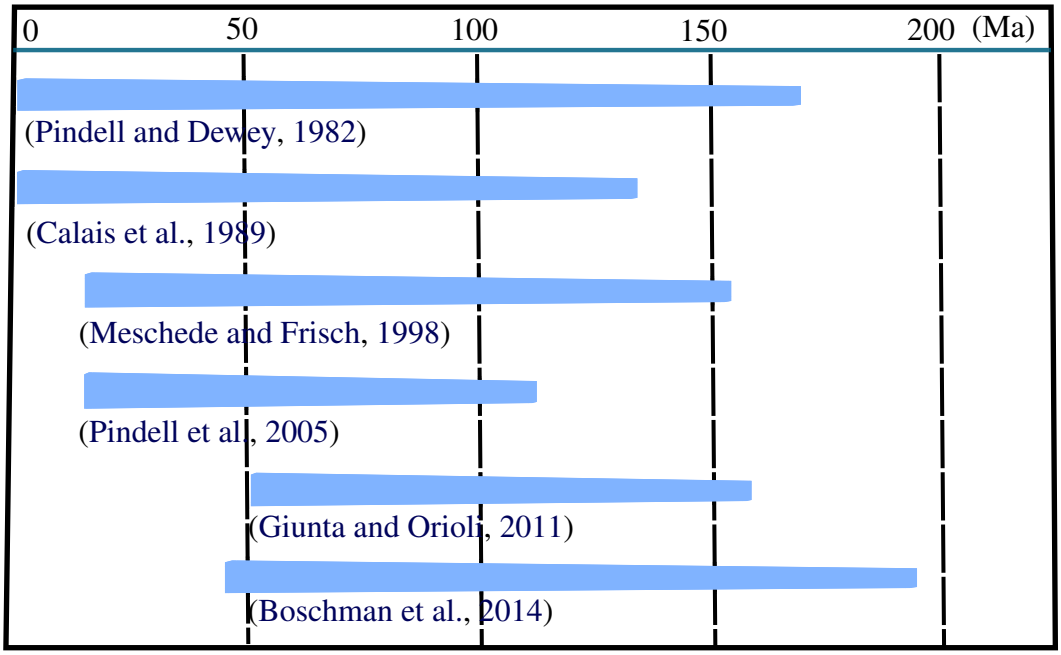

Figure 1.5 – Comparison of time span between different models about the origin of the Caribbean plate

(c. 65 Ma), Calais et al. (1989), Pindell and Dewey (1982) and Boschman et al. (2014) proposed two leading families of models for the origin of the Caribbean plate. The first family assumes that the plate came from far away in the west, i.e., a Pacific origin. In these models, the Caribbean plate is a fragment of the Farallon oceanic crust isolated from the eastern Pacific and emplaced between North and South America starting from the latest Cretaceous time onwards (see Fig. 1.3) (Duncan and Hargraves, 1984; Pindell and Dewey, 1982). These models also imply a convergence and collision of the Caribbean plate versus the proto-Caribbean during the Upper Cretaceous-Paleocene and large-scale sinistral strike-slip faults active from the Eocene until present (e.g., Calais et al., 1989). A second family assumes a local formation, i.e., Intra-America or Atlantic origin.

1.2.3.1 Arguments supporting the Pacific origin of the Caribbean plate

1. Reconstruction of plate circuits of the Caribbean Plateau - Farallon Plate – Pacific Plate – Antarctica – Africa, with South and North America moving relative to Africa suggests a Pacific provenance for the Caribbean plate (e.g., Nerlich et al., 2014) (see Fig. 1.6);
2. Acton et al. (2000) used paleomagnetic data from ODP Sites 999 and 1001, to propose a paleo-latitude for the Caribbean plate at 5°–15° south of its current position at approx. 80 Ma, which agrees with an origin in the Pacific Ocean west of the subduction zones active in the Central American region during the Cretaceous, but also with an origin within the Central American region.

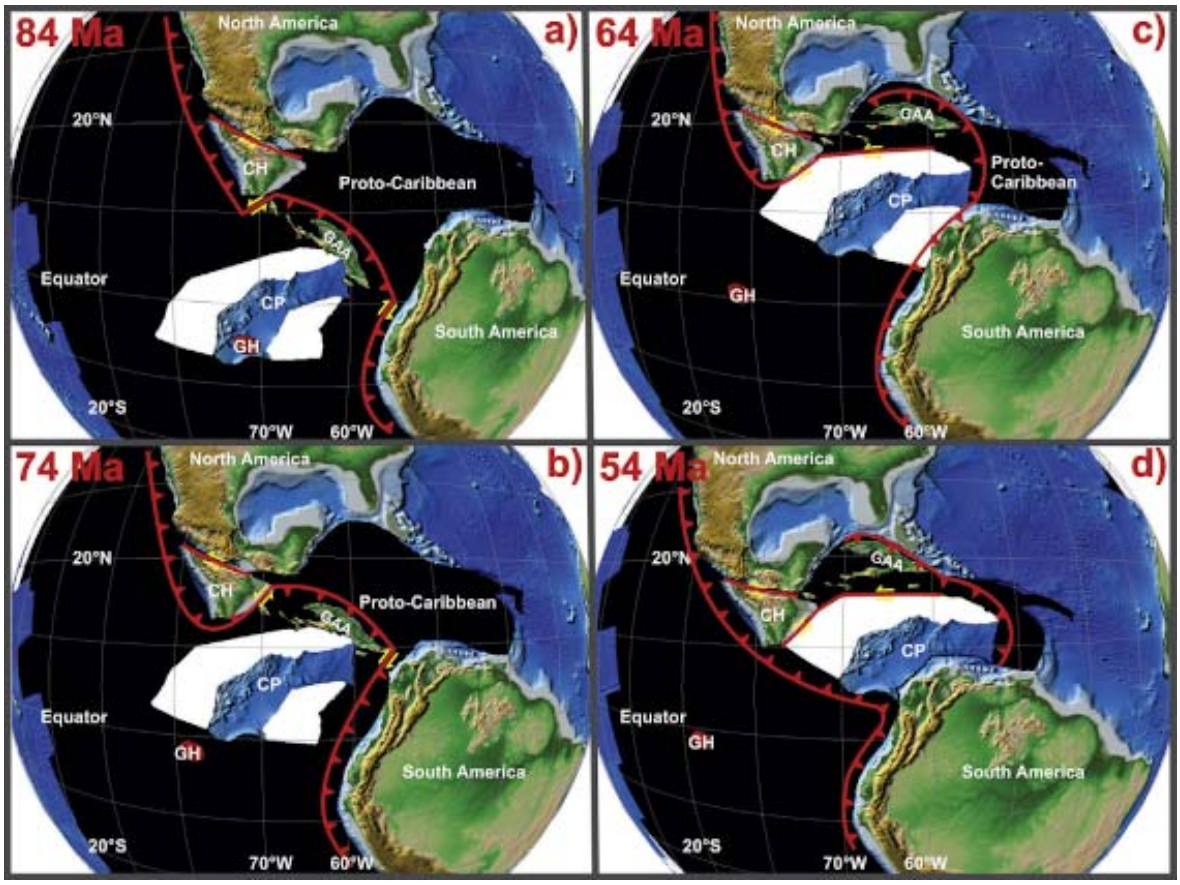

Figure 1.6 – Coincidence of the Galapagos hotspot (red) and the Caribbean Plateau-polygon at 94 Ma Nerlich et al. (2014)

1.2.3.2 Arguments supporting the Intra-Americas origin of the Caribbean plate

- Paleomagnetic data, which covers an age ranging from Jurassic to Paleocene, indicates that the ophiolite complexes in Costa Rica and Panama formed in an equatorial position;
- The position of the ophiolites relative to South America remained unchanged since their origin;
- Basaltic rocks of the lower part of the ophiolites are of mid-ocean ridge type suggesting formation at a spreading center. Those basaltic rocks formed as part of the proto-Caribbean crust at a spreading axis in an intra-American position during Jurassic and Early Cretaceous times;
- The upper part of the ophiolites is mainly built up by island-arc and intraplate basalts. The island-arc basalts evolved at the Central American land bridge which started in the Middle Cretaceous;
- Meschede and Frisch (1998) related the Caribbean plateau basalt to intraplate basalts, which thickened and stopped the movement of the Caribbean crust in the Middle Cretaceous to probably Campanian times;
- Orientations and time sequences of paleostress tensors calculated from fault-slip data in southern Mexico and Costa Rica reflect changes in relative plate motions along the Middle American convergent plate margin;
- And plate-tectonic reconstructions show an overlap between South America and parts of southern Mexico in Triassic to Middle Jurassic times (Pindell and Barrett, 1990; Ross and Scotese, 1988). To solve the space problem, Meschede and Frisch (1998) postulated that large-scale sinistral strike-slip movements along the Mojave-Sonora 'Megashear' in Northern Mexico (Amato et al., 2009; Anderson et al., 2005), the Trans-Mexican Volcanic Belt (Cebull and Shurbet, 1987), the Motagua–Polochic fault system in Guatemala (e.g., Rosencrantz et al., 1988) and several second-order shear zones were active during the Early Mesozoic.

1.2.4 Inner Caribbean plate

It is generally accepted that a Cretaceous Oceanic Plateau made the Caribbean plate core, 'known as the Caribbean Large Igneous Province (CLIP)'. Extensive lava flows and distinct thickness of sediments which covers an igneous basement characterize the Caribbean plate. Lu and McMillen (1982) and Bowland (1993) over the Colombia Basin and Ladd and Watkins (1980), Ladd et al. (1990) and Diebold et al. (1999) in the Venezuelan Basin described several seismic units with typical oceanic material. The thickness of the crust in those units is around 5 km. Moreover, in the Venezuelan Basin, Colombian Basin, south of the Beata Ridge and in the Lower Nicaraguan Rise, seismic reflection and drills allowed the

identification of the Carib Beds (Caribbean typical prominent reflection horizons A" and B") (Corbeau et al., 2016, and references therein.).

1.2.4.1 Yucatán basin

Basement structural provinces The Yucatán borderland, along the west side of the basin parallel to the Yucatán platform, represents the eastern extension of the platform, truncated by a complex paleo-transform boundary fault zone along its outer edge. A small, deep and rectangular oceanic basin of Paleogene age formed by rifting within the transform zone (66-23 Ma) dominates the central deep basins province east of the borderland. The Cayman Rise province, covering the eastern two-thirds of the basin, includes a prominent ENE - WSW trending linear topographic rise of unknown but probable volcanic origin (Rosencrantz, 1996). Rosencrantz (1996) interpreted the rise that intersects and dips beneath the Cuban margin to the east along a buried trench to be a remnant of the Cretaceous subduction zone associated with the Cuban arc.

Crustal thickness Seismic refraction profiles and regional gravity interpretations indicate that crust beneath the deep north-central and western parts of the basin is oceanic, and that it thickens southward to more than 18 km beneath the Cayman Ridge (e.g., Bowin, 1968; Dillon et al., 1972; Dillon and Vedder, 1973; Ewing et al., 1960). In contrast, heat flow and depth to basement measurements in the western part of the basin suggest that the underlying oceanic crust may be as young as Late Paleocene to Middle Eocene in age (Rosencrantz, 1996, and references therein.). In the Central deep basins, the basement depths range from 5 to 7 km, with an average of 6 km approximately. The basement horizon is relatively flat with a moderate relief of 200 to 500 m, and has a seismic reflection character typical of oceanic crust (nested, high-amplitude diffraction hyperbola) (Rosencrantz, 1990). There is no obvious structural break between the basement under the rise and deep basement to the south, however, and the seismic character of the two are similar. The orientation of the stepped terraces is unknown (Rosencrantz, 1996).

Age The age of the oceanic crust underlying the northern Yucatán basin (and presumably the Cayman Rise) is unknown (Rosencrantz, 1996). Even though, it seems that the opening of the Cayman Trough started in the Early Eocene age (49 Ma, Ypresian) (Leroy et al., 2000).

1.2.4.2 Cayman Trough

Pubellier et al. (2000) proposed first in the eastern part of the Gonâve microplate based on paleotectonic reconstructions and magnetic mapping the presence of tilted blocks belonging to the Eastern Cayman Trough passive margin. The easternmost tilted block of the Eastern Cayman Trough passive margin imaged in previous surveys was the Holmes bank near north-

east Jamaica (Leroy and Mauffret, 1996). This passive continental margin related with the rifting episode of the Cayman Trough may extend until the Southern Peninsula of Haiti (Corbeau et al., 2016). The identification of the reflectors A", B" and V on seismic profiles may indicate that the CLIP extends until the southern part of the Jamaica Passage, at the north-eastern extreme of the Lower Nicaraguan Rise (Fig. 1.7) (from Corbeau et al., 2016)

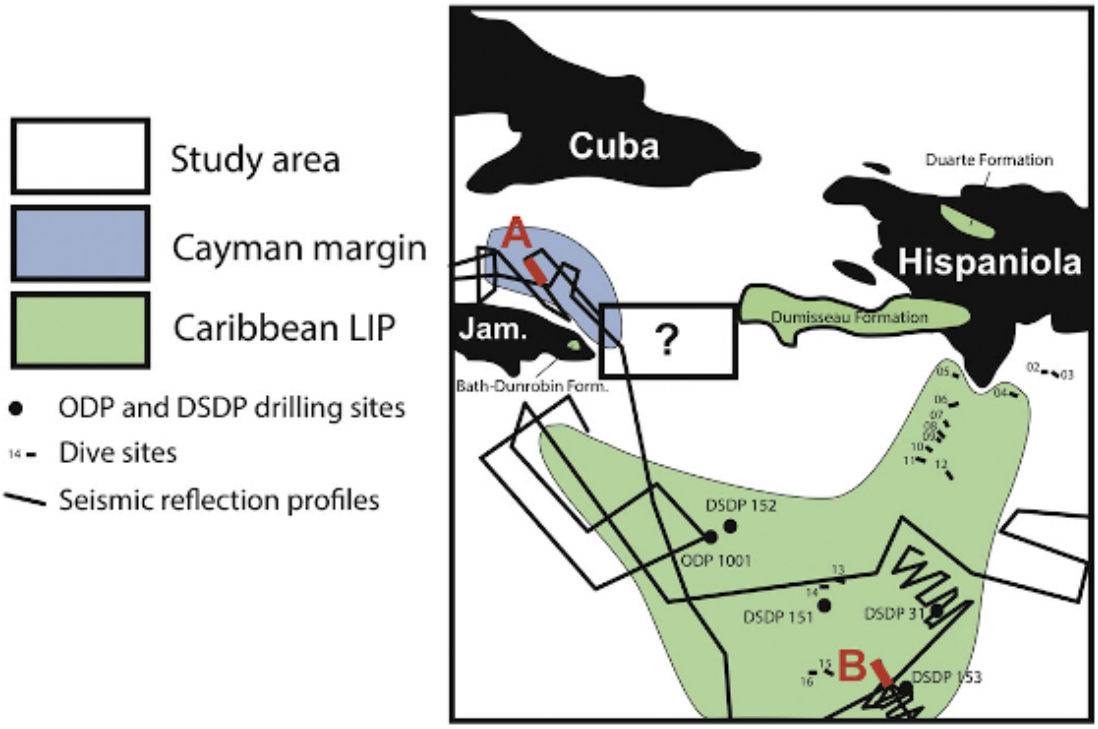

Figure 1.7 – Map of the extent of the Caribbean LIP and eastern Cayman Trough passive margin in the Jamaica passage (Corbeau et al., 2016)

1.2.4.3 Colombian Basin

A smooth, continuous and typically high amplitude acoustic basement characterizes most of the Colombian Basin. This reflector is comparable to the "smooth" horizon B" of the Venezuelan Basin. The smooth horizon B" in the Colombian Basin has never been sampled but may correspond to the top of basaltic sills interbedded with Upper Cretaceous sediments cored during Deep Sea Drilling Project (DSDP) Leg 15 (Sigurdsson et al., 1997). The crust in the Colombian Basin is relatively thin (approx. 8.5 km) where the acoustic basement is deepest and relatively thick (-15 km) beneath basement highs, such as the Mono Rise. The topography of the acoustic basement mirrors crustal thickness (Ewing et al., 1960; Houtz and Ludwig, 1977). A rough basement that shows many characteristics of oceanic crust underlines the southern parts of the Venezuela and Colombia basins (Mauffret and Leroy, 1997).

1.2.4.4 Nicaragua Rise

The Nicaragua Rise (NR) is adjacent to the Colombian Basin, but it remains unexplored with only a few wells drilled on its carbonate platforms. The NR comprises two main structural provinces: the Northern Nicaragua Rise and the Southern Nicaragua Rise.

The Nicaragua Rise has a highly variable relief, and it is the product of an extensive deformation, including faults, troughs, and young volcanoes. The reflectors B", A", and eM are of Campanian, Middle Eocene, and Early Miocene ages respectively (Mauffret and Leroy, 1997).

Northern Nicaragua Rise Tectonic activity modified the bathymetry of the northern Nicaraguan Rise and the Isthmus of Panama (Roth et al., 2000). Cunningham (1998), and references therein, places the initiation of tectonic activity and mini-basin formation in the Pedro Channel area at 16–11 Ma. Leroy and Mauffret (1996) related that activity to the change from a relatively extended period of quiescence on the northern Nicaraguan Rise to the uplift of Jamaica in the late middle Miocene. Carbonate banks that have remains of areas of neritic carbonate since the late Eocene drowned banks and reefs observed in Pedro Channel and Walton Basin formed an east-west barrier along the northern Nicaraguan Rise from the late Eocene to early Miocene. Some of the carbonate banks and barriers subsided and drowned as late as the late middle Miocene (Cunningham, 1998; Roth et al., 2000).

Lower Nicaragua Rise Ewing et al. (1960), Edgar et al. (1971) and Holcombe et al. (1990) regarded the Lower Nicaragua Rise as of oceanic origin, similar to the crust in the Colombian Basin to the south. Its character is different from the northern Nicaragua Rise (Holcombe et al., 1990). A recent left-lateral transtensional tectonics is observed in the lower Nicaragua Rise; the Colombia Basin might have a motion towards the north-east relative to the rise (Mauffret et al., 2001a). The Lower Nicaragua Rise probably formed in the Pacific Ocean during the Mesozoic (approx. 88 Ma) as an oceanic plateau associated with the Galápagos hot-spot (Sigurdsson et al., 1997) and seems to be part of the CLIP. In the results of the IODP site 1001, Sinton et al. (2000) reported an 81 ± 1 Ma age volcanic eruption (Campanian basalts). Additionally the K/T boundary, tektites and carbonates recovered in this hole date from the Middle/Upper Miocene boundary. Results at ODP site 1001 reveal that the rise originated over a volcanic edifice likely located near the paleo-equator, as suggested by the very shallow paleomagnetic inclinations obtained from the basalt and overlying sediments.

Ash layers register three episodes of volcanism: 1. A Paleocene-early Eocene explosive volcanism documented at site 998 and attributed to the Cayman Ridge; 2. A smaller peak in the Early Paleocene, attributed to the Central American arc and 3. A brief episode in mid-Campanian time, perhaps associated with the activity of central

volcanoes on the Caribbean Oceanic Plateau.

Boundaries The Hess Escarpment delimits the southern boundary of the Nicaragua Rise. Burke (1988) and Burke et al. (1984) interpreted the Hess Escarpment as a left-lateral fault boundary of the Caribbean plate, active during the Campanian (approx. 80 Ma). A diffuse zone of rifting and related volcanism between the Hess Escarpment and the Pedro fracture zone was active since the Miocene producing intraplate deformation. The base of the escarpment began between horizons B" and A", based on the occurrence of a sediment-filled, faulted half-graben at the base of the escarpment. 'The demise of carbonate neritic banks in the northern part of Pedro Channel and the central part of Walton Basin led to the observed modern configuration of shallow carbonate banks segmented by north-south oriented channels' (Roth et al., 2000, and references therein).

Hess Escarpment Bowland (1993) interpreted the Hess Escarpment to be a transcurrent fault. Schwindrofska et al. (2016) suggested two contradictory origins for the Hess Escarpment: in the first one, the escarpment was part of the continental Chortis Block whereas in the second one volcanic rocks of the escarpment are related to the CLIP. Unlike the proposition that the Hess Escarpment is part of the continental Chortis Block, results show that the structure is of volcanic origin and most likely also belongs to the CLIP (Schwindrofska et al., 2016). Its morphology also confirms the volcanic nature. The Hess Escarpment represents a significant fault zone but, including the area north of the Escarpment, it also consists of seamounts, guyots, and ridges often located on the vast plateau like structures (Schwindrofska et al., 2016). Erosional channels, which are the result of sediment transport from the lower Nicaragua Rise into the Colombian Basin characterize the escarpment.

1.2.4.5 Venezuelan Basin

Diebold et al. (1981) documented pre-existing thin oceanic crust in the Venezuelan Basin. Diebold (2009), and references therein, also indicated that dozens of volcanic edifices marked the Venezuela Basin (Fig. 1.8) and associated them to the final phase of volcanism. They interpreted the seamounts in the Venezuela Basin as channels for the primary upper volcanic sequence.

1.2.4.6 Beata Ridge

It is generally accepted that the Beata Ridge is part of the CLIP. Schwindrofska et al. (2016) attributed an age between 94 to 86 Ma to the Beata Ridge. The Beata plateau is a marginal unit of the Beata Ridge, where Mauffret and Leroy (1997) documented active transpressional deformation. The geochemical data show that the Beata Ridge has a composition typical for the CLIP (Schwindrofska et al., 2016).

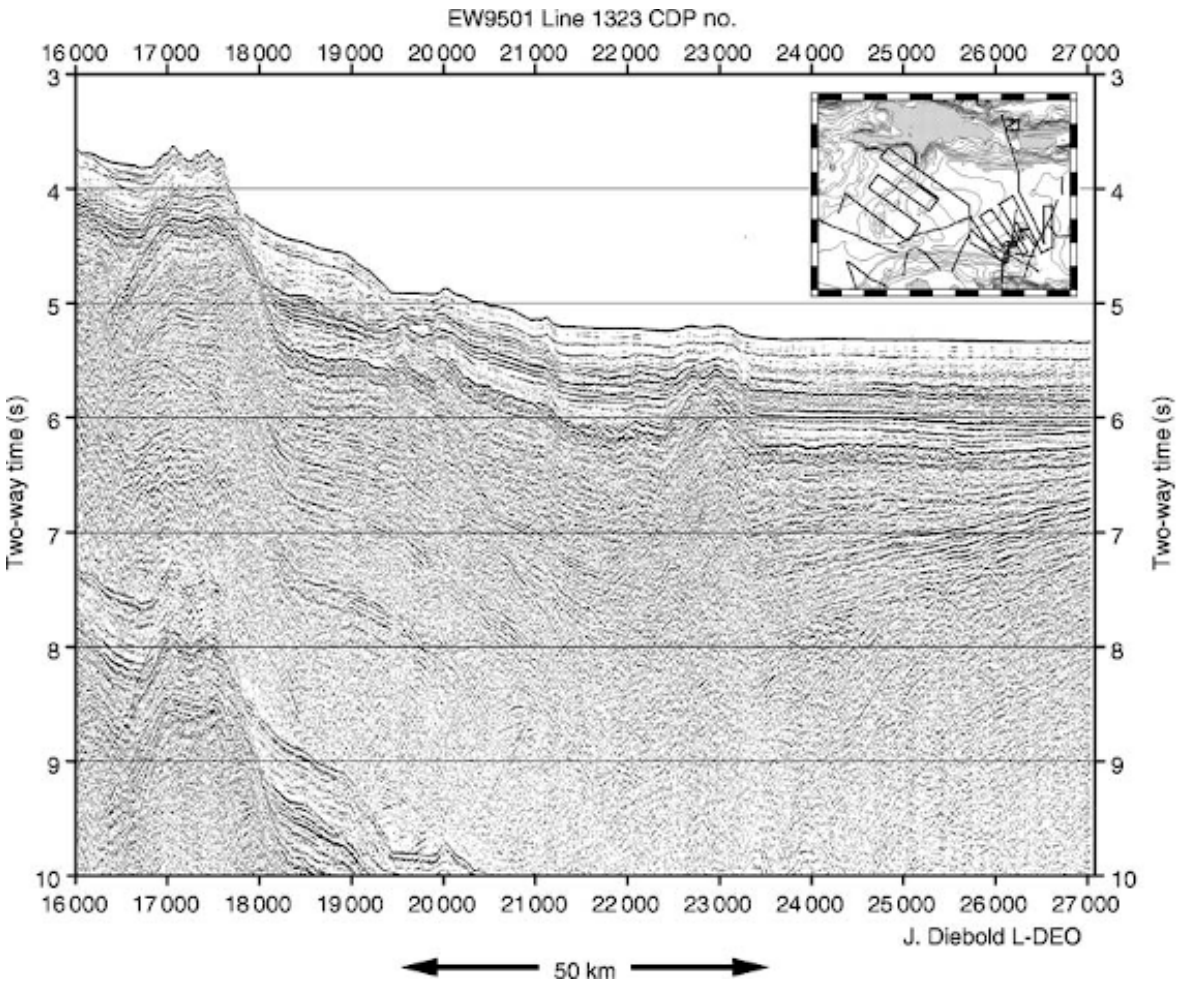

Figure 1.8 – Unmigrated stacked seismic section on the Beata Ridge (Diebold, 2009)

Limits The central part of Hispaniola along a transverse NE alignment collides with the northern part of Beata Ridge, which constitutes a morpho-structural limit (Núñez et al., 2016). The western flank of the Beata Ridge looks undeformed in the sediments, while the eastern flank looks deformed. Granja-Bruña et al. (2014) defines the northern Beata Ridge as a sequence of asymmetrically uplifted and faulted blocks of oceanic crust. Diebold (2009) identified on the eastern flank of the Beata Ridge, "thrust faults superimposed upon a regional flexure resulting from extension" on seismic profiles. Such regional flexure presumably resulted from the extension that uplifted Beata Ridge and thinned the Haiti Basin (Mauffret and Leroy, 1997). It is unclear if compression preceded the extension or if it was the opposite (Diebold, 2009). Kerr et al. (1997a) interpreted evidence on land for deformation of the volcanic plateau and attributed it to plateau or arc collision.

Structure The bathymetry and decreasing thickness towards La Hispaniola strongly influenced the sedimentary layer in the Haiti sub-basin (e.g., Mauffret and Leroy, 1997). The upper mantle thickness is between 20 km and 24 km below the Beata Island (Núñez et al., 2016). Refraction data indicate that the crust is thin beneath the Haiti sub-basin. The upper part of the margin restricts the current compression (Mauffret

and Leroy, 1997). The upper crustal layer is a complex sequence, whose stratigraphy shows that the thickest part of the Caribbean volcanic plateau was experiencing east-west compressional deformation during the last stages of its emplacement (Diebold, 2009). Diebold (2009) identified Moho reflection over all seismic lines acquired over the Venezuela Basin in contrast with intense deformation of the observed along the flanks of Beata Ridge and less often identification of the Moho reflection, and where it was "practically imperceptible the middle and lower crust." The upper crust is thick under Beata Island, suggesting to some authors that it is a thinned continental or transitional crust (Núñez et al., 2016).

Origin The Beata Ridge is more probably an oceanic plateau, and the thick crust formed during the Cretaceous volcanic event is not the result of thickening during the compressional deformation (Leroy and Mauffret, 1996). The formation of the South Caribbean deformed belt and the uplift of its edges disturbed the initial topography of the Beata Ridge during the early Miocene (Leroy and Mauffret, 1996). Révillon et al. (2000) proposed an intrusive origin for the Beata Ridge, "consisting of a dike and sill complex built during three volcanic episodes at 55, 76 and 90 Ma". The arrival of the Sala y Gomez and Galápagos plume at the base of the lithosphere produced a melting episode at 90 Ma and 'potentially' at 76 Ma (Révillon et al., 2000). Lithospheric extension and thinning possibly initiated the 55 Ma episode (Révillon et al., 2000). A different hypothesis proposes that the oblique convergence of the Caribbean plate against the inactive Greater Antilles Island Arc originated the Beata Ridge (e.g., Granja-Bruña et al., 2014). Such oblique convergence resulted in the collision and impingement of the thickened crust of the Beata Ridge into southern Hispaniola Island (Granja-Bruña et al., 2014).

1.2.4.7 Aves Ridge

Some authors favour a no subduction model beneath the Aves volcanic arc because of the lack of evidence. The Aves volcanic arc probably formed after the collision located South of Yucatán (Mauffret et al., 2001a). The Aves Ridge is considered by others to be a remnant arc that precedes the Lesser Antilles arc (after. Bouysse, 1984). Drills at DSDP site 148 found nannofossils within volcano-clastics sediments of Campanian-Maastrichtian age 83–65 Ma together with radiolarians of possibly Paleocene age (Edgar, 1973). Although, the acoustic basement in the Aves Ridge is likely Middle Cretaceous age (Mauffret et al., 2001a). Although, petrological, trace element and isotopic constraints indicate that the granitoids have an oceanic crustal source and formed by melting of the lower arc, oceanic or oceanic plateau crust (Neill et al., 2011).

1.2.5 Caribbean volcanic province

Several thick volcanic plateaus separated by deep basins contrasting with thinner crust comprise the Caribbean volcanic province (Mauffret and Leroy, 1997). The observed sills and dipping horizons on seismic profiles contributed to identify volcanism (Mauffret and Leroy, 1997). Diebold (2009) reported two sequences in this plateau: the upper sequence that shows reflecting horizons and the lower sequence that does not exhibit any reflector. The reflector B" indicates the top of the Cretaceous volcanic flows. The DSDP Leg 15 and the ODP Leg 165 drilled the reflector B" (Sigurdsson et al., 1997).

In the Venezuelan Basin, the upper sequence extends beyond the limits of the lower sequence, appearing to flow onto the pre-existing thin oceanic crust (Diebold et al., 1981). The thickness and volume of the upper volcanic sequence decrease from 10 km or more near the summit of the Beata Ridge to zero to the South-east (Diebold, 2009). Despite the variable thickness and the ridges and domes documented on the lower sequence, its thickness is usually higher than that of the thin oceanic crust of the SE Venezuelan Basin. Diebold (2009) suggested that the upper volcanic sequence was not merely superimposed upon pre-existing oceanic crust and that the original crust must have been thickened by, and likely entrained within, the material forming the lower sequence.

Based on melting trends, Krawl (2014) proposed that composition samples from the CLIP implied a contribution from a more enriched source than a depleted source. The mantle source of the CLIP is heterogeneous at a length scale of $\sim 10^2$ to 10^3 km (Krawl, 2014).

1.2.5.1 Origin

The origin of the Caribbean volcanic plateau remains controversial (e.g., Diebold, 2009). Recent models propose that the CLIP originated at 2000–3000 km east of the modern Galápagos hotspot (Boschman et al., 2014) (see Fig. 1.9). Diebold et al. (1999) concluded that the lower sequence predates the upper, which well correlated with models for a plume-generated oceanic plateau (e.g., Farnetani et al., 1996; Kerr et al., 1997b). By analogy with results from ODP site 1001 samples (Sigurdsson et al., 1997), the inner sections of 'inflated flows' likely formed much of the massive basalts. These flows may reach tens of kilometres in length as a result of lava injection into preexisting, insulating, extrusives (Umino et al., 2006). On the other hand, dolerite sills and gabbros dominated on samples taken nearby with only occasional pillow basalts (Mauffret et al., 2001b; Révillon et al., 2000). This dichotomy suggests either a sampling scheme favouring a few competent sills, or a high degree of lateral heterogeneity in the CLIP, one in which transitions between flow-dominated emplacement and sill-dominated emplacement can take place within a short distance of much thicker sequences of flows (Diebold, 2009).

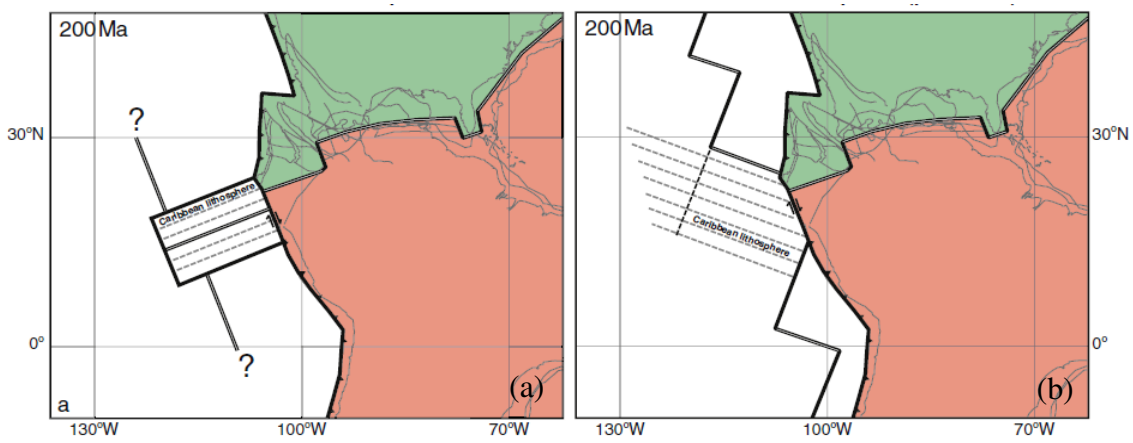

Figure 1.9 – Conceptual plate boundary configurations illustrating the origin of the Caribbean lithosphere at 200 Ma. Proto-Caribbean/Atlantic origin (a), Panthalassa origin (b) (from Boschman et al., 2014)

1.2.6 Island Arcs of the Caribbean

The intrusion of the oceanic Farallon plate into the Caribbean domain and the dispersion of the Gondwanan Block and the Laurentian Block resulted in the Caribbean volcanic arc (e.g., Villeneuve and Marcaillou, 2013).

1.2.6.1 Greater Antilles

The Jamaica Island, Cuba Island, La Hispaniola Island and Puerto Rico Island made up from west to east the Greater Antilles. In this section we synthesize the most relevant events in their geological history:

Cuba Cuban arc sequences include island-arc tholeiitic, calc-alkaline, and alkaline bimodal suites of volcanic and plutonic rocks. Remnants of Proto-Caribbean oceanic lithosphere occur as exhumed mélange bearing eclogite, blueschist, and garnet-amphibolite-facies tectonic blocks (oldest age ca. 120 Ma) within a serpentinite matrix intercalated with, or at the base of, the over-thrusted ophiolitic bodies (Iturralde-Vinent et al., 2016). The Cuban orogenic belt defined the leading edge of the Caribbean plate in late Cretaceous (Rosencrantz, 1996). During the Jurassic, the Pangea breakup and associated passive margin and the oceanic sedimentary layers and magmatic history are present in Cuba Island (Iturralde-Vinent et al., 2016; Woodring, 1928). Thick sequences of Jurassic-Cretaceous strata and interlayered basaltic rocks characterize the passive margin sequences found in the Guaniguanico terrane, allowing to relate the western Cuba with the Maya block passive margin, the Gulf of Mexico and the Bahamas Platform (Iturralde-Vinent et al., 2016). The collision and suturing of allochthonous Cuba terranes with the passive margin of the Bahamas platform followed the development of the Yucatán Basin (Pindell et al., 2005). Over the Cuba Island, Iturralde-Vinent et al. (2016) observed a sedimentary,

magmatic, and metamorphic evolution of an intra-oceanic Cretaceous-Paleogene ophiolite-arc complex. Iturralde-Vinent et al. (2016) proposed evidence of Paleogene "soft collision" and transfer of the NW Caribbean plate allochtonous (and Cuba) to the North American plate in Cuba Island (Iturralde-Vinent et al., 2016). In eastern Cuba, a new arc developed during Paleocene–middle Eocene times. The collision, which included overriding of the ophiolitic and arc units over both subducted and non-subducted passive margin sequences, also produced synorogenic basins and filled them, a process that continued until ca. 40 Ma. A local uplift and subsidence succeeded this fold belt to form late Eocene and Recent unconformable post-orogenic continental basins (Iturralde-Vinent et al., 2016).

Jamaica In the Jamaica Island, post-Jurassic arc and plateau rocks have been found in the igneous rocks of the Blue Mountains, Central, Above Rocks and Benbow Cretaceous Inliers and the Tertiary Wagwater Belt (Hastie, 2007) (Fig. 1.10). Hastie (2007) proposed that at 55 Ma Jamaica collided with the Yucatán peninsula and it was subsequently transported to the east due to the transtensional opening of the Cayman Trough. Corbeau et al. (2016) interpreted two crustal domains in the Jamaica passage: the first associated with the Eastern passive margin of the Cayman Trough and the second related with the CLIP, which may extend up to the north-eastern extreme of the Lower Nicaraguan Rise (Corbeau et al., 2016) (Fig. 1.7). Geochemical analysis confirmed the presence of a Cretaceous oceanic plateau section within the Blue Mountains and Cretaceous island-arc sequences, while in the Tertiary Wagwater Belt were discovered basalts and adakites (Hastie, 2007). Hastie (2007) proposed that the Bath-Dunrobin plateau lavas derive from a 90 Ma mantle plume which is distinct from the source regions for other Caribbean oceanic plateau lavas.

Hispaniola The north of the Hispaniola is colliding with the edge of the Bahamas Platform, as evidenced by offshore compressional structures (Calais et al., 2016, and references therein). The deformation observed might also be due to the transpression related to the collision of the Beata Ridge with its northern part and the left-lateral motion of the Enriquillo fault (Heubeck and Mann, 1991; Mercier de Lepinay et al., 1988).

1.2.6.2 Lesser Antilles

The Lesser Antilles form an archipelago with a North-South orientation that comprises several islands: Barbados, Carriacou, Dominica, Grenada, Grenadines, Guadeloupe, Martinique, Saint Lucia, Saint-Vincent, Tobago, and Trinidad. Along the northern Lesser Antilles arc, the North American and Caribbean plates converge in a roughly ENE direction, at a rate between 1.8 to 2 cm/yr (DeMets et al., 2000). Subduction of Atlantic seafloor chiefly absorbs this motion under the arc (Feuillet et al., 2002, and references therein.). Feuillet et al. (2002) interpret troughs orthogonal to the Lesser Antilles arc as a result from slip-partitioning and extension perpendicular to plate convergence and as result of the interaction between the

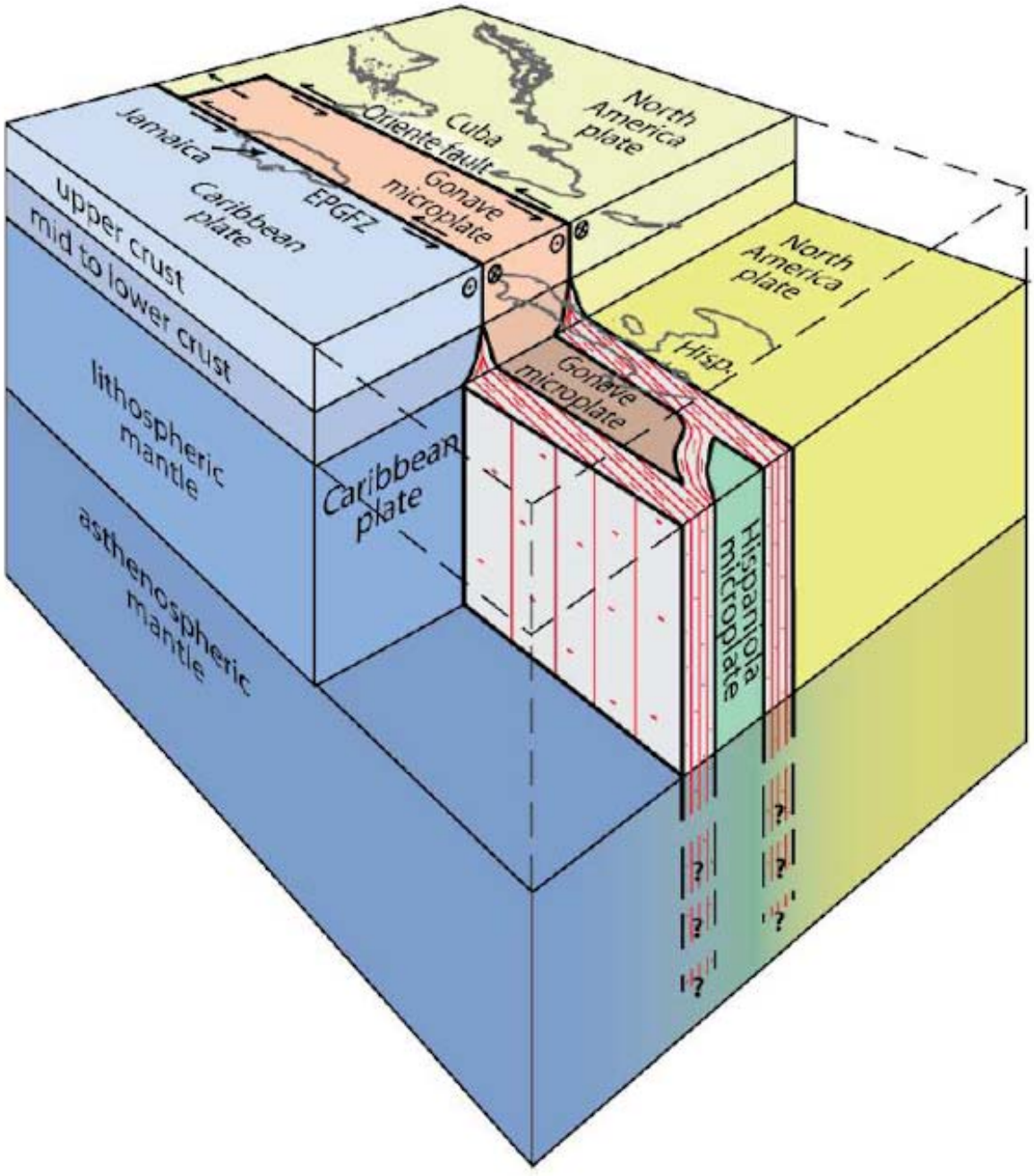

Figure 1.10 – Three-dimensional model for the lithosphere in the northern Caribbean. Fabric (red) has a vertical foliation and horizontal lineation and is localized at borders of microplates, whereas the interior of microplates has no fabric (from Benford, 2012)

Caribbean and North American plates. In the upper plate, arc-parallel and arc-perpendicular faults create graben and crosscut the volcanic arc in echelon pattern respectively. Those faults are the result of the left-lateral trench parallel component of the convergence which is accommodated above the subduction interface (Feuillet et al., 2002). From the Early Cretaceous to the Paleocene, an active island-arc occupied the northern part of the Lesser Antilles as far as the southern part of the Guadeloupe archipelago, representing the southeast termination of the Greater Antilles arc. This island-arc extended to the Aves swell sensu stricto, which was probably offset by a transform fault. The new evidence of an Early Cretaceous age for the La Desirade cherts interbedded in an island-arc complex supports the above hypothesis (Bouysse et al., 1983).

1.3 References

Acton, G. D., Galbrun, B., and King, J. W. (2000). 9. Paleolatitude of the Caribbean plate since the Late Cretaceous. *Atlantic*, 25:25.

Amato, J. M., Lawton, T. F., Mauel, D. J., Leggett, W. J., González-León, C. M., Farmer, G. L., and Wooden, J. L. (2009). Testing the Mojave-Sonora megashear hypothesis: Evidence from Paleoproterozoic igneous rocks and deformed Mesozoic strata in Sonora, Mexico. *Geology*, 37(1):75–78.

Anderson, T. H., Silver, L. T., Nourse, J., McKee, J., and Steiner, M. (2005). The Mojave-Sonora megashear-Field and analytical studies leading to the conception and evolution of the hypothesis. *SPECIAL PAPERS-GEOLOGICAL SOCIETY OF AMERICA*, 393:1.

Audemard, F. A. (2009). Key issues on the post-Mesozoic southern Caribbean plate boundary. *Geological Society, London, Special Publications*, 328(1):569–586.

Baquero, M., Grande, S., Urbani, F., Cordani, U., Hall, C., and Armstrong, R. (2015). New Evidence for Putumayo Crust in the Basement of the Falcon Basin and Guajira Peninsula, Northwestern Venezuela. In *AAPG Special Volumes*.

Benford, B. (2012). *Faulting and strain partitioning in Jamaica from GPS and structural data: Implications for Gonave and Hispaniola microplate kinematics, northern Caribbean*. PhD thesis, The University of Wisconsin-Madison.

Boschman, L. M., van Hinsbergen, D. J., Torsvik, T. H., Spakman, W., and Pindell, J. L. (2014). Kinematic reconstruction of the Caribbean region since the Early Jurassic. *Earth-Science Reviews*, 138:102–136.

Bouysse, P. (1984). The Lesser Antilles island-arc-structure and geodynamic evolution. *Initial Reports of the Deep Sea Drilling Project*, 78(AUG):83–103.

Bouysse, P., Pubellier, M., and Garcia, A. (2016). Structural Map of the Caribbean. In *35th International Geological Congress, Cape Town, South Africa*, number 5243 in -.

Bouysse, P., Schmidt-Effing, R., and Westercamp, D. (1983). La Desirade Island (Lesser Antilles) revisited: Lower Cretaceous radiolarian cherts and arguments against an ophiolitic origin for the basal complex. *Geology*, 11(4):244–247.

Bowin, C. O. (1968). Geophysical study of the Cayman Trough. *Journal of Geophysical Research*, 73(16):5159–5173.

Bowland, C. L. (1993). Depositional history of the western Colombian Basin, Caribbean Sea, revealed by seismic stratigraphy. *Geological Society of America Bulletin*, 105(10):1321–1345.

Burke, K. (1988). Tectonic evolution of the Caribbean. *Annual Review of Earth and Planetary Sciences*, 16(1):201–230.

Burke, K., Cooper, C., Dewey, J. F., Mann, P., and Pindell, J. L. (1984). Caribbean tectonics and relative plate motions. *Geological Society of America Memoirs*, 162:31–64.

Calais, E., Stephan, J., Beck, C., Carfantan, J.-C., Tardy, M., Thery, J., Olivet, J., Bouysse, P., Mercier de Lepinay, B., Tournon, J., et al. (1989). Évolution paléogéographique et structurale du domaine caraıbe du lias al'actuel: 14 étapes pour 3 grandes périodes. *CR Acad. Sci. Paris*, 309:1437–1444.

Calais, É., Symithe, S., de Lépinay, B. M., and Prépetit, C. (2016). Plate boundary segmentation in the northeastern Caribbean from geodetic measurements and Neogene geological observations. *Comptes Rendus Geoscience*, 348(1):42–51.

Cebull, S. and Shurbet, D. (1987). Mexican Volcanic Belt: an intraplate transform. *Geofísica International*, 26:1–14.

Christeson, G. L., Mann, P., Escalona, A., and Aitken, T. J. (2008). Crustal structure of the Caribbean–northeastern South America arc-continent collision zone. *Journal of Geophysical Research: Solid Earth*, 113(B8).

Christofferson, E. (1973). Linear magnetic anomalies in the Colombia Basin, central Caribbean Sea. *Geological Society of America Bulletin*, 84(10):3217–3230.

Corbeau, J., Rolandone, F., Leroy, S., de Lépinay, B. M., Meyer, B., Ellouz-Zimmermann, N., and Momplaisir, R. (2016). The northern Caribbean plate boundary in the Jamaica Passage: structure and seismic stratigraphy. *Tectonophysics*, 675:209–226.

Cunningham, A. (1998). Neogene evolution of the Pedro Channel carbonate system. *Northern Nicaragua Rise [Ph. D. thesis]: Houston, Texas, Rice University*.

DeMets, C., Jansma, P. E., Mattioli, G. S., Dixon, T. H., Farina, F., Bilham, R., Calais, E., and Mann, P. (2000). GPS geodetic constraints on Caribbean-North America plate motion. *Geophysical Research Letters*, 27(3):437–440.

Diebold, J. (2009). Submarine volcanic stratigraphy and the Caribbean LIP's formational environment. *Geological Society, London, Special Publications*, 328(1):799–808.

Diebold, J., Driscoll, N., et al. (1999). New insights on the formation of the Caribbean basalt province revealed by multichannel seismic images of volcanic structures in the Venezuelan Basin. *Sedimentary Basins of the World*, 4:561–589.

Diebold, J., Stoffa, P., Buhl, P., and Truchan, M. (1981). Venezuela Basin crustal structure. *Journal of Geophysical Research: Solid Earth*, 86:7901–7923.

Dillon, W. P., Vedder, J., and Graf, R. (1972). Structural profile of the northwestern Caribbean. *Earth and Planetary Science Letters*, 17(1):175–180.

Dillon, W. P. and Vedder, J. G. (1973). Structure and development of the continental margin of British Honduras. *Geological Society of America Bulletin*, 84(8):2713–2732.

Duncan, R. and Hargraves, R. (1984). Plate-tectonic evolution of the Caribbean region in the mantle reference frame. *The Caribbean-South American plate boundary and regional tectonics*.

Edgar, N. T. (1973). Site 148. *Initial Reports of the Deep Sea Drilling Project*, 15:217. Affiliation (analytic): Scripps Inst. Oceanogr., Deep Sea Drilling Project, La Jolla, CA.

Edgar, N. T., Ewing, J. I., and Hennion, J. (1971). Seismic refraction and reflection in Caribbean Sea. *AAPG Bulletin*, 55(6):833–870.

Escalona, A. and Mann, P. (2011). Tectonics, basin subsidence mechanisms, and paleogeography of the Caribbean-South American plate boundary zone. *Marine and Petroleum Geology*, 28(1):8–39.

Ewing, J., Antoine, J., and Ewing, M. (1960). Geophysical measurements in the western Caribbean Sea and in the Gulf of Mexico. *Journal of Geophysical Research*, 65(12):4087–4126.

Farnetani, C. G., Richards, M. A., and Ghiorso, M. S. (1996). Petrological models of magma evolution and deep crustal structure beneath hotspots and flood basalt provinces. *Earth and Planetary Science Letters*, 143(1-4):81–94.

Feuillet, N., Manighetti, I., Tapponnier, P., and Jacques, E. (2002). Arc parallel extension and localization of volcanic complexes in Guadeloupe, Lesser Antilles. *Journal of Geophysical Research: Solid Earth*, 107(B12).

Giunta, G. and Orioli, S. (2011). The Caribbean plate evolution: trying to resolve a very complicated tectonic puzzle. In *New Frontiers in Tectonic Research-General Problems, Sedimentary Basins and Island Arcs*. InTech.

Granja-Bruña, J., Carbó-Gorosabel, A., Estrada, P. L., Muñoz-Martín, A., Ten Brink, U., Ballesteros, M. G., Druet, M., and Pazos, A. (2014). Morphostructure at the junction between the Beata ridge and the Greater Antilles island arc (offshore Hispaniola southern slope). *Tectonophysics*, 618:138–163.

Hastie, A. R. (2007). *Tectonomagmatic evolution of the Caribbean plate: Insights from igneous rocks on Jamaica*. Cardiff University (United Kingdom).

Heubeck, C. and Mann, P. (1991). Geologic evaluation of plate kinematic models for the North American-Caribbean plate boundary zone. *Tectonophysics*, 191(1-2):1–26.

Holcombe, T. L., Ladd, J. W., Westbrook, G., Edgar, N. T., and Bowland, C. L. (1990). Caribbean marine geology; ridges and basins of the plate interior. *The Caribbean Region, The Geology of North America, vol. H, Geological Society of America*, pages 231–260.

Houtz, R. E. and Ludwig, W. J. (1977). Structure of Colombia Basin, Caribbean Sea, from profiler-sonobuoy measurements. *Journal of Geophysical Research*, 82(30):4861–4867.

Iturralde-Vinent, M., García-Casco, A., Rojas-Agramonte, Y., Proenza, J., Murphy, J., and Stern, R. (2016). The geology of Cuba: A brief overview and synthesis. *GSA Today*, 26(10):4–10.

Kerr, A. C., Marriner, G., Tarney, J., Nivia, A., Saunders, A., Thirlwall, M., and Sinton, C. (1997a). Cretaceous Basaltic Terranes in western Columbia: elemental, chronological and Sr–Nd isotopic constraints on petrogenesis. *Journal of petrology*, 38(6):677–702.

Kerr, A. C., Tarney, J., Marriner, G. F., Nivia, A., and Saunders, A. D. (1997b). The Caribbean-Colombian Cretaceous igneous province: the internal anatomy of an oceanic plateau. *Large igneous provinces: Continental, oceanic, and planetary flood volcanism*, pages 123–144.

Krawl, K. A. (2014). *A petrogenetic model for the Caribbean Large Igneous Province*. PhD thesis, Oregon State University.

Ladd, J. W. and Watkins, J. S. (1980). Seismic stratigraphy of the western Venezuela Basin. *Marine Geology*, 35(1-3):21–41.

Ladd, J. W., Westbrook, G. K., Buhl, P., and Bangs, N. (1990). Wide aperture seismic reflection profiles across Barbados ridge complex. *Proceedings of the Ocean Drilling program, Scientific resutls*, 110.

Leroy, S. and Mauffret, A. (1996). Intraplate deformation in the Caribbean region. *Journal of Geodynamics*, 21(1):113–122.

Leroy, S., Mauffret, A., Patriat, P., and de Lépinay, B. M. (2000). An alternative interpretation of the Cayman trough evolution from a reidentification of magnetic anomalies. *Geophysical Journal International*, 141(3):539–557.

Lu, R. and McMillen, K. (1982). Multichannel seismic survey of the Colombia Basin and adjacent margins. In *Studies in Continental Margin Geology*, volume 34, pages 395–410. American Association of Petroleum Geologists Tulsa, Okla.

Lugo, J. and Mann, P. (1995). Jurassic-Eocene tectonic evolution of Maracaibo basin, Venezuela.

Mann, P., Escalona, A., and Castillo, M. V. (2006). Regional geologic and tectonic setting of the Maracaibo supergiant basin, western Venezuela. *AAPG bulletin*, 90(4):445–477.

Mann, P., Taylor, F., Edwards, R. L., and Ku, T.-L. (1995). Actively evolving microplate formation by oblique collision and sideways motion along strike-slip faults: An example from the northeastern Caribbean plate margin. *Tectonophysics*, 246(1):1–69.

Mauffret, A. and Leroy, S. (1997). Seismic stratigraphy and structure of the Caribbean igneous province. *Tectonophysics*, 283(1):61–104.

Mauffret, A., Leroy, S., d'Acremont, E., Maillard, A., de Lepinay, B. M., Dos Reis, A. T., Miller, N., Nercessian, A., Perez-Vega, R., and Perez, D. (2001a). Une coupe de la province volcanique Caraibe: premiers resultats de la campagne sismique Casis 2. *Comptes Rendus de l'Academie des Sciences-Series IIA-Earth and Planetary Science*, 333(10):659–667.

Mauffret, A., Leroy, S., Vila, J.-M., Hallot, E., De Lépinay, B. M., and Duncan, R. A. (2001b). Prolonged magmatic and tectonic development of the Caribbean Igneous Province revealed by a diving submersible survey. *Marine Geophysical Researches*, 22(1):17–45.

Mercier de Lepinay, B., Mauffret, A., Jany, I., Bouysse, P., Mascle, A., Renard, V., Stéphan, J.-F., and Hernández, E. (1988). Une collision oblique sur la bordure nord-caraïbe à la jonction entre la ride de Beata et la fosse de Muertos. *Comptes rendus de l'Académie des sciences. Série 2, Mécanique, Physique, Chimie, Sciences de l'univers, Sciences de la Terre*, 307(10):1289–1296.

Meschede, M. and Frisch, W. (1998). A plate-tectonic model for the Mesozoic and Early Cenozoic history of the Caribbean plate. *Tectonophysics*, 296(3):269–291.

Neill, I., Kerr, A. C., Hastie, A. R., Stanek, K.-P., and Millar, I. L. (2011). Origin of the Aves Ridge and Dutch–Venezuelan Antilles: interaction of the Cretaceous 'Great Arc'and Caribbean–Colombian Oceanic Plateau? *Journal of the Geological Society*, 168(2):333–348.

Nerlich, R., Clark, S. R., and Bunge, H.-P. (2014). Reconstructing the link between the Galapagos hotspot and the Caribbean Plateau. *GeoResJ*, 1:1–7.

Núñez, D., Córdoba, D., Cotilla, M. O., and Pazos, A. (2016). Modeling the Crust and Upper Mantle in Northern Beata Ridge (CARIBE NORTE Project). *Pure and Applied Geophysics*, 173(5):1639–1661.

Pérez-Díaz, L. and Eagles, G. (2014). Constraining South Atlantic growth with seafloor spreading data. *Tectonics*, 33(9):1848–1873.

Pérez-Díaz, L. and Eagles, G. (2017). South Atlantic paleobathymetry since early Cretaceous. *Scientific reports*, 7(1):11819.

Pindell, J. and Dewey, J. F. (1982). Permo-Triassic reconstruction of western Pangea and the evolution of the Gulf of Mexico/Caribbean region. *Tectonics*, 1(2):179–211.

Pindell, J., Kennan, L., Maresch, W. V., Stanek, K.-P., Draper, G., and Higgs, R. (2005). Plate-kinematics and crustal dynamics of circum-Caribbean arc-continent interactions: Tectonic controls on basin development in Proto-Caribbean margins. *Geological Society of America Special Papers*, 394:7–52.

Pindell, J. L. and Barrett, S. F. (1990). Geological evolution of the Caribbean region: a plate tectonic perspective. *The Caribbean region: Boulder, Colorado, Geological Society of America, Geology of North America, v. H*, pages 405–432.

Pubellier, M., Mauffret, A., Leroy, S., Vila, J. M., and Amilcar, H. (2000). Plate boundary readjustment in oblique convergence: Example of the Neogene of Hispaniola, Greater Antilles. *Tectonics*, 19(4):630–648.

Révillon, S., Hallot, E., Arndt, N., Chauvel, C., and Duncan, R. (2000). A complex history for the Caribbean Plateau: petrology, geochemistry, and geochronology of the Beata Ridge, South Hispaniola. *The Journal of Geology*, 108(6):641–661.

Rosencrantz, E. (1990). Structure and tectonics of the Yucatan Basin, Caribbean Sea, as determined from seismic reflection studies. *Tectonics*, 9(5):1037–1059.

Rosencrantz, E. (1996). Basement structure and tectonics in the Yucatan basin. *Ofiolitas y Arcos Volcánicos de Cuba. Miami, USA, IGCP Project*, 364:36–47.

Rosencrantz, E., Ross, M. I., and Sclater, J. G. (1988). Age and spreading history of the Cayman Trough as determined from depth, heat flow, and magnetic anomalies. *Journal of Geophysical Research: Solid Earth*, 93(B3):2141–2157.

Ross, M. I. and Scotese, C. R. (1988). A hierarchical tectonic model of the Gulf of Mexico and Caribbean region. *Tectonophysics*, 155(1-4):139–168.

Roth, J. M., Droxler, A. W., Kameo, K., et al. (2000). The Caribbean carbonate crash at the middle to late Miocene transition: linkage to the establishment of the modern global ocean conveyor. In *Proceedings of the Ocean Drilling Program, Scientific Results*, volume 165, pages 249–273. Ocean Drilling Program College Station, TX.

Sabaka, T. J., Olsen, N., and Purucker, M. E. (2004). Extending comprehensive models of the Earth's magnetic field with Ørsted and CHAMP data. *Geophysical Journal International*, 159(2):521–547.

Schlaphorst, D., Kendall, J.-M., Baptie, B., Latchman, J. L., and Tait, S. (2017). Gaps, tears and seismic anisotropy around the subducting slabs of the Antilles. *Tectonophysics*, 698:65–78.

Schwindrofska, A., Hoernle, K., van den Bogaard, P., Hauff, F., and Werner, R. (2016). Submarine structures of the Caribbean Large Igneous Province: Age and Geochemistry of the Beata Ridge and Hess Escarpment. In *2nd European Minerogical Conference, Rimini, Italy*.

Sigurdsson, H., Leckie, R., Acton, G., and et al (1997). *Proceedings of the Ocean Drilling Program. A.: Initial Reports: Vol. 165*. Ocean Drilling Program, Texas A&M University.

Sinton, C. W., Sigurdsson, H., and Duncan, R. A. (2000). Major element oxides and 40Ar/39Ar plateau and isochron ages of ODP Hole 165-1001A. *Proceedings of the Ocean Drilling Program, Scientific Results, College Station, TX*, 165:1–4.

Stéphan, J., Mercier de Lepinay, B., Calais, E., Tardy, M., Beck, C., Carfantan, J.-C., Olivet, J., Vila, J., Bouysse, P., Mauffret, A., et al. (1990). Paleogeodynamic maps of the Caribbean: 14 steps from Lias to Present. *Bull. Soc. Géol. Fr.*, 6(8):6–919.

Symithe, S., Calais, E., Chabalier, J., Robertson, R., and Higgins, M. (2015). Current block motions and strain accumulation on active faults in the Caribbean. *Journal of Geophysical Research: Solid Earth*, 120(5):3748–3774.

ten Brink, U. S., Coleman, D. F., and Dillon, W. P. (2002). The nature of the crust under Cayman Trough from gravity. *Marine and Petroleum Geology*, 19(8):971–987.

Umino, S., Nonaka, M., and Kauahikaua, J. (2006). Emplacement of subaerial pahoehoe lava sheet flows into water: 1990 Kūpaianaha flow of Kilauea volcano at Kaimū Bay, Hawaii. *Bulletin of Volcanology*, 69(2):125–139.

Villeneuve, M. and Marcaillou, B. (2013). Pre-Mesozoic origin and paleogeography of blocks in the Caribbean, South Appalachian and West African domains and their impact on the post "variscan" evolution. *Bulletin de la Société Géologique de France*, 184(1-2):5–20.

Woodring, W. P. (1928). *Miocene Mollusks from Bowden, Jamaica: Pelecypods and Scaphopods*. The Carnegie Institution of Washington.

Chapter 2

Marine magnetic anomaly map of the Caribbean and the Gulf of Mexico

> Indian America: "The first men who came (during the Discovery of America), among them Columbus, had the desire of finding here what was not here, what they brought in their minds. The most glaring and visible fact is the fact of calling Indians to the inhabitants of this continent, they were not Indians, Indians are the people of India. However, the first mistake was to think that this was Asia, Columbus thought that he had reached the coast of Asia and that therefore those beings who were there were Indians, that is to say, they belonged to India, they were Asiatic. Moreover, it was because Columbus did not know that he had found a new continent, and he would not know it until much later"
>
> — ARTURO USLAR PIETRI

Abstract

The Caribbean plate and the Gulf of Mexico remain partly controversial concerning their origin and age. Magnetic anomalies are the ideal tool to explore the oceanic crust and decipher its age. We compiled available marine magnetic tracks to retain the short wavelengths of the magnetic signal and hence, to build a suitable dataset for plate reconstructions and perform a crustal magnetic interpretation.

The thick sediments in the basins and the proximity of the magnetic Equator made this goal a daunting challenge. Magnetic anomalies produced near the Equator result in low amplitudes approaching the noise level (e.g., Horner-Johnson and Gordon, 2003) that might equally be affected by the Equatorial Electrojet (EEJ) current, depending on the daytime of the acquisition. The EEJ is an ionospheric current that circulates eastward which peak-to-peak amplitude is varying between 20 to 30 nT along the geomagnetic dip equator, and that

depends on the longitude, local time, season, and solar flux (Thébault et al., 2017). The EEJ estimation is still under discussion (e.g., Benaissa et al., 2017; Hamid et al., 2017) and beyond the scope of this research.

In this chapter, we present the methodology used to derive the magnetic anomalies from total magnetic field measurements over the Caribbean region and the Gulf of Mexico and the encountered obstacles during the compilation process. To assess and to validate our results, we performed a qualitative and quantitative comparison with the MF7 (Maus, 2010), GRIMM-L model (Lesur et al., 2013), the North American Magnetic Anomaly map (NAMAG) (Bankey et al., 2002) and the World Digital Anomaly Map (WDMAM v.2.0) (Dyment et al., 2015; Lesur et al., 2016) respectively. Both analyses allow us to be confident in the obtained results.

Furthermore, we will revisit the magnetic anomalies of the Caribbean region, which will allow us to provide an interpretation of the most prominent geological features that strike the study area.

2.1 Introduction

During the last decades, the increasing spatial and temporal resolution of the satellite measurements of the Earth's magnetic field allowed denser measurements (e.g., Friis-Christensen et al., 2006; Reigber et al., 1999). The density and the global coverage of the satellite measurements facilitated the mapping of lithospheric structures and revealed them with further details (e.g., Olsen et al., 2017; Thébault et al., 2016). Therefore, satellite long-wavelength magnetic anomalies are an adequate data for imaging the lithosphere (e.g., Purucker and Dyment, 2000).

However, for plate tectonic reconstruction and regional geophysical interpretation, it is necessary to access the short-wavelength magnetic anomalies. They provide information related to the shallowest lithospheric structures (e.g., Thébault et al., 2010), particularly in marine areas where the extrusive basaltic layer has the largest contribution (e.g., Dyment and Arkani-Hamed, 1995; Gee and Kent, 2007).

In addition, marine magnetic anomalies contain information related to the fluctuations of the magnetic field intensity (e.g., Cande and Kent, 1992; Granot et al., 2012). Hence, it is necessary to have a dataset that covers the entire wavelength spectrum of the magnetic lithosphere. At the altitude of the SWARM satellite measurements, the magnetic anomalies represent 0.01% of the field strength (Thébault et al., 2017). Consequently, near-surface or near-bottom data are more suitable to recover short-wavelength marine magnetic anomalies. Nevertheless, their compilation has to be exhaustive and detailed, mainly because of the intrinsic difficulties of the data acquisition and pre-processing. A proper compilation will result in a better magnetic anomaly map and therefore a more accurate interpretation.

Many efforts have been made to integrate near-surface and satellite data and to produce global (e.g., Dyment et al., 2015) and regional maps (e.g., Bankey et al., 2002; Golynsky et al., 2001). Nevertheless, problems remain in those areas where the marine track coverage is weak, or where the navigation system pre-dates the Global Positioning System.

Within the Caribbean region and the Gulf of Mexico (GoM) (see Fig. 2.1) the acquisition of magnetic data spans almost 50 years, which constitutes part of the difficulty to compile an accurate marine magnetic map (see Fig. 2.2). Therefore, an adequate magnetic processing is necessary in this area to discard discrepancies and identify errors related to navigation or malfunctioning of the instruments, among others, in a way similar Quesnel et al. (2009) considered it on a global scale.

The importance of identifying and correcting or discarding problematic surveys lies on the fact that those will induce artifacts into the compilation. The levelling procedure does part of the correction of the marine track lines, but often it is an empirical procedure which criteria to retain or remove a survey remain subjective.

Therefore, in this chapter, we envisage shedding light upon the lithospheric structures on the Caribbean plate and the Gulf of Mexico, revisiting magnetic anomalies in an area that still remains controversial (e.g., Bird et al., 1993; Bouysse, 1988; Christeson et al., 2008; Christofferson, 1973; Ghosh et al., 1984; Guevara et al., 2013).

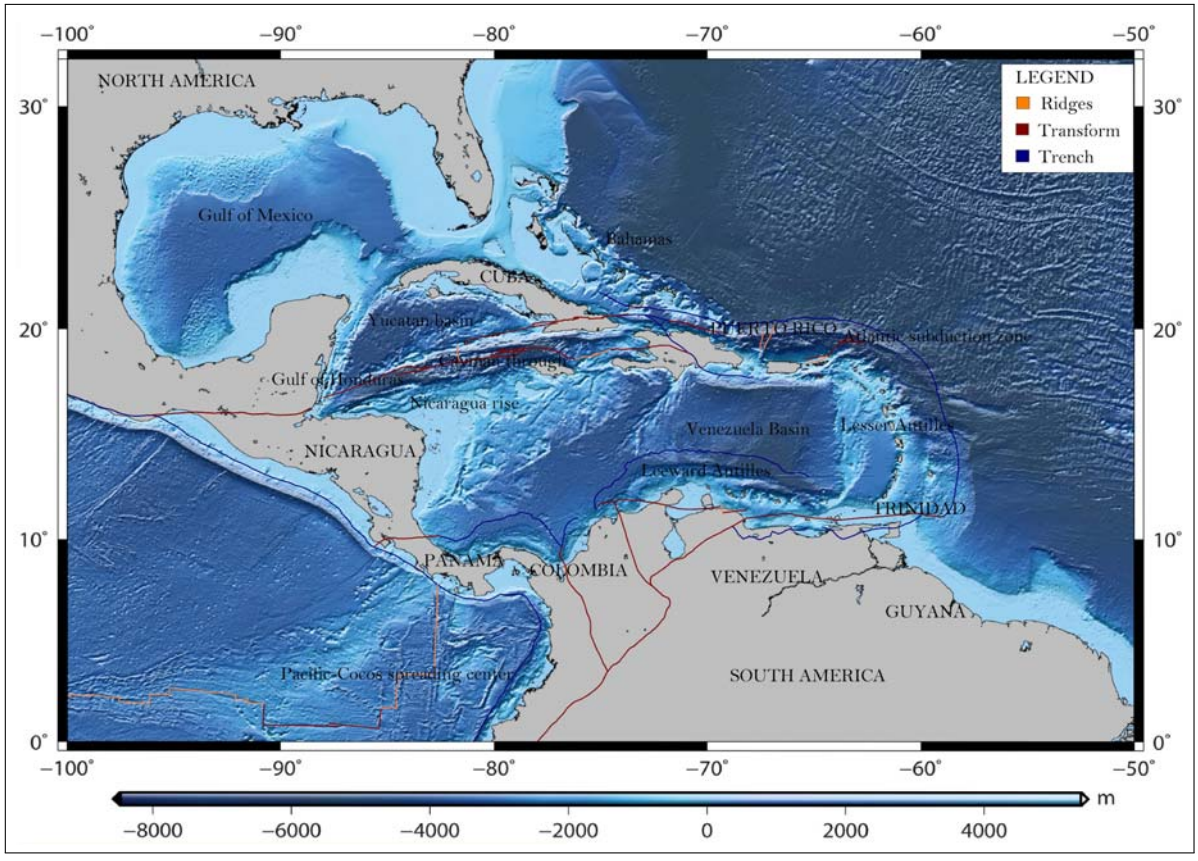

Figure 2.1 – Main geographical features on the Caribbean region

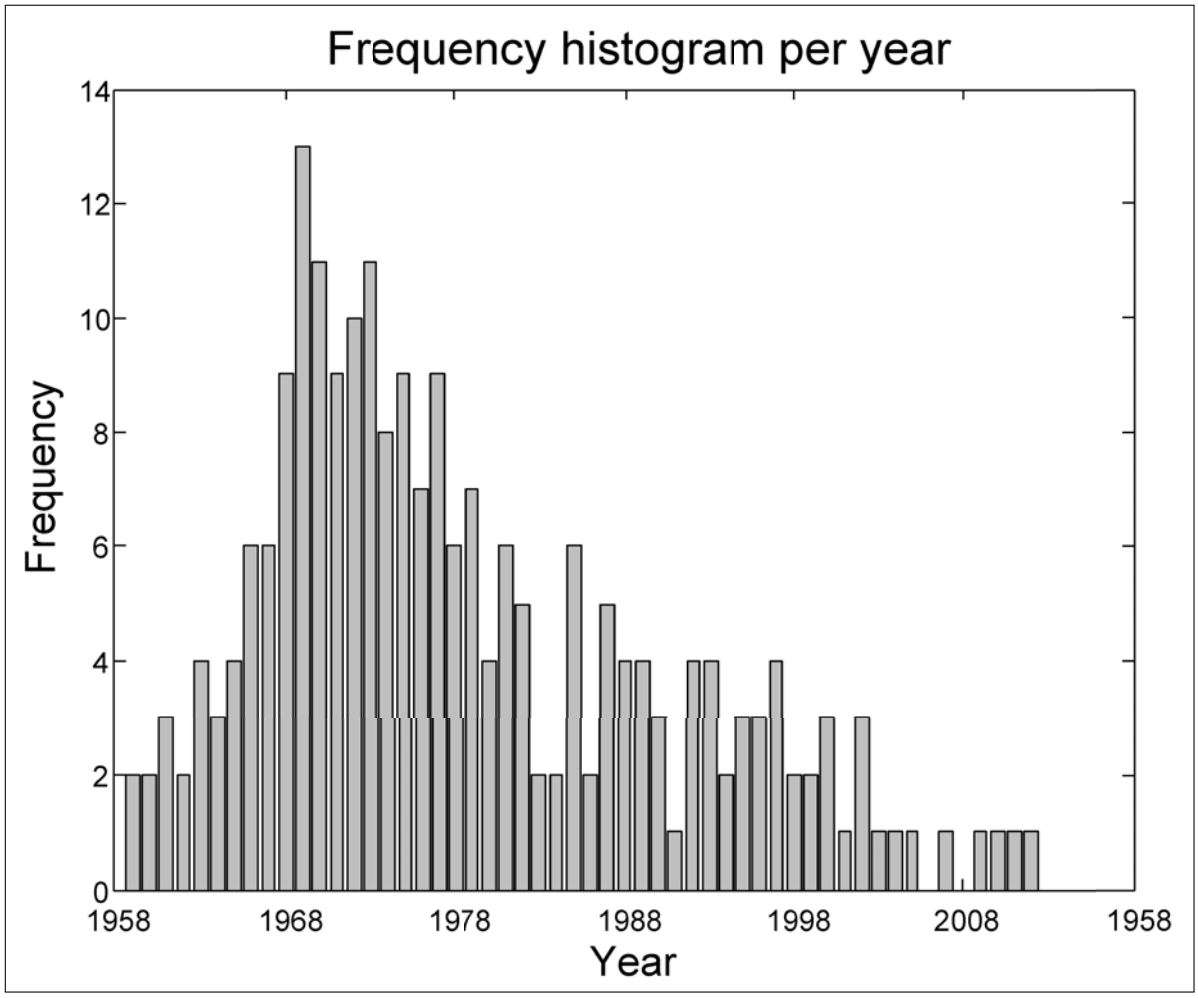

Figure 2.2 – Histogram of surveys per year

2.2 Objectives

- To exploit the available marine magnetic surveys to build a regional magnetic anomaly map of the Caribbean plate and surroundings;
- To obtain a better-resolved model of the magnetization contrasts, decipher lithospheric structures and unravel the plate tectonic evolution of the area;
- Delineate the tectonic boundaries that are visible from magnetic data;
- To delimitate the oceanic and continental tectonic blocks from the attributes of the potential field data;
- To produce an integrated interpretation from potential field data.

2.3 Theory

2.3.1 Main internal magnetic field

The fluid Earth's core is the primary contributor to the Earth's magnetic field intensity. Different spherical harmonics models of the internal Earth's magnetic field have been proposed from the launching of the first satellite mission with geomagnetic field measurement purposes, since more than half a century ago (e.g., Zmuda, 1969) (see Fig. 2.3).

More accurate satellite positioning and the possibility of collecting satellite, ground and observatory data allows to count on global models of the Earth's magnetic field and its secular variation with more precision in space and time (e.g., Hulot et al., 2002; Olsen et al., 2006).

The comprehensive model CM4 derived from ground-based observatories and satellite mapping missions and extend in time from 1960 to 2002.5 with knot spacing equal to 2.5 yr (Sabaka et al., 2004). The eleventh generation of the International Geomagnetic Reference Field (IGRF-11) extends from 1900 A.D. until 2009 and derives from observations collected by satellites, at magnetic observatories, and during magnetic surveys (Finlay et al., 2010).

This model provides the main magnetic field model for the epoch 2010, and its secular variation prediction is from 2010 to 2015 (Finlay et al., 2010).

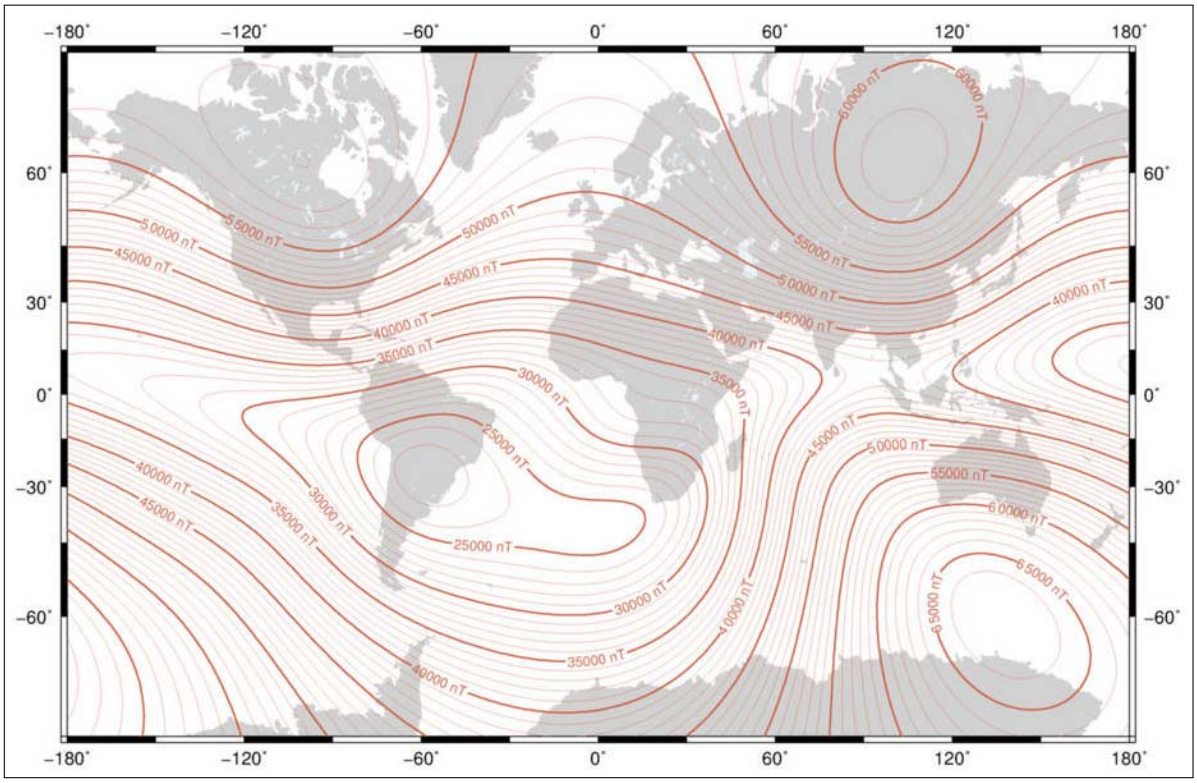

Figure 2.3 – Total magnetic field intensity IGRF12 (http://www.gfz-potsdam.de)

2.3.2 Magnetic anomalies

Magnetic anomalies have been widely used to explore the crust regarding the age, depth and extension of the magnetic sources (e.g., Bowin, 1968). Magnetic anomalies measure the magnetic contribution of the Earth's lithosphere and result from separating the Earth's core magnetic field of the total magnetic field (e.g., Purucker and Whaler, 2007).

The standard method to obtain the total magnetic anomaly comprises the removal of the temporal variation of the magnetic field, removal of the contribution of the main magnetic field, levelling of all data, filtering, gridding, and magnetic mapping (e.g., Luyendyk, 1997; Reeves, 2005). Usually, levelling process uses crossover data from tie-lines to correct the misfit over crossing points. Aeromagnetism frequently employs this technique, in which tie-lines are nearly perpendicular to the flight lines of each survey (e.g., Reeves, 2005; Urquhart, 1988). Ishihara (2015) and Beamish et al. (2015) proposed additional levelling methods for marine and aeromagnetic surveys without using crossover data or tie-lines.

For geophysical exploration, the geological bodies that lay within the crust produced a quasi-steady magnetic contribution (Voorhies, 1998); even though a magnetic contribution of the upper mantle is still under discussion (Ferré et al., 2014; Friedman, 2015). In average, the wavelength for the lithospheric magnetic field ranges to few meters until hundreds of kilometres. Wavelength estimation of the lithospheric magnetic field depends on the bottom depth of the magnetic lithosphere, i.e., the maximum depth of the magnetic sources.

Marine magnetic anomalies (see Fig. 2.4) depend on factors such as the location of creation and observation respectively; the age and the spreading rate and in the case of seafloor magnetic anomalies, the thickness and depth of the magnetic layer (e.g., Vine and Matthews, 1963).

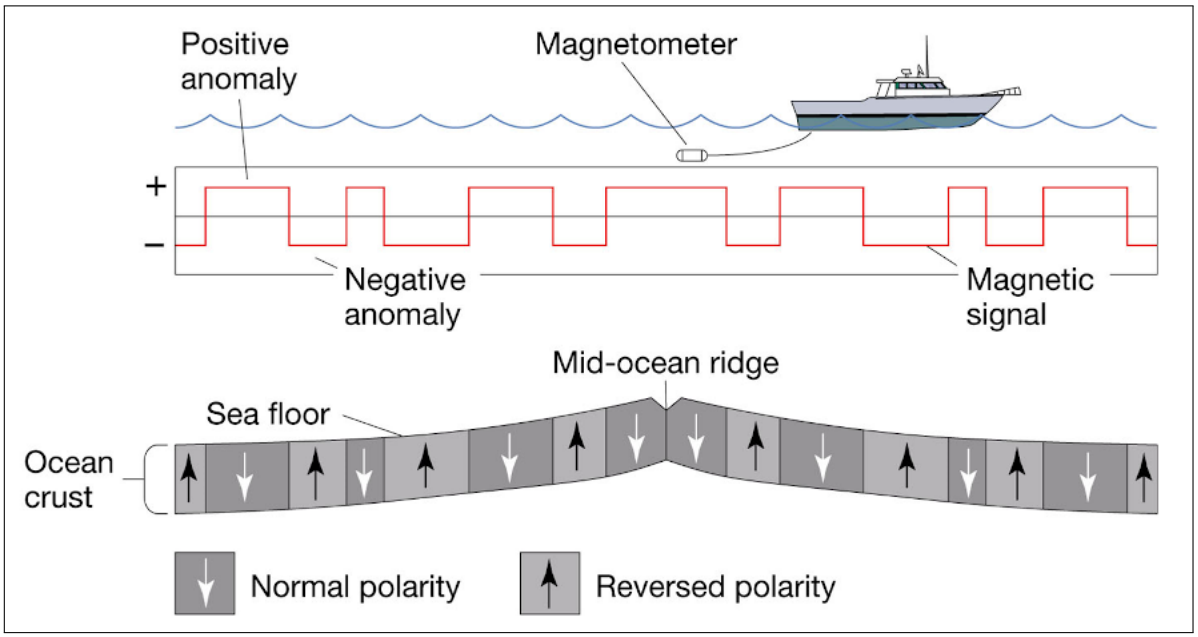

Figure 2.4 – Marine magnetic anomalies (From Burger et al. (2006))

Further difficulties arise if the magnetic anomalies formed near the magnetic Equator, resulting in low amplitudes approaching the noise level (e.g., Beard et al., 2000; Horner-Johnson and Gordon, 2003). Therefore, their imaging depends on the quality of the available dataset of total magnetic field measurements and also on the temporal and spatial resolution of the model of the internal Earth's magnetic field.

2.3.3 Source of errors

Luyendyk (1997) reviewed the sources of errors (SEs) for aeromagnetic surveys that include variations in the induced magnetization due to changes in the aircraft motion, altitude variations, navigational effects, ground clearance variation, wave noise due to large bodies of water and time variation in the magnetic field. Wessel and Watts (1988) also reported navigation problems and instrumental influence as SEs in marine gravity surveys.

Additional SEs in marine magnetic measurements may be due to the difficulty to correct the external magnetic field, the variations of the induced magnetization of the ship due to changes in the magnetic heading and the unavailability of a proper geomagnetic model of the main internal field. Quesnel et al. (2009) found further SEs during the compilation of marine magnetic data process.

Despite the identification of the SEs or noise in marine and aerial magnetic surveys in previous works, in the Caribbean region some conditions restrict on knowledge on the behavior of those sources in time or space and hence make difficult to apply a proper crossover data correction.

Those conditions include:

1. Lack of control on external magnetic field behaviour due to the very sparse location of geomagnetic observatories (Actually two geomagnetic observatories are operating in the Caribbean and Gulf of Mexico region: The Stennis Space Center (BSL) in Mississippi, US, and the San Juan observatory (SJG) in Puerto Rico, US. The BSL has been operating from 1986 until present, and the SJG has been operating from 1903 until present (Intermagnet, 2017));

2. Proximity to the equatorial electrojet (EEJ), which strongly varies latitudinally and which estimation from ground-based data is often impossible given the difficulty in locating a station precisely at the dip latitude (Hamid et al., 2014) and;

3. Proximity to the magnetic Equator that produces total magnetic anomalies of very low amplitude (Gee and Kent, 2007) which may be of the same order of the noise.

   Actually, the amplitude depends on direction: a N-S elongated body will have a zero magnetic anomaly, and an E-W elongated body will have an anomaly of amplitude half of the same body at the pole.

2.3.3.1 Heading effect

The geometry and the heading of a ferromagnetic vehicle (ship or aircraft) can severely affect the magnetic measurements, because of the intensity of vehicle's magnetic field (e.g., Abdel-Kader et al., 2017; Bullard and Mason, 1961; Leliak, 1961). The heading effect is part of the magnetic noise and depends on the induced and remanent magnetisation of the field respectively.

Bullard and Mason (1961) stated for marine measurements that "if the total magnetic field is measured at a point fixed relative to the ship as a function of the ship heading and expressed as a Fourier series, only a constant term and sine and cosine terms in the heading and twice the heading should occur."

For marine measurements, the equation for predicting the effect of the ship's magnetic field is:

$$F_Q = F\ C_0\ C_1 cos\theta\ C_2 cos2\theta\ S_1 sin\theta\ S_2 sin2\theta \tag{2.1}$$

Where θ is the magnetic heading measured clockwise from north, F_Q is the total field at location Q, F is the background magnetic field, and C_0, C_1, C_2, S_1, and S_2 are constants dependent on the ship's magnetic contribution (Bullard and Mason, 1961). For a symmetrical ship, the terms S_1 and S_2 are negligible compared with the cosine terms.

The variation of the field with ship heading disappears at the magnetic poles and is maximum at the equator. Thus, it is necessary to model the ship magnetisation to estimate the variation of the coefficients with the distance.

2.3.4 Spectral analysis

Total intensity power spectrum can be obtained from a spherical harmonic approach but also from local total intensity data (Maus, 2008), and represents the sum of expected core and crustal spectra (Voorhies, 1998). The local averaged spectrum is mostly used for local intensity data (Maus, 2008). The equation that governs the radial average of the power spectrum is given by Blakely (1996):

$$\Phi_{\Delta_T}(|\kappa|) = A\Phi_M(|\kappa|)e^{-2|\kappa|d}(1-e^{-|\kappa|t})^2 \tag{2.2}$$

where $\Phi_{\Delta_T}(|\kappa|)$ is the radial average of the power-density spectra of the total field anomaly, A is a constant that depends on the orientation of the magnetization and regional field, Φ_M is the power-density spectra of the magnetization (if $M(x,y)$ is random and uncorrelated then $\Phi_M(|\kappa|)$ is a constant), κ is the wavenumber, d is the depth of the top of a horizontal layer where the total-field anomaly is measured, and t is the thickness of that horizontal layer.

In general, log-log power spectrum decays with a nearly constant slope at the wavelength less than 50 km, continuously decreases from wavelengths between 50-500 km associated

with crustal magnetization and is nearly flat at the wavelength ranging between 500-2500 km (Maus, 2008).

Spatially, the crustal and the internal magnetic field spectra are uncorrelated, and above λ=2500 km the main internal field masks the crustal energy (Maus, 2008). Blakely (1983) discussed the spectral properties of marine magnetic anomalies and factors that influence the shape of $|R(k)|^2$. Short-wavelength increases proportionally to crust aging (Blakely, 1983).

2.3.5 Principal component analysis

Principal component analysis (PCA) is a tool to explore the patterns within a matrix but also to detect outliers over datasets with a complex correlation structure. PCA is the basis of the multivariate analysis, where the pattern between two or more datasets is determined (Wold et al., 1987).

The basic goal in PCA is to decorrelate the signal by projecting the data onto orthogonal axes (Clifford, 2005). Pearson (1901) formulated PCA from the analysis of "lines and planes of closest fit to systems of points in space". In the formulation of PCA, Pearson (1901) considered the problem of determining the best-fitting plane through *n* non-coplanar points. Hence, PCA extracts the dominant 'object pattern' **rows of T** and complementary 'variable pattern' **columns of P'** of a data matrix **X** (Wold et al., 1987).

PCA allows to projecting the matrix onto the eigenvectors of the covariance matrix. The calculation of the eigenvalue 'λ' is the first step to determine the eigenvector ν of a matrix **X**. This process consists in to determine a singular value for the data matrix **X** so that if:

$$\mathbf{C} = X^T\mathbf{X} \tag{2.3}$$

then it exists an eigenvector ν such that satisfies the condition:

$$\mathbf{C}\nu = \lambda\nu = 0 \tag{2.4}$$

The eigenvalue is determined by solving the characteristic equation:

$$(\mathbf{C} - \lambda\mathbf{I})\nu = 0 \tag{2.5}$$

Further details about the method can be found in Pearson (1901).

2.4 Data and methods

2.4.1 Aeromagnetic

2.4.1.1 Data

Geoterrex (MENEVEN S.A. contractor) acquired the reprocessed aeromagnetic data used in this study between 1982 and 1984 (Fig. 2.5) and INTEVEP (Venezuelan Oil Research Institute) provided it in 2013. The total magnetic measurements cover the northern part of the Venezuela territory (northern of the Orinoco river), and included the main petroliferous basins (to the north: Maracaibo Basin, Falcón Basin, Cariaco Basin; to the south: Barinas-Apure Basin and the Eastern Venezuela Basin). Geoterrex also acquired data on further important geological structures, including the Baúl Massif, Espino Graben, Paraguaná Peninsula, the Gulf of Paria and the Central Coastal Range.

Herrero O. and Navarro (1989) published the first public domain map derived from this campaign. Geoterrex acquired a total of 202.354,6 linear kilometres of magnetic lines (MENEVEN, 1983) and covered about 501.330 km^2 (54,70 $\%$ of the total area of the Venezuelan territory) during that campaign. The dataset comprises nine blocks acquired with a North-South preferential direction of flight for the regular lines and East-West for the tie lines. The spacing between them was about 3 km and 9 km respectively. The height of flight ranged between 497.9 m and 2614.45 m.

The calculated height gradient from ground magnetometers data was ∼0.02 nT/m. MENEVEN (1983) reported some disturbed periods during the survey, including both magnetic storm, micropulsation activity and additional acquisition problems.

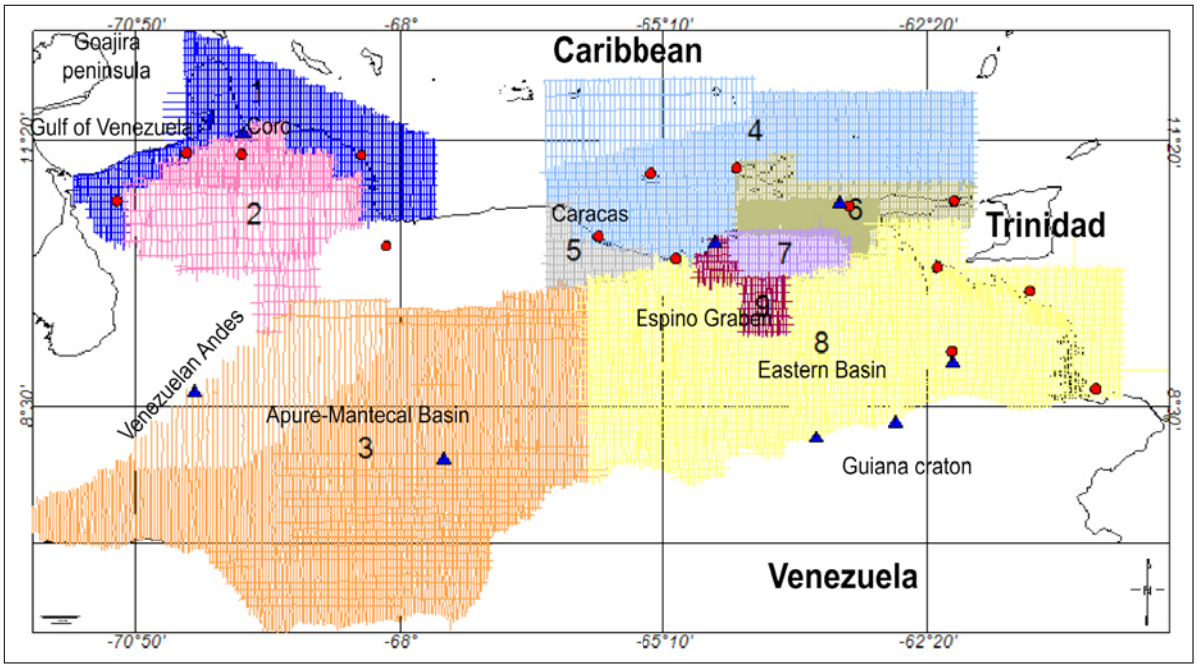

Figure 2.5 – Aeromagnetic tracklines location (Legend: Red circles indicate Syledis navigation stations location, blue triangles indicate ground magnetometer location) (MENEVEN, 1983)

2.4.1.2 Method

We used the Comprehensive magnetic field (CM4) (Sabaka et al., 2004) to remove the main internal magnetic field. We identified the outliers from frequency histograms analysis. We applied a standard levelling by block due to the regular geometry of the acquisition (further details in: Reeves, 2005). During the levelling, we built a function from the crossovers data by line. We also inspected the frequency histogram of the gradients at the cross-overs and we used averaged gradients as quality control criteria. We discarded cross-overs with steep gradients for the correction. We smoothed the resulting function and used it to correct the crossovers data. After, we decomposed the total magnetic anomalies into long wavelength and short wavelength.

2.4.2 Marine data

2.4.2.1 Data

The gathered data amount 516 surveys which represent 2.612.994 data points between epochs 1958 and 2012 (see Table No. 2.1). The initial database includes both magnetic anomalies and total magnetic field stored in the National Centers for Environmental Information (NCEI) (formerly the National Geophysical Data Center) and French Research Institute for Exploitation of the Sea (IFREMER) system.

We calculated the magnetic anomaly from the total magnetic field measurements (see Fig. 2.6). The descriptive statistics of the marine total magnetic field measurements show that the mean was about 40.226 nT, and the standard deviation along the tracks ranged between 2,90 nT and 5.730,9 nT, indicating a variable distribution of magnitudes of the total magnetic field. The inline resolution was variable and ranged between 2 m up to 40,39 km.

The total distance for the marine track lines was about 1.758,60 Mm (see Table No. 2.1). The values of marine magnetic anomalies recovered from NCEI and IFREMER ranged from -9.759 nT to 9.809 nT.

Table 2.1 – Description of track lines and total magnetic field measurements

Pre-processed data	
N	2.612.994
No. Surveys	516
Total dist. (km)	1.758,60 Mm
Resolution inline (km)	(0,002 - 40,39)
Mean	40.226,90
Std. dev.	(2,90 - 5.730,90)
Range TMF*	(30.098-71.903,90)

**TMF = Total magnetic field*

N= number of measurements, mean, and standard deviation (in nT for marine data)

2.4.2.2 Method

During the preprocessing, we exhaustively reviewed all the available acquisition documentations of each magnetic survey present in the dataset. Also, we performed a detailed visual inspection track-by-track. The latter task was time-consuming; however, it guaranteed the success of the final goal: the magnetic mapping. A limitation is, the protocol followed by each provider Institution to derive the anomaly from NCEI and IFREMER was often unavailable.

A preliminary comparison within the NCEI/IFREMER magnetic anomalies revealed that almost 38% of the surveys are anti-correlated with the other ones, i.e., these magnetic anomalies have an erroneous sign. Mapping our results confirmed that observation. We concluded that the processing procedure on these surveys was erroneous.

Also, we confirmed that the sign of the NCEI magnetic anomaly was correct and suspect that total magnetic field erroneously reconstituted from the magnetic anomalies resulted in this wrong sign when computed anomalies. To overcome this limitation, we retained the polarity of the NCEI magnetic anomalies.

The MGD77 format (NCEI format for the marine tracks) gathered most of the needed acquisition information although ambiguities remained concerning the main internal field used to derive the magnetic anomaly or to the procedure used to reconstitute the total magnetic anomaly. In the available documentation is unclear whether a baseline distinct

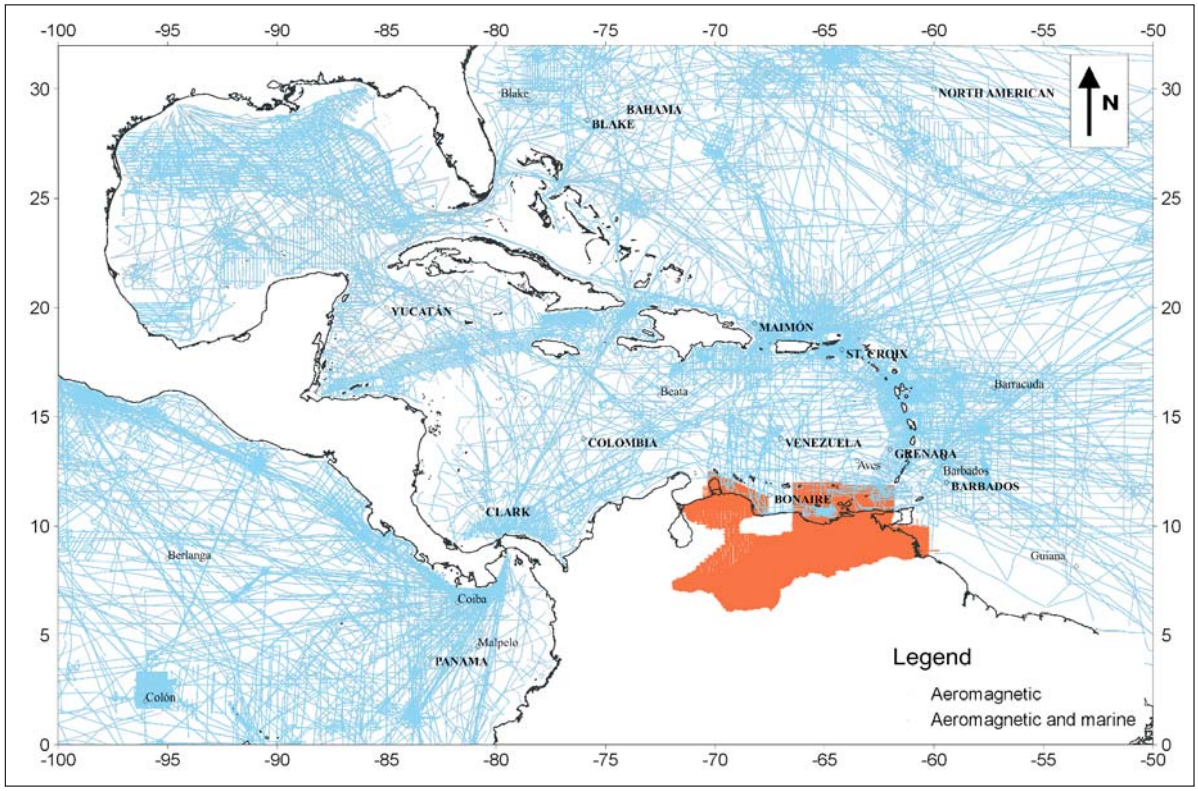

Figure 2.6 – Marine and aerial tracks location

from zero was used or not.

As part of a traditional practice during the acquisition, surveyors often added a constant value to the entire database, but that information may be omitted in the documentation if written some time after the survey. For these reasons and to take advantage of all possible magnetic data, we performed a detailed track-by-track inspection of the data to identify and correct (if possible) all data with systematic differences concerning the dataset.

Also, we evaluated the magnetic heading effect and corrected the data from that effect although statistical analysis suggested that this correction only brings a marginal improvement.

2.4.3 Main internal magnetic field removal

We calculated the internal magnetic field of the Earth by using the Comprehensive Magnetic Model v.4 (CM4), for a time interval between 1960 and 2002.5, while we used the IGRF-11 to deduce the magnetic anomalies acquired outside the time range of the CM4 model. We processed 2118438 total magnetic field values with CM4 and 494556 measurements using the International Geomagnetic Reference Field (IGRF).

In order to calculate the CM4 internal magnetic field contribution, we used DST coefficients and Local time values. The CM4 processing also considers the geodetic and geocentric coordinates. In this case, we converted the geocentric latitude to geodetic latitude. Then, we calculated the magnetic anomaly by substracting the CM4 internal magnetic field from the total magnetic field (F). The values of total field range between -5693.6 to 38676.0 nT.

2.4.4 Preprocessing of marine magnetic anomalies

We preprocessed total magnetic anomalies using the following protocol:

2.4.4.1 Detecting outlying surveys

We plotted all surveys at every 2.5° of latitude and longitude, respectively, to identify the outlying surveys. We identified huge discrepancies visually. We identified as outliers the surveys LCATO07MV, LKA68G, LU671AT, LCAG71IDO, LV1603 and LV1612 from the plotting of surveys between longitude 55°W and 52.5°W (see Fig. 2.7). We discarded the survey LODP207JR due to its out of range amplitude. We applied similar criteria from plots: 2.8, 2.9, and, 2.10. Once done the previous step, we used visual inspection of the frequency histogram of magnetic anomalies by survey as a tool for the tracks assessment.

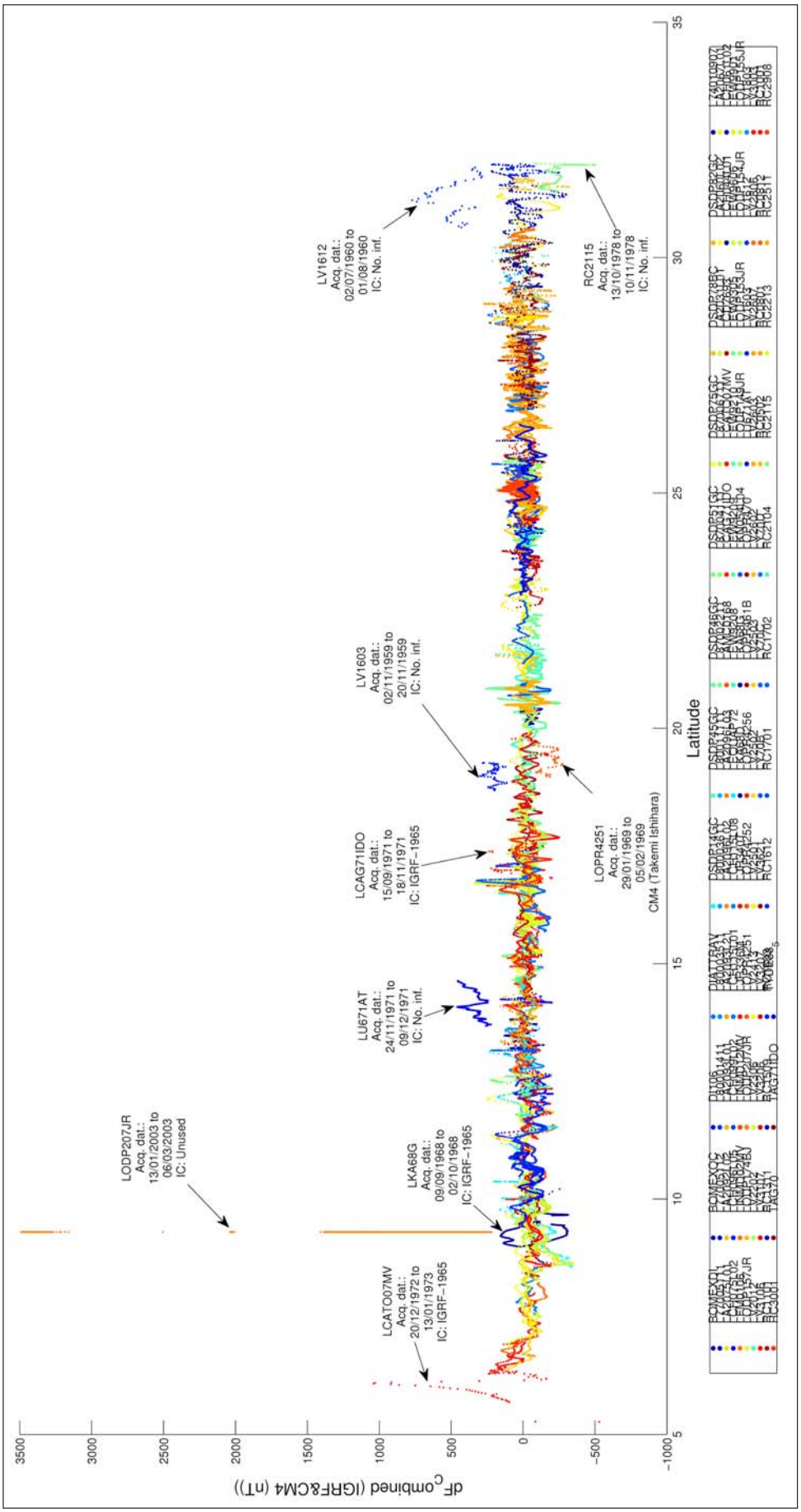

Figure 2.7 – Plot of marine magnetic anomalies located between 55°W and 52.5°W showing outliers

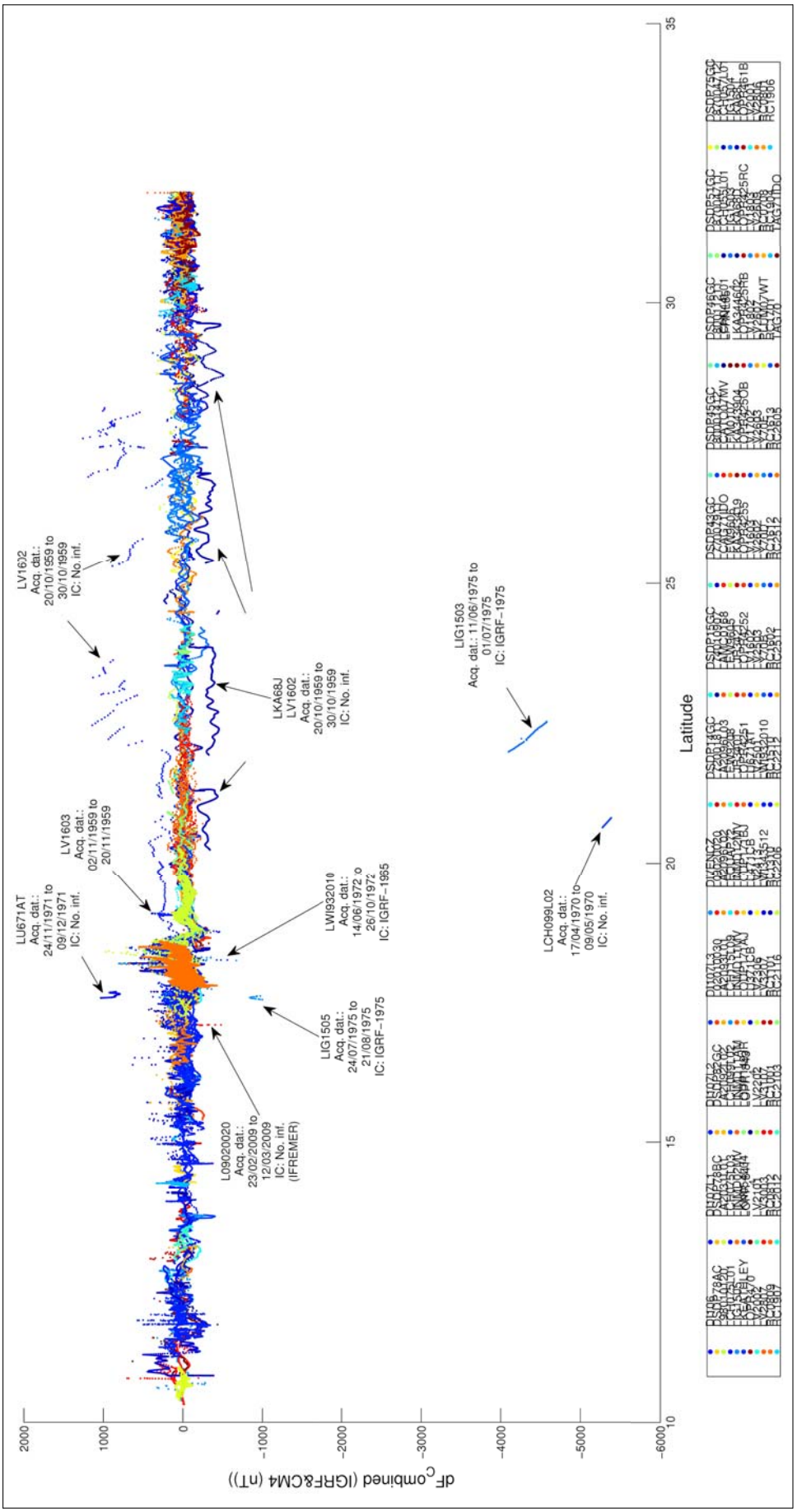

Figure 2.8 – Plot of marine magnetic anomalies located between 65°W and 62.5°W showing outliers

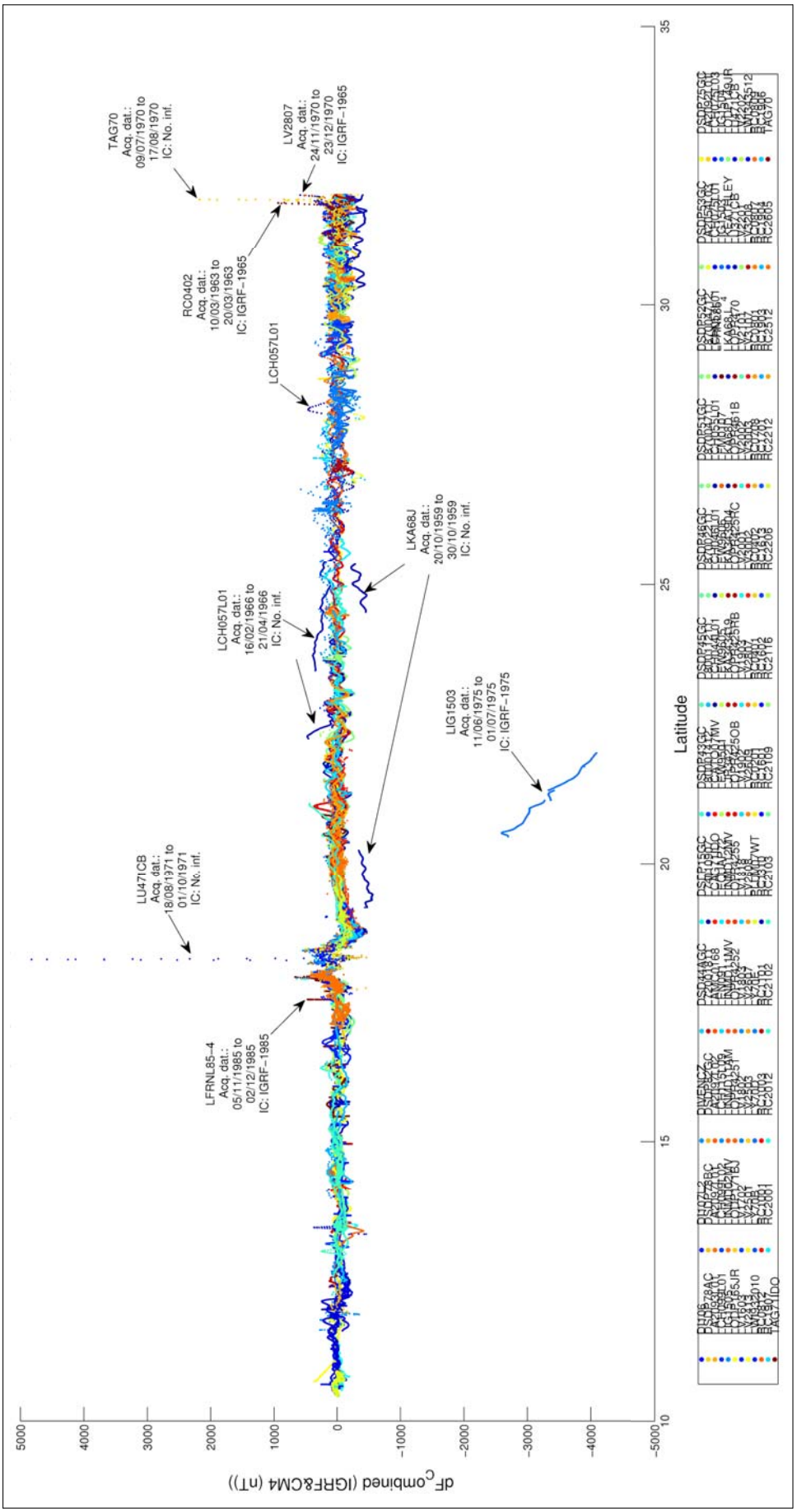

Figure 2.9 – Plot of marine magnetic anomalies located between 65°W and 67.5°W showing outliers

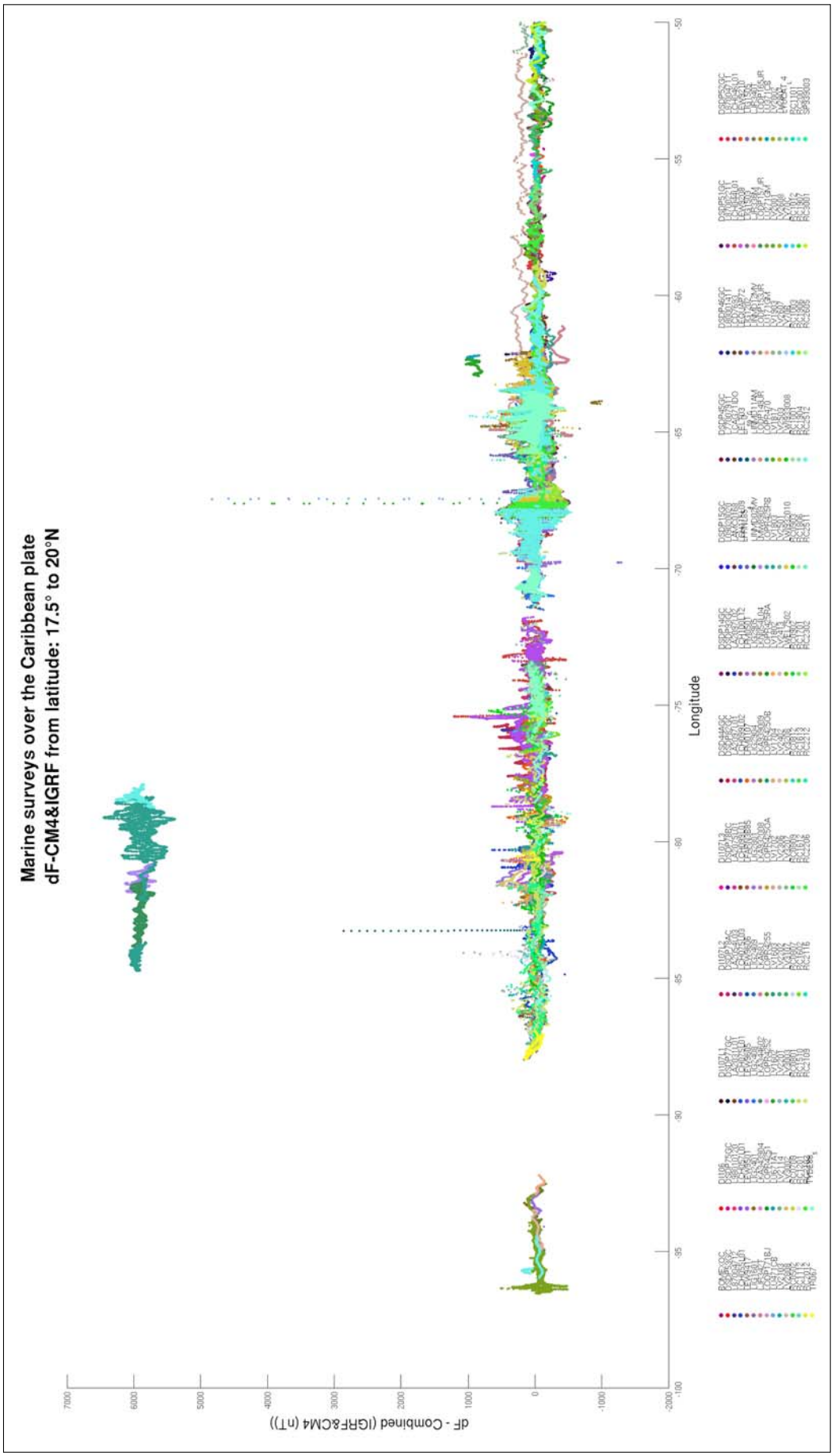

Figure 2.10 – Plot of marine magnetic anomalies located between 17.5°N and 20°N showing outliers

2.4.4.2 Detecting erroneous acquisition time

An erroneous acquisition time in the dataset can affect the determination of the magnetic main internal field, due to the time dependency of the model. We plotted the decimal year vs. the magnetic anomalies by track to evaluate errors in the registered acquisition time. We detected errors as duplicate acquisition time or improper values of magnetic anomalies (see Fig. 2.11). Also, we plotted the velocity of the ship vs the accumulated distance to identify

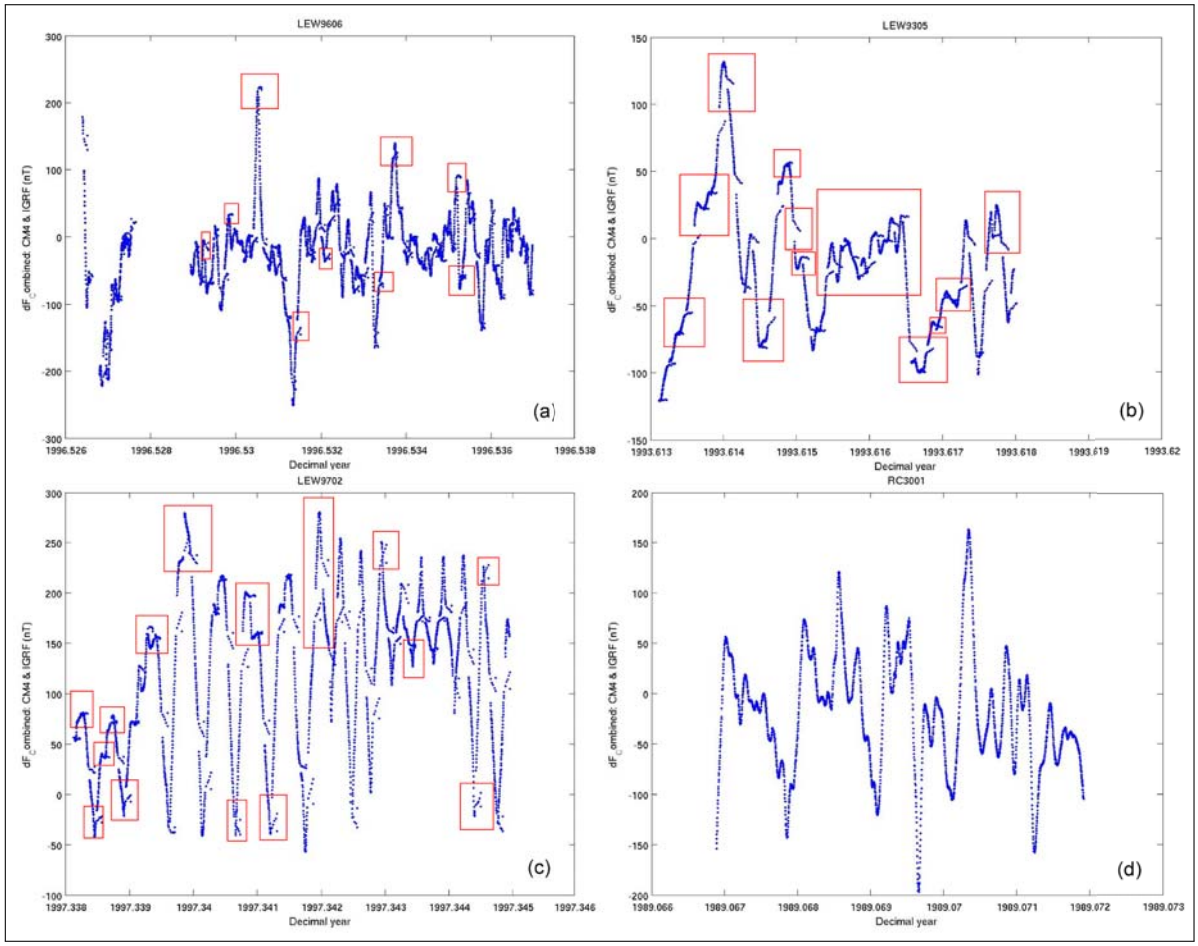

Figure 2.11 – Magnetic anomalies versus decimal year showing erroneous registered acquisition time (Labels "a", "b", and "c" exhibit errors whilst "d" has a correct time, red boxes indicating identified erroneous time)

potential location problems, as for example, negative velocities and reverse time (see Fig. 2.12 and Fig. 2.13).

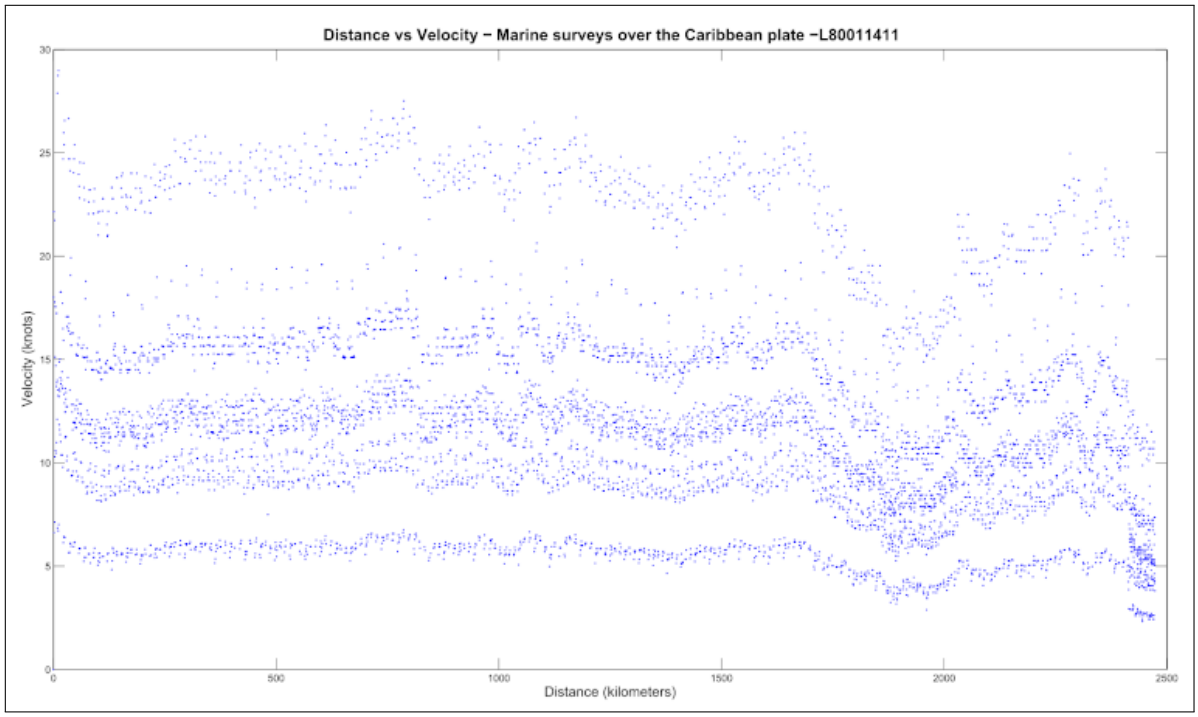

Figure 2.12 – Accumulated distance vs. ship velocity

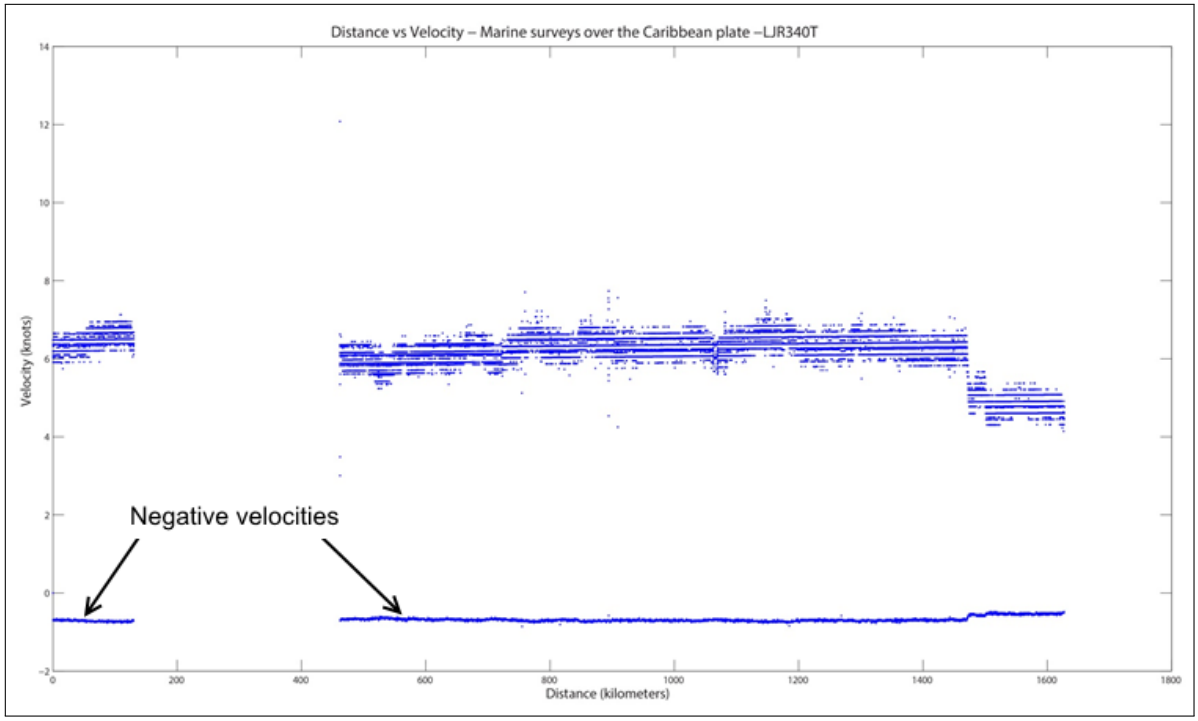

Figure 2.13 – Accumulated distance vs. Ship velocity (featuring negative velocities)

2.4.4.3 Evaluation of the magnetic heading effect

We plotted the magnetic heading in degrees versus the magnetic anomaly for evaluating the magnetic heading effect (e.g., see Fig. 2.14). We determined the magnetic heading effect by using the relationship proposed by Bullard and Mason (1961) (see Eq. 2.1). We obtained the coefficients C_1 and C_2 of the Eq. 2.1 at the cross-overs points. We deduced the coefficient Co from the cosine equation at heading equal to zero degrees. Statistics showed no improvement in the magnetic anomalies after apply this correction (see Fig. 2.15). Then, we did not used the magnetic heading correction.

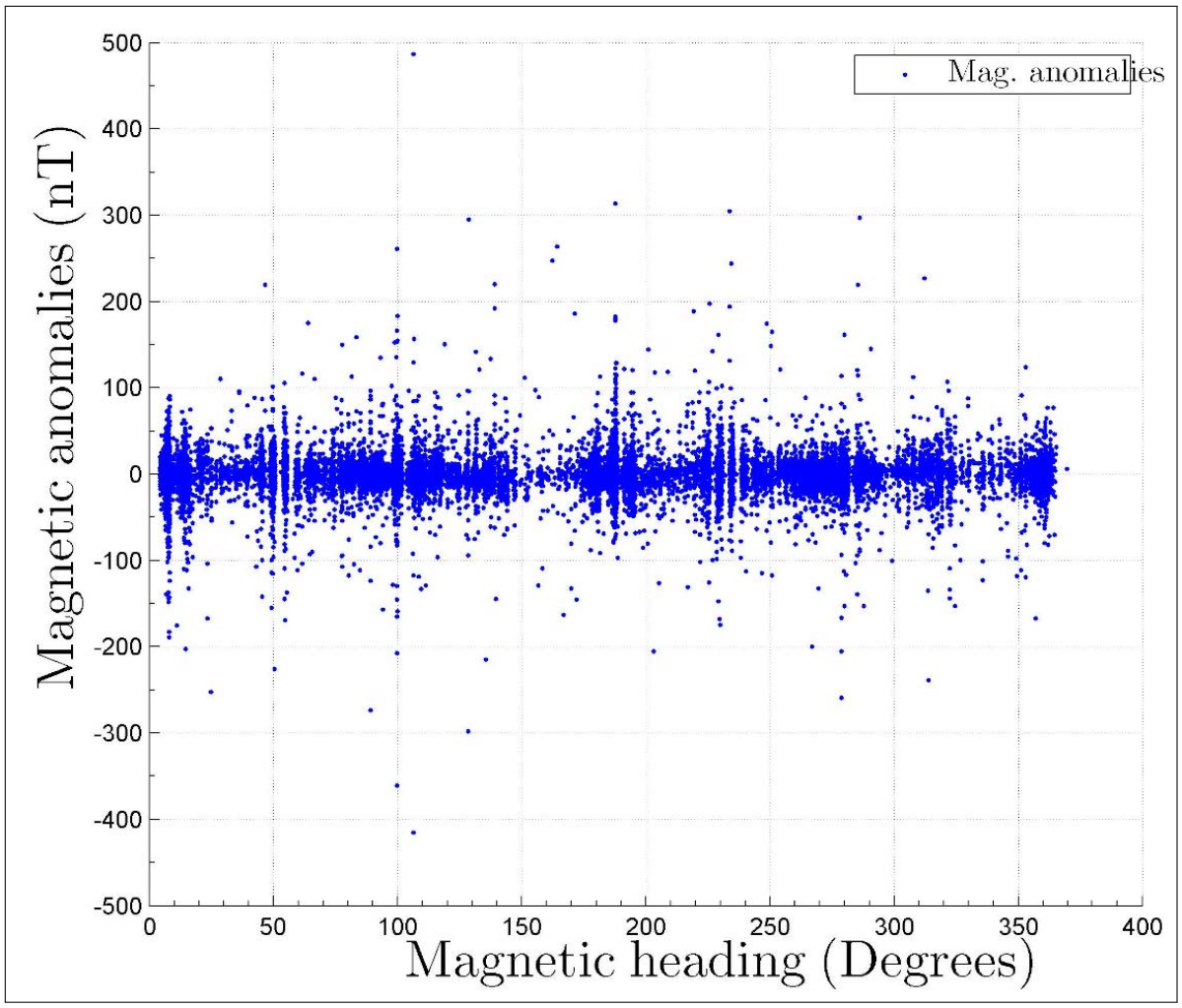

Figure 2.14 – Magnetic anomaly vs. magnetic heading on the survey LWI932010

2.4.5 Levelling

2.4.5.1 Detection of internal and external crossovers

We detected internal and external crossovers for the entire dataset using the package x2sys (Wessel, 2010). Because the methodology followed to detect and correct crossover data partially relies on the method proposed by Wessel (2010), we discriminated the

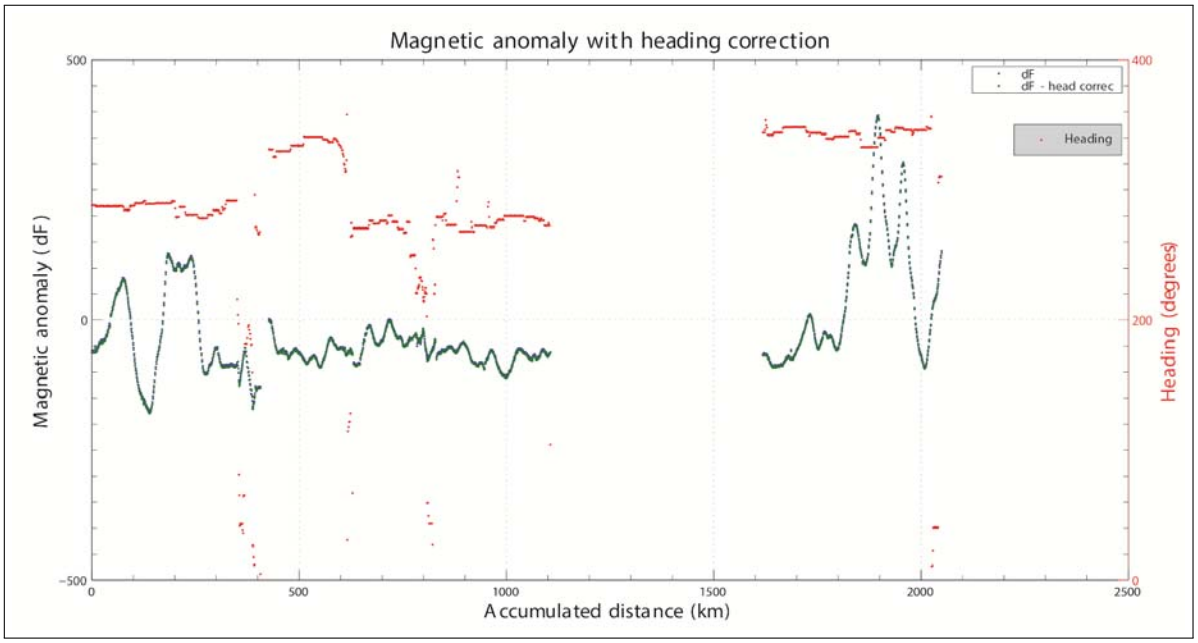

Figure 2.15 – Heading effect and correction on magnetic anomalies

crossovers between crossovers within the same survey, hereafter called 'internal crossovers' and crossovers between two different surveys, hereafter called 'external crossovers.'

First, we defined the parameters for the internal cross-overs detection. In this sense, we took the survey DI107L3 as sample, for which the number of internal cross-overs was known in advance. We tested the crossover detection using a maximum gap ranging from 0 to 1000 km and maintaining a fixed bin size of 0.009 degrees (i.e., 1 km at the equator), for each chosen maximum gap. We compared the different results and parameters (see Fig. 2.16).

That first step allowed us to establish an empirical criterion to define the parameters for the cross overs detection within survey: The bin size (see Eq. 2.6), which is depending on the mean distance between adjacent measurements and the gap distance. The gap distance was then defined as the mean of the distance between contiguous measurements plus the standard deviation of this distance (see Eq. 2.7).

$$bz = mean(diff(d))\ 0.1mean(diff(d)) \tag{2.6}$$

where: bz is the bin size and, dg is the gap distance, d is the accumulated distance, and $diff(d) = d_{i1} - d_i$.

$$dg = mean(diff(d))\ std(diff(d)) \tag{2.7}$$

For the external crossover detection, we used a bin size of 0.5 degrees for the entire dataset. In general, external crossover errors ranged between 0 and 150 nT, showing extreme values up to 2265 nT (see Fig. 2.17).

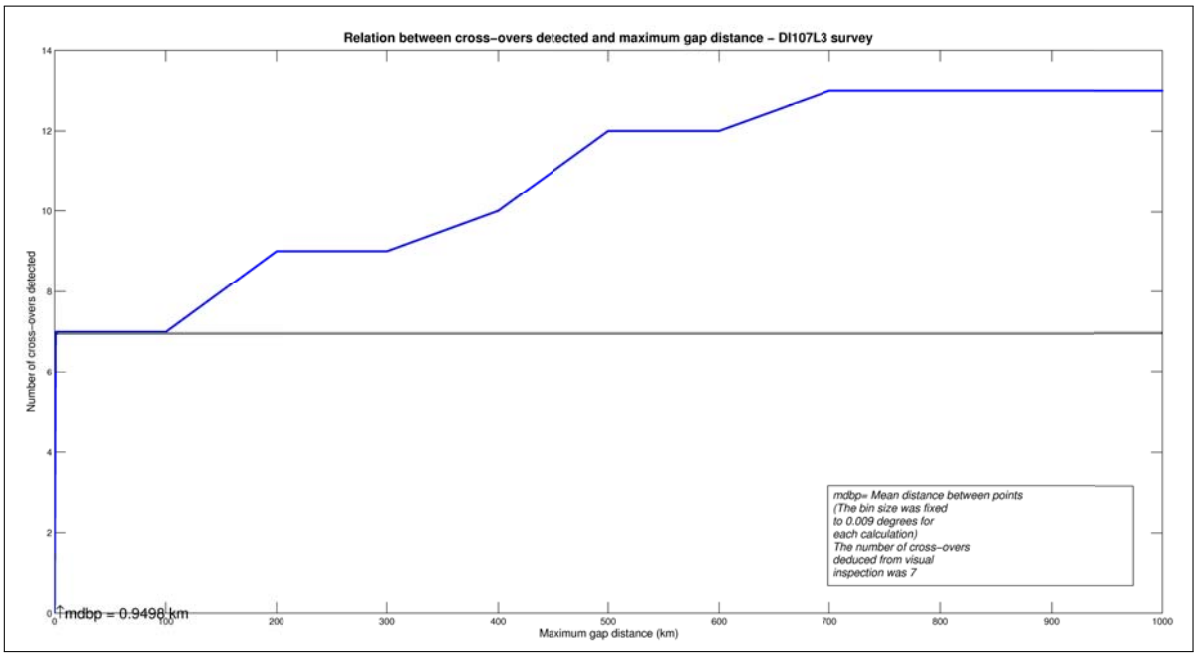

Figure 2.16 – First criterion used to determine the parameters for the internal cross-overs detection

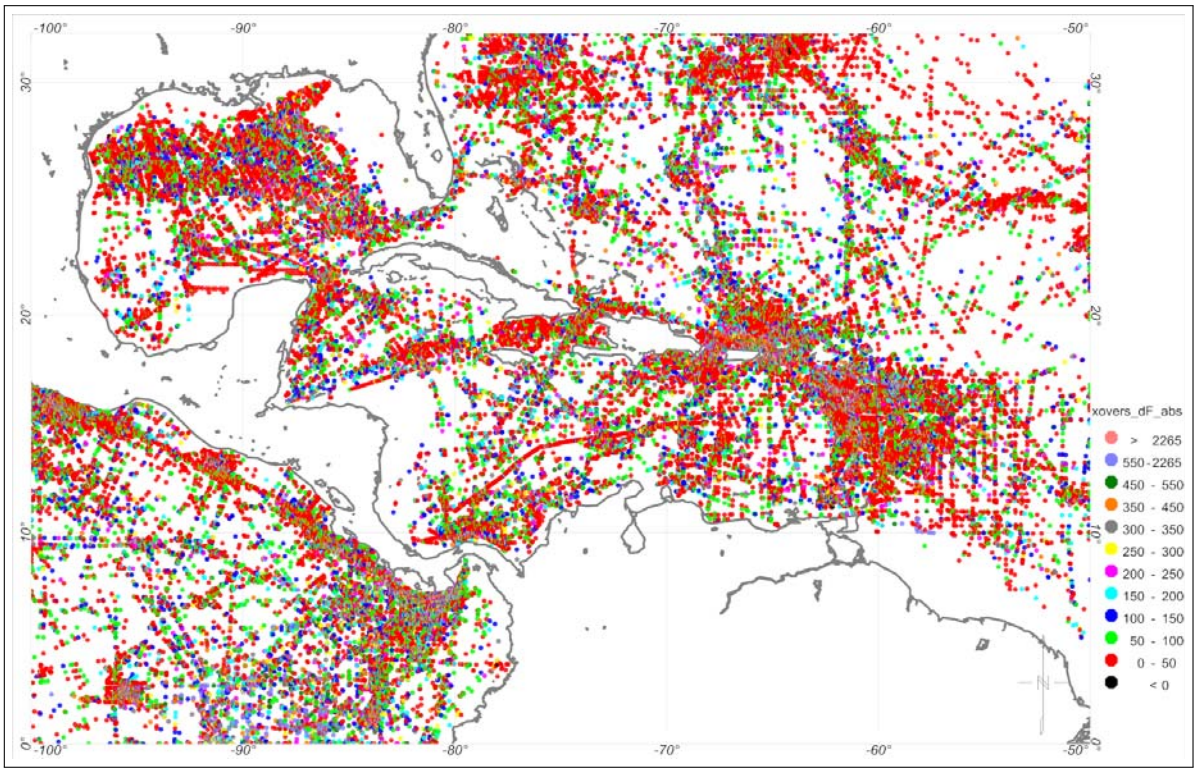

Figure 2.17 – Amplitude of the external crossovers for the marine tracklines

2.4.5.2 Internal levelling

We built a Matlab algorithm for the correction of internal crossovers, allowing to distribute the misfit along each track using a 'piecewise cubic Hermite' function (see further details in Fritsch and Carlson, 1980) in the space domain. We chose the 'piecewise cubic Hermite' interpolation function because of its simplicity, and because it warranted a monotonicity in the correction curve at least between two knots (here 'cross-overs') and hence, it preserved the shape of the function build by the accumulated distance and the magnetic anomalies in every track (e.g., see Fig. 2.18).

We retained the internal crossover data for errors between -360 and 360 nT from the frequency histogram analysis. We performed an exhaustive and iterative review track-by-track to discard inconsistent crossovers points.

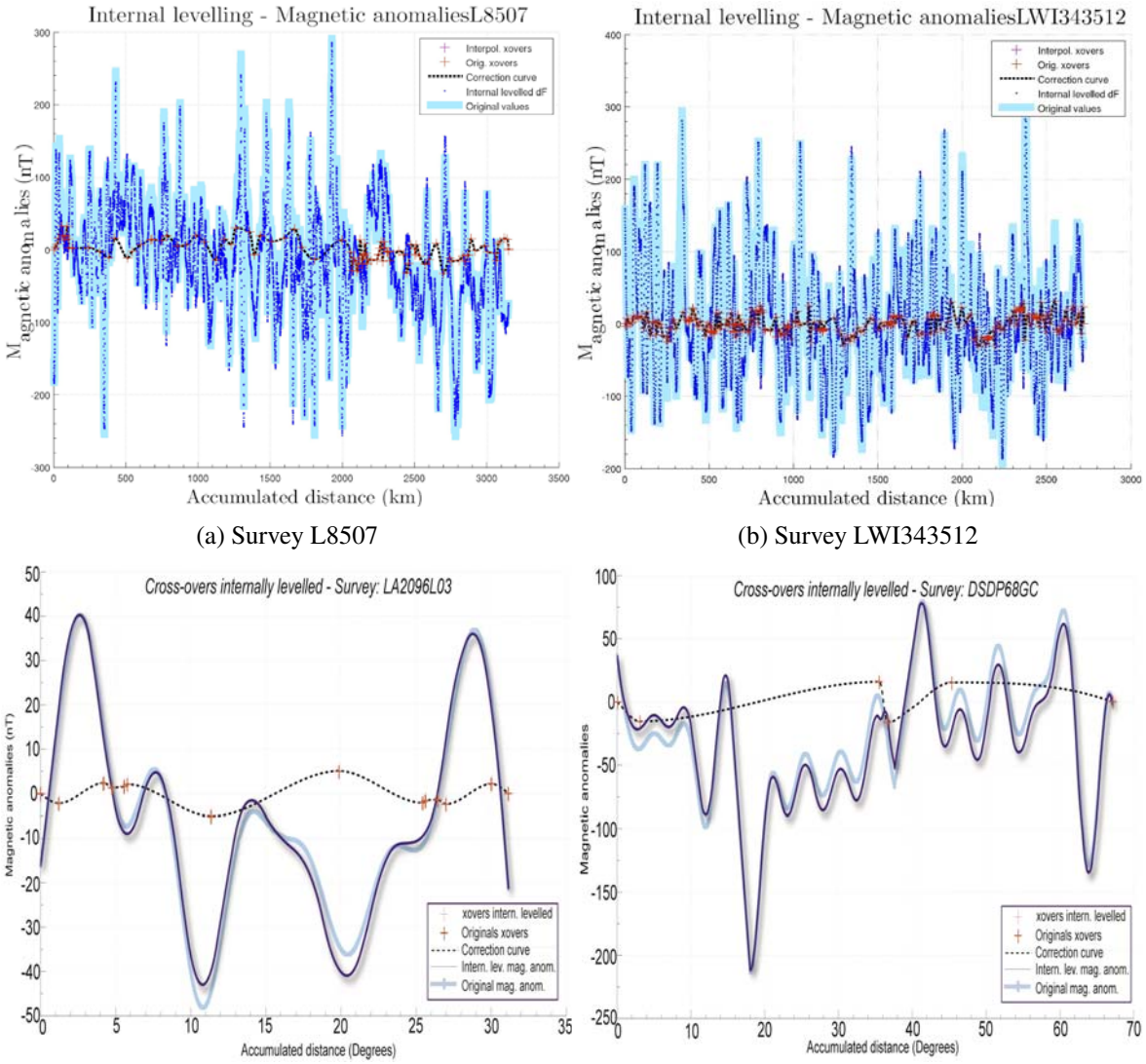

(a) Survey L8507

(b) Survey LWI343512

(c) Survey LA2096L03

(d) Survey DSDP68GC

Figure 2.18 – Internal levelling and correction curve

2.4.5.3 External levelling

2.4.5.3.1 Unshifting: "Unshifting" a survey consists in defining a criterion for the selection of a proper baseline. A prevalent practice during the acquisition is to assume a baseline equal to zero and hence, remove the mean in each survey. This criterion might be only valid for more extended surveys, i.e., more than approx. 1500 km of roughly straight length because it is expected that the total wavelength content will be contained in that distance.

For shorter surveys the mean may just represent the trend of a transect and may be different to the baseline, suggesting that this practice should be applied cautiously. Subtracting the mean when such differences exist between trend and baseline can have an undesirable effect on the compilation.

For that reason, we tested the unshifting in two different ways: 1) For the first test, we subtracted the mode (the value that occurs most often in the dataset) of every track, if the mode was in the interval between -280 and 280 nT, 2) The second test consisted of using the mean of a selected survey with broad spatial coverage and low amplitude of its crossovers (50 nT) and to compare the results of both tests.

We selected the VEMA surveys following this approach. Figure 2.19 shows the magnetic anomalies before and after the unshifting procedure for the DLDR01HO survey. We applied the unshifting procedure using Matlab.

2.4.5.3.2 Distribution of the crossovers data using x2sys: After unshifting the surveys requiring to corrected, we applied the method for correcting external crossovers errors proposed by Wessel (2010), which was initially designed for marine gravity data. The statistics confirmed the importance of this processing and improved the internal and external crossovers, with in particular, an apparent reduction of the extreme values (see table No. 2.2).

2.4.6 Frequency analysis and band-pass filtering

We calculated and compared the spectrum of the total magnetic anomaly (see Eq. 2.2) to the spectrum of the following models and datasets: GRIMM-L (Lesur et al., 2013), MF7 (Maus, 2010), WDMAM v.2.0 (Dyment et al., 2015) and NAMAG (Bankey et al., 2002). We only kept the wavelengths less or equal to 2500 km. because of the uncertainties related to the lithospheric magnetic field at scales larger than 2500 km (Thébault et al., 2010).

The used method to study the spectral content of the obtained total magnetic anomalies relies on methodologies cited above. We applied a bandpass filter to keep wavelengths in the interval between 300 km and 2500 km. We filtered the resultant marine and aeromagnetic grids using a bandpass filter in the same wave band.

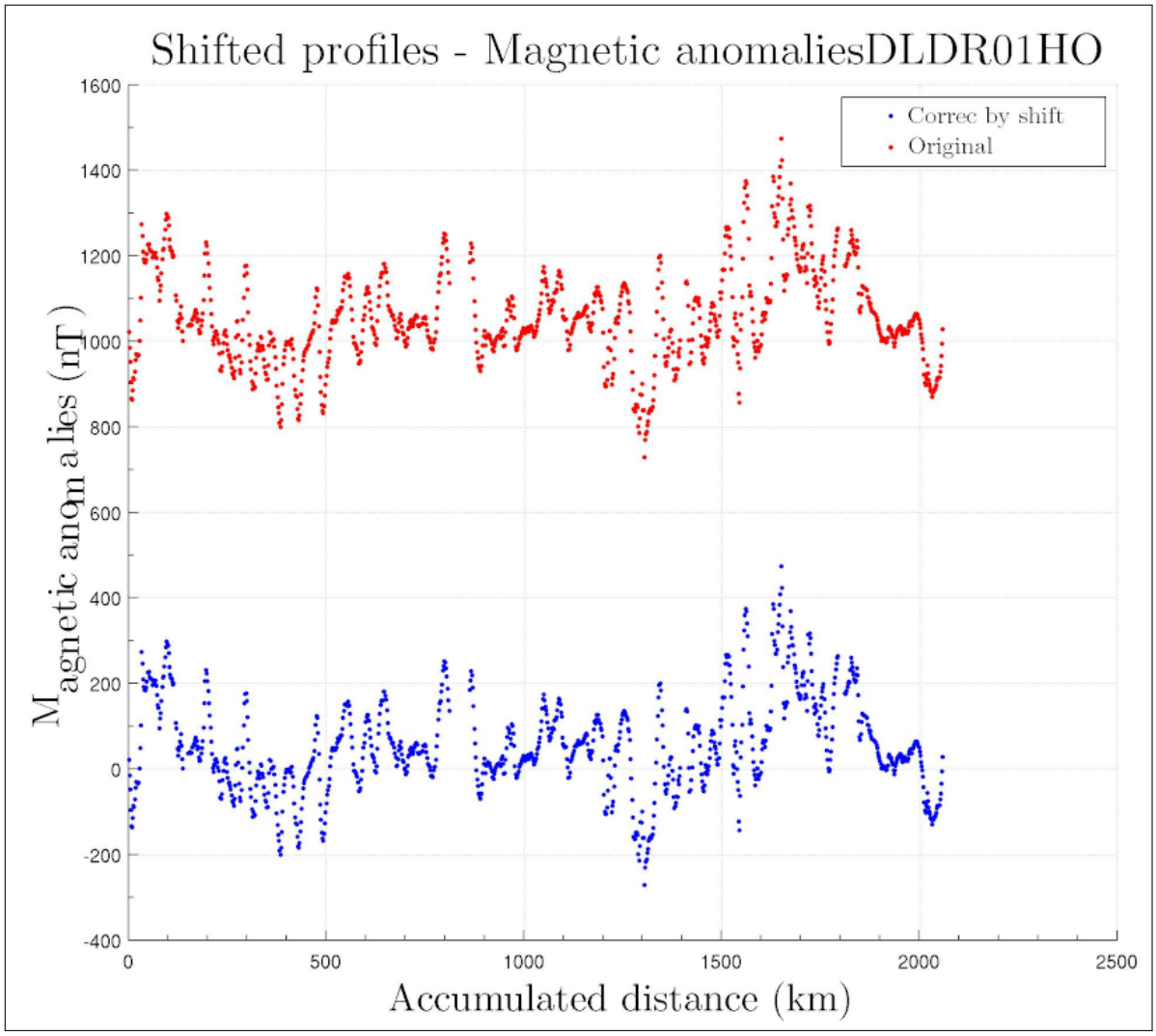

Figure 2.19 – DLDR01HO survey before and after the unshifting step

2.4.7 Statistical validation of the maps: Principal component analysis on the magnetic anomalies and error ellipses.

We validated data within the spatial domain. We performed a multivariate frequency analysis following the next steps:

- Centering the data: We removed the mean from each dataset in order of centring them. The resulting datasets were centred at zero nT;
- Then we calculated the accumulative frequency of magnetic anomalies from the two compared datasets. We performed this calculation using a Matlab algorithm;
- We implemented the principal component analysis by the calculation of the eigenvalues and the eigenvectors;
- We determined the confidence error ellipses as follows: the direction of the major and minor axis of the ellipses corresponded to the direction of the eigenvectors; whereas we calculated the radius of each ellipse from a Chi statistical distribution and the

Table 2.2 – Statistics of the magnetic anomalies before and after the internal levelling

	Min. (nT)	Max. (nT)	Mean (nT)	Std (nT)	N
Internal crossovers					
Before internal levelling	-496,72	655,48	0,52	43,42	
After internal levelling	-81,50	96,50	0,025	5,72	
External crossovers					
Before internal levelling	-1903,53	2263,14	12,31	169,48	97658
After internal levelling	-1869,91	2263,14	10,37	158,62	
Crossovers of normal surveys					
Before internal levelling	-409,52	340,50	-0,52	41,09	8675
After internal levelling	-68,71	64,13	0.000271	5,428	
Magnetic anomalies of the entire database					
NGDC/IFREMER	-9759	9809	-6.78	832,52	
Before internal levelling	-1851	2318	-7,69	126,62	2354148
After internal levelling	-1851	2360	-8,49	122,36	
Magnetic anomalies of normal surveys					
NGDC/IFREMER	-2340	9809	-119,88	246,01	
Before internal levelling	-1267,28	2201,25	-9,98	109,79	1900897
After internal levelling	-1283,13	2201,25	-10,20	109,97	
Magnetic anomalies of the surveys with internal crossovers					
Before internal levelling	-1303,32	2318,84	-7,70	119,69	2303539
After internal levelling	-1287,46	2360,82	-7,59	119,99	

eigenvalues;

- And finally, we determined the optimal confidence ellipse from the visual inspection of each plot (see Fig. 2.20). Using a Chi-distribution has the advantage of facilitating the calculation of the percentage of confidence between both datasets.

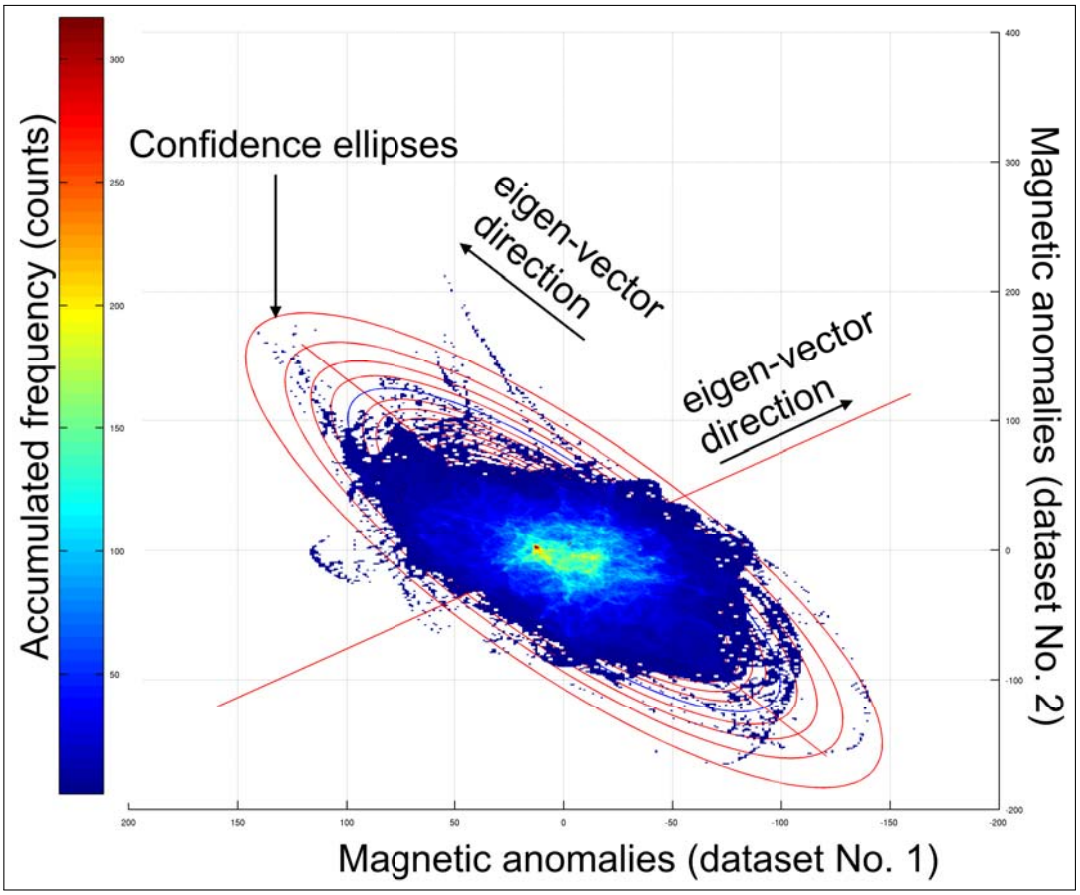

Figure 2.20 – Example of the frequency analysis used

2.5 Results

2.5.1 Aeromagnetic data

We obtained three aeromagnetic anomaly maps of the Venezuelan territory from the processed total magnetic field measurements and from its spectral decomposition (see Fig. 2.21).

2.5.1.1 Long wavelength magnetic anomaly map

The long wavelength magnetic anomaly map comprises wavelengths ranging between 2500 to 300 km and allows to illuminate the magnetic sources that lay above $\sim$ 500 km depth in the subsurface (see 'a' in Fig. 2.21). This map, in general, is well correlated to the geological structures documented in this area.

We interpret the grabens that parallel the northern Orinoco river from west to east as follows: the Apure-Mantecal Graben and the Espino Graben respectively, related with a negative trend of magnetic anomalies. A magnetic dipole at the longitude $\sim$ 68°W approx. interrupts those anomalies. The amplitude of the magnetic dipole ranges between -100 to 100 nT and its positive and oblate pole is pointing to the south. We associate this magnetic dipole with the igneous-metamorphic structural high El Baúl, also described in previous geological and potential field publications (Orihuela Guevara et al., 2011; Tabare and Orihuela Guevara, 2013; Viscarret and Urbani, 2005).

We interpret the elongated absolute negative magnetic anomaly close to the northern border of the Orinoco river as part of a magnetic corridor that characterises from the magnetic point of view the Venezuelan territory, and which constitutes a frontier between the Paleozoic and the Precambrian provinces, as interpreted in previous works (García-Reyes, 2009; Orihuela Guevara et al., 2011).

Unfortunately, the airborne data is not covering the southern part of the Orinoco river, and we are not able to interpret more than the spectacular magnetic anomaly along the Orinoco river provided by satellite data. Our observations might suggest that the tectonic or thermal events were more intense in the continental area, and they occurred prior from the event that produces the interaction between the Caribbean plate and the South American plate.

We observed the correlation of the long wavelenghs with the structural geology uniquely on the mapped continental part. Because the magnetic signature of the continental part significantly differs from the magnetic signature of the marine areas, we define the boundary zone between the Caribbean plate and the South American plate as a zone of sharp magnetic gradient located approx. at 10° of North latitude, which shows a quasi-linear and elongated pattern with orientation WE.

A characteristic of this plate boundary is that no correlation is observed with the structural

provinces present in the area as was observed in the continental part. Also, the continuity observed along the plate boundary put in evidence the magnetic homogeneity along the boundary (in deep). The linear character of this signature may be due to the transcurrent tectonics that is governing the boundary, although, the magnetic gradient along the plate boundary is not constant and becomes sharper to the east.

We interpret the increasing gradient from west to east as reflecting the narrow from west to east of the zone of interaction between the two plates, due to a greater influence of the plate convergence in the eastern part of the boundary. Farther to the north, over the marine area, the flat magnetic gradient allows us interpreting this area as magnetically homogeneous, maybe because the deepest magnetic sources were not defined enough to imprint the magnetic signature (exclusively regarding the area contained in the map).

An exception is the remarkable positive magnetic anomaly with N-S direction to the north-west of the Margarita Island and that curves to the south-west in the eastern part of the island. We relate this magnetic anomaly to a deep geological structure that may involve the Aves Ridge.

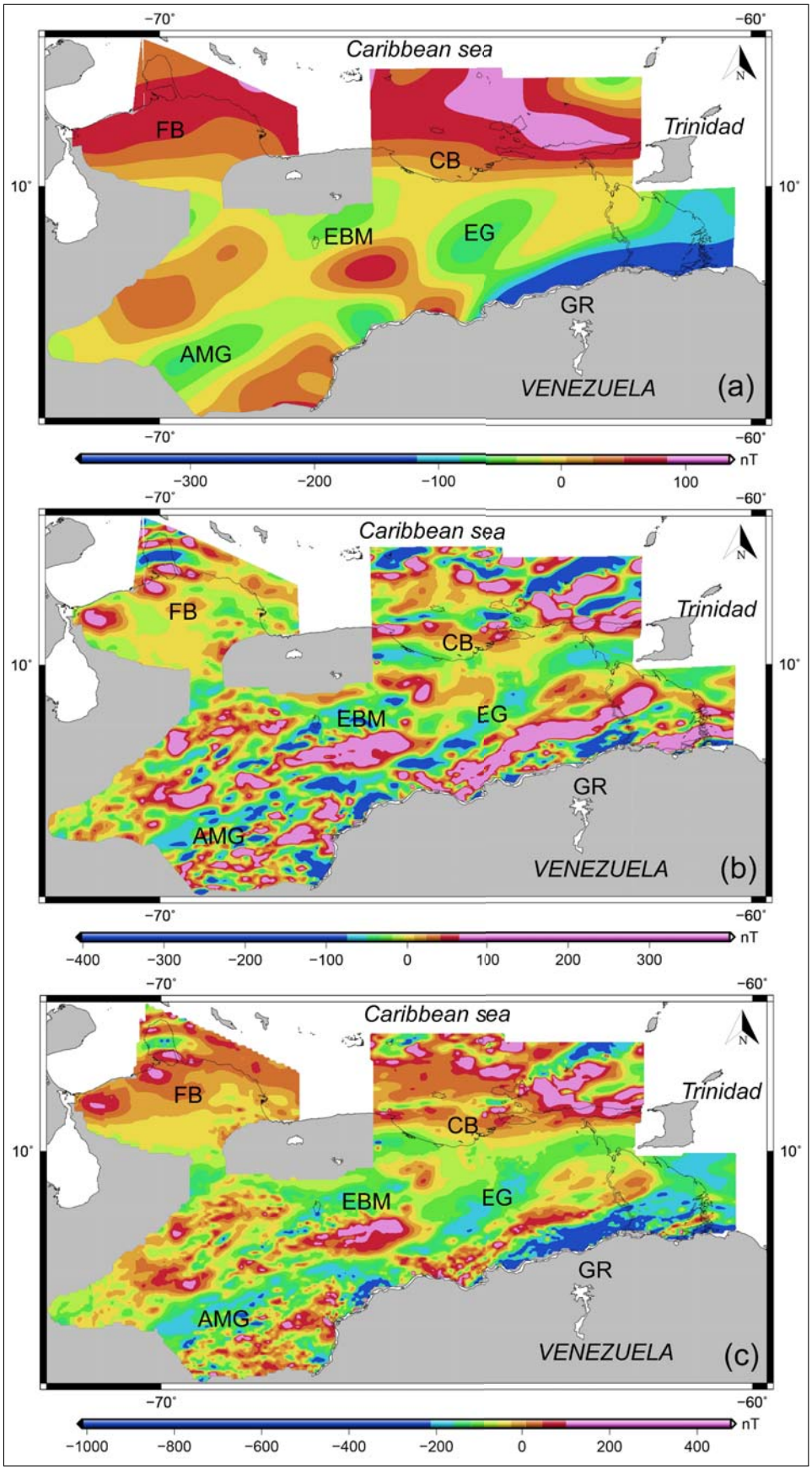

Figure 2.21 – Aeromagnetic maps over Venezuela from processed magnetic anomalies (Legend: (a) Long wavelength map, (b) Short wavelength map, (c) Total magnetic anomaly map); Acronyms: FB=Falcón Basin, AMG= Apure-Mantecal Basin, EG= Espino Graben, CB=Cariaco Basin, EBM= El Baúl Massif, GR= Lake Guri)

2.5.1.2 Short wavelength magnetic anomaly map

From west to east, we distinguish four major magnetic provinces from the short wavelength magnetic anomaly map:

1) The first province is characterised by a zone of low gradient, and negative magnetic anomalies that range from -50 nT to 0 nT on average and that is related to the Falcón Basin (see 'FB' in 'b', Fig. 2.21). We observed a sequence of magnetic highs in this province from south to north, bounding the western coastline of the Falcón state, and that we relate with the igneous magnetic sources, interpreted previously by Baquero et al. (2015) and Urbani et al. (2013). Two elongated magnetic highs with WE direction and a maximum amplitude of 200 nT entirely cross the Paraguaná Peninsula. In the Falcón Basin, we observe a continuous pattern of these anomalies to the west. We propose that shallowing of the igneous bodies at the west of the Falcón Basin produces these anomalies and that the magnetic sources that produce them may extend to the east of the basin;

2) The second magnetic province is characterized by a zone with high content of short wavelengths which amplitude is ranging between -400 and 200 nT and with preferential orientation N85°E approx. We relate the narrow and elongated anomalies to the Barinas-Apure Basin and El Baúl Massif (see 'AMG' and 'EBM' in 'b', Fig. 2.21). Compared with the total magnetic anomaly map, this map better illuminates the magnetic signature associated to the Apure-Mantecal Graben, which is characterized by a sequence of negative magnetic anomalies whose amplitude oscillates between -150 and -300 nT, with preferential orientation SW-NNE, and whose wavelengths become larger from west to east. Local igneous intrusions, thermal activity, tectonics or a combination of them might be responsible for the very short wavelengths observed in the Barinas-Apure Basin;

3) The third magnetic province is composed of a negative magnetic corridor that extends from the west boundary of the Espino Graben and goes farther to the east offshore (see 'EG' in 'b', Fig. 2.21). The magnetic structures in this province have a similar orientation to the main structures observed in the province '2' and that we relate to the Venezuelan Eastern Basin. Although, the absence of short wavelengths and the low amplitude of the anomalies suggests that the geological evolution and possibly the nature of the magnetic basement of this area differ from those typical of the Barinas-Apure Basin. Thus, it is expected a deeper depocenter for the basin respect to the Barinas-Apure Basin. Additionally, it is unavoidable to consider that the Espino Graben, present in this province, records the Pangea rifting history. Therefore, on the southern flank of the Espino Graben, there is large chronological record that ranges between the Precambrian, with rocks of the Guiana craton (where the basement is outcropping) and the Paleozoic, proposed age for the magnetic basement of the Eastern Venezuelan Basin, which depocenter reaches up to 10-13 km depth (García-Reyes, 2009; Rodriguez Millan, 2014, citing just a few.). The presence of the magnetic signature associated to the Espino Graben in the long wavelength map and the short wavelength map

suggests that this structure is profound and involves the deep crust;

4) The last province identified is characterized by positive magnetic anomalies mostly located to the north of the plate boundary and that we relate to the island-arcs described in this area (see 'CB' in 'b', Fig. 2.21). Two negative magnetic anomalies located to the north of the Ensenada de Barcelona and which constitutes a magnetic depression describes well the two depocenters of the Cariaco Basin. Farther to the north, we associate three elongated negative magnetic bands with the south of the Grenada Basin, among others.

2.5.1.3 Frequency histogram analysis

The frequency histogram of the total magnetic anomalies shows a unimodal distribution with slightly negative skew, from which it is not possible to differentiate the continental from the oceanic magnetic crust (see Fig. 2.22).

On the contrary, the frequency histogram of the long wavelength magnetic anomalies shows a bimodal distribution. This bimodal distribution can be due to the presence of continental and oceanic plates over the area. Here we associate the distribution of long wavelengths mainly composed by negative magnetic anomalies with those located over continental areas; on the other side, we associate the distribution of long wavelengths composed by positive magnetic anomalies to the broad plate boundary between the southern Caribbean plate and the northern South American plate.

The short wavelength frequency histogram shows a unimodal and symmetrical distribution well-correlated with the total magnetic anomaly frequency histogram; this behaviour is expected due to the fact that shallowest magnetic sources have the main contribution on the magnetic anomalies and hide the frequency distribution of the long wavelength magnetic anomalies.

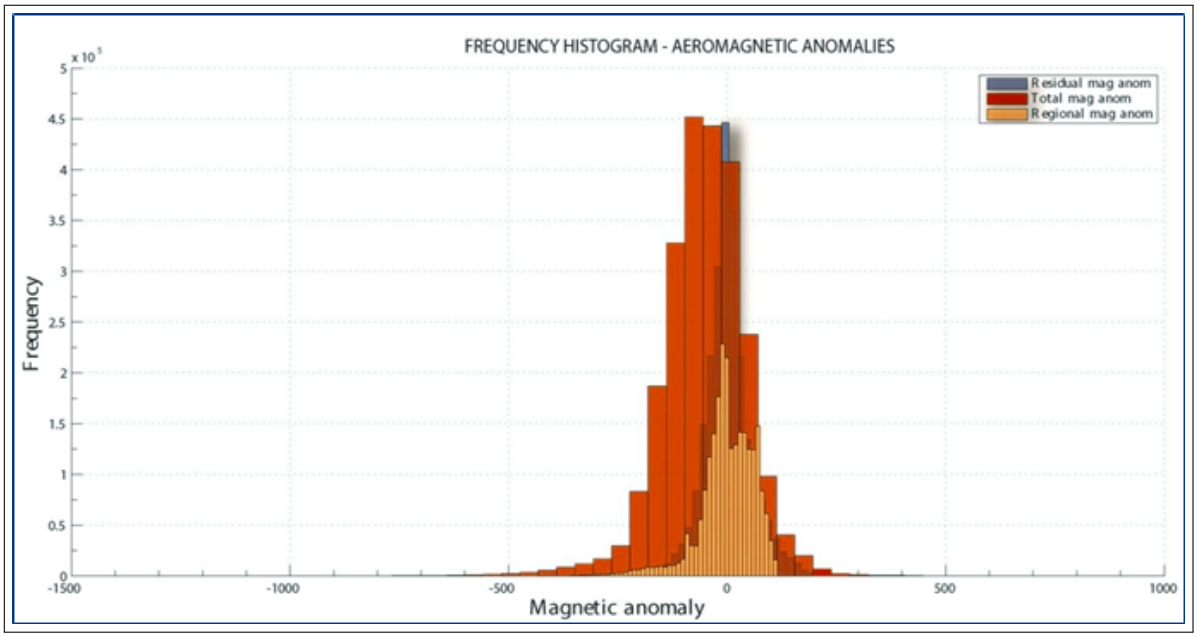

Figure 2.22 – Frequency histogram from aeromagnetic data

2.5.2 Compiled database

We present a reprocessed magnetic anomalies database covering the Caribbean plate and the Gulf of Mexico. We obtained this database from total magnetic field measurements using only marine data for offshore areas and airborne data over the northern part of the Venezuelan territory. In marine areas, the range of the processed magnetic anomalies is about 1.382 nT showing a significant decrease with respect to the range of the NCEI/IFREMER magnetic anomalies (see Table. 2.3).

We observed significant improvement in the statistics of the dataset over the marine total magnetic anomalies standard deviation which decreased from 836 nT before the processing to 81 nT after the processing. Also, the standard deviation of the aeromagnetic anomalies diminished from 142 nT to 77 nT.

Long wavelength magnetic anomalies present a standard deviation equal to 33 nT which is lower than the standard deviation of 90 nT exhibited by the short wavelength magnetic anomalies. These differences may suggest that more diverse magnetic sources affect the short wavelengths. The resultant dataset has a mean of -30 nT, a standard variation of 86 nT and a range of 3022 nT.

Table 2.3 – Basic statistics of magnetic anomalies before and after their reprocessing

Type	λ	Status	min	max	mean	Std. Dev.	Range
M	< 2500	Before	-9759	9809	-6,78	832,52	19568
A	< 2500	Before	-1486,50	641,56	-199,3	141,78	2128
M	< 2500	After	-714	667,74	-17,07	81,24	1382
M	2500-300	After	-166,49	309,40	-2,94	33,30	475,90
M	< 300	After	-214,37	186,38	18,66	89,63	400,80
A	< 2500	After	-2353,80	1367,10	0,93	76,59	3721
C	< 2500	Merged	-2353,80	-667,74	-30,24	85,81	3022

M= marine data, A= airborne data, C= combined data, λ= wavelength in kilometres. Min, max, mean, std. dev., and range are in nanotesla unit.

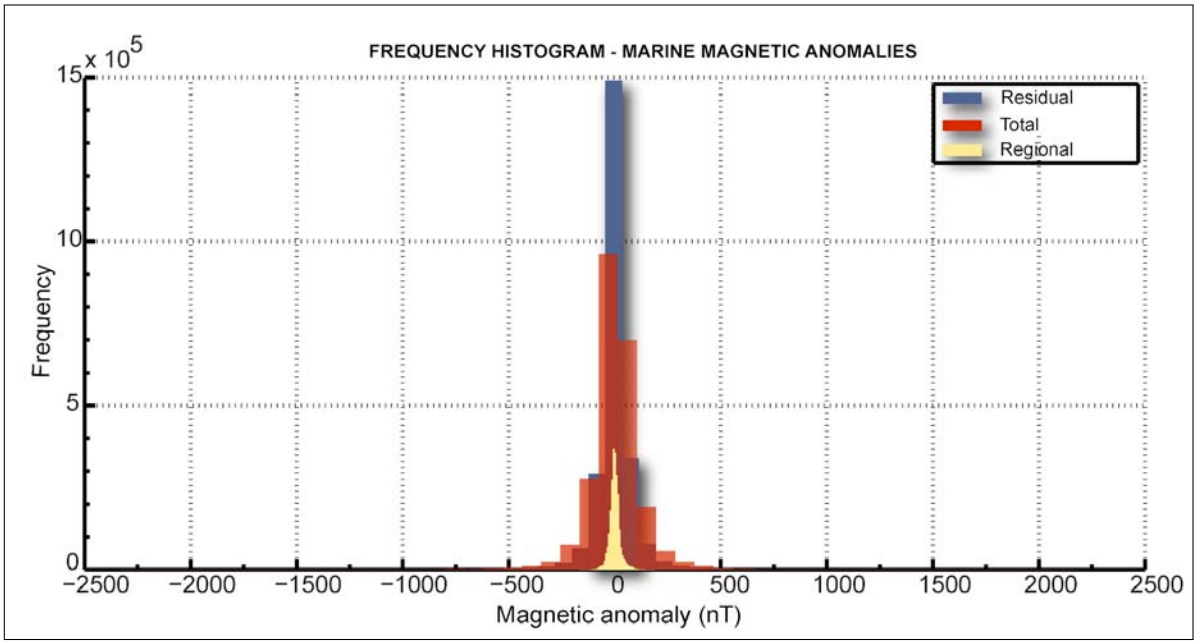

Figure 2.23 – Frequency histogram of magnetic anomalies before and after processing

2.5.3 Marine magnetic anomalies

The total magnetic anomaly map of the Caribbean plate and Gulf of Mexico region (see Fig. 2.24) comprises wavelengths less than 2500 km and compiles marine data over the Caribbean plate and the Gulf of Mexico and airborne data over the northern part of the Venezuelan territory. Below is our general interpretation of the magnetic domains identified on the map. Our interpretation makes particular emphasis in the Caribbean.

2.5.3.1 Caribbean domain and surroundings

Below we show the magnetic domains identified within the total magnetic anomaly map:

1. Atlantic Ocean and Pacific Ocean: We associate the first and most evident pattern with

the seafloor spreading structures located over the Pacific Ocean domain (e.g., Nazca and Cocos plates) and the Atlantic Ocean domain (e.g., North American plate). As expected, linear magnetic anomalies of high amplitude and produced by the extrusive layer of the seafloor characterize those oceanic areas.

2. **Yucatán Block and Florida Block:** Excluding the pattern associated with purely and well-known oceanic structures, we recognize a second pattern related to the contrast between allocthonous continental crust and the surrounding oceanic crust. In this sense, we relate a prominent block of positive magnetic anomalies to the Yucatán Block which signature towards the Gulf of Mexico allows defining the Continent-Ocean Boundary (COB) in the Southern Gulf (see Chapter 3 for further explanation).

3. **Western Caribbean and surroundings:** Within the Western Caribbean, positive magnetic signature and wavelengths shorter than those observed over the continental blocks characterize active island-arcs. We interpret the group with linear and parallel magnetic anomalies in the Colombian Basin as related to seafloor spreading. The second group consists of linear, not parallel, and segmented or often isolated magnetic anomalies, that we interpret as the result of the transcurrent tectonic (e.g., linear magnetic anomaly along the Hess escarpment or along the Beata Ridge). We associate a third group of shorter, linear and parallel marine magnetic anomalies over the Cayman Ridge to seafloor spreading, as suggested by other authors (e.g., Leroy et al., 2000). Finally, we point out the existence of a positive magnetic anomalies belt that fringes the limits of the western Caribbean plate which is of particular interest because of its marked and prominent character, as can be observed in the long wavelength map (see Fig. 2.25). Counil et al. (1989) associated these positive magnetic anomalies with fast subduction zones to the south, but its northern part can be related to the allochthonous blocks of continental nature (see Chapter 4 for further explanation).

4. **Eastern Caribbean:** We relate two N-S positive magnetic structures which enclose the Venezuelan Basin to the Beata Ridge and the Aves Ridge, respectively. Both on the Venezuelan Basin and on the Lesser Antilles, the magnetic anomalies show lateral variations from west to east and also from north to south possibly, revealing the magnetic heterogeneity of the plate. Positive marine magnetic anomalies ranging between 30 nT to 70 nT mark the Lesser Antilles, the Anegada Passage, Puerto Rico and Hispaniola Islands. The magnetic pattern that we observe in the Venezuelan Basin will be discussed in Chapter 4.

5. **Subduction zone:** In the Middle American Trench, we identify a positive marine magnetic pattern with amplitudes ranging between 40 nT and 60 nT. This pattern parallels the Oaxaca and Chiapas terranes. Farther north, offshore Yucatán and Chortis blocks we identify an elongated magnetic pattern of positive magnetic anomalies higher than 70 nT with N70°W trend (see '4' in Fig. 2.24), that we relate to the

prolongation offshore of the continental rocks of the Yucatán and western Chortis blocks. The eastern section of this domain correlates with the smooth-rough boundary delineated by seamount chains as proposed by Hey (1977). Clark et al. (1985) and Vasicek et al. (1988) proposed that magnetization contrasts between the cold oceanic slab and the surrounding hotter, nonmagnetic mantle produced those anomalies.

6. **North Andean subduction domain:** The North-Andean-Trench correlates with an elongated and segmented corridor of negative magnetic anomalies, with NS preferred orientation that parallels the continental margin. We observe that the magnetic signature of the North-Andean-Trench differs from the magnetic signature of the Middle-American-Trench. The observed differences are maybe due to differences in the geometry of subduction but also to the properties of the subducted slab mentioned above.

The correlation of this map with the most relevant geological and tectonic structures of the Caribbean plate and the Gulf of Mexico serves as first validation test and proves the consistency of the results.

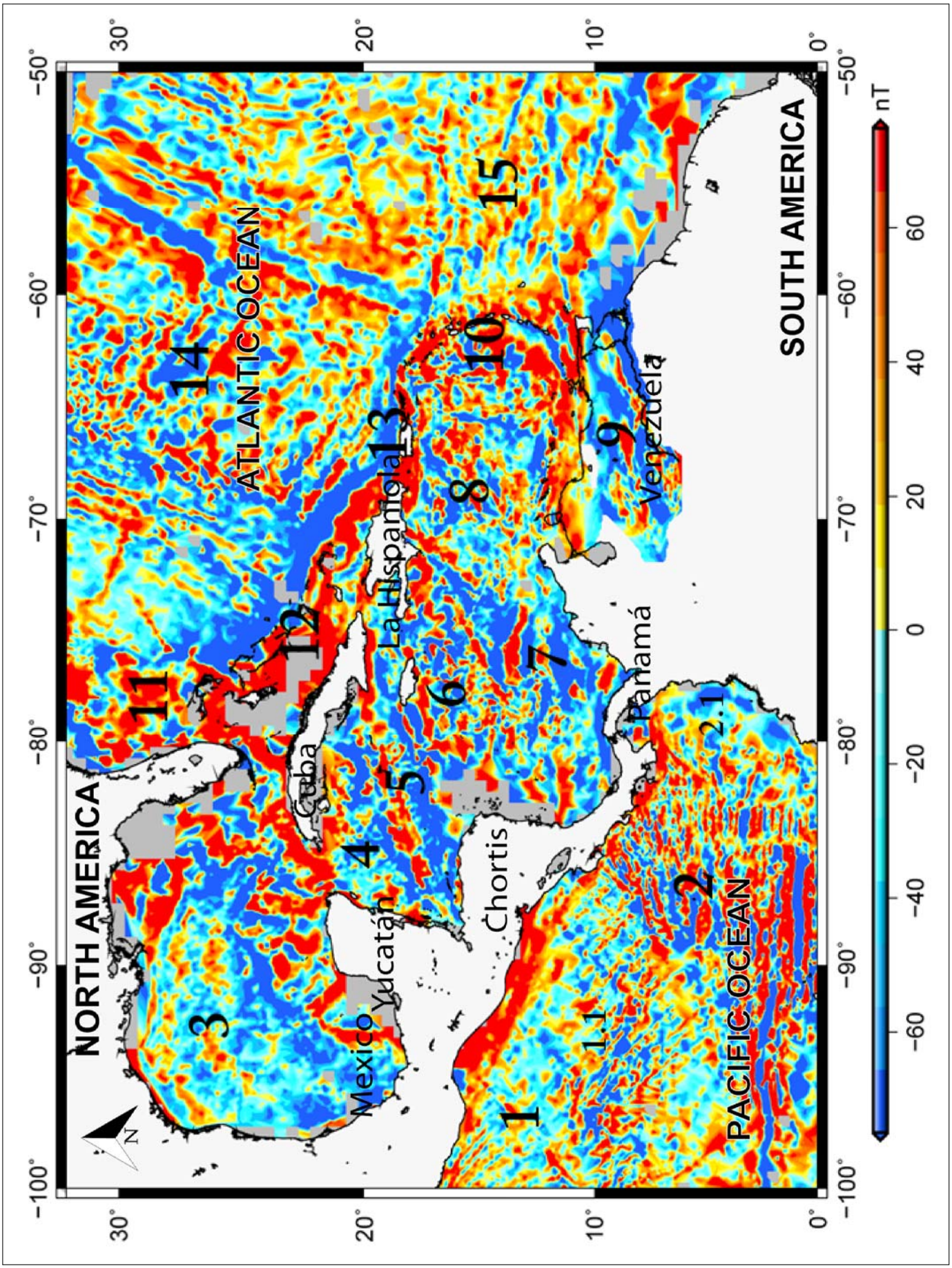

Figure 2.24 – Total magnetic anomaly map

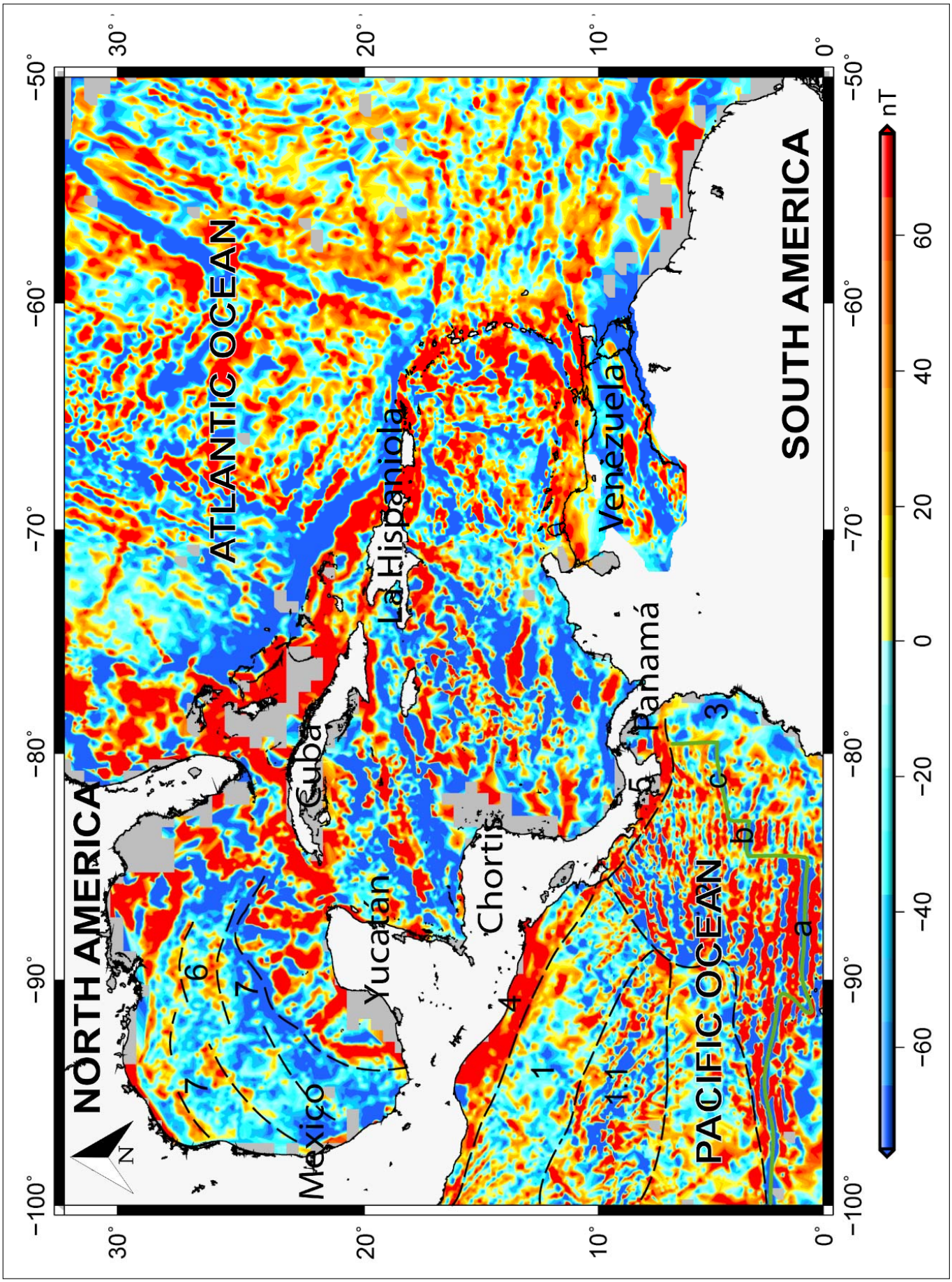

Figure 2.25 – Short-wavelength magnetic anomaly map

2.5.4 Comparison of the long wavelength map with previous works

In this section, we compare the long wavelength magnetic anomaly map obtained in this study with the long wavelength magnetic anomaly maps from the WDMAM v.2.0 compilation, MF7 model, and the GRIMM-L model respectively (see Fig. 2.26). The strong positive magnetic anomalies belt that surrounds the Middle American Trench seems to contour and delimit the Caribbean domain. This belt is a prevalent feature in all the maps. We interpret the high amplitudes observed along this belt as possibly created by the natural high magnetization of the continental blocks. Moreover, the magnetic belt seems to be continuous along the active island-arcs (e.g., the Greater Antilles and the Lesser Antilles) in our map and within the MF7 map. However, the continuity of magnetic belt along La Hispaniola and Puerto Rico islands is less clear in the WDMAM map, and is not observed on the map produced using GRIMM-L data. Instead, we observe a negative corridor NS between La Hispaniola and the Puerto Rico islands.

In both our and MF7 maps, the centre of the Gulf of Mexico is marked by a magnetic low produced by the contrast between oceanic and continental crust of the Yucatán Block, as reported in the previous section. Our map seems to better resolve the long wavelength structures in the North Atlantic and Pacific oceans. This good result over oceanic areas makes us confident about the magnetic patterns observed within the Caribbean plate and that are described below.

Along the Cayman Ridge, the magnetic signature on our map seems similar to MF7. On the other side, the Nicaragua Rise looks problematic since the four maps show very different patterns. Within the plate, GRIMM-L exhibits anomalies that are mostly elongated NS, suggesting an influence of the satellite orbits or the filtering used during the processing. We observe a similar pattern on the Venezuelan Basin between MF7 and our dataset.

Neither the Aves Ridge nor the Beata Ridge appear as a North-South prominent magnetic anomaly. The differences observed in the four maps in the inner Caribbean plate are significant and might be due to the data used and the applied processing method.

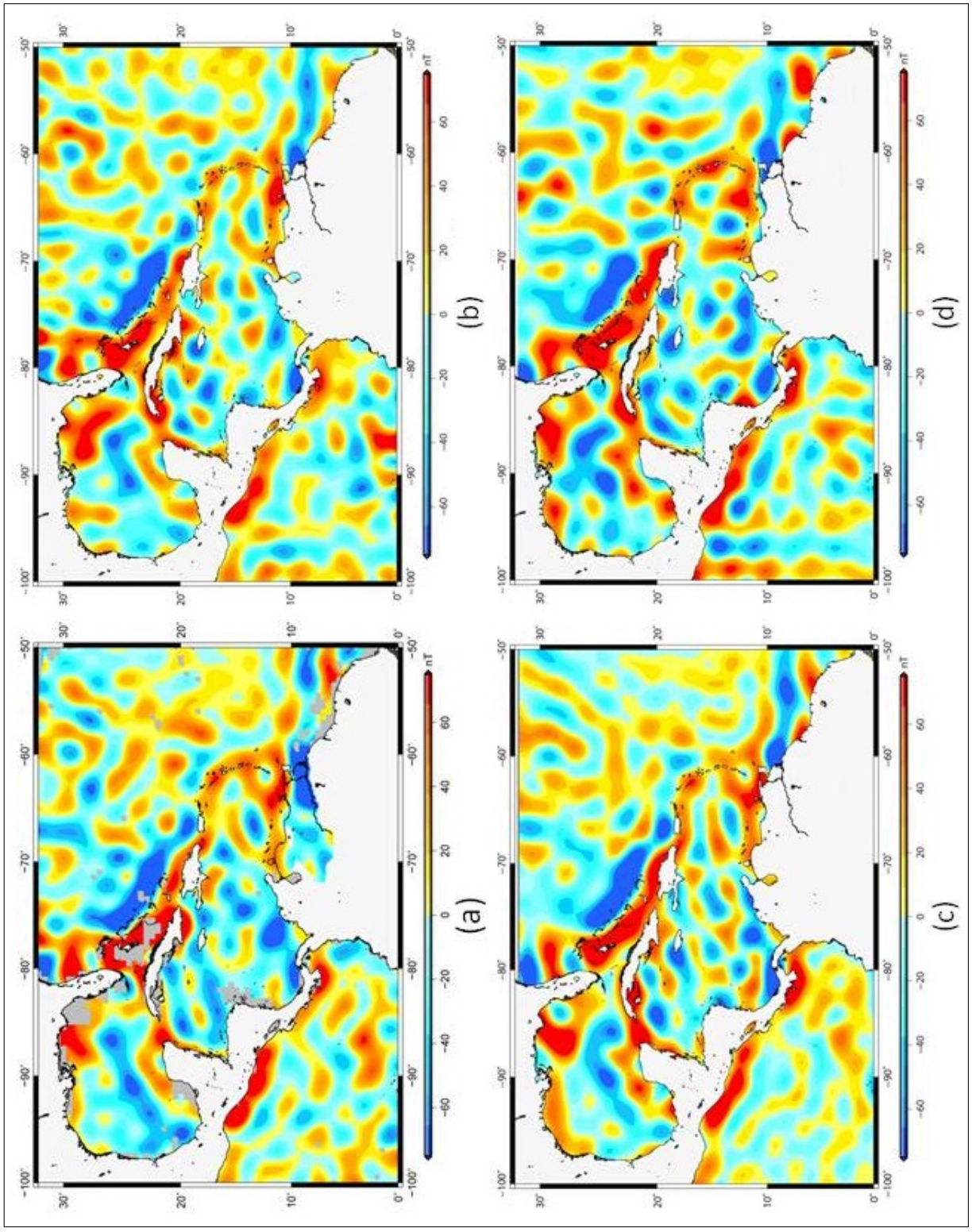

Figure 2.26 – Long wavelength magnetic anomaly maps (a: Reprocessed magnetic anomalies, b: WDMAM, c: MF7, d: GRIMM-L)

2.5.5 Comparison of the short wavelength map with previous works

In this section, we compare the short wavelength magnetic anomaly map obtained in this study with its homologous maps from the WDMAM v.2.0 compilation and NAMAM respectively (see Fig. 2.27). Over the Pacific domain, the WDMAM v.2.0 exhibits a similar pattern to our map, although linear features associated, with the Galápagos rift, the Panamá rift within the Nazca plate, and the smooth-rough boundary within the Cocos plate are better defined in our map, as can be observed on Fig. 2.27.

The magnetic response of the Yucatán Block has a similar signature in the three datasets. Further details are given below, where a comparison between maps is held of the Yucatán Basin, the Nicaragua Rise and the Eastern Caribbean.

2.5.5.1 Short-wavelengths on the Yucatán Basin

The Yucatán Basin is bounded in the west by the eastern part of the Yucatán Block, in the east by the southern part of the Cuba Island and, in the south by the Cayman Ridge. Positive magnetic anomalies appear on both NAMAM and our map; but not on the WDMAM, whereas the inner part of the basin is showing negative magnetic anomalies (see Fig. 2.28). West of this basin, Rosencrantz (1996) reported normal oceanic crust. The very short wavelength anomalies observed over the NAMAM do not correlate with the dominant magnetic pattern. They may be the signature of marine tracklines along which the anomalies were not properly levelled. The WDMAM does not show such artifacts in the inner basin, maybe because of its spatial resolution; however the linear magnetic anomalies associated with the Cayman Ridge or those surrounding the Jamaica Island are not as well observed as in our map. We observed substantial differences north of Jamaica: whereas our map and NAMAM are showing a negative magnetic anomaly, the WDMAM does not show any significant magnetic low.

2.5.5.2 Short-wavelengths on the Eastern Caribbean plate

A pattern of curved positive magnetic anomalies, concave to the west, characterizes the Lesser Antilles. This pattern constitutes the western boundary of the Caribbean plate (see Fig. 2.29). We observe a similar magnetic signature in NAMAM and WDMAM, but several artifacts on NAMAM make difficult a proper reading. Within the Grenada Basin, we observe an east-west pattern of magnetic anomalies over our processed map. The magnetic signature of the Grenada Basin is fuzzy on NAMAM and less defined over WDMAM. In general, the Aves Ridge appears as a quasi NS linear and segmented structure. The interpretation of the central and southern Aves Ridge is difficult at the west of the Grenada Basin because its linear pattern is missed (see Chapter 4 for further explanation).

2.5.5.3 Short-wavelengths on the Nicaragua Rise

The Nicaragua Rise is characterized by very short wavelengths magnetic anomalies with no preferential direction in both NAMAM and WDMAM (see Fig. 2.31). A linear pattern of parallel magnetic anomalies with direction approx. N20°W characterizes the lower Nicaragua Rise, suggesting an oceanic nature for this block (see Fig. 2.32). This linear pattern is neither clear on NAMAM nor WDMAM. The Northern Nicaragua Rise shows longer and stronger magnetic anomalies than the Southern Nicaragua Rise. The pattern observed over the Northern Nicaragua Rise may extend until the Jamaica Island. Because of the observed amplitude of the magnetic anomalies on the Northern Nicaragua Rise, we propose a continental nature for this crust (see Fig. 2.32). The linear magnetic anomaly related to the Hess Escarpment is also well defined in this map, including the linear and parallel magnetic anomalies within the Colombian Basin.

2.5.6 Validation of the dataset

2.5.6.1 Power spectrum of the magnetic anomalies

The power spectrum expresses the distribution of energy of a function (here the magnetic field) in the frequency domain. We must take in consideration that the power spectrum is only calculable over integrable functions, hence the function should be defined on the whole area of investigation. This condition is not always satisfied because of the lack in some places. Significant errors in estimation of the energy spectrum may occur if the dataset does not cover the totality of the area. Blank areas must be filled, either with another dataset or with synthetic 'data'. In the case of marine data, we can adopt an existing data to fill land areas.

The magnetic anomalies obtained in this study show higher energy than WDMAM at wavelengths ranging between approx. 2500 km and 370 km, and similar slope (see. Fig. 2.33). At the same scale, the energy of the GRIMM-L model is lower than the MF7 model but is similar to WDMAM at longer wavelengths. At wavelengths less than approx. 1000 km GRIMM-L shows more energy than MF7 and WDMAM. We calculated the radially averaged power spectrum for WDMAM and NAMAM, and also for our map at wavelengths less than approx. 300 km (see Fig. 2.34). The result shows that NAMAM power spectrum is lower at wavelengths between 285 km and 195 km. At wavelengths ranging between 195 km and 135 km the energy of NAMAM is similar to the energy of WDMAM and higher that the energy of the dataset produced in this work. Finally, for wavelengths less than 135 km WDMAM shows slightly more energy but similar slope than our map.

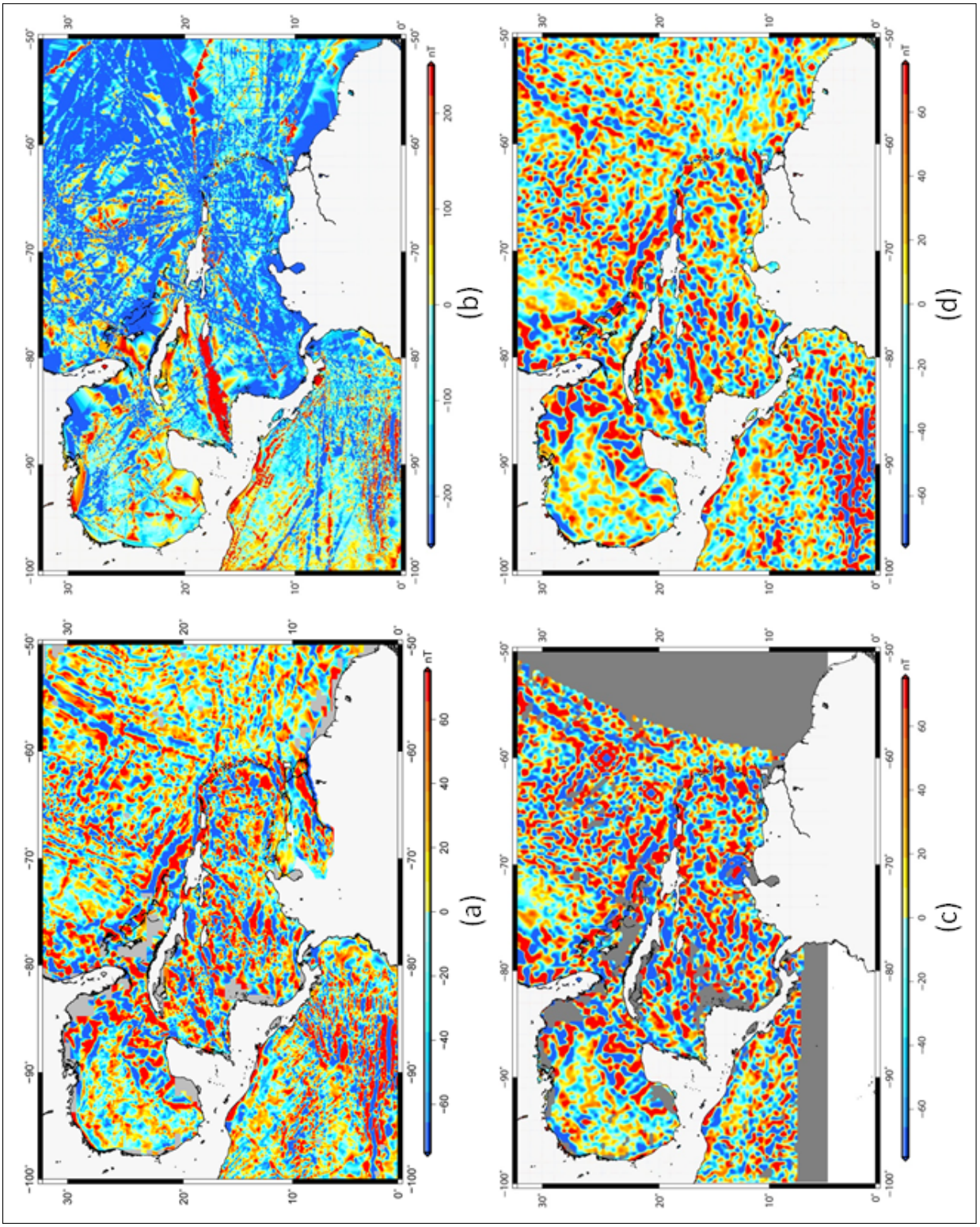

Figure 2.27 – Short wavelength magnetic anomaly maps. (a: Reprocessed magnetic anomalies, b: Processed by NGDC, c: NAMAM, d: WDMAM)

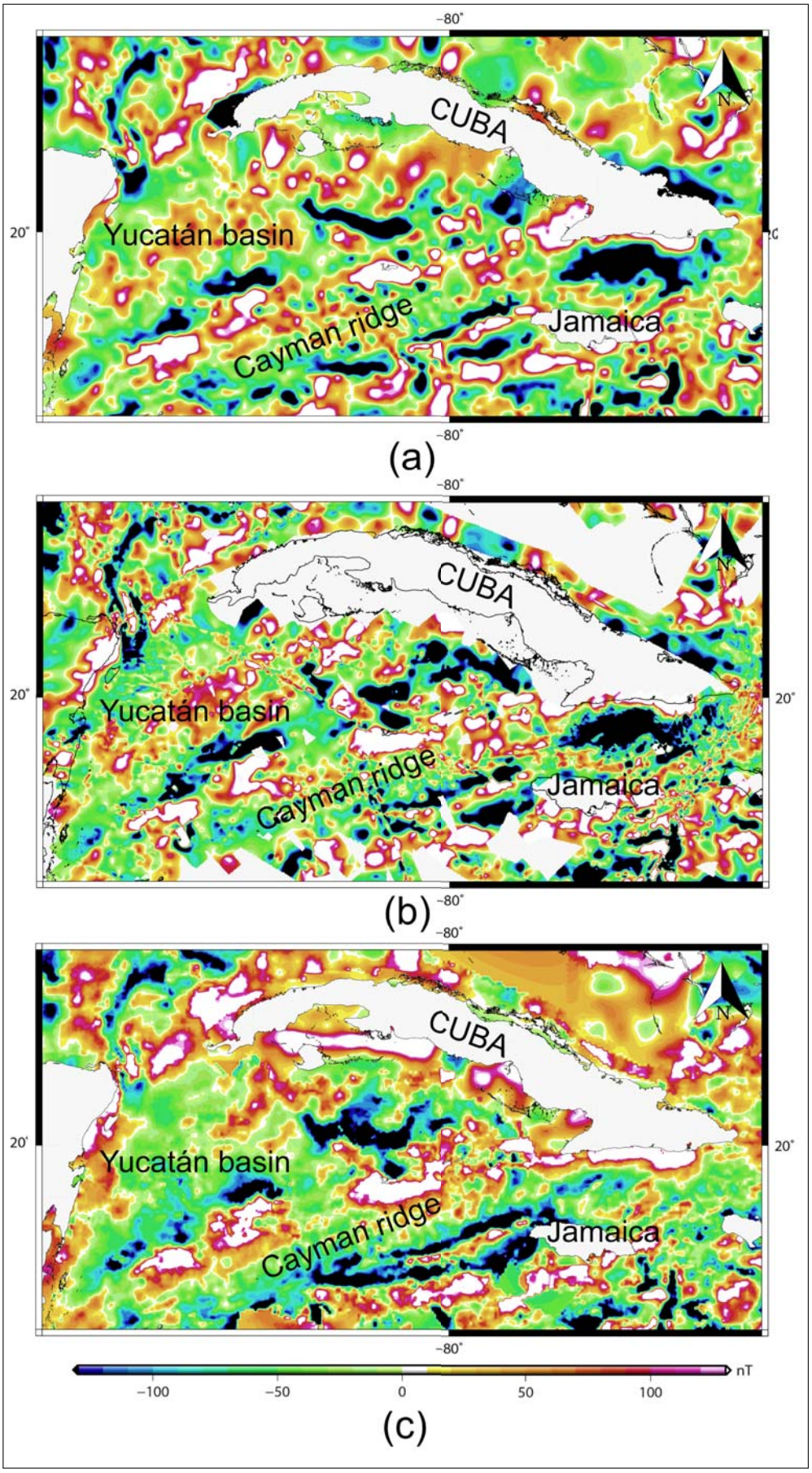

Figure 2.28 – Short wavelength magnetic anomaly map of Yucatán Basin. (a: Reprocessed magnetic anomalies, b: NAMAM, c: WDMAM)

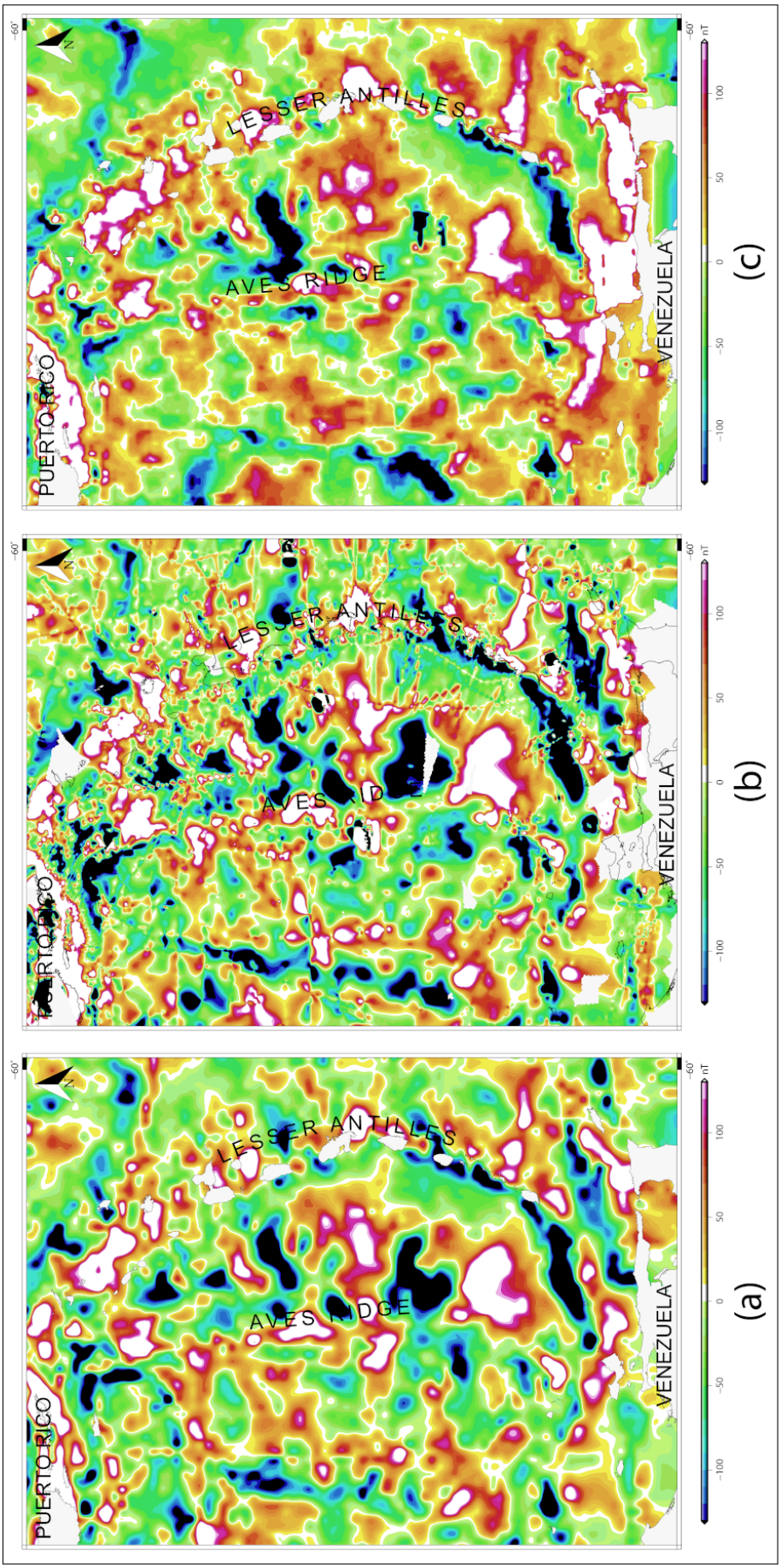

Figure 2.29 – Short wavelength magnetic anomaly map of Eastern Caribbean plate. (a: Reprocessed magnetic anomalies, b: NAMAM, c: WDMAM)

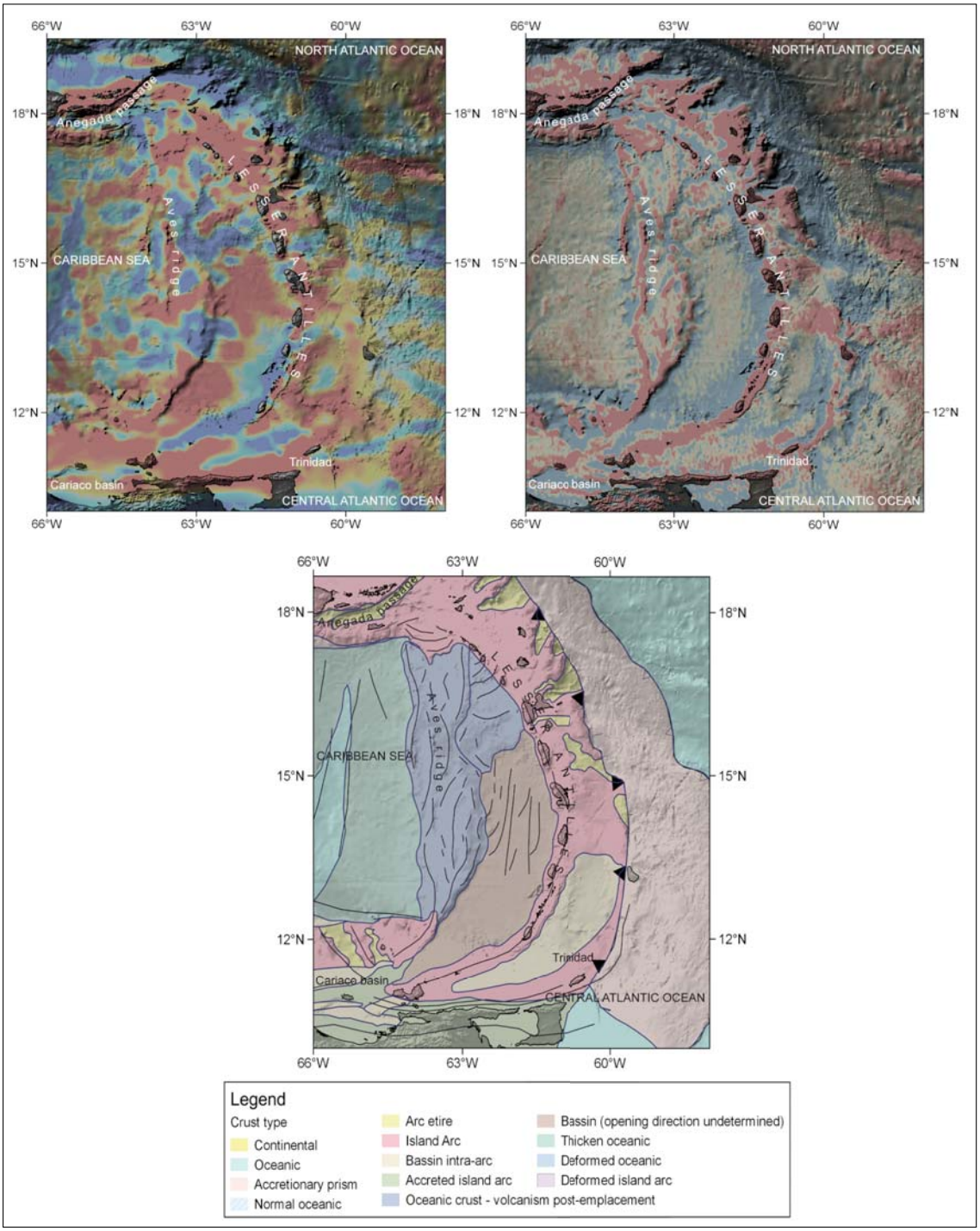

Figure 2.30 – Crust type in the Aves Ridge interpreted from potential field data

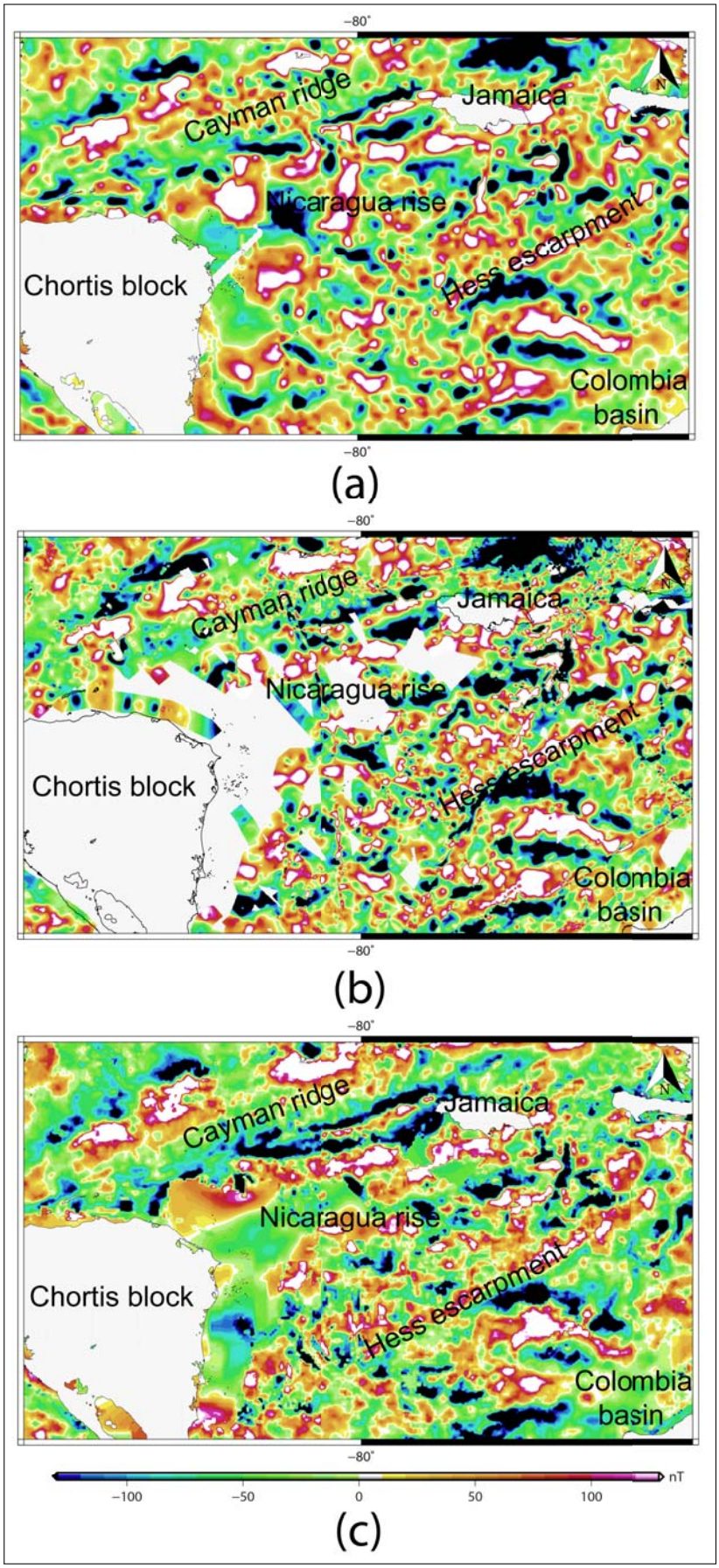

Figure 2.31 – Short wavelength magnetic anomaly map of Nicaragua rise. (a: Reprocessed magnetic anomalies, b: NAMAM, c: WDMAM)

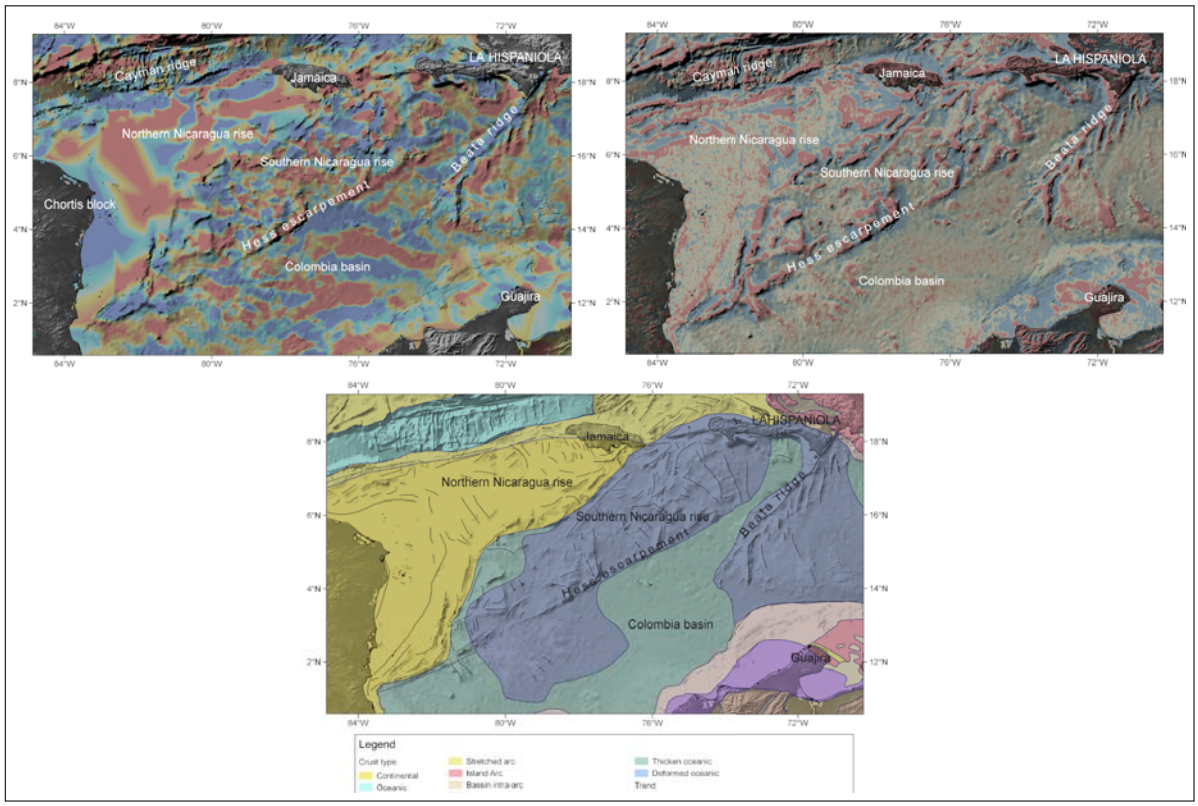

Figure 2.32 – Crust type in the Nicaragua Rise interpreted from potential field data

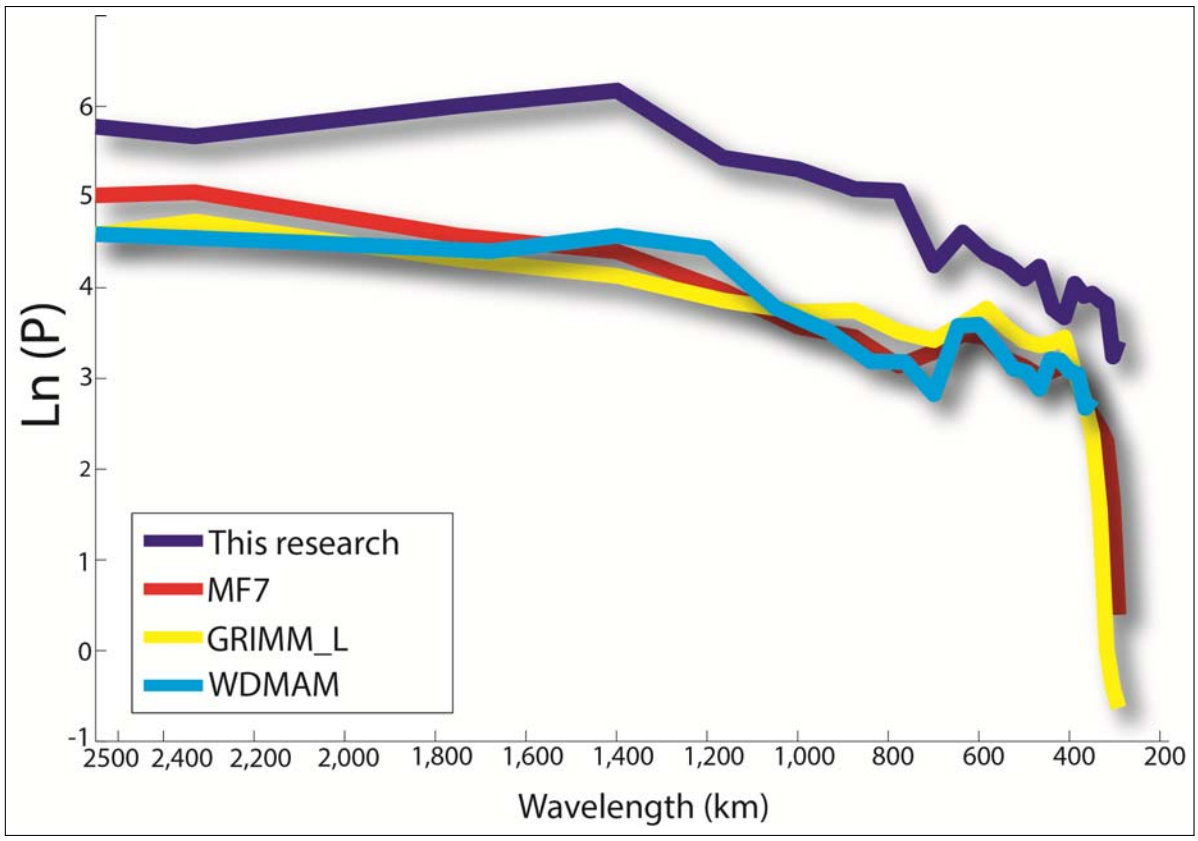

Figure 2.33 – Radially averaged spectrum of the magnetic anomalies for long wavelengths over the Caribbean region and the Gulf of Mexico

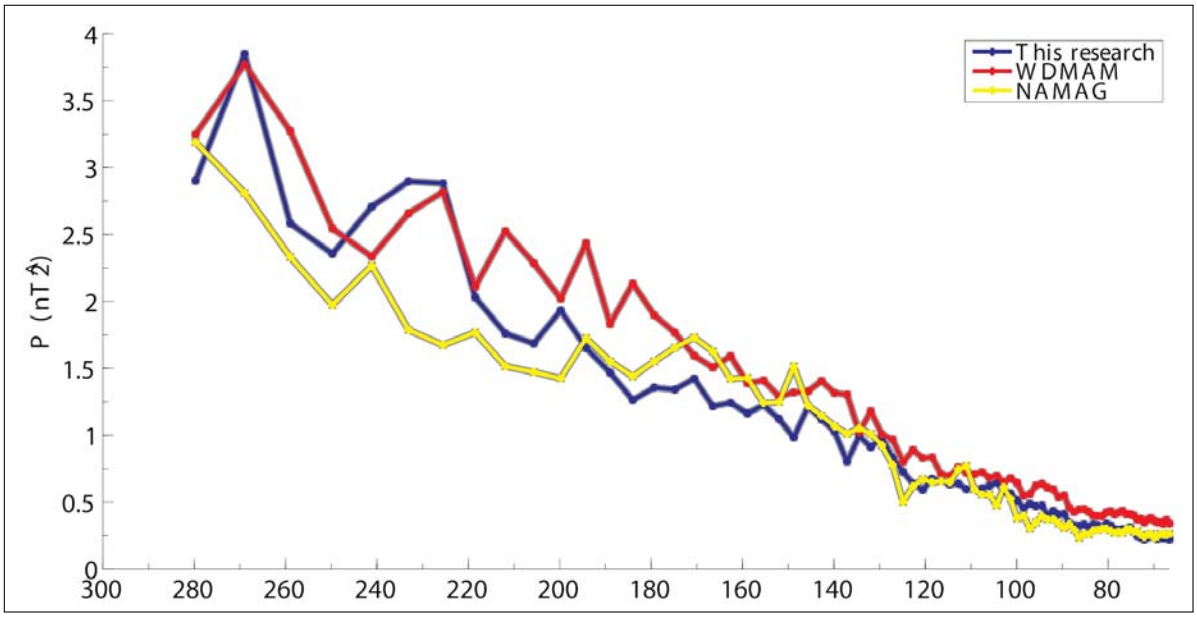

Figure 2.34 – Radially averaged spectrum of the magnetic anomalies for short wavelenghts over the Caribbean region and the Gulf of Mexico

2.5.6.2 Statistical validation: Principal component analysis on the magnetic anomalies and error ellipses.

We performed the principal component analysis over the GRIMM-L, MF7 and WDMAM datasets in order of spatially identify areas with significant discrepancies between these datasets. We can observe to the left of the Fig. 2.35, the plain view of the accumulated frequency of magnetic anomalies between two datasets, the error ellipses and also the eigen vectors, and to the right, the tridimensional view. Two datasets are correlated when the slope of the major axis of the ellipse is near 45°. In this test, the highest slope of the major axis of the ellipse was equal to 38,85°. We obtained it from the MF7 dataset and ours, indicating that MF7 dataset correlate better with our dataset. On the other hand, we obtained the lowest slope of the major axis of the ellipse from the WDMAM and our dataset and it is equal to 33,86°, thus, the WDMAM is spatially less correlated with our dataset.

We held a similar analysis for the long wavelengths (see Fig. 2.36) and for the short wavelengths (see Fig. 2.37) respectively. For the short wavelengths, we observe a more linear relationship between our dataset and NAMAM, while we observe a more disperse but quasi-ellipsoidal relationship for the WDMAM dataset. Regarding the long wavelengths, we observe a more linear relationship between the frequency of the magnetic anomalies of WDMAM and ours.

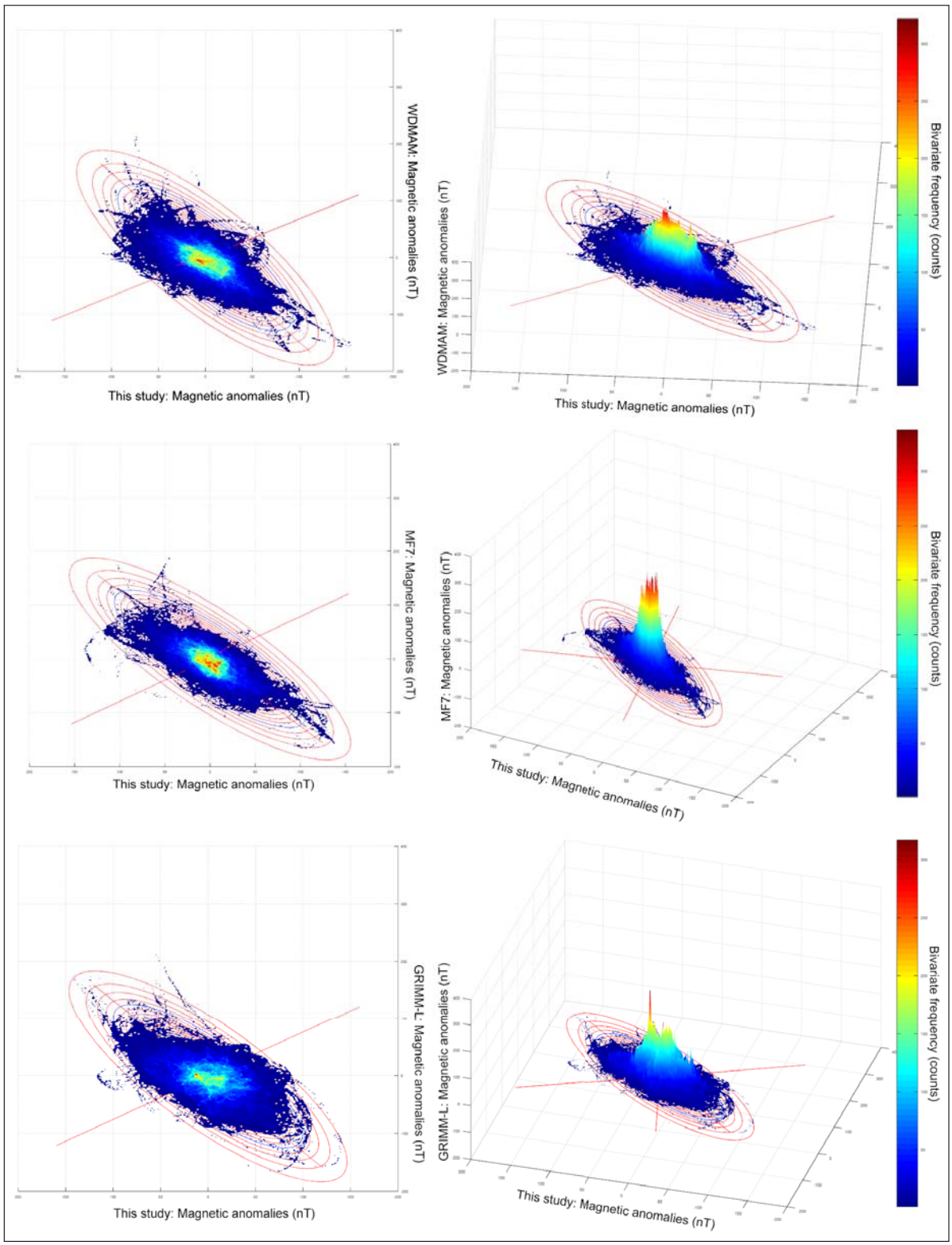

Figure 2.35 – Plain and tridimensional view of the bivariate frequency calculated from the magnetic anomalies of the GRIMM-L, WDMAM and MF7 datasets and the magnetic anomalies from this study in the Caribbean region and the Gulf of Mexico

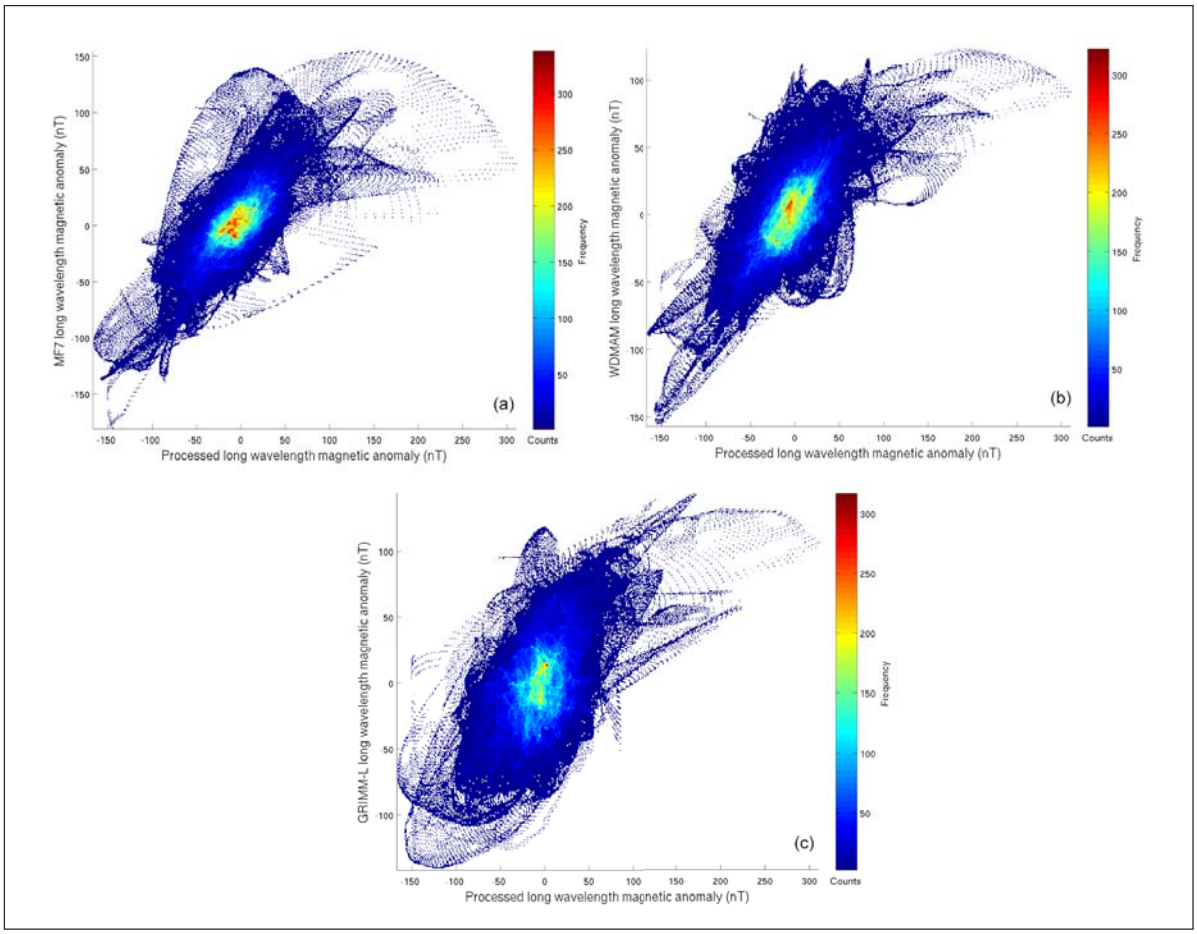

Figure 2.36 – Bivariate frequency from long wavelength datasets. (Using: MF7 (a), WDMAM (b) and GRIMM-L (c))

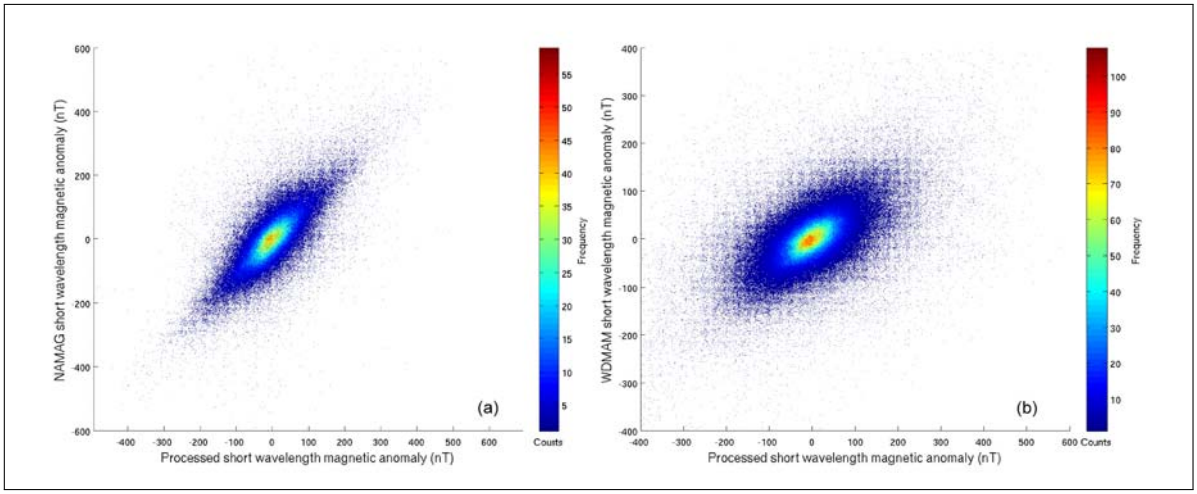

Figure 2.37 – Bivariate frequency from short wavelength datasets. (Using: NAMAG (a) and WDMAM (b)

For the long wavelengths, we plotted the measurements with discrepancies or lying outside the chosen confidence ellipse (see Fig. 2.38). In that sense, we observe that discrepancies are mostly located over the northern part of the Bahamas platform, over the eastern part of the Gulf of Mexico, in the Middle American Trench and offshore of the Panamá Arc. These discrepancies can be due to the lack of marine magnetic data on those areas, and hence, in our dataset. Both MF7 and GRIMM-L models, and WDMAM have data on land. The short wavelength discrepancies between NAMAM, WDMAM and our dataset are located mostly on the inner Caribbean plate: within the Colombian Basin, over the Cayman Ridge, the Lesser Antilles, the Greater Antilles and the Nicaragua Rise (see Fig. 2.39). The statistics show a significant reduction of the standard deviation in our dataset after detecting and excluding problematic measurements (see Table No. 2.4).

Table 2.4 – Statistics before and after the bivariate frequency analysis

RMS_error (before)	**RMS_error (after)**	**Std. dev. (before)**	**Std. dev. (after)**	**Model**	**Wavelength (km)**
27.06	23.63	34.98	30.28	WDMAM	2500-300
25.43	21.37	34.98	28.34	MF7	2500-300
33.04	30.75	34.98	31.03	GRIMM-L	2500-300
115.75	58.27	69.81	69.6	NAMAM	300
62.05	50.41	74.8	62.06	WDMAM	300

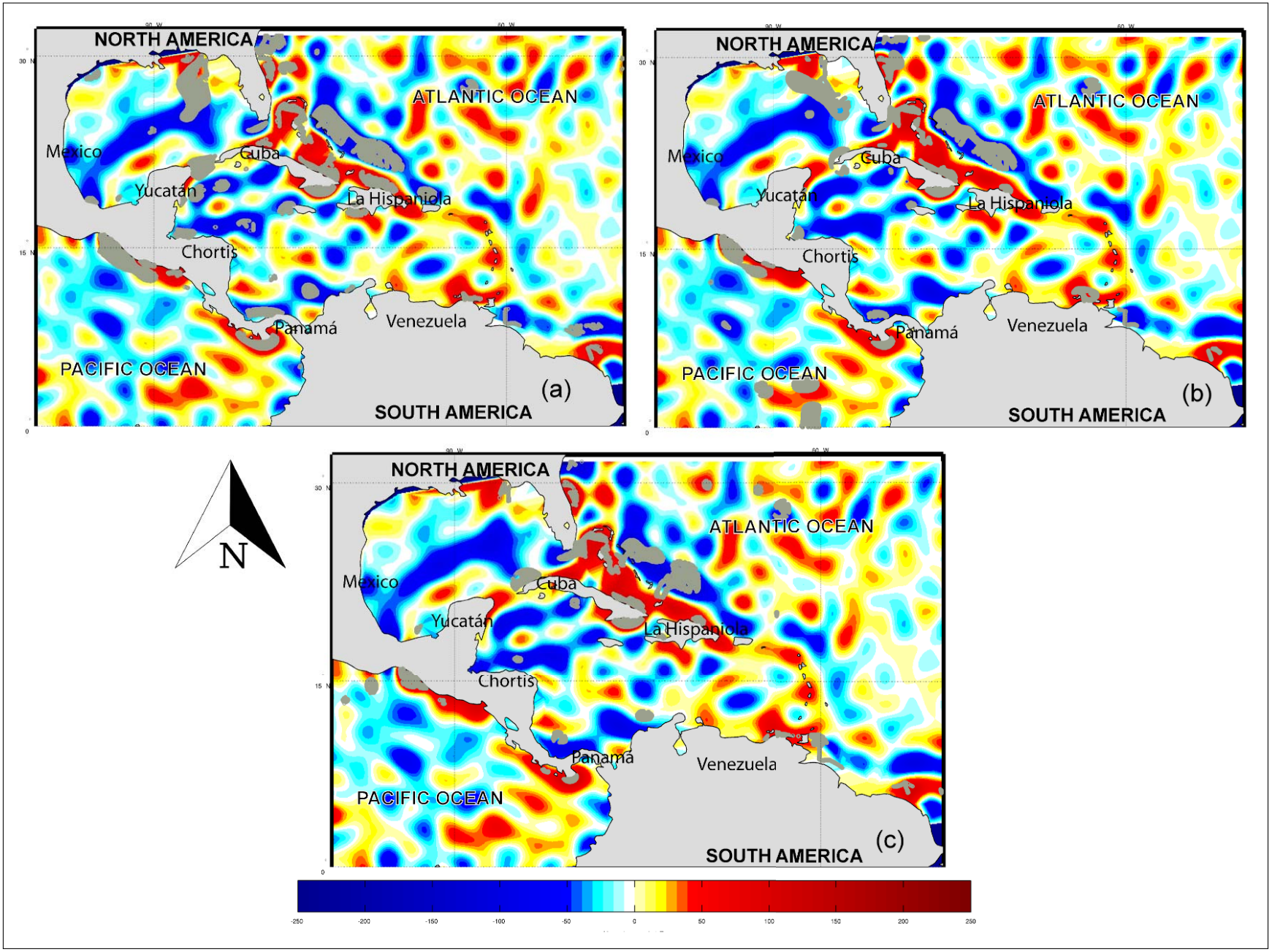

Figure 2.38 – Location of the discrepancies between previous datasets and the processed magnetic anomaly for long wavelengths (Using: MF7 (a), WDMAM (b) and GRIMM-L (c))

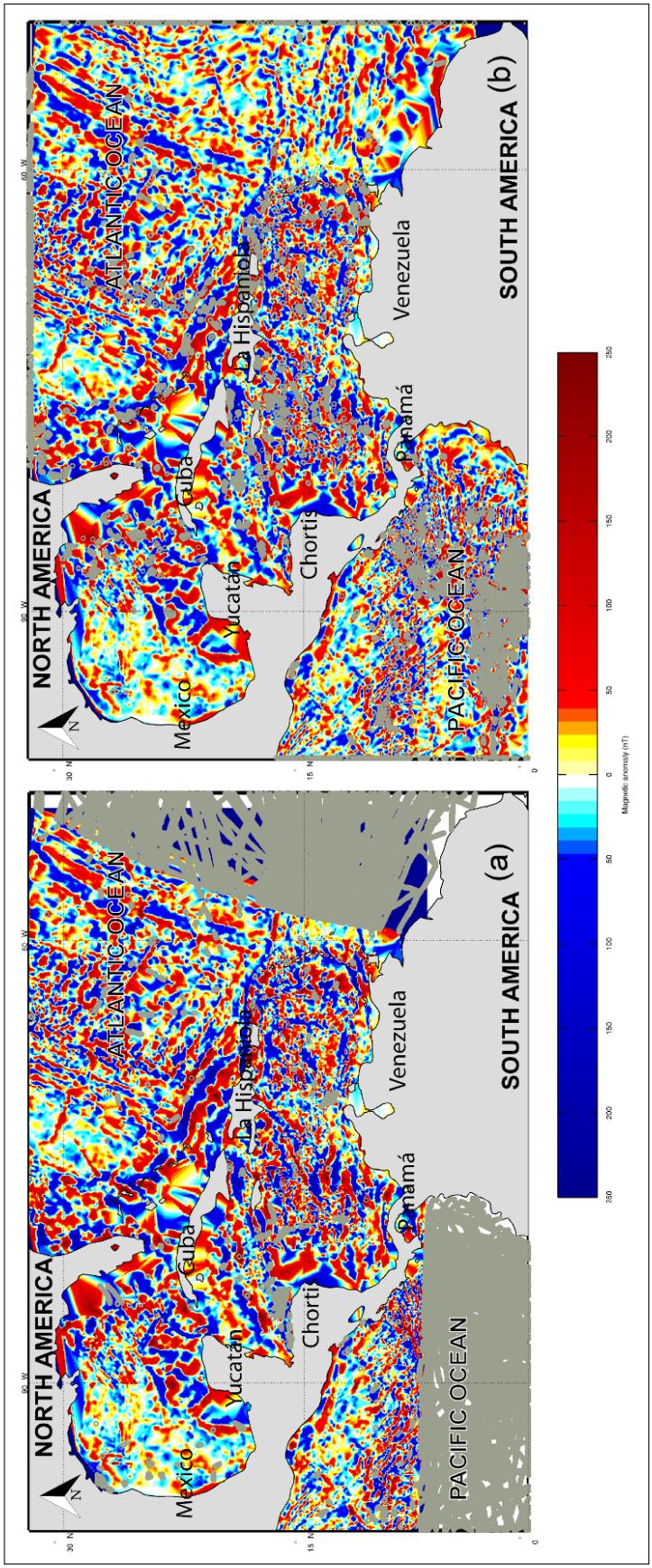

Figure 2.39 – Location of the discrepancies between previous datasets and the processed magnetic anomaly for short wavelengths (Using: NAMAG (a) and WDMAM (b)

2.6 Conclusions

Long wavelength magnetic anomalies present a standard deviation equal to 33,3 nT, lower than the standard deviation of 89,63 nT exhibited by the short wavelength magnetic anomalies. This difference suggests that more diverse magnetic sources affect short wavelengths magnetic anomalies.

We define the boundary zone between the Caribbean plate and the South American plate as a zone of sharp magnetic gradient located approx. at 10° of North latitude, which shows a quasi-linear and elongated pattern with orientation WE. Moreover, we interpret the increasing magnetic gradient from west to east along the Caribbean plate-South American boundary as a narrowing of the zone of interaction between the two plates from west to east, due to a greater influence of the plate convergence in the eastern part of the boundary. Within the Caribbean region, positive magnetic signature and wavelengths shorter than those observed over the continental blocks characterize active island arcs.

Due to the observed amplitude of the magnetic anomalies on the Northern Nicaragua Rise, we suggest a continental nature for this crust. Offshore Central America, the strong positive magnetic anomalies belt that surrounds the Middle American Trench seems to contour and delimit the Caribbean domain. This belt is a prevalent feature in all the long wavelength maps and may be produced by the natural high magnetization of the continental blocks.

In the Eastern Caribbean, we relate the remarkable NS positive magnetic anomaly north-west of Margarita Island, which curves to the south-west eastward of the island, to a deep geological structure possibly related to the Aves Ridge. The magnetic signature of the Grenada Basin is fuzzy on NAMAM and less defined over the WDMAM. In general, the Aves Ridge appears as a quasi NS linear and segmented structure. The interpretation of the central part of the Aves Ridge until its southern edge is difficult because its linear pattern is missed at the western part of the Grenada Basin.

Over the Venezuela territory, the absence of short wavelengths in the Eastern Venezuelan Basin and the low amplitude of the anomalies suggests that the geological evolution and possibly the nature of the magnetic basement of this area differ from the basement of the Barinas-Apure Basin. We interpret the Espino Graben as a structure that might involve the deep crust, from the magnetic signature associated to it in the long wavelength map and the short wavelength map. Also we propose that local igneous intrusions, thermal activity, tectonics or a combination of them might be responsible for the very short wavelengths observed in the Barinas-Apure Basin.

2.7 References

Abdel-Kader, K., El-Kabbani, A., Yahya, A., Soliman, F., Ismail, A., and Abdel-Maksood, A. (2017). A New Electronic Technique for Real-Time Correction of Heading and DC-

Shift Noises in Airborne Magnetic Data. *Journal of Multidisciplinary Engineering Science and Technology*, 4(6):7390–7396.

Bankey, V., Cuevas, A., David, D., Finn, C. A., Hernandez, I., Hill, P., Kucks, R., Warner, M., Pilkington, M., Carter, R., Rystrom, W., Shearer, V., Snyder, S., Sweeney, R., Velez, J., J.D., P., Ravat, D., et al. (2002). Digital data grids for the magnetic anomaly map of North America. *U.S. Geological Survey Open-File Report 02-414 U.S. Geological Survey Denver Colorado USA*.

Baquero, M., Grande, S., Urbani, F., Cordani, U., Hall, C., and Armstrong, R. (2015). New Evidence for Putumayo Crust in the Basement of the Falcon Basin and Guajira Peninsula, Northwestern Venezuela. In *AAPG Special Volumes*.

Beamish, D. et al. (2015). Levelling aeromagnetic survey data without the need for tie-lines. *Geophysical Prospecting*, 63(2):451–460.

Beard, L., Goitom, B., and Reidar, J. (2000). Interpretation of Low Latitude magnetic anomalies. *NGU Report, Geological Survey of Norway*, 2000:31.

Benaissa, M., Berguig, M., Doumbia, V., and Bouraoui, S. (2017). The equatorial electrojet (EEJ) current deduced from CHAMP satellite and ground magnetic measurements in West Africa. *Arabian Journal of Geosciences*, 10(15):329.

Bird, D. E., Hall, S. A., Casey, J. F., and Millegan, P. S. (1993). Interpretation of magnetic anomalies over the Grenada Basin. *Tectonics*, 12(5):1267–1279.

Blakely, R. J. (1983). Statistical averaging of marine magnetic anomalies and the aging of oceanic crust. *Journal of Geophysical Research: Solid Earth*, 88(B3):2289–2296.

Blakely, R. J. (1996). *Potential theory in gravity and magnetic applications*. Cambridge University Press.

Bouysse, P. (1988). Opening of the Grenada back-arc basin and evolution of the Caribbean Plate during the Mesozoic and early Paleogene. *Tectonophysics*, 149(1-2):121–143.

Bowin, C. O. (1968). Geophysical study of the Cayman Trough. *Journal of Geophysical Research*, 73(16):5159–5173.

Bullard, E. and Mason, R. (1961). The magnetic field astern of a ship. *Deep Sea Research (1953)*, 8(1):20–27.

Burger, H. R., Sheehan, A. F., and Jones, C. H. (2006). *Introduction to applied geophysics: Exploring the shallow subsurface*. WW Norton.

Cande, S. C. and Kent, D. V. (1992). Ultrahigh resolution marine magnetic anomaly profiles: a record of continuous paleointensity variations? *Journal of Geophysical Research: Solid Earth*, 97(B11):15075–15083.

Christeson, G. L., Mann, P., Escalona, A., and Aitken, T. J. (2008). Crustal structure of the Caribbean–northeastern South America arc-continent collision zone. *Journal of Geophysical Research: Solid Earth*, 113(B8).

Christofferson, E. (1973). Linear magnetic anomalies in the Colombia Basin, central Caribbean Sea. *Geological Society of America Bulletin*, 84(10):3217–3230.

Clark, S. C., Frey, H., and Thomas, H. H. (1985). Satellite magnetic anomalies over subduction zones: the Aleutian Arc anomaly. *Geophysical Research Letters*, 12(1):41–44.

Clifford, G. (2005). Singular Value Decomposition and Independent Component Analysis. *J. Biomedical and Image Processing*.

Counil, J.-L., Achache, J., and Galdeano, A. (1989). Long-wavelength magnetic anomalies in the Caribbean: Plate boundaries and allochthonous continental blocks. *Journal of Geophysical Research: Solid Earth*, 94(B6):7419–7431.

Dyment, J. and Arkani-Hamed, J. (1995). Spreading-rate-dependent magnetization of the oceanic lithosphere inferred from the anomalous skewness of marine magnetic anomalies. *Geophysical Journal International*, 121(3):789–804.

Dyment, J., Lesur, V., Hamoudi, M., Choi, Y., Thebault, E., Catalan, M., the WDMAM Task Force*, the WDMAM Evaluators**, and the WDMAM Data Providers** (2015). World Digital Magnetic Anomaly Map version 2.0. `http://www.wdmam.org`.

Ferré, E. C., Friedman, S. A., Martín-Hernández, F., Feinberg, J. M., Till, J. L., Ionov, D. A., and Conder, J. A. (2014). Eight good reasons why the uppermost mantle could be magnetic. *Tectonophysics*, 624:3–14.

Finlay, C., Maus, S., Beggan, C., Bondar, T., Chambodut, A., Chernova, T., Chulliat, A., Golovkov, V., Hamilton, B., Hamoudi, M., et al. (2010). International geomagnetic reference field: the eleventh generation. *Geophysical Journal International*, 183(3):1216–1230.

Friedman, S. A. (2015). *Investigation of the upper mantle as a source for contribution to magnetic anomalies*. Southern Illinois University at Carbondale.

Friis-Christensen, E., Lühr, H., and Hulot, G. (2006). Swarm: A constellation to study the Earth's magnetic field. *Earth, planets and space*, 58(4):351–358.

Fritsch, F. N. and Carlson, R. E. (1980). Monotone piecewise cubic interpolation. *SIAM Journal on Numerical Analysis*, 17(2):238–246.

García-Reyes, A. (2009). Mapas de anomalías de gravedad y magnetismo de Venezuela generados a partir de datos satelitales. *Dissertation. Universidad Central de Venezuela, Caracas*, 175:191.

Gee, J. S. and Kent, D. V. (2007). Source of oceanic magnetic anomalies and the geomagnetic polarity time scale. *Treatise on Geophysics, Vol. 5: Geomagnetism*, pages 455–507.

Ghosh, N., Hall, S., and Casey, J. (1984). Seafloor spreading magnetic anomalies in the Venezuelan Basin. *Geological Society of America Memoirs*, 162:65–80.

Golynsky, A., Chiappini, M., Damaske, D., Ferraccioli, F., Ferris, J., Finn, C., Ghidella, M., Isihara, T., Johnson, A., Kim, H., et al. (2001). ADMAP–Magnetic Anomaly Map of the Antarctic, 1: 10 000 000 scale map. *BAS (Misc.)*, 10:1109–1112.

Granot, R., Dyment, J., and Gallet, Y. (2012). Geomagnetic field variability during the Cretaceous Normal Superchron. *Nature Geoscience*, 5(3):220–223.

Guevara, N. O., García, A., and Arnaiz, M. (2013). Magnetic anomalies in the Eastern Caribbean. *International Journal of Earth Sciences*, 102(3):591–604.

Gutscher, M.-A., Spakman, W., Bijwaard, H., and Engdahl, E. R. (2000). Geodynamics of flat subduction: Seismicity and tomographic constraints from the Andean margin. *Tectonics*, 19(5):814–833.

Hamid, N., Liu, H., Uozumi, T., Yoshikawa, A., and Annadurai, N. (2017). Peak time of equatorial electrojet from different longitude sectors during fall solar minimum. In *Journal of Physics: Conference Series*, number 1 in 852. IOP Publishing.

Hamid, N. S. A., Liu, H., Uozumi, T., Yumoto, K., Veenadhari, B., Yoshikawa, A., and Sanchez, J. A. (2014). Relationship between the equatorial electrojet and global Sq currents at the dip equator region. *Earth, Planets and Space*, 66(1):146.

Hayes, G. P., Wald, D. J., and Johnson, R. L. (2012). Slab1. 0: A three-dimensional model of global subduction zone geometries. *Journal of Geophysical Research: Solid Earth*, 117(B1).

Herrero O., E. and Navarro, J. (1989). Mapa de anomalías magnéticas de Venezuela. *Direccion de Geologia*.

Hey, R. (1977). Tectonic evolution of the Cocos-Nazca spreading center. *Geological Society of America Bulletin*, 88(12):i–vi.

Horner-Johnson, B. C. and Gordon, R. G. (2003). Equatorial Pacific magnetic anomalies identified from vector aeromagnetic data. *Geophysical Journal International*, 155(2):547–556.

Hulot, G., Eymin, C., Langlais, B., Mandea, M., and Olsen, N. (2002). Small-scale structure of the geodynamo inferred from Oersted and Magsat satellite data. *Nature*, 416(6881):620–623.

Idárraga-García, J., Kendall, J.-M., and Vargas, C. (2016). Shear wave anisotropy in northwestern South America and its link to the Caribbean and Nazca subduction geodynamics. *Geochemistry, Geophysics, Geosystems*, 17(9):3655–3673.

Intermagnet (2017). International Real-time Magnetic Observatory Network. `http://intermagnet.org`. Accessed: January 23, 2017.

Ishihara, T. (2015). A new leveling method without the direct use of crossover data and its application in marine magnetic surveys: weighted spatial averaging and temporal filtering. *Earth, Planets and Space*, 67(1):1–14.

Iturralde-Vinent, M., García-Casco, A., Rojas-Agramonte, Y., Proenza, J., Murphy, J., and Stern, R. (2016). The geology of Cuba: A brief overview and synthesis. *GSA Today*, 26(10):4–10.

Langseth, M. G. and Silver, E. A. (1996). The Nicoya convergent margin—A region of exceptionally low heat flow. *Geophysical Research Letters*, 23(8):891–894.

Leliak, P. (1961). Identification and evaluation of magnetic-field sources of magnetic airborne detector equipped aircraft. *IRE Transactions on Aerospace and Navigational Electronics*, 3(ANE-8):95–105.

Leroy, S., Mauffret, A., Patriat, P., and de Lépinay, B. M. (2000). An alternative interpretation of the Cayman trough evolution from a reidentification of magnetic anomalies. *Geophysical Journal International*, 141(3):539–557.

Lesur, V., Hamoudi, M., Choi, Y., Dyment, J., and Thébault, E. (2016). Building the second version of the World Digital Magnetic Anomaly Map (WDMAM). *Earth, Planets and Space*, 68(1):1–13.

Lesur, V., Rother, M., Vervelidou, F., Hamoudi, M., and Thébault, E. (2013). Post-processing scheme for modelling the lithospheric magnetic field. *Solid Earth*, 4(1):105.

Luyendyk, A. (1997). Processing of airborne magnetic data. *AGSO Journal of Australian Geology and Geophysics*, 17:31–38.

Maus, S. (2008). The geomagnetic power spectrum. *Geophysical Journal International*, 174(1):135–142.

Maus, S. (2010). Magnetic field model MF7.

MENEVEN (1983). Aeromagnetic survey 1981-1982, Contract CAR-62. Technical Report 1, GEOTERREX LTD and CGG. 199pp.

Olsen, N., Lühr, H., Sabaka, T. J., Mandea, M., Rother, M., Tøffner-Clausen, L., and Choi, S. (2006). CHAOS—a model of the Earth's magnetic field derived from CHAMP, Ørsted, and SAC-C magnetic satellite data. *Geophysical Journal International*, 166(1):67–75.

Olsen, N., Ravat, D., Finlay, C. C., and Kother, L. K. (2017). LCS-1: A high-resolution global model of the lithospheric magnetic field derived from CHAMP and Swarm satellite observations. *Geophysical Journal International*, 211(3):1461–1477.

Orihuela Guevara, N., Tabare, T., et al. (2011). Mapas de gravedad y anomalía gravimétrica de venezuela derivados de datos satelitales. *Revista de la Facultad de Ingeniería Universidad Central de Venezuela*, 26(1):51–58.

Pearson, K. (1901). LIII. On lines and planes of closest fit to systems of points in space. *The London, Edinburgh, and Dublin Philosophical Magazine and Journal of Science*, 2(11):559–572.

Purucker, M. and Whaler, K. (2007). Crustal magnetism. *Treatise on geophysics*, 5:195–237.

Purucker, M. E. and Dyment, J. (2000). Satellite magnetic anomalies related to seafloor spreading in the South Atlantic Ocean. *Geophysical research letters*, 27(17):2765–2768.

Quesnel, Y., Catalán, M., and Ishihara, T. (2009). A new global marine magnetic anomaly data set. *Journal of Geophysical Research: Solid Earth*, 114(B4).

Ranero, C. R., Morgan, J. P., McIntosh, K., and Reichert, C. (2003). Bending-related faulting and mantle serpentinization at the Middle America trench. *Nature*, 425(6956):367–373.

Reeves, C. (2005). Aeromagnetic surveys: principles, practice and interpretation. *Published by Geosoft*, page 155.

Reigber, C., Schwintzer, P., and Lühr, H. (1999). The CHAMP geopotential mission. *Boll. Geof. Teor. Appl*, 40:285–289.

Rodriguez Millan, I. (2014). *Gravity Anomalies, Geodynamic Modelling and the Eastern Venezuela Basin Evolution.* PhD thesis, Durham University.

Rosencrantz, E. (1996). Basement structure and tectonics in the Yucatan basin. *Ofiolitas y Arcos Volcánicos de Cuba. Miami, USA, IGCP Project*, 364:36–47.

Sabaka, T. J., Olsen, N., and Purucker, M. E. (2004). Extending comprehensive models of the Earth's magnetic field with Ørsted and CHAMP data. *Geophysical Journal International*, 159(2):521–547.

Sandwell, D. T., Müller, R. D., Smith, W. H., Garcia, E., and Francis, R. (2014). New global marine gravity model from CryoSat-2 and Jason-1 reveals buried tectonic structure. *Science*, 346(6205):65–67.

Stern, R. J. (2002). Subduction zones. *Reviews of geophysics*, 40(4).

Tabare, T. and Orihuela Guevara, N. (2013). Estudio geofísico integrado del macizo ígneo-metamórfico de El Baúl, región central de Venezuela. *Revista Venezolana de Ciencias de La Tierra GEOS*, 45(1):171. ISSN: 0435-5601.

Thébault, E., Lesur, V., Kauristie, K., and Shore, R. (2017). Magnetic field data correction in space for modelling the lithospheric magnetic field. *Space Science Reviews*, 206(1-4):191–223.

Thébault, E., Purucker, M., Whaler, K. A., Langlais, B., and Sabaka, T. J. (2010). The magnetic field of the Earth's lithosphere. *Space Science Reviews*, 155(1-4):95–127.

Thébault, E., Vigneron, P., Langlais, B., and Hulot, G. (2016). A Swarm lithospheric magnetic field model to SH degree 80. *Earth, Planets and Space*, 68(1):126.

Urbani, F., Grande, S., Baquero, M., Mendi, D., Fournier, H., Alemán, A., Camposano, L., and Baritto, I. (2013). Los diques de basalto de la quebrada Yaracuyabare, Municipio Silva, Estado Falcón, Venezuela. *Revista Venezolana de Ciencias de La Tierra*.

Urquhart, T. (1988). Decorrugation of enhanced magnetic field maps. In *SEG Technical Program Expanded Abstracts 1988*, pages 371–372. Society of Exploration Geophysicists.

Vasicek, J. M., Frey, H. V., and Thomas, H. H. (1988). Satellite magnetic anomalies and the Middle America Trench. *Tectonophysics*, 154(1-2):19–24.

Vine, F. J. and Matthews, D. H. (1963). Magnetic anomalies over oceanic ridges. *Nature*, 199(4897):947–949.

Viscarret, P. and Urbani, F. a. (2005). Algunos aspectos de la geología de la región de El Baúl, estado Cojedes. *Revista Venezolana de Ciencias de la Tierra GEOS*, 38:49–51. ISSN: 0435-5601.

Voorhies, C. (1998). *Elementary theoretical forms for the spatial power spectrum of Earth's crustal magnetic field*. Number 1. 36pp.

Wessel, P. (2010). Tools for analyzing intersecting tracks: The x2sys package. *Computers & Geosciences*, 36(3):348–354.

Wessel, P. and Watts, A. B. (1988). On the accuracy of marine gravity measurements. *Journal of Geophysical Research: Solid Earth*, 93(B1):393–413.

Wold, S., Esbensen, K., and Geladi, P. (1987). Principal component analysis. *Chemometrics and intelligent laboratory systems*, 2(1-3):37–52.

Zmuda, A. (1969). International Geomagnetic Reference Field. *Transactions-American Geophysical Union*, 50(4):134.

Chapter 3

Plate tectonics on the Gulf of Mexico from gravity and magnetic data

> "Je crois toujours que l'un des chemins positifs de l'humanité est le métissage. Plus il est grand, plus la fusion des races est grande, plus on peut éliminer le chauvinisme, le patriotisme, les nationalismes des frontières absurdes et folles. J'espère en même temps que l'homme soit toutes les hommes"
>
> — JULIO CORTÁZAR

Abstract

The structure, age and evolution of the Gulf of Mexico (GoM) have long been controversial. It is generally agreed that oceanic crust is present within the Gulf, although its extension is debated. Recent satellite-derived Vertical Gradient of Gravity (VGG) data revealed the presence of N-S fracture zones in the Western GoM. We compiled, corrected and gridded all publicly available marine magnetic data to build an improved magnetic anomaly map of the GoM. This map allows delineating the COB by recognizing marked changes of magnetic anomaly patterns. Strong anomalies mark both the Yucatán Block and the Florida Block, whereas weaker magnetic signal characterizes the GoM. The magnetic anomaly map reveals long-wavelength lineated bands of anomalies: five positive anomalies represent two pairs of conjugate isochrons bounding the fossil spreading centre.

Reconstructions based on the COB, these isochrons, and the FZs revealed by the VGG depict a consistent opening by counter-clockwise rotation of the Yucatán Block. Refining this history to get details of the geomagnetic polarity reversals recorded in the GoM oceanic crust and date this evolution was proven impossible, as the data quality and distribution are inadequate for such an exercise. Instead we isolated the long-wavelengths of the M-series Geomagnetic Polarity Time Scale (GPTS) for different cut-off (different possible spreading

rates) and compared the anomalies to the filtered GPTS.

Our best guess gives ages of M17 and M24n (143 and 153 Ma) for the fossil axis and the older conjugate isochron. Concurrent with available dating of rock samples, seafloor spreading in the GoM would have started before Kimmeridgian and ceased during Berriasian. We determined spreading rates (with strong variations due to the nearby rotation pole) and asymmetry, offering a complete plate tectonic evolution model for the GoM.

3.1 Introduction

The Pangea super-continent breakup is intimately connected to the Atlantic opening and its basins. Small basins in the western side of the Atlantic, such as those that lie in the Caribbean Sea or the Gulf of Mexico (GoM), are located in low magnetic latitudes. Magnetic anomalies at low magnetic latitudes have low amplitude and superimposed electrojet currents usually disturb them. We discussed these arguments in further detail in Chapter 2. Those conditions make the processing and interpretation of magnetic anomalies in the Caribbean and surroundings a real challenge with implications in the knowledge of the Equatorial and Central Atlantic opening and consequently in the geological evolution of Caribbean plate.

After seafloor spreading is proven valid (Vine and Matthews, 1963) marine magnetic tracks design generally approximate the seafloor spreading direction, in order to record the succession of magnetic isochrons (record of reversals of the magnetic field) and hence contributes to the mapping of the magnetic signature of seafloor spreading (e.g., Dyment et al., 2015; Hemant et al., 2007). These magnetic records together with geological information provide constraints about the age of the seafloor and allow to trace the relative motions of the involved plates, giving access to the kinematics of plate tectonics.

Plate tectonics continue to be the most successful theory to explain the actual position of the large continental blocks surrounding the Atlantic Ocean (e.g., Biari et al., 2017; Seton et al., 2012). Nevertheless, plate tectonic reconstructions depend on the computational capacities, availability of data and accuracy of the chosen features (proper location and resolution). For example, assuming the shape of the Earth as a sphere simplifies performing rotations of the tectonic blocks, although considering a similar curvature in every place of the Earth can lead to unrealistic results. In practice, the curvature of the Earth increases from to the geographical Equator towards the geographical poles. Also, results can be different depending on which feature was chosen to perform the initial continental reconstruction, either the shelf break or the continent-ocean boundary (COB). The offset between the shelf break and the COB is usually not uniform along the margins. This non uniformity is due to different amount of crustal extension on the continental margins, especially during the rifting phase.

The Gulf of Mexico is part of the longitudinal band of small basins located in the

Caribbean realm which origin has been related with the Central Atlantic Ocean opening. For a long time, it has been proposed the GoM to be created during the Jurassic age, thanks to the counter-clockwise rotation of the Yucatán Block by analogy to the Central Atlantic. Perhaps, this most accepted age is still controversial because of the lack of geophysical and geological data to confirm it. Vertical gradient of gravity (VGG) exhibit spectacular fracture zones (FZ) in the western GoM (Bonvalot et al., 2012; Sandwell et al., 2014), but we do not observe a clear signal related to fracture zones either in the Central part or the East of the GoM. Magnetic tracks from open access data lack at first sight any distinctive magnetic anomalies that could be related to seafloor spreading. In the northern GoM, the predominant gravity signal comes from the salt bodies which mask the signal of possible fracture zones. Drilling wells do not reach the acoustic basement, and the orientation of the FZ suggests that the location of the Yucatán Block before the seafloor opening is not compatible with the previously proposed models.

In this work, we revisit the potential field data over the GoM, to integrate gravity and magnetic in a unique plate tectonic reconstruction model that can contribute to the knowledge of the GoM opening and discuss its role in the Caribbean tectonic evolution but also the derived implications for the Pangea break up.

3.2 Problem statement

During many decades, the entire Gulf of Mexico (hereafter GoM) has been explored intensively. A consensus after the exploration is the certainty that s.l. the nature of the crust that underlies the GoM seafloor is oceanic (see Fig. 3.1). This crust was first imaged by seismic data, and more recently vertical gradient of gravity (VGG) has illuminated fracture zones west of the GoM (e.g., Bonvalot et al., 2012; Sandwell et al., 2014). However the nature of the crust in some areas remains unclear, i.e., in its central part, the absence of a clear signature in the potential field data does not help to decipher whether the crust there is oceanic or not.

Understanding the nature of the crust in the GoM is of interest because: in the first place, the GoM represents a model of an isolated ocean basin that is not connected with the oceanic crust of the Atlantic, Indian and Pacific oceans. Additionally, its kinematics is crucial for the outline of the southern margins of Laurentian and the Precambrian terranes of North America. Furthermore, the sedimentary prisms that it encloses harbor to one of the richest prolific petroleum provinces of the World (Dickinson, 2009).

Several authors interpreted the COB in the GoM from gravity, magnetics, seismic refraction, seismic reflection and by plate kinematic models (cf. Bird et al., 2005; Bouysse, 2009; Christeson et al., 2014; Hudec et al., 2013; Marton and Buffler, 1994; Pindell, 1994; Sandwell et al., 2014; Sawyer et al., 1991; Schouten and Klitgord, 1994; Seton et al., 2012),

although the interpretations of the authors may differ.

Such differences are smaller in the southern part of the GoM than in the north, where the geophysical data is not conclusive (see Fig. 3.2). The presence of the Sigsbee salt province and the high thickness of sediments underlying the salt province contribute to the weakness of the potential field signal.

About the geological evolution of the Gulf, most of the existing models place the Yucatán Block near the Louisiana coast, before the basin opening (e.g., Pindell, 1994) (see Fig. 3.3). However, those models are not closing the GoM entirely, and in some way they are unable to explain, for instance, the similarity between the observed magnetic anomalies of the Yucatán and Florida blocks.

A first option is to consider only the sharp vertical gradient of gravity for the tectonic reconstruction of this small basin and place the eastern part of the Yucatán Block together with the western part of the Florida Block (e.g., Keppie and Keppie, 2012), even though such models are in disagreement with the orientation of the FZ revealed by VGG. From the potential field data point of view, a valid model must satisfy the observed FZs from gravity data, and ideally, the model must close entirely the Gulf.

Concerning the crustal nature in the GoM, we considered two hypotheses: (A) A prevailing and straightforward hypothesis, which considers the oceanic crust of the Gulf

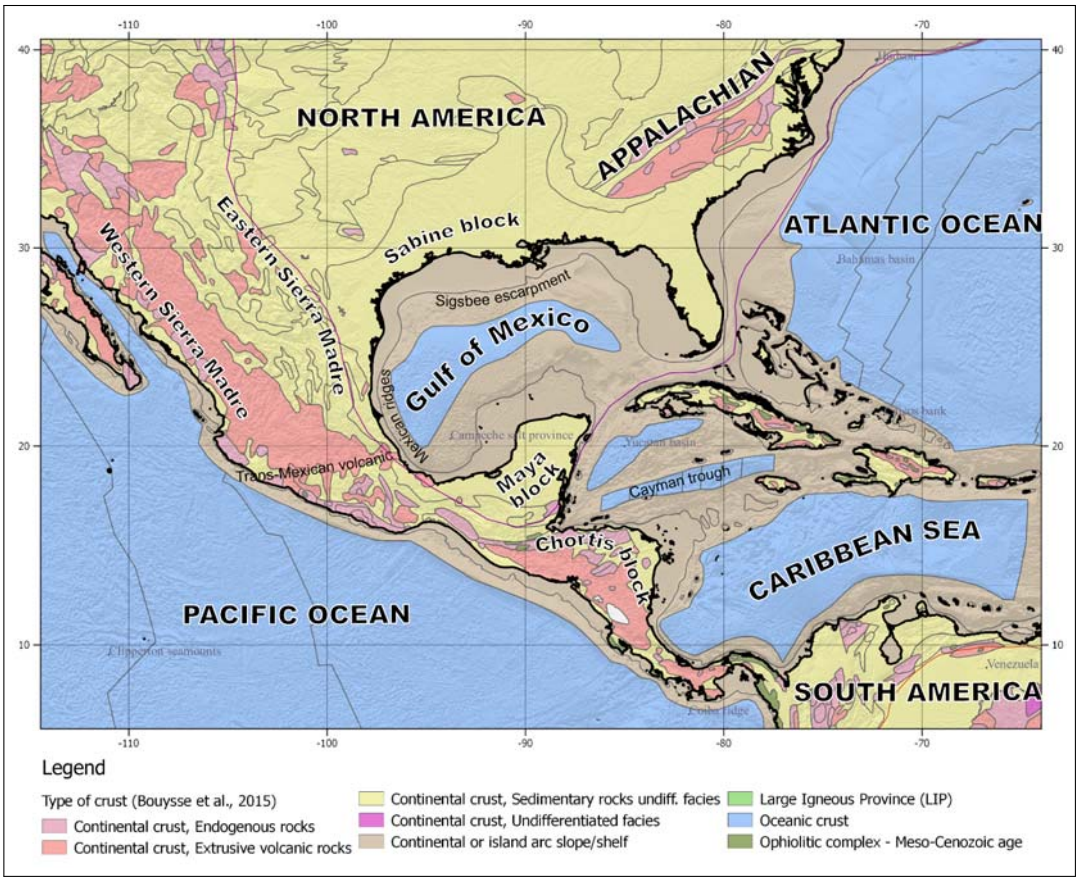

Figure 3.1 – Simplified geology of the Gulf of Mexico (from Bouysse et al., 2015)

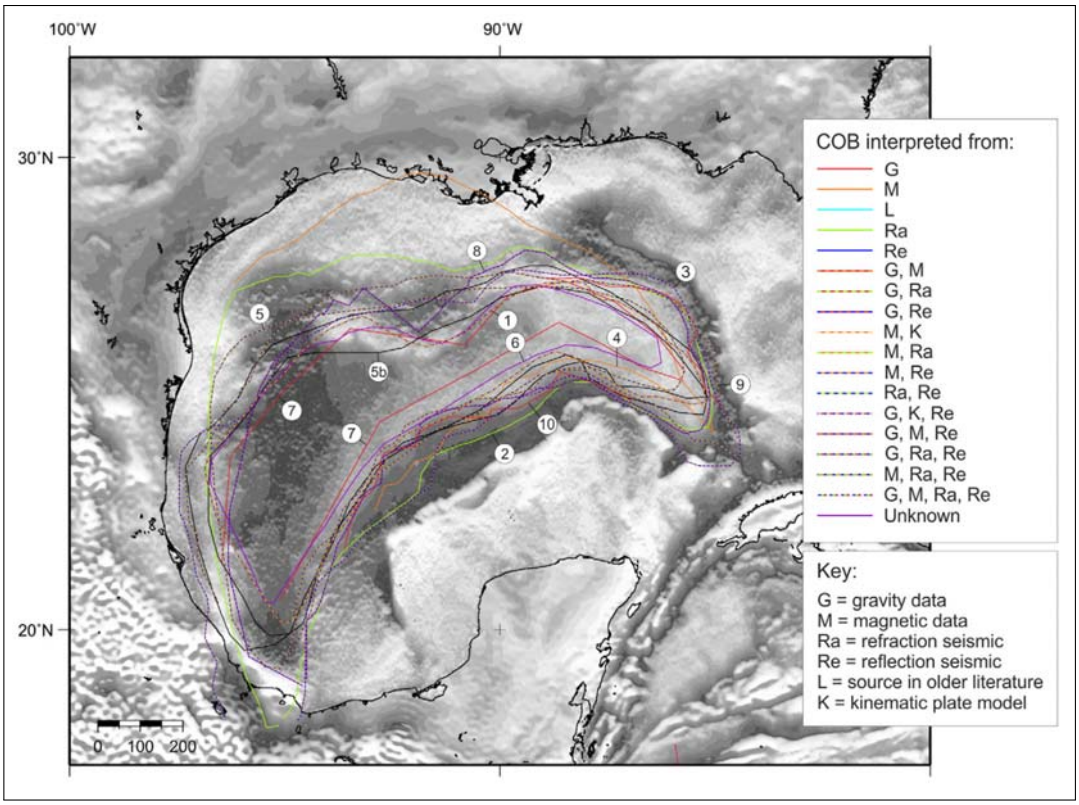

Figure 3.2 – COB estimations from different authors (Eagles et al., 2015)

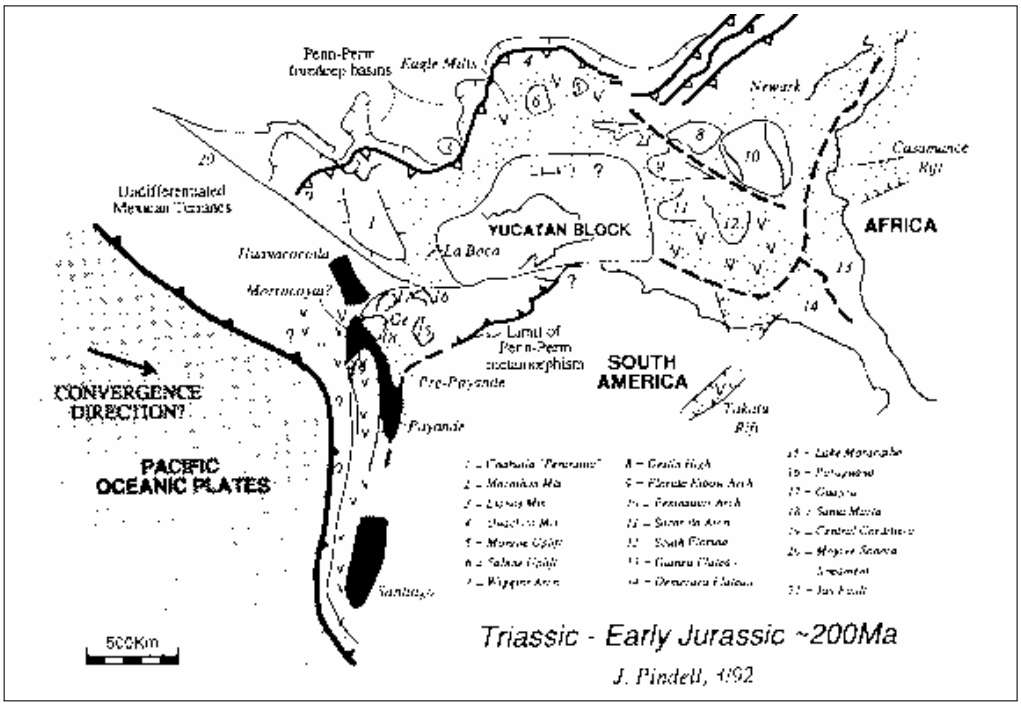

Figure 3.3 – Plate tectonic reconstruction in the GoM at 200 Ma (from (Pindell, 1994))

of Mexico as formed by a unique event of seafloor spreading, within one or more rotation stages; and (B) a second and less simple hypothesis which considers the GoM formed as a small oceanic basin through several episodes of spreading, resulting in fragments of trapped oceanic crust.

We resume the current issues in the reconstruction of the GoM as follows:

i The potential field signal of the COB in the central part of the GoM is vague;

ii We do not observe short wavelengths VGG associated to extinct FZ neither in the central part nor observed in the eastern part of the GoM;

iii A model that places the Yucatán Block close to Texas-Louisiana shelf before the seafloor spreading is not compatible with the orientation of the FZ observed by VGG;

iv The tectonic model must satisfy the observed potential field features;

v And the thickness of the salt layer and sediments must be considered given that their signal is overprinting the signal of the underlying oceanic crust.

The latter arguments are part of the motivation to revisit the potential field data over the GoM and to perform plate tectonic reconstruction from potential field data. The signal of potential field data is ambiguous. The layer composed of sediments and evaporites hindered the continent-ocean boundary signal. Relevant evidence of the location of the Euler pole to the east of the GoM is the close distance that exists between the Florida Block and the Yucatán Block in the eastern part of the GoM and the decrease of this distance from east to west. The small separation between the Florida Block and the Yucatán Block justify the lack of identification of any FZs in the central part and eastern part of the Gulf. Magnetic anomalies are, in principle, neither significantly altered by the presence of sediments nor altered by the presence of salt bodies, but the thickness of the sediments layer can be responsible for the attenuation or disappearance of the magnetic signal.

It should be noted that the width of the Gulf varies from 160 km to the East to 1200 km at the West. We can therefore expect to recover higher resolution signals in the west than in the east. The tectonic model of the GoM has to be adaptable enough to take into account all the pieces that are present in this puzzle and to infer missing pieces if needed.

3.3 Aim

The Gulf of Mexico and its surroundings have been widely studied for almost 50 years, and the geological information available is abundant and overwhelming. Even though, questions regarding the crustal structure of the Gulf, nature and age of its opening are still under debate.

Magnetic and gravity data are useful tools to characterize the crust, so we aim to perform a plate tectonic reconstruction of the Gulf of Mexico based on potential field data, that at

the same time can contribute to the debate about the delimitation of the continent-ocean boundary within the Gulf and its opening age. First of all, here we review the tectonic models proposed in the GoM up to now and the characteristics of its crust.

The aim of this research is to use the marine magnetic anomalies (Garcia-Reyes et al., 2017) and VGG to produce a tectonic map of the GoM and to identify the magnetic isochrons, hence to propose an opening age for the Gulf. The combination of these two results will converge in a tectonic model for the opening of the GoM with derived implications in the understanding of the Pangea break-up and in the evolution of the Caribbean region.

3.3.1 Limitations from potential field data

- We observe a sharp gradient from VGG at the north-eastern part of the Yucatán Block which is similar to that observed at the south western part of the Florida Block (see 1 and 2 in Fig. 3.4). We do not observe this pattern in the rest of the GoM margins, thus it is very tempting to propose affinity between the Yucatán Block and the Florida Block and to conceive a tectonic reconstruction where the Florida Block and the Yucatán Block were initially next to each other;
- We observe no similarity between the gravity pattern in the western part of the GoM compared to the one in the east;
- And we only well observe the gravity signal related to FZs in the western part of the GoM.

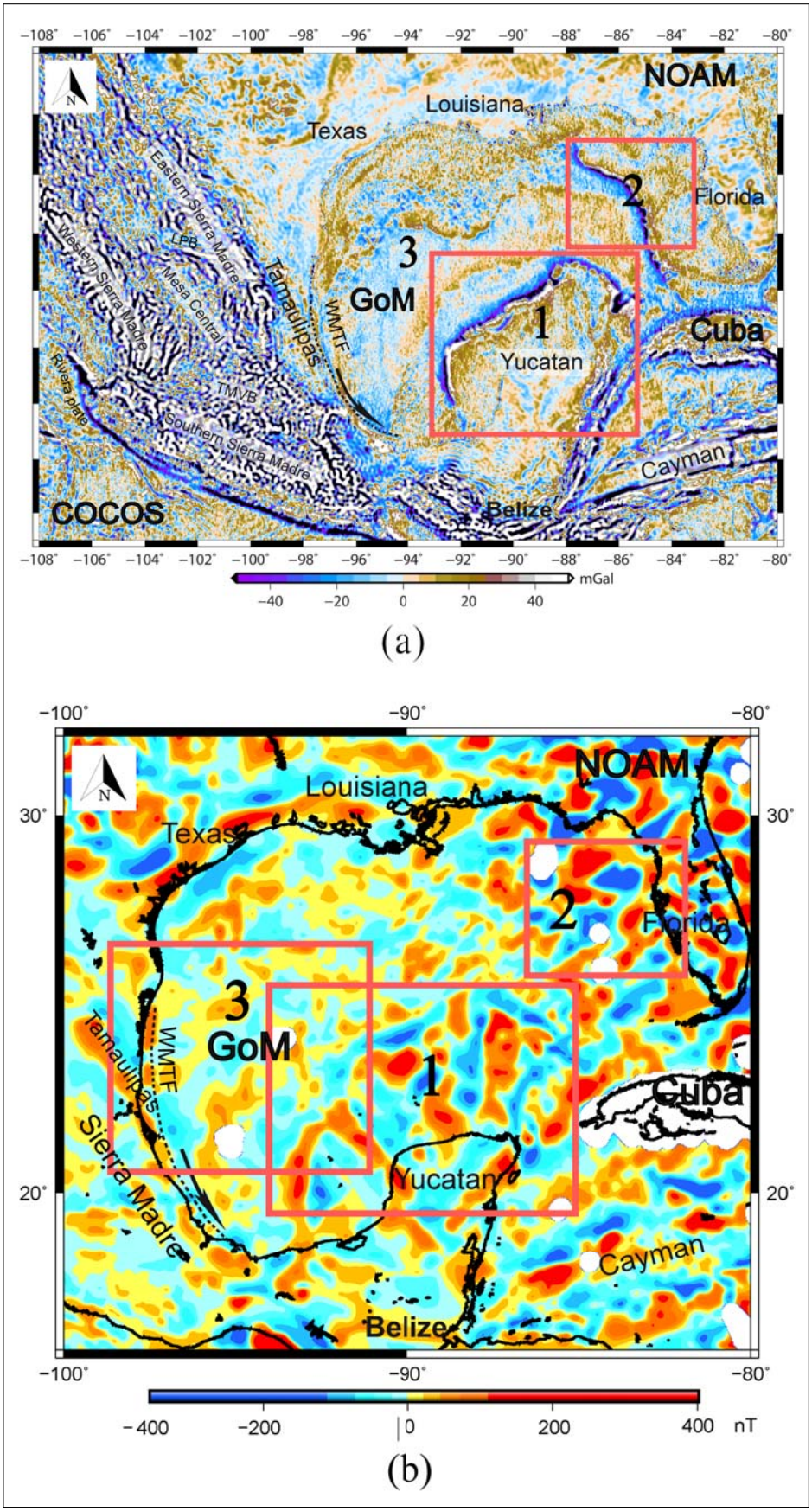

Figure 3.4 – Base maps of this study: Vertical gradient of gravity (Sandwell et al., 2014) (a) and marine magnetic anomalies (b)

3.4 Geological background

3.4.1 Margins

The Mississippi River sediment-dispersal system dominates the northern continental margin of the GoM (Blum et al., 2017) (see Fig. 3.5). Short and curved normal faults dipping in various directions characterize this margin (Fort and Brun, 2012). Fort and Brun (2012) imaged the basal salt in the northern continental margin as very thin below the actual shelf. On the other side, tectonic blocks formed during the Paleozoic and Mesozoic delimit the western margin of the GoM. Centeno-García (2017) considered these blocks as the result of the complex interaction between Laurentia, Gondwana and the paleo-Pacific plate. Thomas et al. (2006) and Stephens (2009) interpreted transfer faults, grabens, and rifts affecting the basement in the Sigsbee salt province and covering part of the western part of the GoM (see Fig. 3.5).

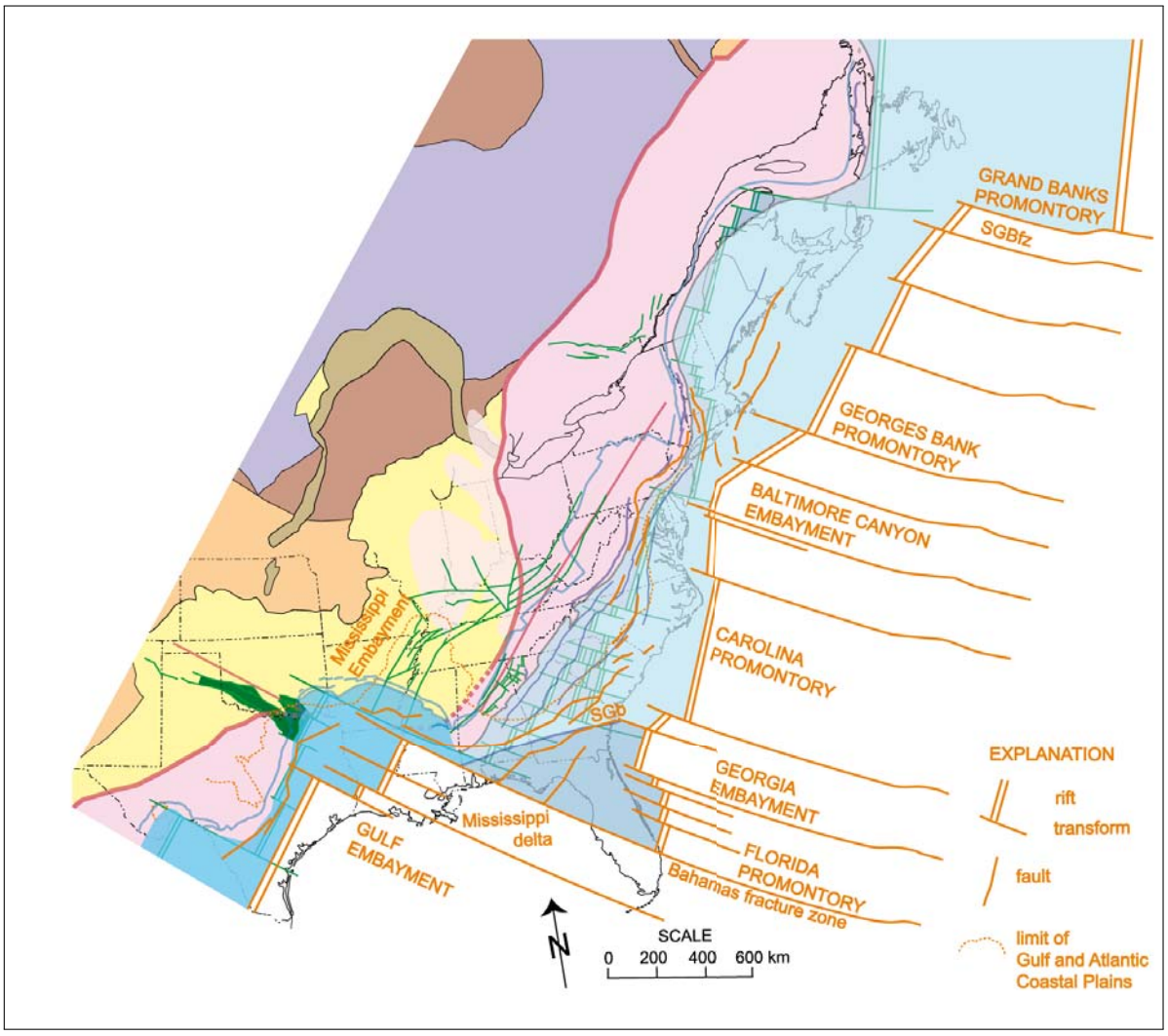

Figure 3.5 – Previously interpreted fracture zones over Eastern North America (from (Thomas et al., 2006))

3.4.2 Models of opening of the GoM

Pangea breakup

The Late Triassic breakup of the Pangea super-continent preceded the ultimate assembly of Mexico and consequently the beginning of the Gulf of Mexico opening (Bird et al., 2006, and references therein.). Welsink et al. (1989) reported the breakup of Pangea to occur ca. 230 Ma ago. The westward separation of the Yucatán Block from Northern South America followed the breakup of Pangea (e.g., Bartok, 1993; Hall et al., 1982), probably forming a now disappeared basin. A number of fault-bounded rift basins related to the initial rifting of Pangea parallels the eastern margin of North America and the western margin of Africa (Olsen, 1997).

3.4.2.1 Principal tectonic events that occurred from 200 to 164 Ma

1. Poorly dated red beds and volcanics of the Eagle Mills Formation mark the rifting in the Gulf of Mexico which started approximately in the Norian (228,4–209,5 Ma); (Moy and Traverse, 1986); approximately synchronous with rifting along the Central Atlantic margin along the U.S. East Coast (Olsen et al., 1996);
2. The Central Atlantic Magmatic Province (CAMP) probably initiated at approx. 200 Ma (Blackburn et al., 2013; Marzoli et al., 1999). First dated pulse of CAMP magmatism is approx. 201.56 Ma age (Blackburn et al., 2013). The CAMP is considered a large igneous province and different mechanisms have been proposed for its initiation (Whalen et al., 2015, and references therein.). The Eastern North America magmatism is related to CAMP;
3. Seafloor spreading in the Central Atlantic started around 180–200 Ma (e.g., Sahabi et al., 2004; Schouten and Klitgord, 1994; Withjack et al., 1998);
4. The Coahuila transform is also known as the Mojave-Sonora megashear (see Fig. 3.3). Amato et al. (2009) considered this megashear as a Late Jurassic transcurrent fault crossing northern Mexico south eastward from southern California with approx. 800 km of displacement;
5. (Withjack et al., 1998) documented rift-drift transition in the southern United States. After, stretching of the Yucatán Block occurred;
6. Eastward ridge jump in the Central Atlantic (transfering African lithosphere on the western flank) at 170 Ma (Bird et al., 2011);
7. And the westward ridge jump in the Central Atlantic (transfering North American lithosphere on the eastern flank) at 160 Ma (Bird et al., 2011).

3.4.2.2 Single mantle plume model

More recent models introduce the presence of a single mantle plume in the Central and Western GoM. Those models are produced from gravity and seismic data (Bird et al., 2006). Among most of the researchers there is a consensus regarding the evolution and geological history of the Gulf of Mexico (from Nguyen and Mann, 2016):

- First stage of Triassic continental rifting, related to the continental breaking apart of North America, the Yucatán Block and South America;
- A short period of syn-rift, thick salt deposition during the latest Jurassic;
- A period of oceanic spreading and transform faulting that rotated the Yucatán Block by approximately 40° in a counterclockwise direction that ceased in the Early Cretaceous;
- And finally, a period of subsidence of the Gulf margins formed by carbonate platforms and thick sedimentary layers. The eastern margin did not recorded subsidence.

"Previous models of Yucatán Block motion and Gulf of Mexico opening since the breakup of Pangea in the Mesozoic seem to provide no explanation for the Yucatán slab structure. Most models suggest that the Yucatán Block rotated in counter-clockwise fashion away from the northern Gulf of Mexico margin during the Jurassic" (Pindell and Kennan, 2009).

3.4.3 Regional geological structures

3.4.3.1 Western Main Transform Fault

This fault located ∼100 km offshore eastern Mexico defines its continent-ocean boundary (Nguyen and Mann, 2016, and references therein.) (see Fig. 3.4). A sharp transition from 6.5 to 10 km characterizes the crustal thickness within this boundary. Nguyen and Mann (2016) proposed that stretched continental crust constitutes the eastern Mexico margin.

3.4.3.2 Sabine Block

In the north, the Sabine Block is recognised as a distinct block in comparison with the Gondwanan terranes around the Gulf of Mexico (Clift et al., 2018, and references therein.) (see Fig. 3.7). The Sabine Block may have been accreted to North America before 1.4 Ga and affected by the Grenville orogeny (Clift et al., 2018).

3.4.3.3 Yucatán Block

The Yucatán Block is also known as the Maya Block. The granitoids, volcanic rocks, clastic sedimentary strata and minor limestone rocks that make up the Yucatán Block are mostly of Paleozoic age (Martens et al., 2010, and references therein). Kring et al. (2017) found granitic rocks in the uplifted peak ring of the Chicxulub crater in IODP wells, which confirms the continental nature of the Yucatán Block. Bartok (1993) defined the

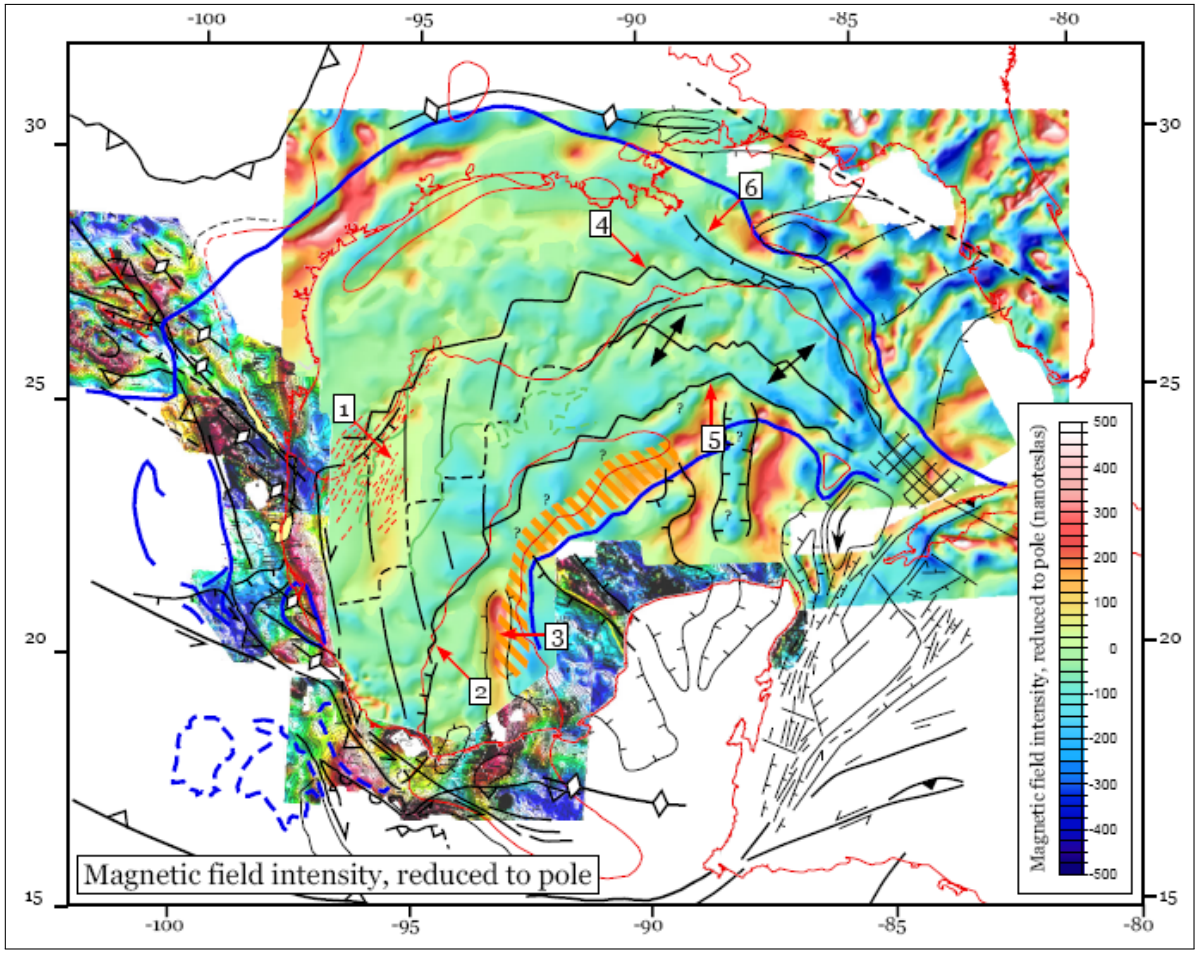

Figure 3.6 – Structural interpretation of the GoM from magnetic anomalies (from Tectonic Analysis)

Yucatán Block as formed by small cratonic centers located in north central Guatemala and Yucatán and the Chiapas Massif. This block agglutinates the Maya mountains of Belize, the Cuchumatanes Range to the south and the Chiapas Massif. Keppie and Keppie (2014) pointed out that mountains in Belize have no counterpart in Texas, our observation interpreted by Bartok (1993) as reflecting a Laurentian origin for the Yucatán Block, with a Laurentian/Gondwana suture at the west of the Maya mountains. Bartok (1993) also documented vestiges of Pan-African aged belts from the Appalachians.

The Yucatán and Florida Blocks show affinity in their seismic velocities with relation to the rest of Mexico and the western GoM, suggesting a connection between the Yucatán Block and the Florida Block in the past (Kim et al., 2011). This connection lasted tentatively from the early Mesozoic until the Jurassic breakup of Pangea (Dickinson and Lawton, 2001; Pindell et al., 2005; Salvador, 1991). Martens et al. (2010) used results from igneous zircons dating in the Maya mountains to propose a location for the Yucatán Block along the West Amazonia side of Gondwana during the Cambrian-Silurian age. Moreover, paleomagnetic studies over sedimentary and plutonic rocks suggest that the Yucatán Block was not located between the North and South American plates during the Permian (Steiner and Anderson, 2005).

Keppie (2013) considered the two different hypotheses for the origin of the Yucatán Block: Laurentian or Gondwanan. Some models require a north-south oriented transform fault offshore eastern Mexico (see Fig. 3.3) (e.g., Marton and Buffler, 1994; Pindell, 1994). Bird et al. (2006) proposed that the Yucatán Block first rotated away from North America with a 24º counterclockwise of continental extension; at ∼150 Ma, an additional 20º counterclockwise rotation of seafloor spreading gave birth to the Gulf of Mexico; at ∼140 Ma the formation of the Gulf of Mexico was completed (e.g., Bird et al., 2006, and references therein.).

3.4.3.4 Florida Block

The crystalline basement in northern and central Florida is also called Gondwanan Suwannee Terrane (GST) (see Fig. 3.7) (e.g., Dallmeyer, 1989; Mueller et al., 2014). Undeformed early Paleozoic sedimentary rocks considered of Gondwanan-African derivation of Mesoproterozoic age formed this terrane (Mueller et al., 2014). Heatherington and Mueller (2003) found Mesozoic rocks with tholeiitic basalts and diabases in drill holes and dated at 183-189 Ma in northern Florida. The GST likely originated from its separation from Gondwana during the Atlantic Ocean rifting along a Mesoproterozoic–Neoproterozoic suture (e.g., Mueller et al., 2014).

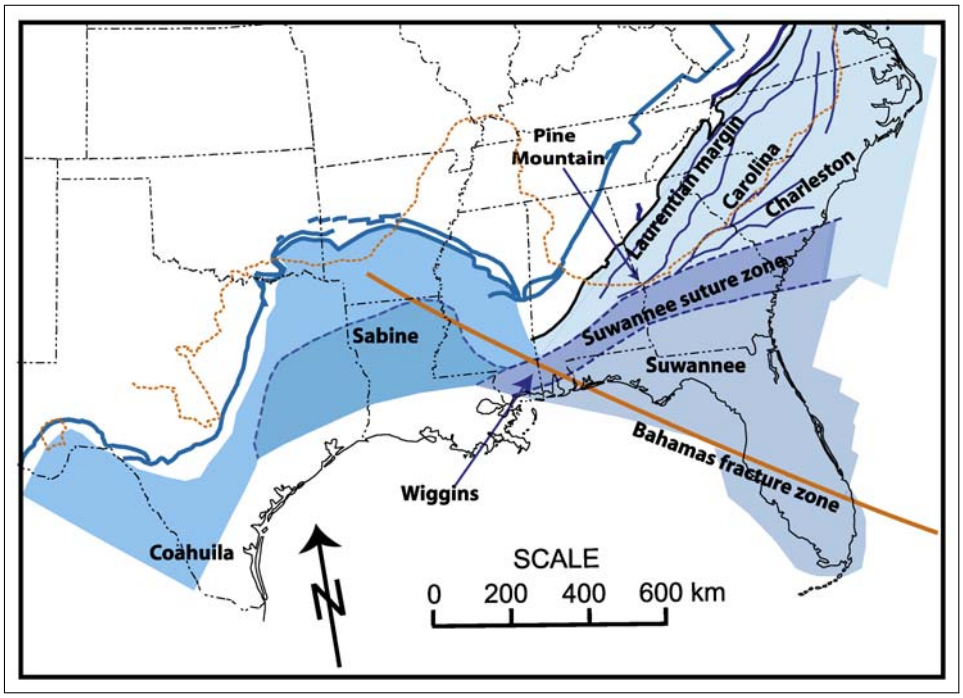

Figure 3.7 – Map showing Gondwana terranes along the Atlantic and GoM (From (Mueller et al., 2014))

3.4.4 Crust in the GoM

3.4.4.1 Stratigraphy

Cretaceous marine strata have been reported in Deep Sea Drilling Project (DSDP) drills in the Western GoM. Buffler (1984); Worzel and Watkins (1973) interpreted these deposits as to record stable sedimentation at the Eastern part of the Gulf of Mexico during the Cenozoic. The northern Gulf of Mexico basin records five main episodes (from Worrall and Snelson, 1989):

1. Late Triassic-Early Jurassic terrestrial syn-rift deposition during crustal attenuation;
2. Late Middle-Jurassic evaporite (Louann province) and aeolian sand deposition over a major regional unconformity;
3. Late Jurassic-Early Cretaceous carbonates and updip evaporite deposition followed by progradation of terrigenous clastics;
4. Two major shelf-margin reef cycles during the Early and Middle Cretaceous; and lastly;
5. Widespread Late Cretaceous drowning of reefs and associated extensive sedimentation of chalks, marls, and shales and the development of the post-"Mid-Cretaceous" unconformity.

3.4.4.2 Thickness

In the Northwest of the GoM, Van Avendonk et al. (2015) and Eddy et al. (2018) interpreted stretched continental crust of about 12 km thickness from seismic sections. Eddy et al. (2014) defined the COB from the seismic line GUMBO2 (central Gulf of Mexico) and proposed changes in the crustal thickness from 10 km to 7 km (the thickness of normal oceanic crust). Also Eddy et al. (2014) associated the magnetic highs observed in the GUMBO 2 profile with high seismic velocities. Eddy et al. (2014) interpreted those results as produced by the presence of magmatic intrusive bodies that were emplaced in the lower continental crust during the rifting stage. East of the GoM, near the coast of Florida, Christeson et al. (2014) interpreted thinned continental crust with a Moho depth of about 32 km to 33 km, with an average of sediments equal to 6 km and an average crustal thickness of 27 km. In the marine eastern part of the GoM, Christeson et al. (2014) interpreted oceanic crust with a thickness between 5.6-5.7 km, together with an extinct spreading center and a full spreading rate of 2.2 cm/yr. Seismic images show normal oceanic crust at depth (Ibrahim et al., 1981). Deeper, Van Avendonk et al. (2015) interpreted mantle at depths between 30 km to the Northwest to 18 km to the Southeast from seismic data.

3.4.4.3 Physical properties

Carlson and Herrick (1990) suggested from the analysis of Mid-Atlantic drilling samples that the structure of the seismic velocities in the oceanic crust is related to changes in porosity and alteration (or metamorphic grade). Using empirical models Carlson and Herrick (1990) suggested the following crustal densities and porosities: Layer 2, 2.62—2.69 Mg m—3, 0.10—0.12 and layer 3, 2.92—2.97 Mg m—3.

The estimated average density of the oceanic crust is 2.86 $\pm$ 0.03 Mg m—3 (Carlson and Herrick, 1990). The upper oceanic crust is distinguished by high density and porosity gradient (Carlson and Herrick, 1990).

3.4.4.4 Ages

Stern and Dickinson (2010) considered the Gulf of Mexico a Jurassic "backarc basin". Hall and Najmuddin (1994) and Pindell (1985) proposed that the Yucatán Block rotated counter clockwise approx. 22° between 165.1 Ma to 154.1 Ma from magnetic anomaly data, while a syn-rift salt deposition took place. Jurassic rocks include evaporites of the Oxfordian-Kimmeridgian Minas Viejas Formation exposed only in diapiric bodies in La Popa Basin of northern Mexico (Lawton et al., 2001). In the Coahuilas Block (northern Mexico), Jones et al. (1984) and Garza (2005) dated hornblende (215.9 ± 1.9 Ma), biotite (217.3 ± 1.2 Ma) and potassium feldspar (205.6 ± 1.4 Ma) (see Fig. 3.7).

The U-Pb ages and biostratigraphy indicate a late Oxfordian-early Kimmeridgian salt age in northeastern Mexico (onshore salt basins), younger than the Louann Salt of the GoM

(Lawton and Amato, 2017).

3.4.5 Evolution models

The nature of the crust that underlies the salt provinces and the sea water of the Gulf of Mexico is part of the controverse regarding the evolution of the Gulf. The orientations proposed for the position of the Yucatán Block, before the GoM opening are diverse (Buffler and Sawyer, 1985; Bullard et al., 1965; Carey, 1958; Keppie and Keppie, 2014; Pindell and Dewey, 1982; Ross and Scotese, 1988; Seton et al., 2012). Hall and Najmuddin (1994) proposed that the Yucatán Block rotated about a pole located presently at 24°N, 81.5°W.

Because seafloor magnetic anomalies have not been identified so far (e.g., Christeson et al., 2014), kinematic models on the GoM are based on stratigraphical records (Galloway, 2008), the location of the COB, and the extrapolation of the age of the spreading in the neighbouring basins (Kneller and Johnson, 2011). Most of the plate tectonic models place the South Florida Block moving south along a transform near the Bahamas FZ (e.g., Pindell and Kennan, 2009) (see Fig. 3.7) in the Early and Middle Jurassic, with seafloor spreading beginning East in the Late Jurassic (Christeson et al., 2008) and placing the Yucatán Block and the Pan African margin next to each other during the Late Palezoic. Due to this location of the Gulf during the Late Paleozoic, it plays a fundamental role on the understanding of the Tethys corridor. Bartok (1993) related the northeast-southeast trend that parallels the Guiana craton and the eastern part of the North American craton to the Gondwana-Laurentia suture (see Fig. 3.7).

Meanwhile, the Yucatán Block is defined as a small cratonic block located in northcentral Guatemala and Yucatán and the Chiapas Massif (Bartok, 1993). The Chiapas Massif contains the oldest rocks on the Yucatán Block which have radiometric age dates of 1760 Ma (Van Avendonk et al., 2015). Margins formed when North America and Yucatán continental fragment separated in the Early Jurassic. Synrift magmatism added igneous crust to the margins of the Eastern Gulf of Mexico during the early opening of the basin. Seafloor spreading lasted until the Early Cretaceous when motion between the two plates ceased. Rowan (2014) interpreted a zone of exhumed mantle on the northwest margin of the Gulf from industry seismic reflection data, slow mantle observed seismic velocities may represent localized serpentinized (seawater hydrated) uppermost mantle.

3.4.5.1 Implications (from Van Avendonk et al., 2015)

- North America and Yucatán formed part of the same continental block in the Early Jurassic (Salvador, 1987);
- Yucatán Block rotated 40° counter clockwise with respect to North America and that motion ceased in the Early Cretaceous (Marton and Buffler, 1994; Pindell and Kennan, 2009);

- The two conjugate margins started to form prior to the deposition of a thick evaporitic section that dominated the postrift evolution of the GoM;
- The salt deposited in the Callovian (Jurassic) as a single unit at the end of the rifting phase (approx. 3-4 km thick). Eddy et al. (2014) supported a two-stage kinematic model for the opening of the Gulf of Mexico, which includes the following: (1) Triassic-Middle Jurassic south-western movement of the Yucatán Block until 158-154 Ma, which resulted in strike-slip movement in the eastern Gulf of Mexico; and (2) counterclockwise rotation of the Yucatán Block as it separated from Laurentia until c. 140-137 Ma, accompanied by sea floor spreading in the eastern Gulf basin.

Christeson et al. (2014) located the COB at ∼270-290 km on the GUMBO Line 3 model distance given the following :

1. Crustal seismic velocities and thicknesses seaward of the COB are consistent with oceanic crust;
2. Possible outer wedge seaward dipping reflectors (SDRs) landward of the LOC;
3. A landward dipping step in basement height (i.e., the inner ramp of Hudec et al. (2013)) recognized in coincident MCS data;
4. A sharp decrease in magnetic intensity at the edge of the Gulf Coast Magnetic Anomaly (GCMA) overlaps the COB and;
5. The COB coincides with the seaward limit of autochthonous salt.

The location of the COB and an extinct spreading center at ∼470 km model distance help constrain the extent of ocean crust and support a slow rate of sea floor spreading (∼24 mm/yr).

3.4.6 Salt migration and deposition

The presence of the salt provinces and the load of sediments produced by the Missisipi river characterize the northern GoM. Fort and Brun (2012) reported a massive extrusion of allochthonous salt bodies with 8 km maximum thickness, on top of which are deposited Pliocene-Quaternary minibasins (see Fig. 3.8). There is a consensus that salt in the GoM evolved in SW direction since the Cretaceous comprising three stages (Fort and Brun, 2012). Almost all authors argued that sedimentary loading is the main driving force for salt tectonics in the Gulf of Mexico (e.g., Diegel et al., 1995; Hall, 2002; Peel et al., 1995; Worrall and Snelson, 1989). The development of the salt flow driven by the sedimentary loading or predominantly controlled by gliding above the margin dip (Fort and Brun, 2012, and references therein.). The thermal subsidence after the end of rifting favoured the gravity instability together with a progressive sedimentary loading (Fort and Brun, 2012). The crustal stretching facilitated the progressive thinning of the salt layer and the loss of its

decoupling power, consequently producing the migration of the updip extension oceanwards (Fort et al., 2004). Nguyen and Mann (2016) proposed that the salt province split during the oceanic spreading resulting in two salt provinces located at the northern and southern margins of the Gulf, respectively.

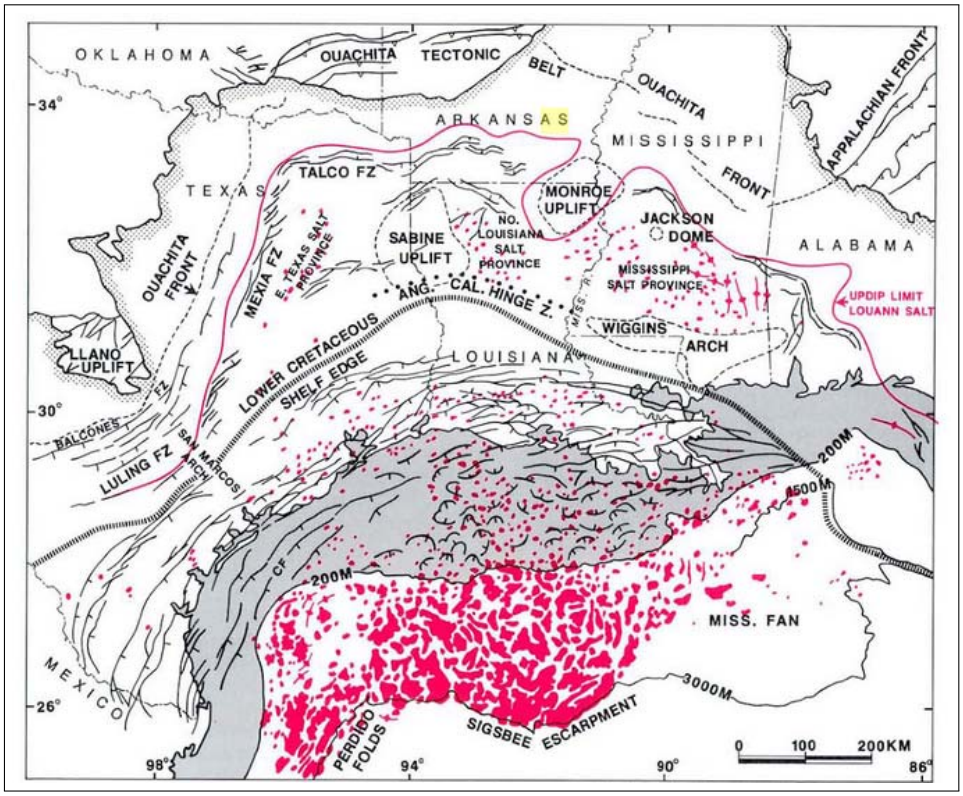

Figure 3.8 – Tectonic map and location of salt domes in the GoM (from (Worrall and Snelson, 1989))

3.5 Data

Magnetic and gravity are the primary data used in this study. The magnetic base map produced from the dataset processed in the framework of this thesis, shows the marine magnetic anomalies with wavelengths less than 300 km (see Fig. 3.4) in the Gulf of Mexico. We produced a grid from the dataset of magnetic anomalies in the GoM at 3 km spatial resolution. Hence, the GoM magnetic map presented in this Chapter has a higher resolution than the magnetic anomaly map covering the Caribbean plate and the Gulf of Mexico presented in Chapter 2. Due to this spatial resolution, it is possible to better appreciate the short wavelength structures associated with seafloor spreading (depending on the spatial resolution of each track line and the coverage of the database). We also used marine tracklines individually (see Fig. 3.9). We performed the individual analysis in those cases in which it was necessary to inspect the magnetic signal directly from the track. We did this step was done in order of detecting discrepancies and to avoid interpretation over artifacts in the grid. However we did not observe marine tracklines well aligned to the orientation of the observed FZ.

Artifacts amid gridded data and track data are common when track lines resolution is low and when the spatial coverage is inadequate, as is the case of the marine track lines coverage for the GoM.

Geomagnetic time scale (GTS) describes the time reversals of the geomagnetic field. We employed three GTS covering the so-called "Mesozoic anomalies" in this study (Gradstein and Ogg, 1996; Kent and Gradstein, 1986; Tominaga and Sager, 2010).

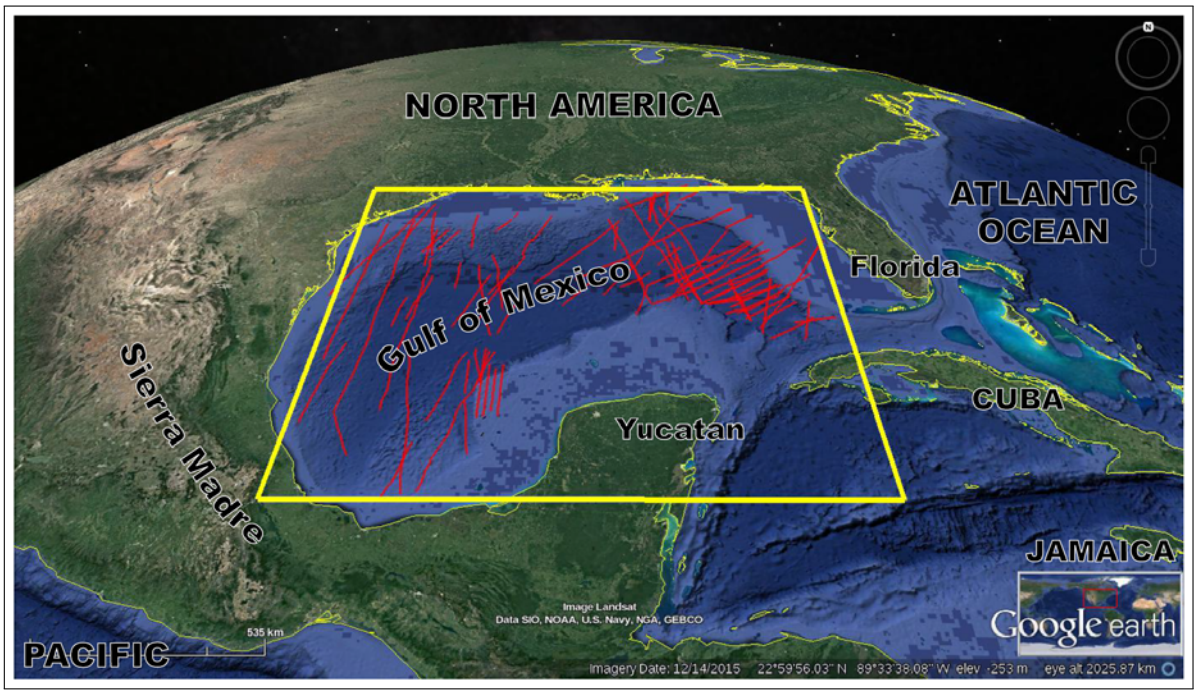

Figure 3.9 – Location of the magnetic profiles used individually in this study

3.6 Methodology

In a practical sense, our first goal is to find and identify magnetic isochrons in the GoM. The spreading direction and the fossil ridge axis can be effectively identified if we recognize magnetic isochrons. Our implemented methodology focus in deciphering and then characterizing the signal of the predominant oceanic structures. The following steps resume the applied methods.

3.6.1 Mapping and interpretation of the magnetic and gravity fabric

Magnetic mapping and interpretation: Linear and parallel magnetic anomalies remain the target in a crust produced by seafloor spreading. To identify such features requires a proper spatial resolution as well as well-oriented profiles and enough closeness to the magnetic source to capture as much signal as possible. We removed spurious data from the dataset and excluded noisy tracks after correcting the sign of those tracks with reverse sign. We used the sign of the magnetic anomalies provided by NCEI as baseline (see Chapter 2).

Identifying seafloor spreading features: We identified features related to seafloor spreading or continental crust, depending on the case. We interpreted the magnetic provinces within the GoM from the analysis of the amplitudes and the magnetic pattern present in the magnetic anomalies at a regional scale. We did that analysis by contrasting the results with the geological provinces in the GoM. High amplitude magnetic anomalies characterize the continental crust which is the result of strongly magnetized rocks. In most cases, the felsic rocks are considered to have a weaker magnetization than mafic rocks (e.g., Hinze et al., 2013). However, mafic rocks in the lower crust in general bear a strong magnetization. Exceptions exist when the presence of certain minerals alters the chemical composition of the crust. The alteration on the chemical composition induces changes in its magnetic properties, the maghemitization results in weaker magnetization (e.g., Hinze et al., 2013; Schnetzler, 1985). On the contrary, magnetic anomalies on the oceanic crust are weaker and exhibit a parallel linear trend. The weakness of the anomalies may be due to the deeper basement. We interpreted the magnetic provinces from the above mentioned criteria but also by juxtaposing that interpretation to the geological and geophysical preliminary information.

Determination of the approximate spreading direction: We used the identified magnetic and gravity anomalies related to seafloor spreading to define the spreading direction and the possible location of the fossil ridge axis along the GoM.

3.6.1.1 Determination of the trial Euler poles from FZs

We used different hypotheses to determine the Euler pole from the identified seafloor spreading isochrons. Bullard et al. (1965) used depth contours of the continental shelf to reassemble the continents. That reconstruction considered the continents as rigid bodies and so their displacementwas a rigid rotation. The basis of the Bullard's exercise was the Euler theorem. The Euler theorem states that "the most general displacement of a rigid body with a fixed point is equivalent to a rotation about an axis through that fixed point". Consequently, if the Earth is considered as a sphere, the rotation is produced around an axis passing through the center of the Earth. In Bullard et al. (1965) exercise, the displacement of each tectonic plate represents the rotation about a suitably chosen axis passing through the center of the Earth. After Bullard et al. (1965), different proposed plate tectonic reconstructions use the same Euler theorem basis (e.g., Müller et al., 1999; Royer et al., 1992). From Euclidean geometry, we know that "the perpendicular raised from the middle of a cord passes through the center of the circle, and through the middle of the arc subtended by that cord" (e.g., Legendre, 1852). Hence, we determined the Euler pole (the center of the circle) from the above considerations and theorem, which was first used in plate reconstructions by Morgan (1968). In our reconstruction we use small circles instead of the great circles employed in Morgan (1968). Hellinger (1979) introduced the discussion about the uncertainties related to the use of small circles and great circles in the plate tectonic reconstruction.

To confirm the first hypothesis raised in this chapter, we calculated the crossings between perpendiculars lines to the interpreted FZs. We wrote a Matlab algorithm to represented those perpendicular lines by great circles (meridians of the rotation) whereas FZs were represented by small circles (parallels of the rotation), and processed in geocentric coordinates. Our algorithm considered trial Euler poles those crossings with high statistical frequency. We built concentric small circles using trial Euler poles to simulate FZ. We exported the results to a Geographical Information System (GIS) and compared them with the initial interpretation of the FZ. We performed that procedure iteratively until the misfit between the interpreted and simulated FZ was minimum. We evaluated that misfit visually.

To confirm the first hypothesis raised in this chapter, we calculated the crossings between perpendiculars lines to the interpreted FZs. Those perpendicular lines were represented by great circles whereas FZs were represented by small circles, and processed in geocentric coordinates. We considered trial Euler poles those crossings with high statistical frequency. Concentric small circles were constructed using trial Euler poles to simulate FZ. The results were exported to a Geographical Information System (GIS) and compared with the preliminary interpretation of the FZ. The chosen Euler poles represent the ones with less misfit.

Selection of a proper geographical projection:

A proper geographical projection can improve the visualization of the FZ and others oceanic structures related to the seafloor spreading. An adequate projection is that capable of transforming seafloor spreading features into simple geometric features. In an adequate projection, the FZs related to the same pole of rotation become linear. The pole of the projection will be the rotation pole. In our calculations we considered the shape of the Earth to be a sphere; thus, we transformed the geographical coordinates into geocentric coordinates for calculations, and then we transformed back them to geographical coordinates for their visualization in the GIS. This change of projection helped us to visualize the FZ for various Euler pole. We plotted the results using an Oblique Mercator Projection, for distances between the trial Euler pole and the FZ higher than 25°. On the contrary, we used a Polar projection with pole at the Euler pole for distances between the trial Euler pole and the FZ less than 25°. If the Euler pole is the correct pole of rotation, each FZ belonging to the same stage of rotation must look parallel among them. In this case, the FZ related to a same stage of rotation must align on concentric circle with respect to the Euler pole of rotation.

In figure 3.11 we show the parameters used to calculate the Oblique Mercator projection. In this case; the principal meridian of the oblique projection is a great circle passing through the Euler pole and a point in the mean of the zone of interest. We calculated the azimuth of the projection from the azimuth of such great circle. As we mentioned before, the pole in the projection will coincide with the Euler pole of rotation.

Ultimately we determined by this way the finite rotation parameters, namely, the longitude and latitude of the pole of rotation, the angle of rotation and age of the rotation (where possible). We could estimate the number of possible stage rotation from the FZ: If an Euler pole can describe the plate motion (i.e. FZ directions), then a single stage of rotation may be sufficient. If the contrary case occurs, more than one single Euler pole is needed to describe the plate motion, and several phases with different poles and angles of rotation occurs.

Estimation of the general asymmetry. This step implied the examination of the previous results together with their comparison with the interpreted features.

Estimation of the local asymmetry.

Generation of flow lines and asymmetry estimation: We produced flow lines on both sides of the fossil ridge axis and estimated the percentage of local asymmetry. The estimated flow lines describe the rotational movement of the plates with respect to its stage Euler pole. Consequently, flowlines are the best fit to the observed FZ but also they provide a prediction for those FZ that are not clearly revealed. We produced the flow lines taking into account the stage(s) of rotation involved in the seafloor rotation.

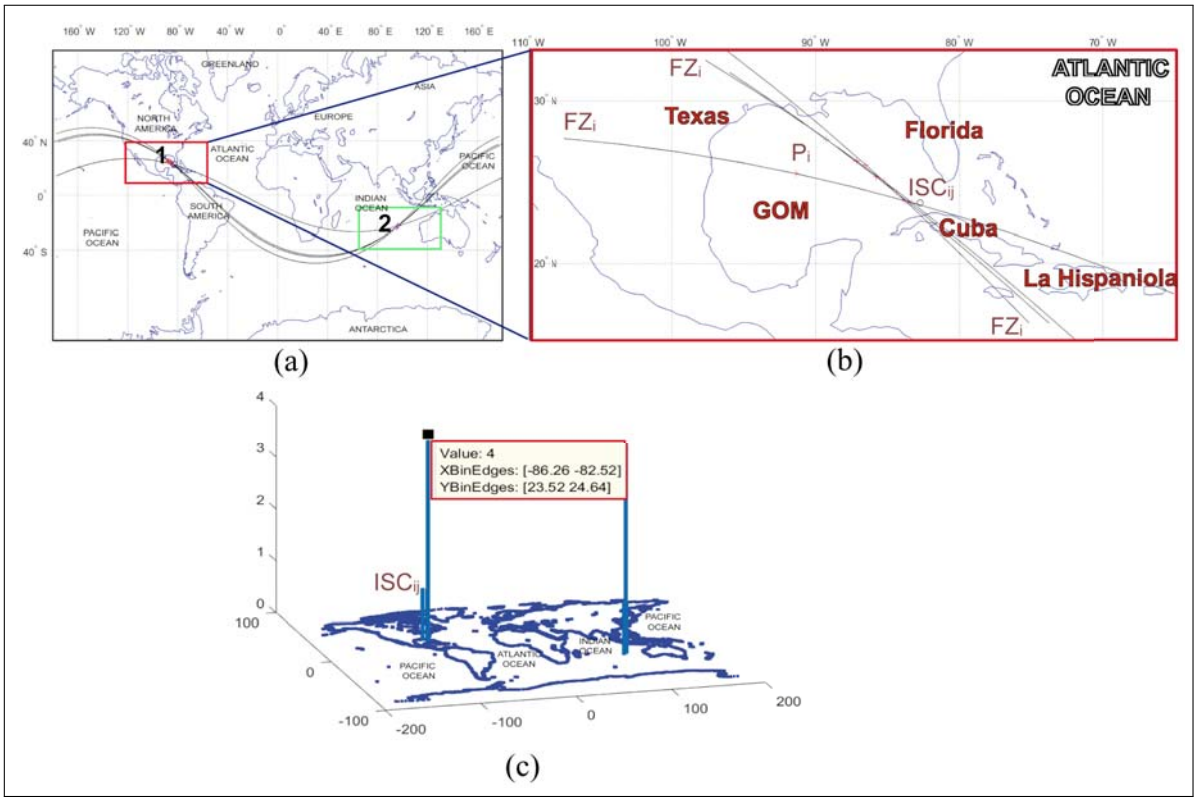

Figure 3.10 – Estimation of the Euler pole produced by our Matlab algorithm. Great circles passing perpendicular to the simulated FZ and by the Euler pole (a); detail of the different great circles calculated in the GoM (b) and, global view showing the two set of solutions for the location of the Euler poles, bars represent the statistical frequency of the crossings between the great circles (c)

3.6.1.2 Identification of magnetic isochrons

1. We used flow lines direction to extract the magnetic profiles from the magnetic grid, in order to attempt identifying the magnetic isochrons;
2. Only long wavelengths lineated magnetic anomalies could be confidently recovered because the direction of the initial profiles used to build the magnetic grid was not optimal to allow recovering details of the isochrons;
3. Consequently, for the sake of comparison we filtered the polarity of the geomagnetic time scale using various Gaussian filters to account for a range of different spreading rates to match the wavelength of the observed magnetic anomalies. We then compared those filtered polarity time scale to the extracted profiles, and the observed lineated magnetic anomalies;
4. We calculated the spreading rate along each flow line. We used the inferred ages of the identified isochrons from three different polarity time scales as reference (Gradstein and Ogg, 1996; Kent and Gradstein, 1986; Tominaga and Sager, 2010). We calculated an average spreading rate along the western, central and eastern part of the GoM respectively.

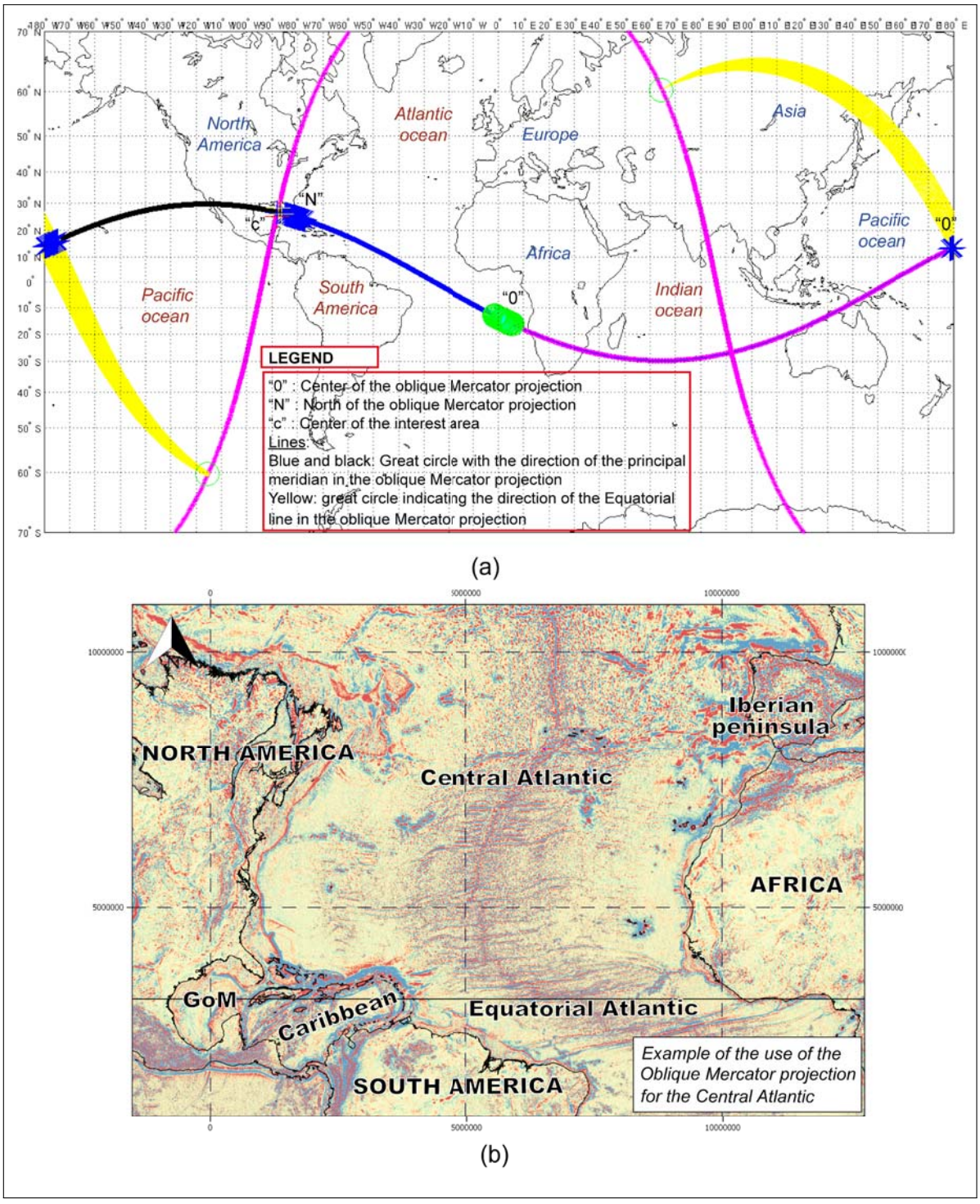

Figure 3.11 – Parameters that we used to apply the oblique Mercator projection (a) and an example of the use of the Oblique Mercator projection for the Central Atlantic (b)

3.7 Results and interpretation

3.7.1 Mapping and interpretation of the magnetic and gravity fabric

3.7.1.1 Surroundings of the Gulf of Mexico

We distinguish four domains on the map of magnetic anomalies of intermediate wavelengths (see Fig. 3.12). From west to east, a first domain associated with the post -accreted terranes at the western margin of the Gulf of Mexico, among which are the Sierra Madre Mountain Range. Magnetic anomalies of low amplitude characterize this domain and whose general orientation is parallel to the direction of the Mountains. To the east, the domain is limited by a NW -SE trending magnetic anomaly associated with the Western Main Transform Fault (see 3.4.3.1).

A second domain corresponds to the Yucatán Block, limited by the Belize Mountains to the south. These magnetic anomalies show greater amplitudes than in the first domain, ranging between -200 nT and 200 nT. Due to their amplitude and pattern, we associate these magnetic anomalies to continental crust. They are linear and parallel by groups and show a distinct pattern compared to those observed in the interior of the GoM. The impact of the Chicxulub meteorite, north of the Yucatán Peninsula, probably produced an aureole reflected in the magnetic anomalies, which superimposed its imprint on the older anomalies of the Yucatán Block. A sharp magnetic gradient interrupts those magnetic anomalies which allows us to delimitate the Yucatán Block. This delimitation corresponds to the COB of the southern part of the GoM.

We identify a third domain of interest Florida. This domain exhibits anomalies with wavelengths similar to those observed in the Yucatán Block, which allows proposing in a first view the analogy between both blocks. For both the Yucatán Block and the Florida Block, the observed pattern of magnetic anomalies interrupts in the direction of the Gulf of Mexico. This interruption of pattern leads to define the southern and northern boundaries of both tectonic blocks, respectively. The salt provinces in the north and south GoM mask the response of the gravitational signal, but for the magnetic data the salt province remains imperceptible. The magnetic signal that we observe directly reflects crustal magnetization.

We identify a fourth magnetic domain located between the Florida Block and the Sierra Madre Mountain Range. This domain shows a magnetic anomaly that parallels the coastline and may reflect the contrast between continental and oceanic crust in this area.

3.7.1.2 Interior of the Gulf of Mexico

The observed magnetic anomalies in the Gulf of Mexico have a tenuous expression. Their pattern is fan -like and arcuate. We do not observe different magnetic domains that would suggest that different types of crust co -exist within the GoM. Considering the amplitude of

the anomalies, their shape and distribution, we suggest they reflect the opening of the ocean floor that gave birth to the Gulf of Mexico. This group of elongated anomalies in the Gulf of Mexico has a maximum of 1.500 kilometres long and covers the GoM from west to east. Numbers one, two and three respectively on Fig. 3.12 indicate the prominent anomalies. We also identified a pair of parallel anomalies located north and south respectively of the prominent anomalies (see '*' in Fig. 3.12). However, given their short extension we are unable to delineate them in a more effective way.

3.7.1.3 Synthesis of the maps interpretation

The synthesis from our interpretation of the magnetic map of the GoM is:

- Magnetic anomalies ranging approximately between -70 nT to 70 nT characterize the crust that forms the GoM;
- We identified a set of W -E elongated and positive magnetic anomalies (see Fig. 3.12). The shape of these magnetic anomalies is fan-like and arcuate towards the South. They are approx. 1500 km long and due their amplitude, shape and distribution we relate them with seafloor spreading structures;
- The northernmost elongated magnetic anomaly lies farther north of the southern boundary of the Sigsbee salt province (see '*' in Fig. 3.12). Such an extension suggests that the opening of the GoM initiated farther north of the Sigsbee salt province;
- In the Central part of the Gulf of Mexico, we recognize magnetic highs and interpreted them as being produced by magmatic intrusions in the lower crust. We related those magmatic intrusions to high seismic velocities (Eddy et al., 2014). However we note that these highs extend from west to east throughout the whole basin. Their extension suggest that they can better explained by seafloor spreading;
- We do not observe tiny magnetic anomalies with a linear and parallel signature (associated with seafloor spreading) in our dataset;
- We propose that due to the misorientation of the marine tracks in the GoM with respect to the spreading direction there is a lack of consistent short wavelength magnetic anomalies;
- Vertical gradients of gravity exhibit N-S linear pattern related to FZs in the southwestern part of the GoM (see '3' in Fig. 3.4). Marine tracks were acquired before the revealed orientation of the FZ (at least at the western part of the GoM) by satellite altimetry (e.g., Bonvalot et al., 2012; Sandwell et al., 2014). Among the poorly-oriented profiles, some data with limited resolution or poor navigated tracks hinder the identification of the magnetic isochrons;
- The Eastern GoM is narrower than the Western GoM. Then we expect that the record of the spreading stages (if there is any) will be more complete and/or better expressed

in the western side;

- Our interpretation pushes the COB significantly to the North, in comparison with that proposed by other authors (e.g., Bird et al., 2005; Christeson et al., 2014; Hudec et al., 2013; Marton and Buffler, 1994; Sandwell et al., 2014; Sawyer et al., 1991; Schouten and Klitgord, 1994; Seton et al., 2012). Consequently to perform the reconstruction an angle of rotation larger than previously proposed is required. Hence, our interpretation is closer to that of Pindell (1994);
- Given that there is no drilling sample of the acoustic basement in the GoM and therefore no magnetic properties measurements, the previously proposed models poorly constrained the magnetic susceptibility (Carlson and Herrick, 1990; Christensen and Mooney, 1995; Hunt et al., 1995);
- We recognize intermediate wavelength magnetic anomalies related to seafloor spreading. We attempt to use them taking into account the FZ signature revealed in the VGG;
- The above mentioned magnetic anomalies are the primary input for our plate tectonic model. We will use the interpreted FZs from the vertical gradients of gravity as secondary input for the tectonic model;
- Hence, the scope of this chapter is the interpretation of the intermediate wavelengths of the magnetic anomaly polarity along the direction of interpreted FZs. This is due to the insufficient resolution and inadequate quality of the marine data.

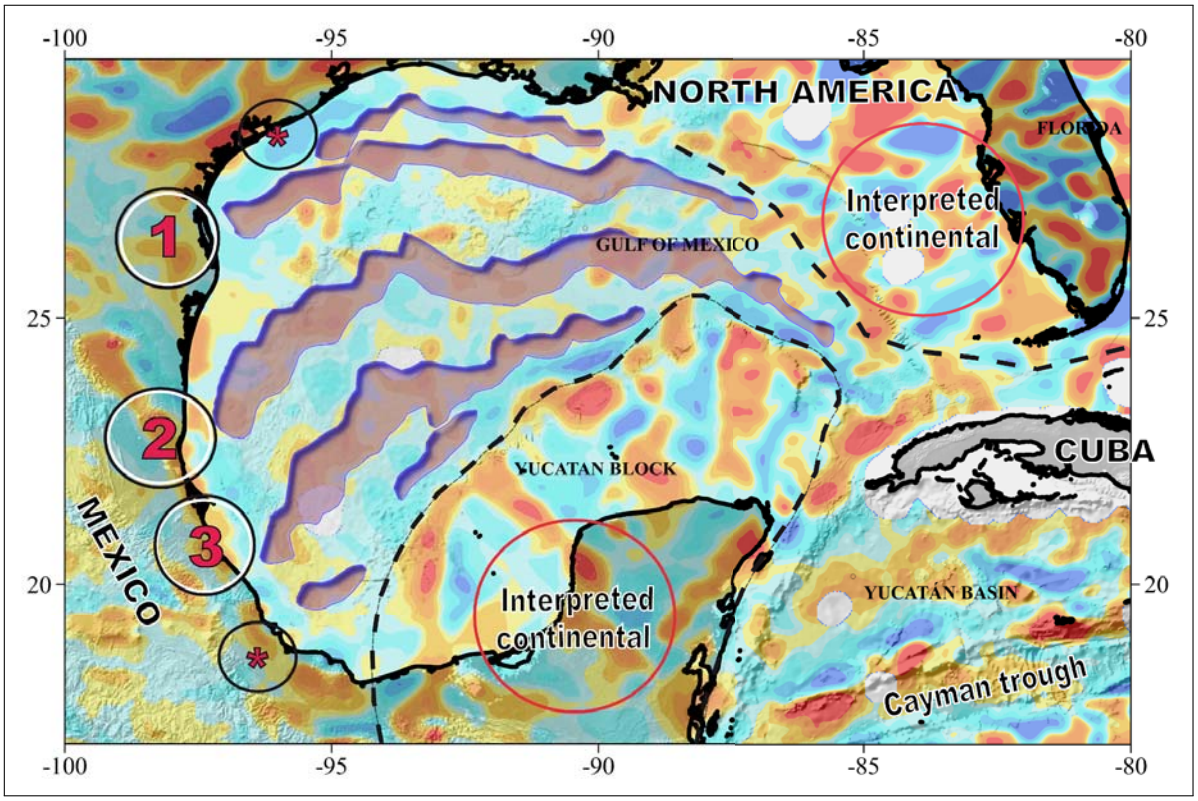

Figure 3.12 – Three fan-like magnetic anomalies on each flank. Central anomalies are marked by 1, 2 and 3; outer anomalies '*'; dashed black lines represent the boundaries of the Yucatán Block and Florida Block respectively

3.7.2 Trial Euler poles

3.7.2.1 Laying the foundations for the plate tectonic reconstruction in the GoM

The reconstruction of the Atlantic turns out to be the starting point for anyone who wants to undertake the global study of the GoM and the Caribbean. The first step in the plate tectonic reconstruction consisted in the determination of the Euler poles for the Central Atlantic and South Atlantic. To define these Euler poles, we used the shelf breaks as reference as they were interpreted from magnetic and gravity data. Fracture zones are fine delimited in the vertical gravity gradients. It is possible to define at least two criteria to select the boundary used for the tectonic reconstruction: either we can choose those features marking the continental break-up (1) or those features marking the continent-ocean boundary (2). Implications of using the first or the second features are different. The break-up boundary may not be parallel to the COB, for different reasons beyond of the scope of this work. Consequently, we may obtain different fits depending on which feature we use.

We performed our fit of the North American and the African continent by using the continent-ocean boundary (COB) interpreted from the vertical gradients of gravity (Sandwell et al., 2014) (see Fig. 3.14). The high gradients of VGG indicate the density contrast between the two types of crust. We used qualitative analysis of the magnetic anomalies pattern to delimitate the COB (see Chap. 2). The COB is marking the transition between the

stretched continental margins and the oceanic crust at the easternmost of the North American continent and the westernmost of the Europe continent. Consequently, the COB marks a phase transition between the continental rifting and the starting of the oceanic spreading. Our calculated finite rotation for the Central Atlantic and South Atlantic conduct us to propose and to confirm that the Yucatán Block obtained its actual position after or during the Pangea break up. The proposed rotation the Yucatán Block implies a Late Triassic opening for the GoM (see Fig. 3.13). Thus, our model supports the counter clockwise rotation of the Yucatán Block after or during the Pangea break up respect to the North American continent, and closely linked to the opening of the Central Atlantic and Equatorial Atlantic. On the US western margin and the western Africa continent, magnetic isochrons allowed constraining the path of the two plates during the oceanic opening.

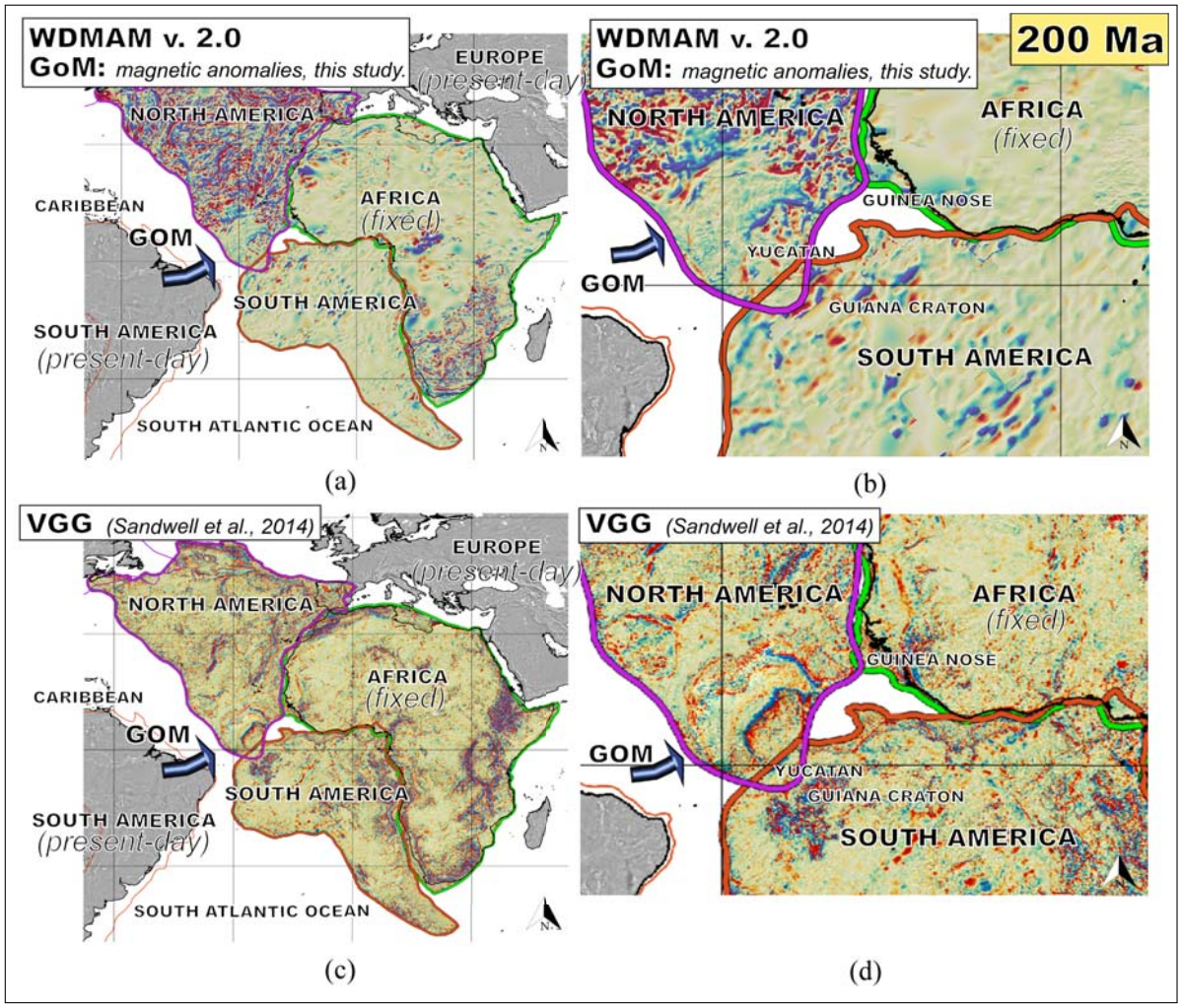

Figure 3.13 – Focus on the Pangea reconstruction from magnetic and gravity data respectively. Pangea reconstruction based in magnetic data from WDMAM 2.0 (a), focus in the Southern North American continent-Northern South American-Western African continent fit 200 Ma ago, observed amplitude of the magnetic anomalies in the North American continent is stronger than those observed over the South American continent and the African continent (b), similar reconstruction were performed using vertical gradients of gravity (c and d)

We do not observe preferential direction in the magnetic anomalies lying off the COB and

no parallel magnetic anomalies related to the continental drift. We base our estimations of the rifting direction on the results of fitting the COB on both sides of the seafloor spreading. In our plate tectonic reconstruction for 200 Ma, if the Yucatán Block is kept in its current position, it overlaps the Venezuelan Central and Eastern Range respectively. This overlap prove that the GoM is at least partially oceanic and should be closed. In order to reconstruct to GoM, we are forced to move the block in a clockwise direction to restore it to its probable initial position. Regarding the Florida Block, its displacement is unnecessary for the GoM plate reconstruction. Our reconstruction underlines affinities between the magnetic anomalies of the South American and African continents. The Florida Block could be adjacent to Guinea Nose. However, the lack of correlation between the magnetic anomalies of both blocks prevents affirming that both blocks are of the same nature. Such differences are unnoticeable in the vertical gradient of gravity, which on the contrary, demonstrates spectacularly the continuity of the anomalies from the reconstruction of Pangea. From this reconstruction, we envisioned that the Yucatán Block could be next to the Guiana craton.

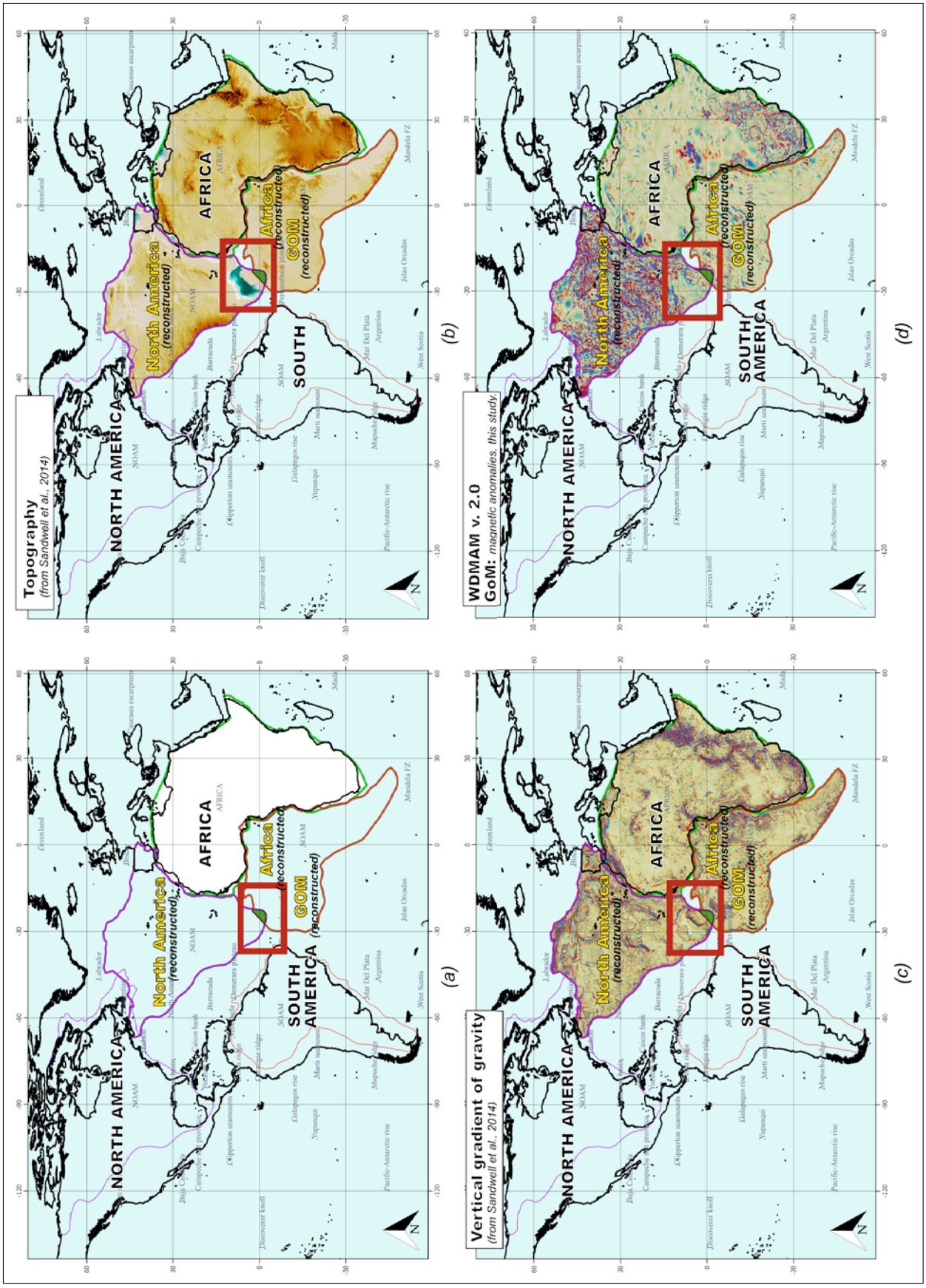

Figure 3.14 – View of the Pangea reconstruction from gravity (b), topographical (c) and magnetic data (d) centred in the Atlantic Ocean

3.7.3 Closure

We obtained the pole of rotation for closure of the GoM from the juxtaposition of the northern limit of the Yucatán Block, interpreted from the magnetic data, with the southern edge of the North American plate at the level of the Gulf of Mexico.

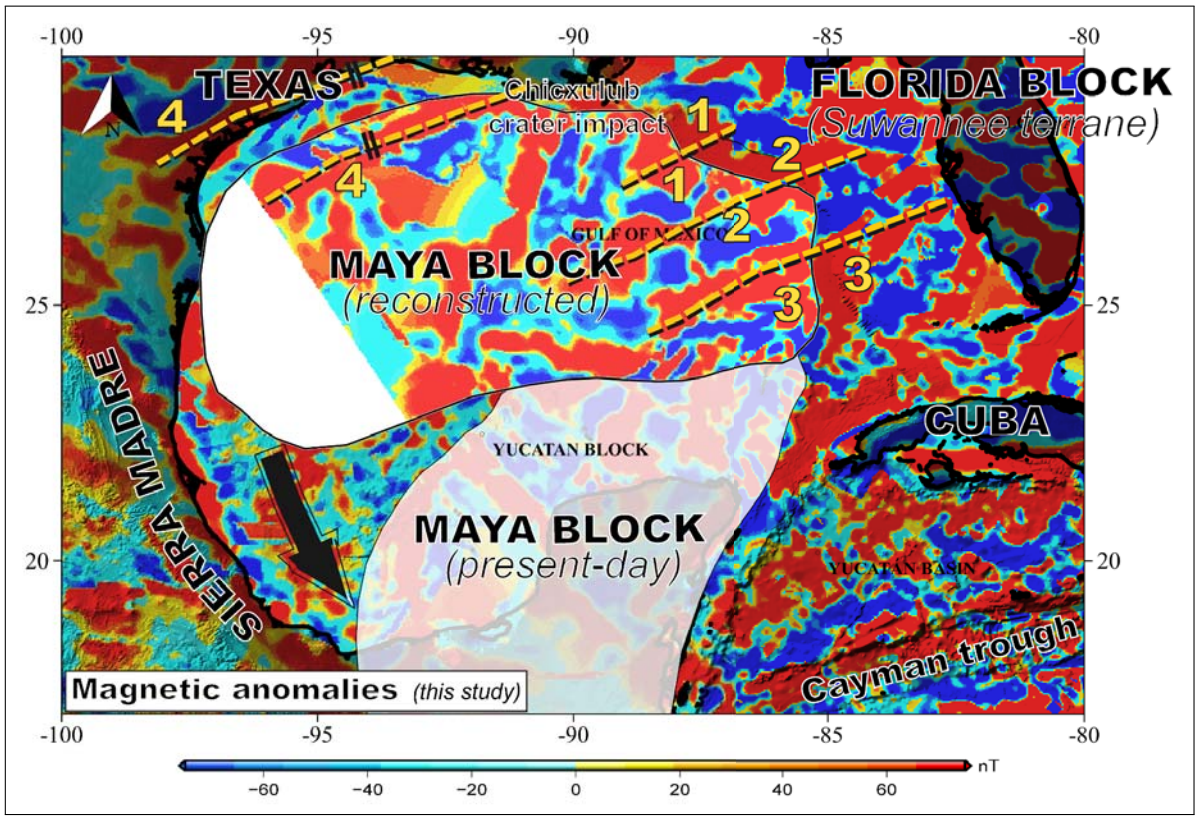

Figure 3.15 – Tectonic reconstruction of the Gulf of Mexico from magnetic anomaly

The rotation pole that best fits the available information is 85.26°W,23.85°N with an angle of 60.25° (see Fig. 3.15). In this plate tectonic reconstruction, we identified a set of magnetic anomalies on the Yucatán Block, named 1, 2 and 3 (see Fig. 3.16). This group of anomalies aligns with conjugate anomalies identified in the Florida Block (see Fig. 3.16). From this adjustment we propose that the area occupied by these anomalies was part of the same magnetic domain before rupture of Pangea. This magnetic domain may correspond to the Suwannee Block. Our model suggests that the Suwannee Block may be a tectonic block belonging to the African continent, detached from this continent during the Pangea rupture, as proposed by other authors (Thomas et al., 2006).

The Bahamas fracture zone affects only our proposed Suwannee Block, which history may predate the formation of the Gulf of Mexico (see Fig. 3.17). The Oblique Mercator projection is the most convenient geographical projection to visualize better the structures related to the plates rotation. We used this projection in the reconstruction of the Central Atlantic and the Equatorial Atlantic.

However, in the Gulf of Mexico we used the Polar projection since the distance between

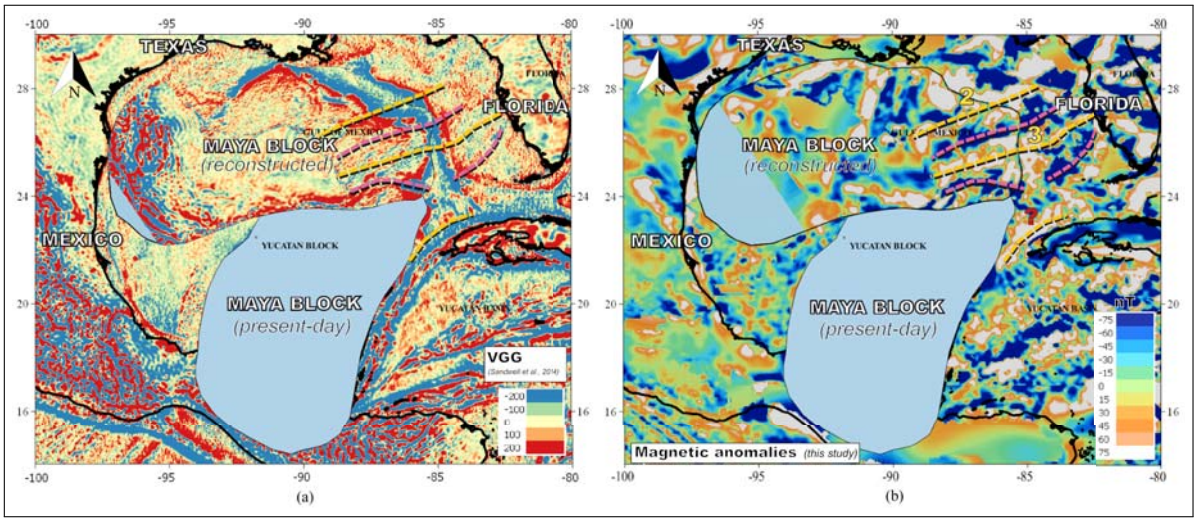

Figure 3.16 – Adopted tectonic model from VGG (a) and magnetic anomaly data (b). Dashed yellow lines represent the correlation that we observe between magnetic anomalies highs of the Yucatán Block and the Florida Block respectively. Dashed fuchsia line represents the respective correlation for the magnetic anomalies lows

the total rotation pole and the fracture zones is extremely short less than 25 degrees (see Fig. 3.18).

3.7.4 Stage poles of rotation and spreading asymmetry

We identified pairs of conjugated anomalies and the ridge axis from the magnetic anomaly map. These conjugated magnetic anomalies helped us to constrain the youngest and oldest rotation stages in the GoM. We reconstructed the conjugated magnetic anomalies marked as '1' and related them to the youngest stage of rotation, whereas we used those ones marked as '2' in Fig. 3.19 to estimate the rotation parameters for the second stage of rotation.

We calculated the distinct stages of rotation using the orientation of the interpreted fracture zones. We interpreted the fracture zones from the vertical gradient of gravity and, from the prominent magnetic anomalies described in the previous section (see Fig. 3.20). We show the stage poles calculated for each stage of rotation in the Table No. 3.1.

Table 3.1 – Stage poles for each rotation stage in the GoM respect to our interpreted ridge axis

Different stages of rotation	Longitude (degrees)	Latitude (degrees)	Angle (+=counterclockwise)
Oldest – South	-86.76	23.81	17.40
Oldest – North	-86.08	25.10	11.40
Youngest – South	-83.95	23.20	18.02
Youngest – North	-83.95	23.20	13.42

We designed an algorithm to estimate the probable location of the Euler pole from the fracture zones. We stored the interpretation of the FZ in shapefiles, and later it was used in

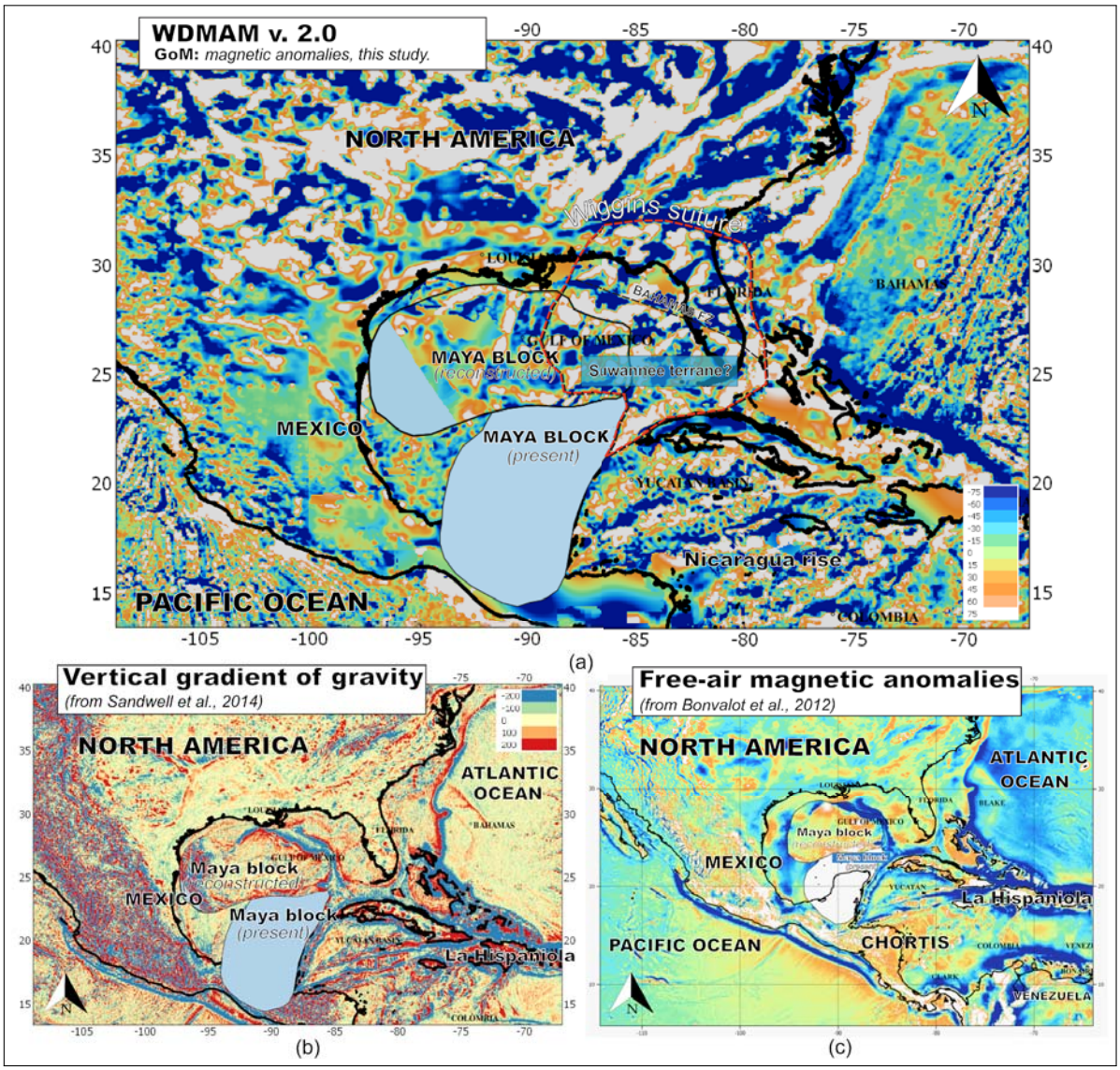

Figure 3.17 – Extended view of the adopted tectonic model from VGG and magnetic anomaly data

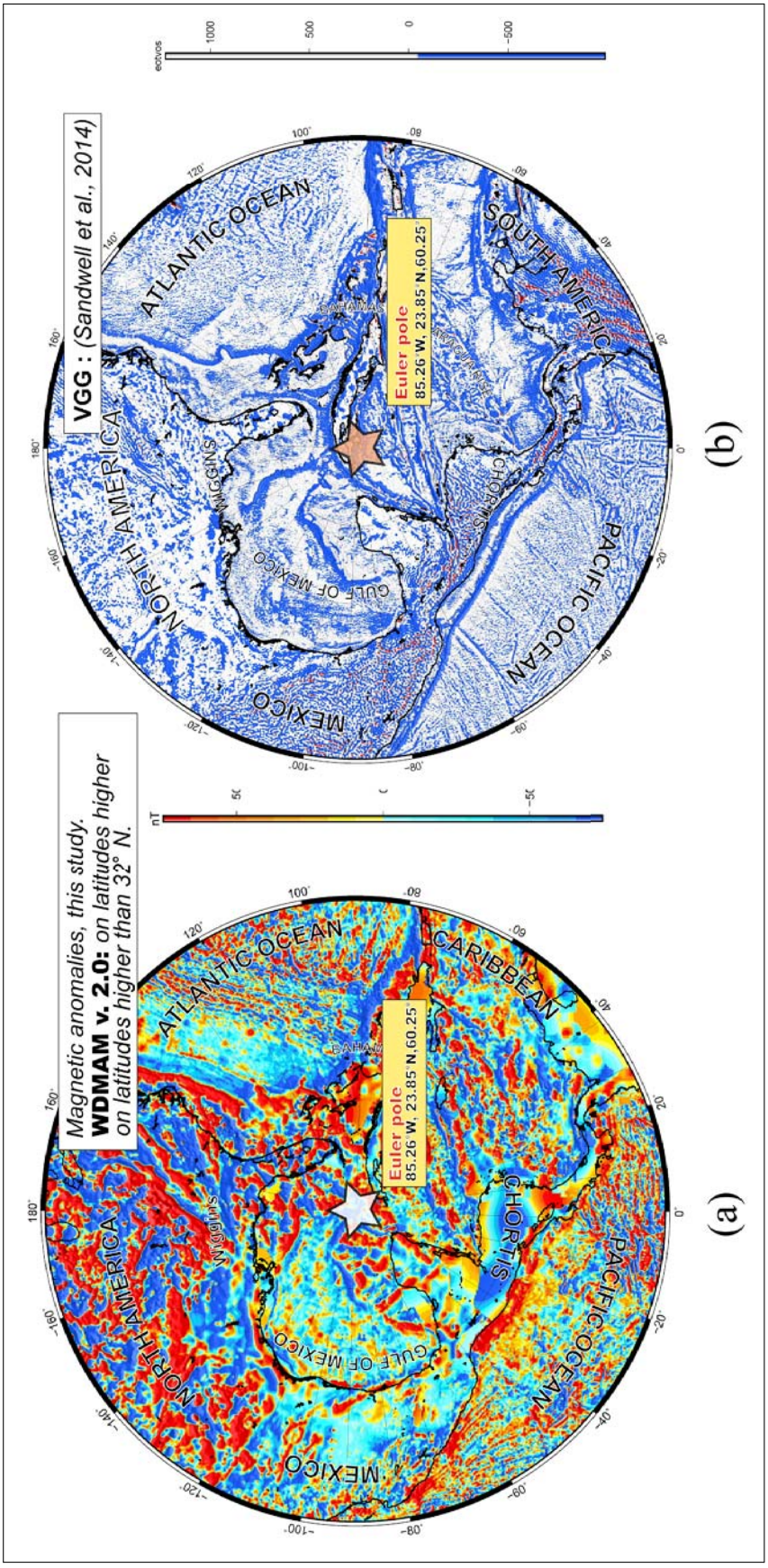

Figure 3.18 – Magnetic and gravity maps in polar projection, using the Total Euler pole as pole of the projection

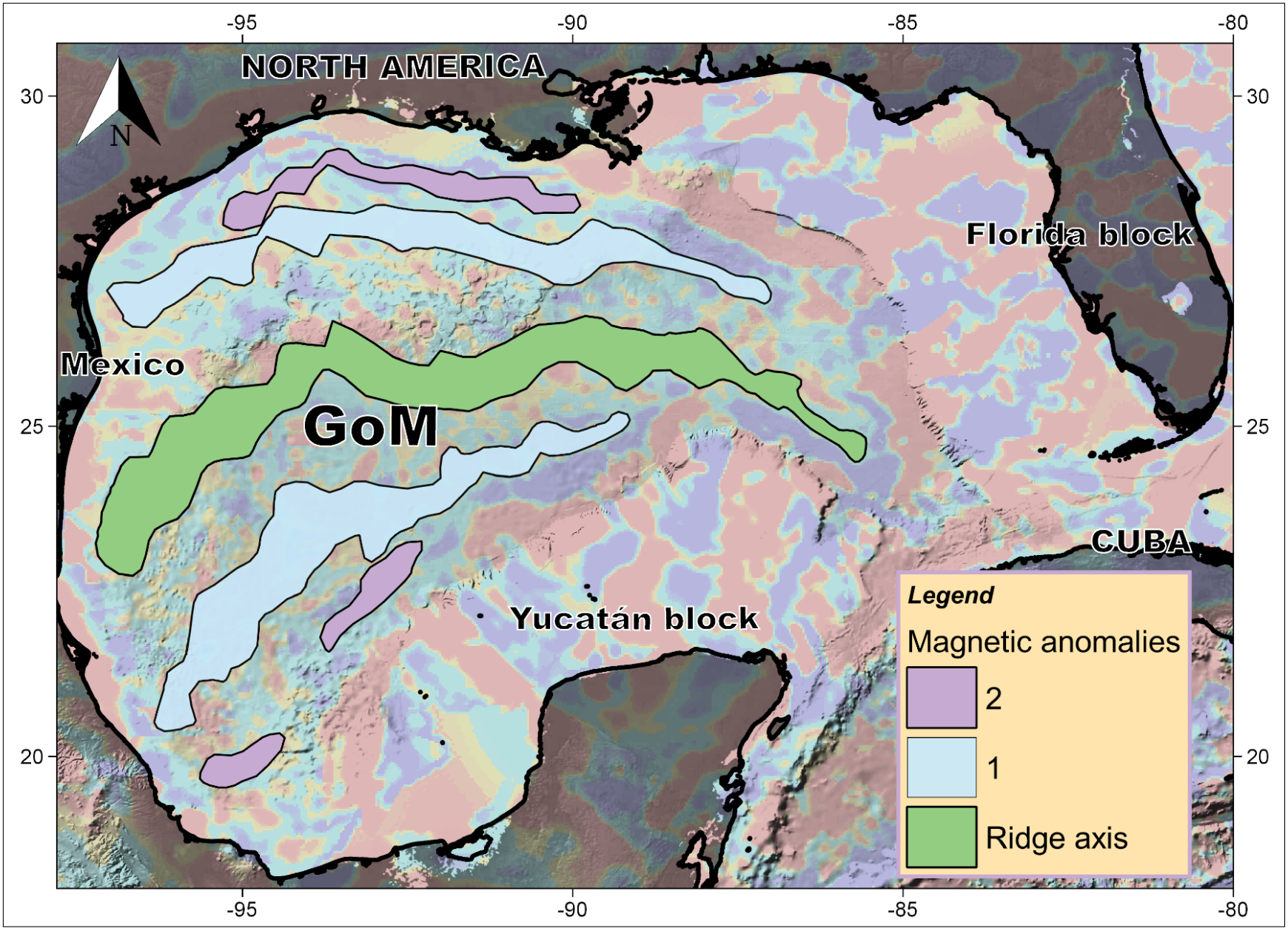

Figure 3.19 – Interpretation of the conjugated magnetic anomalies in the GoM. Colors represent different stages of rotation: Light violet represents a younger rotation stage than darker violet (outer magnetic anomalies)

MATLAB to constraint the rotation results (this was also mentioned in the Methods section).

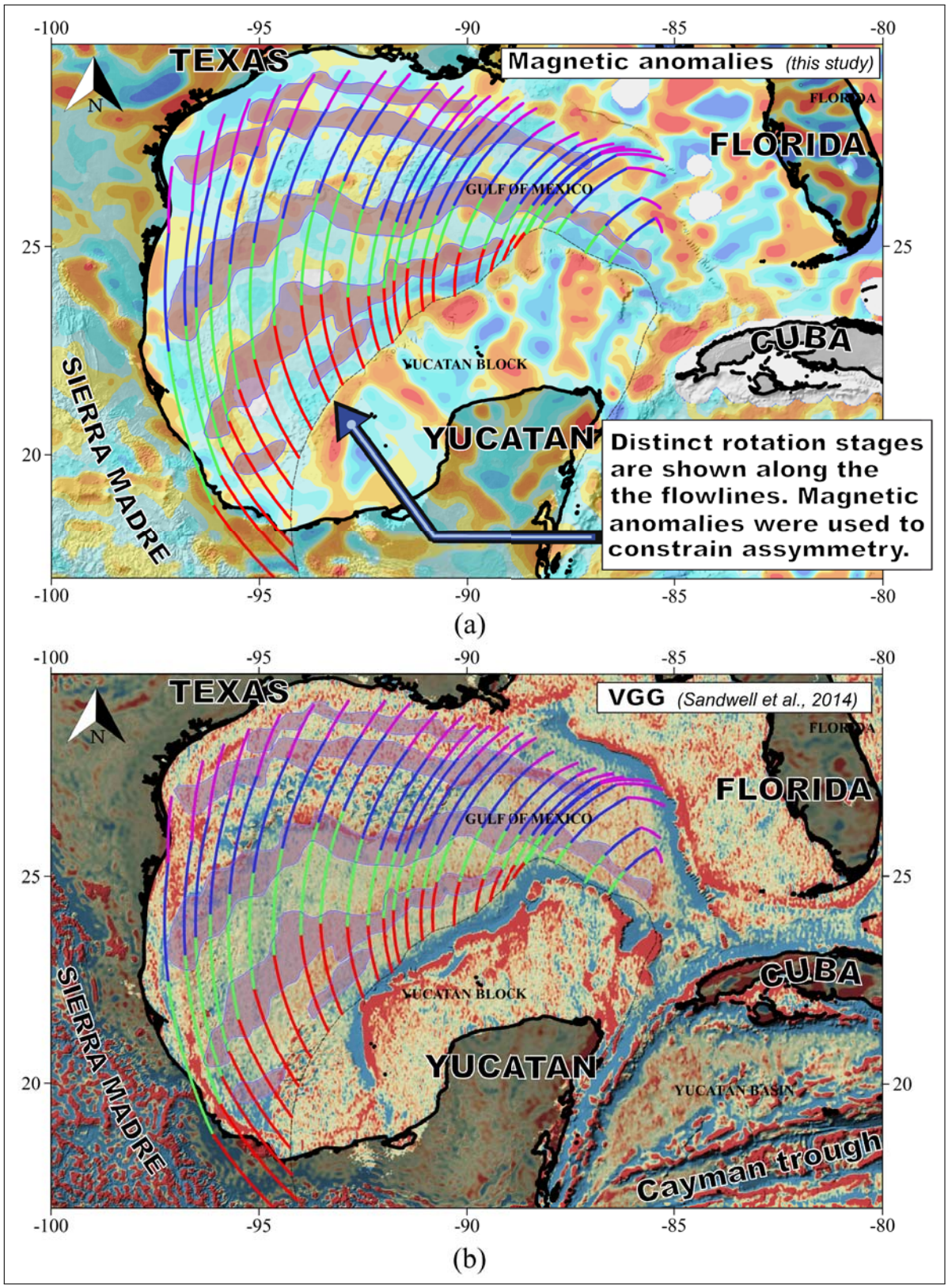

Figure 3.20 – Flow lines showing the different stages of rotation in the GoM

We used the anomalies '*' to determine previous stage of rotation. We generated flow lines for each stage of rotation, to describe the rotation movement of the Yucatán Block (see

Fig. 3.21). The flow lines simulate the shape of the fracture zones in the Gulf.

We computed the asymmetry along each flow line (see Fig. 3.21 and Fig. 3.22). Seafloor spreading was asymmetrical for the different stages of evolution depicted by the magnetic anomalies in the Gulf of Mexico. In the Western GoM, the amount of crust formed was

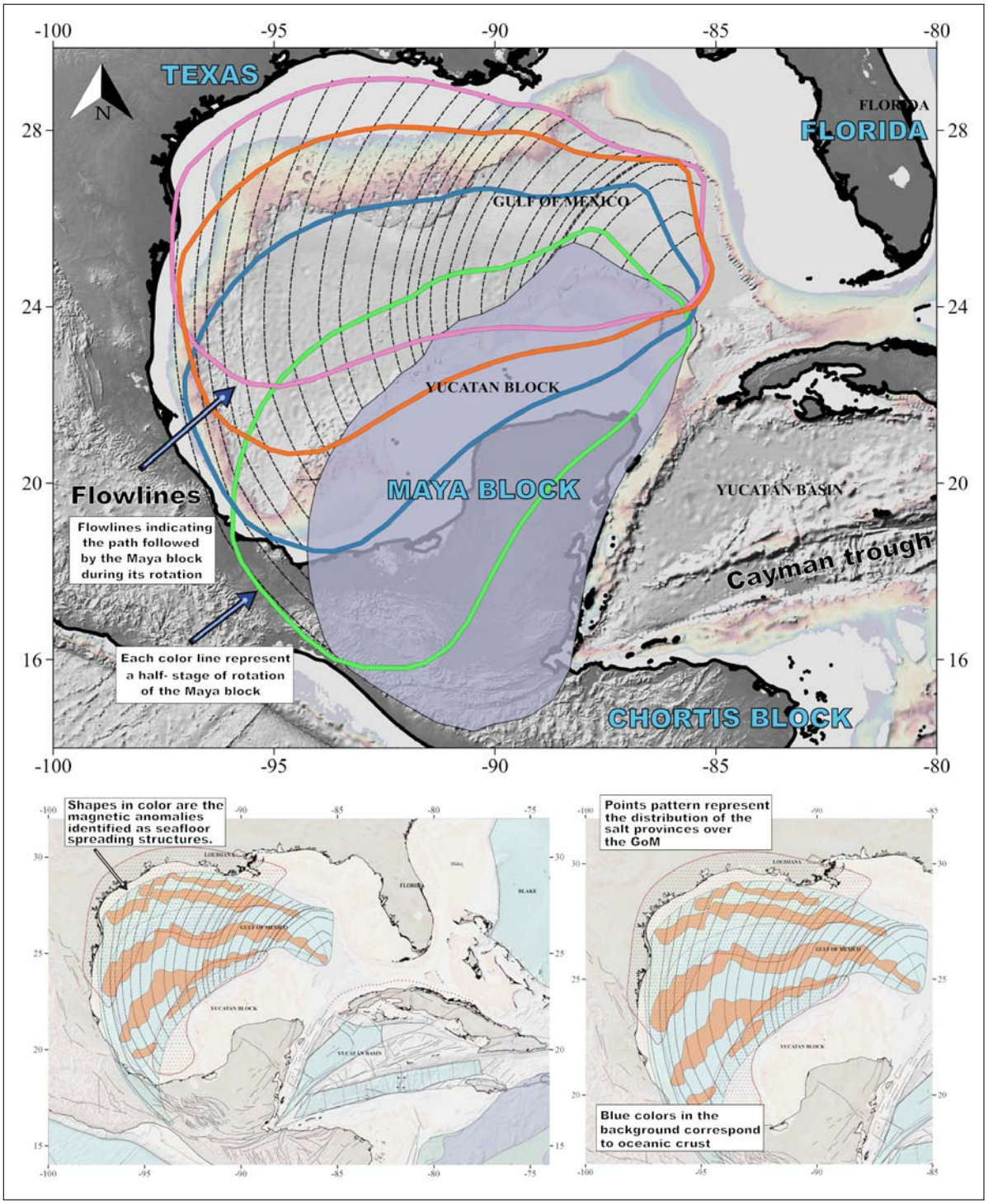

Figure 3.21 – Sketch of the location of the Yucatán Block at different stages of rotation. Legend: Points pattern represent the distribution of the salt provinces over the GoM; flowlines indicate the path followed by the Yucatán Block during the rotation; each color line represent a half-stage of rotation

higher south of the ridge axis. On the contrary, in the Central and Eastern GoM, the amount of crust formed was higher north of the ridge axis (see Table No. 3.2).

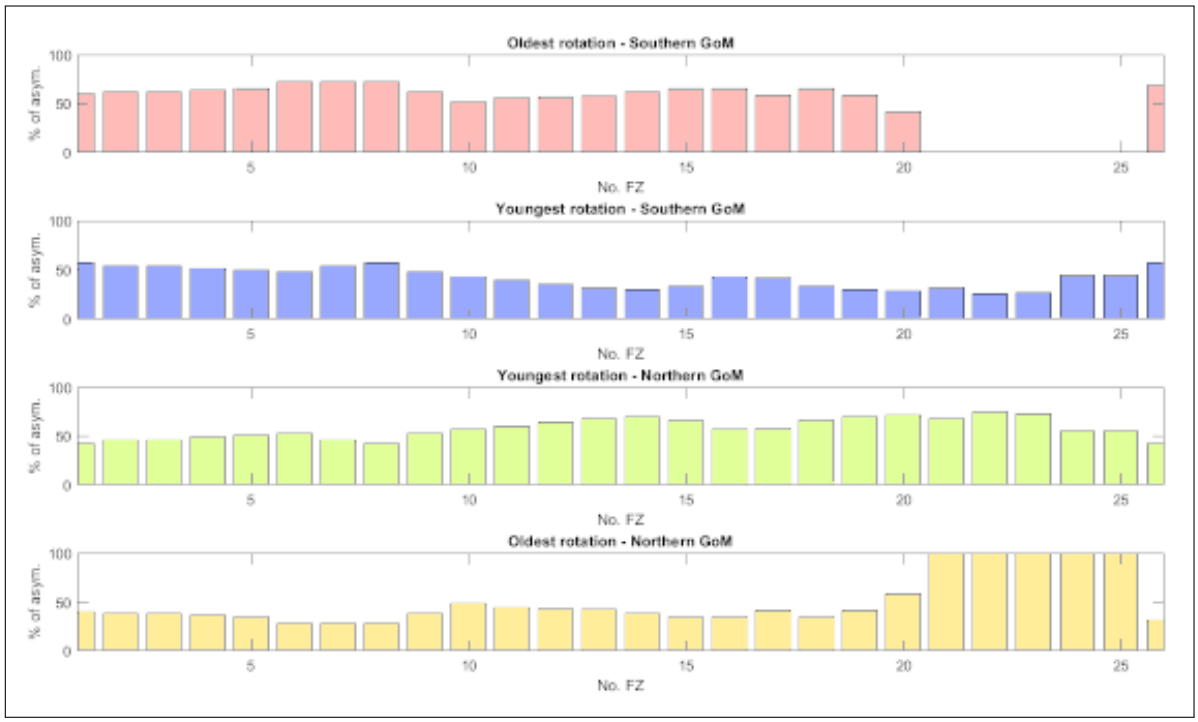

Figure 3.22 – Percentage of asymmetry along the different stages of rotation

We propose that the asymmetry may be responsible for the remaining misfit observed among the FZ direction obtained from gravity and magnetic data respectively. However, the proposed model generally allows reconciling the orientation of the fracture zones obtained from the gravimetric data and the orientation provided by the magnetic data.

The asymmetry may also explain why some short fossil ridge are observed on gravity. They do not correspond to the magnetic anomaly that we interpret as marking the fossil spreading center and most probably represent local ridge jumps as possible for the observed asymmetry.

3.7.5 Magnetic isochrons and Spreading rates on the GoM

To identify the magnetic isochrons, magnetic tracks must resolve wavelengths less than 20 kilometres. However, the magnetic grid lacks data in many places, and the quality of its data is questionable as well. For these reasons, the recovery of the magnetic signal at the minimum required wavelength remains not a straightforward issue. The first intuition we had was the grid resolution would not allow us to identify the magnetic isochrons. However, we wanted to confirm this statement, from along modeled flowline, i.e. inferred spreading center, assuming our rotation pole. We extracted magnetic anomalies from the grid (see Fig. 3.24 and Fig. 3.23). Both vertical and horizontal scales are the same to all the profiles. The uniformity in the scales facilitates the comparison of the profiles and facilitates the

Table 3.2 – Percentage of seafloor spreading symmetry from our proposed model for each stage of rotation

Asymmetry - Entire GoM (%)				
	Old-South	*Young-South*	*Young-North*	*Old-North*
Min	0.00	25.52	42.69	27.44
Max	72.56	57.31	74.48	100.00
Mean	50.10	42.13	57.87	49.90

Western GoM (%)				
	Old-South	*Young-South*	*Young-North*	*Old-North*
Min	60.41	47.77	42.69	27.44
Max	72.56	57.31	52.23	39.59
Mean	66.31	53.02	46.98	33.69

Central GoM (%)				
	Old-South	*Young-South*	*Young-North*	*Old-North*
Min	51.74	30.29	56.99	34.38
Max	65.62	43.01	69.71	48.26
Mean	59.95	36.93	63.07	40.05

Eastern GoM (%)				
	Old-South	*Young-South*	*Young-North*	*Old-North*
Min	41.32	25.52	55.40	41.32
Max	58.68	44.60	74.48	100.00
Mean	14.29	33.24	66.76	85.71

identification of the magnetic isochrons. We present the magnetic profiles from west to east in Fig. 3.23.

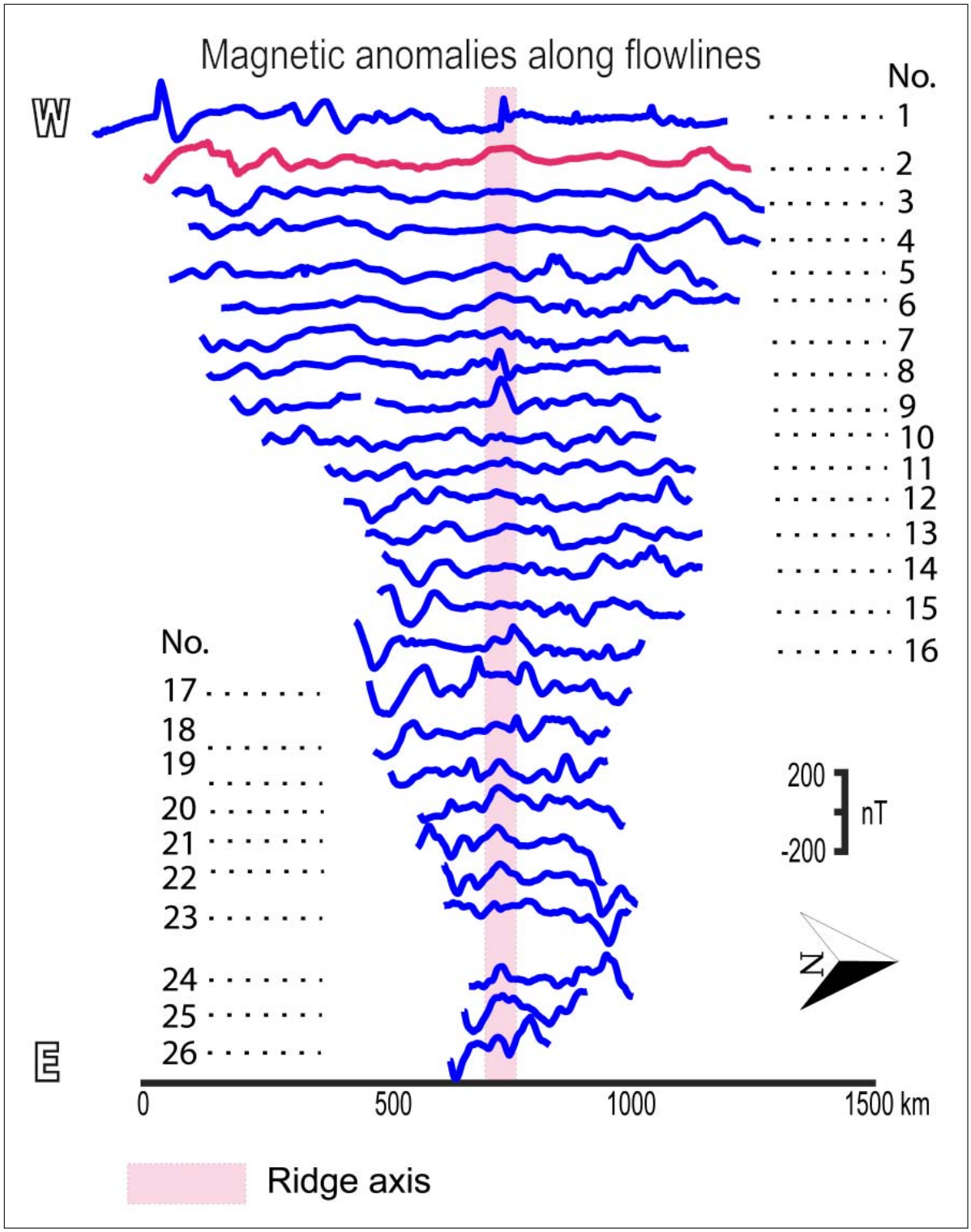

Figure 3.23 – Marine magnetic anomalies from west to east of the GoM as estimate from our grid. We plotted the profiles centered in the ridge axis

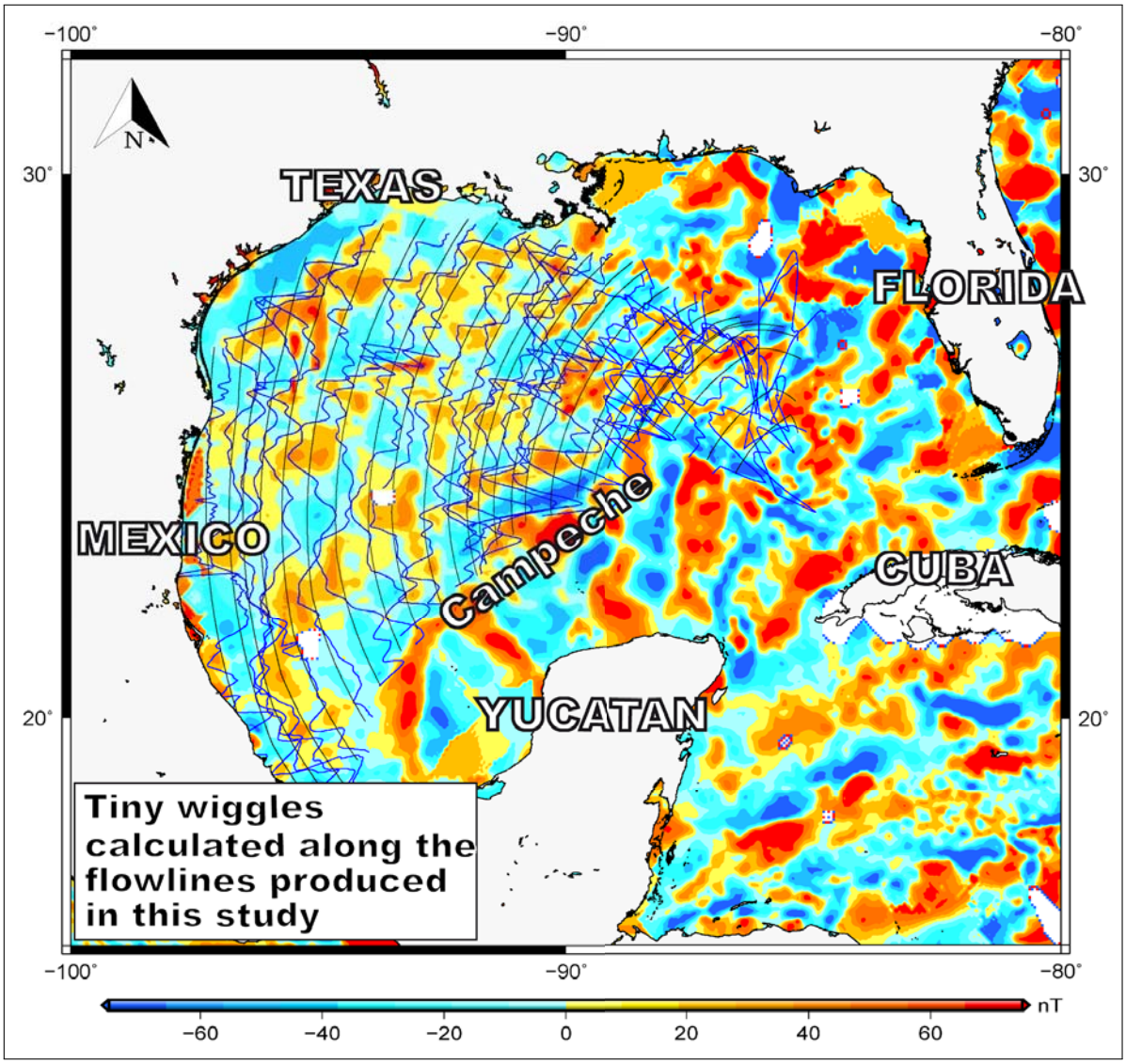

Figure 3.24 – Magnetic wiggles from the previously extracted profiles

We used the ridge axis as reference in the distance axis. The peaks or shapes of the correlated anomalies have intermediate wavelengths. Given the quality of magnetic campaigns, short wavelengths may be unreliable.

The magnetic wavelengths that we observe in the Gulf of Mexico do not allow the proper identification of isochrons in short time intervals. We applied a Gaussian filter to the geomagnetic polarity time scale (see Fig. 3.25) to retain only the long wavelengths of the GPTS for comparison with the data (see Fig. 3.26).

We did not correct the magnetic anomalies skewness. Because magnetic anomalies in the GoM are supposed created near the Equator along an E-W spreading center, they must produce an anomaly centered on the source with normal polarity generating a negative anomaly and reversed polarity a positive anomaly (skewness = 180°). We inverted the GPTS polarity before comparing it with the marine magnetic anomalies (see Fig. 3.26.

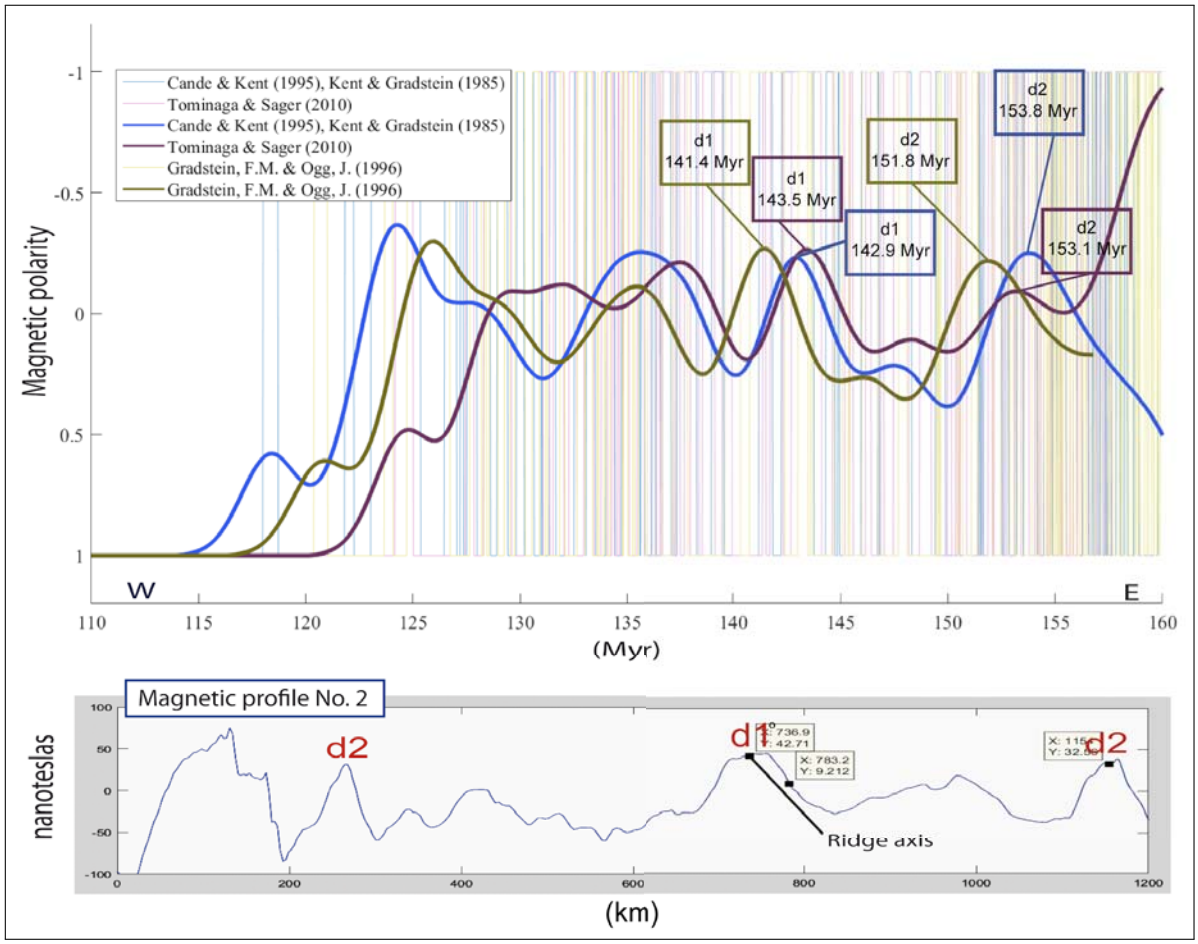

Figure 3.25 – Filtered geomagnetic time scale (normal polarity). In the background, vertical lines in colours represent the geomagnetic polarity time scales before filtering

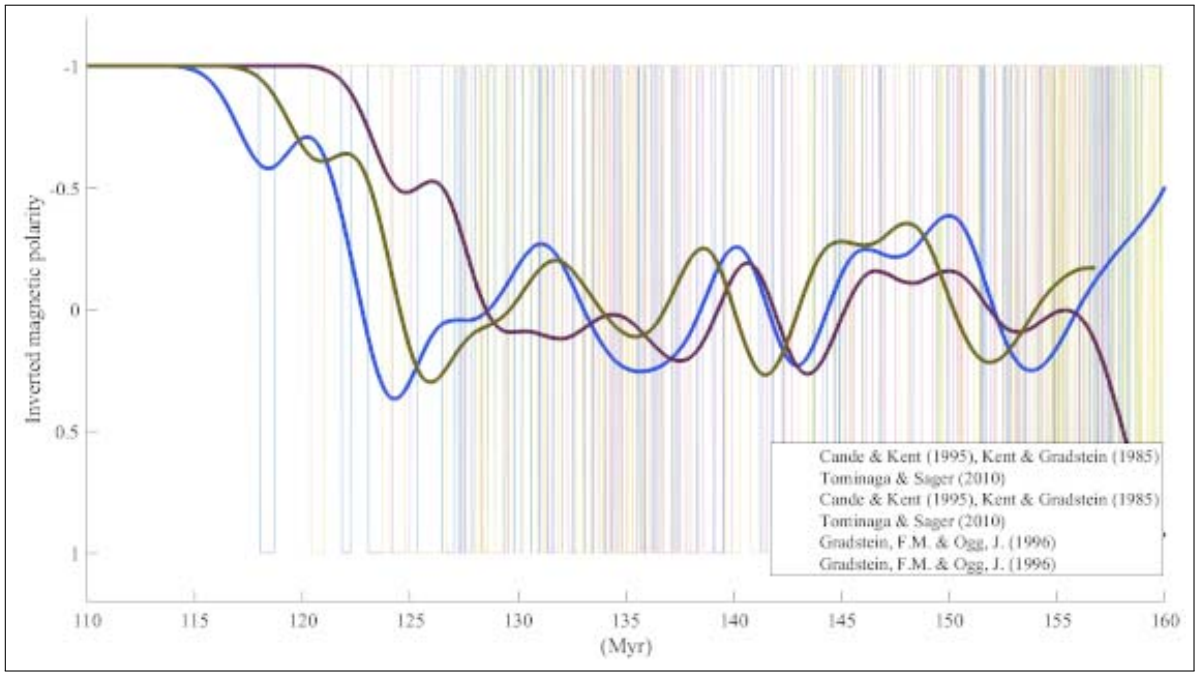

Figure 3.26 – Filtered geomagnetic time scale (inverse polarity). In the background, vertical lines in colours represent the geomagnetic polarity time scales before filtering

We carried out this process was on three GPTS (Gradstein and Ogg, 1996; Kent and Gradstein, 1986; Tominaga and Sager, 2010), to insure that the result does not depend in peculiarities of a given time scale. The results allow us to identify two magnetic isochrons (see Fig. 3.27). The identified magnetic isochrons are the M17 and the M24n in the Tominaga and Sager (2010) and Gradstein and Ogg (1996).

From the identified isochrons we suggest the Gulf of Mexico opened before the Kimmeridgian and seafloor spreading ceased during the Berriasian. We take into account the seafloor spreading asymmetry and calculate averaged spreading rates by area and flank (Western, Central and Eastern parts of the GoM) (see Table 3.3).

As a result the South-western part of the GoM spreads at a more rapid rate than the North-western one. However, the Central and Eastern parts of the GoM exhibit a different behaviour. Indeed, the seafloor of the North-central part of the GoM and the North-eastern part of the GoM spread at rates half of the ones observed in their southern conjugates,

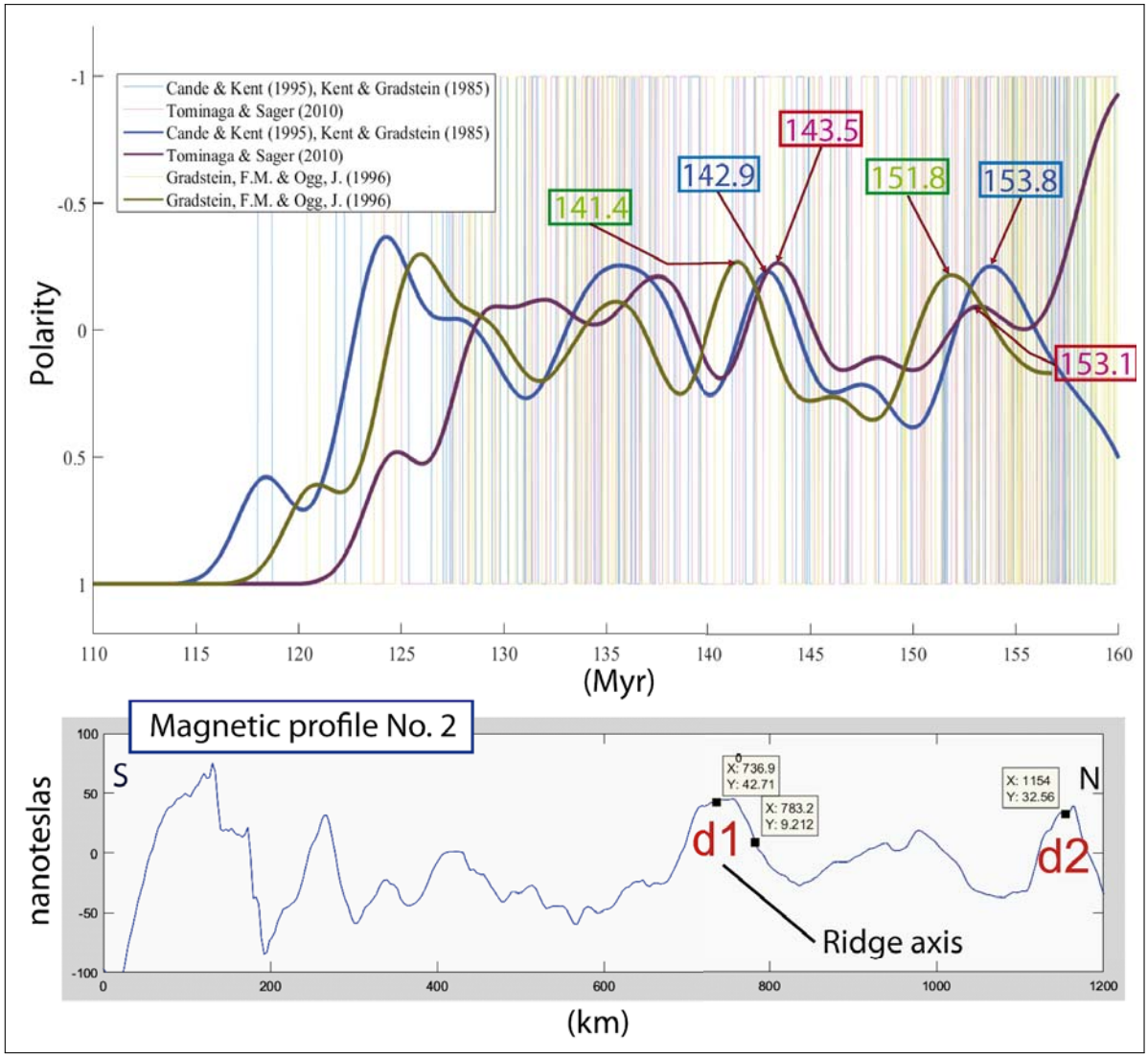

Figure 3.27 – Identified isochrons in the GoM. 'd1' represent the ridge axis whereas 'd2' represent the inner conjugated magnetic anomalies, associated to the isochron M24n

Table 3.3 – Average half-spreading rates for the youngest stage of rotation from the three different GPTS used in this study

	Half-spreading rates averaged for the youngest stage of rotation (mm/yr)		
	(Kent and Gradstein, 1986)	(Tominaga and Sager, 2010)	(Gradstein and Ogg, 1996)
Part of the GoM	South of the ridge axis		
Western (Flow lines No. 1-9)	33.10	34.13	31.51
Central (Flow lines No. 10-21)	13.36	13.78	12.72
Eastern (Flow lines No. 22-26)	7.55	7.79	7.19
	North of the ridge axis		
Western (Flow lines No. 1-9)	29.70	30.63	28.28
Central (Flow lines No. 10-21)	24.08	24.83	22.92
Eastern (Flow lines No. 22-26)	14.73	15.19	14.02

reflecting a significant spreading asymmetry.

3.8 Discussion

Previous tectonic models of the GoM broadly agree on the fact that the GoM originated during the Late Triassic, possibly following a phase of Paleozoic continental drift, followed by a phase of Jurassic rifting. Our plate reconstruction over the GoM suggests the oceanic part of the Gulf originated before the Kimmeridgian, during the Late Jurassic (see Fig. 3.28).

Models from potential field data presented in previous works (e.g., Nguyen and Mann, 2016; Pindell et al., 2016) did not consider the fan-like magnetic anomalies studied in this chapter as related to seafloor spreading (see Fig. 3.29). We point out the fact that there is no strong magnetic anomaly in the interior of the Gulf of Mexico.

In some areas, it is rather difficult to propose an ocean-continent boundary with the available potential field data. The layer associated with the salt province of Sigsbee masks the crustal gravity response. This salt layer does not allow observing neither the continuity of the fracture zones nor the location of possible spreading axes of the oceanic crust. However the magnetic anomalies are only partially attenuated by the sediments in this area. In our model we deduce the age of the GoM on magnetic isochrons. However, dating of rock sample in the Gulf of Mexico led to comparable ages with ours, in locations such as the eastern edge of the Sierra Madre (López-Martínez et al., 2017) and in the channel located between the Florida Block and the Yucatán Block (Marton and Buffler, 2016) respectively.

The total rotation pole of the Yucatán Block with respect to North America allowed us to provide the location of the Continent-Ocean Boundary (see Fig. 3.31).

Our model suggests the Yucatán Block was larger than it currently is, and that parts of the terranes were detached from the block, in part of what are today the Sierra Madre Mountains and the Belize Mountains. It is equally possible that the block had a more significant extension southward, after its rotation. However, part of these southern terranes may have detached from the Southern Yucatán Block due to a lateral collision of the Greater Antilles arc, along a transcurrent fault. The Greater Antilles arc is supposed to have migrated north-eastward after or during the rotation of the Yucatán Block. This hypothesis assumes that the Greater Antilles Arc was coming from the Pacific side. The reconstruction of the Gulf of Mexico represents the first chapter in the evolution of the Caribbean plate, since it defines the starting framework to perform the plate reconstruction in the Caribbean. In the same way, our model allows us to find the possible affinities of the Yucatán Block with terrains of Amazonia, and its possible belonging to the Suwannee Block, part of the African continent (see Fig. 3.30). If this hypothesis is correct, the Jurassic grabens that are part of the Yucatán Block could share history with the Jurassic grabens in South America (Espino Graben and Graben de Takutu).

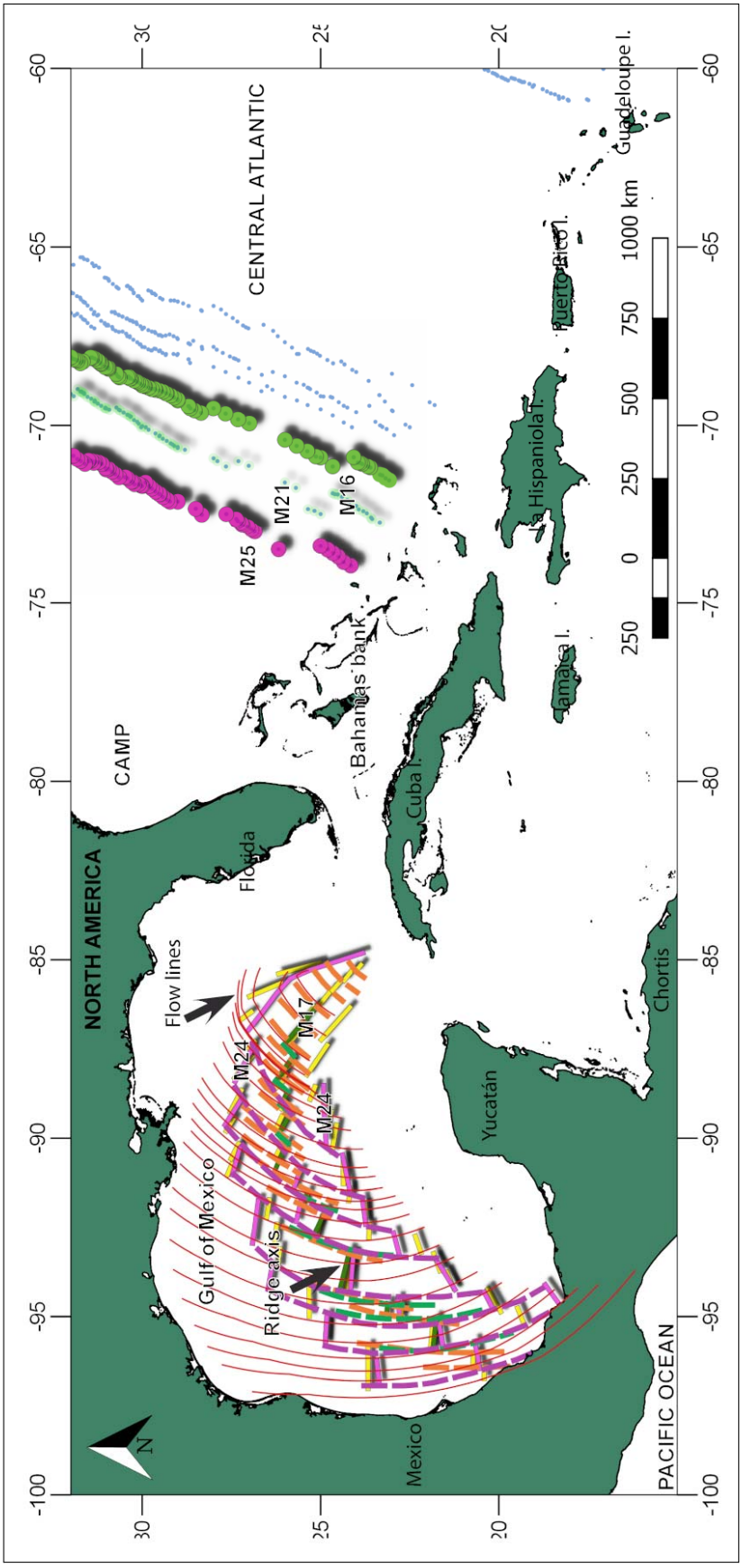

Figure 3.28 – Identified magnetic isochrons in the GoM with previously identified isochrons in the Central Atlantic (Isochrons from (Seton et al., 2014) database updated on July-2018)

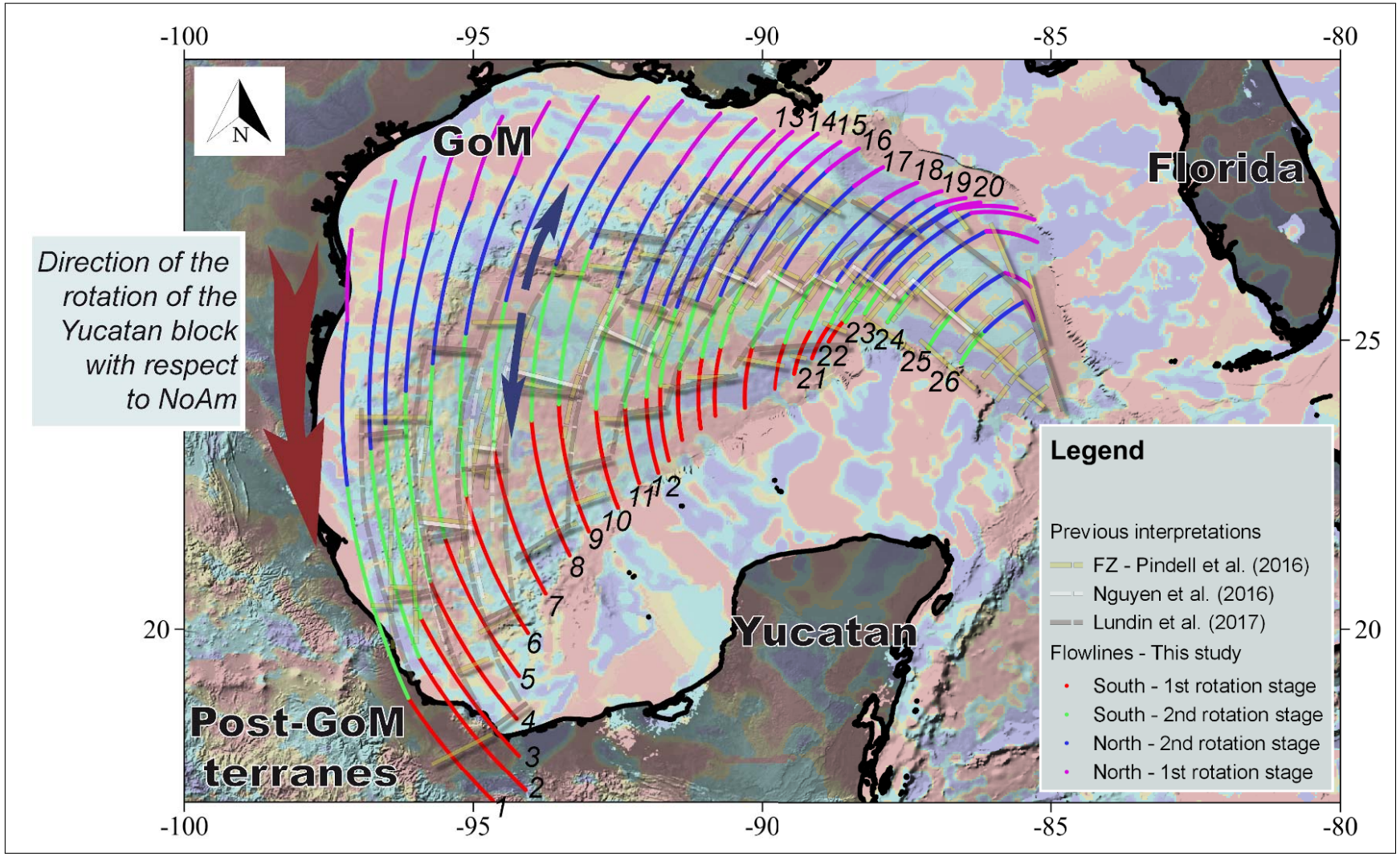

Figure 3.29 – In the figure, our proposed GoM reconstruction is showed together with models suggested by other authors (Lundin and Doré, 2017; Nguyen and Mann, 2016; Pindell et al., 2016)

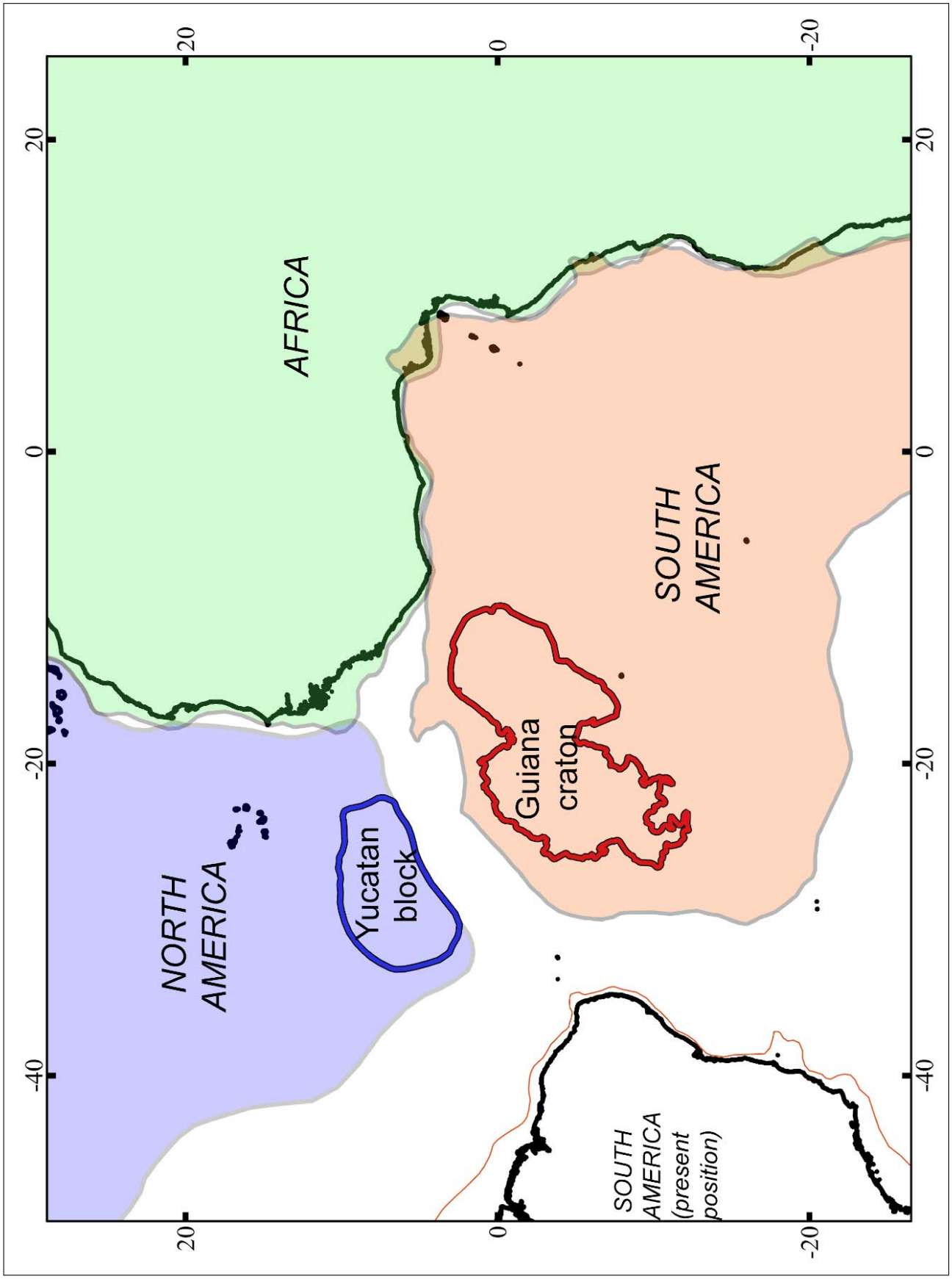

Figure 3.30 – Position of the Yucatán Block at 245 Ma as an implication of our proposed model

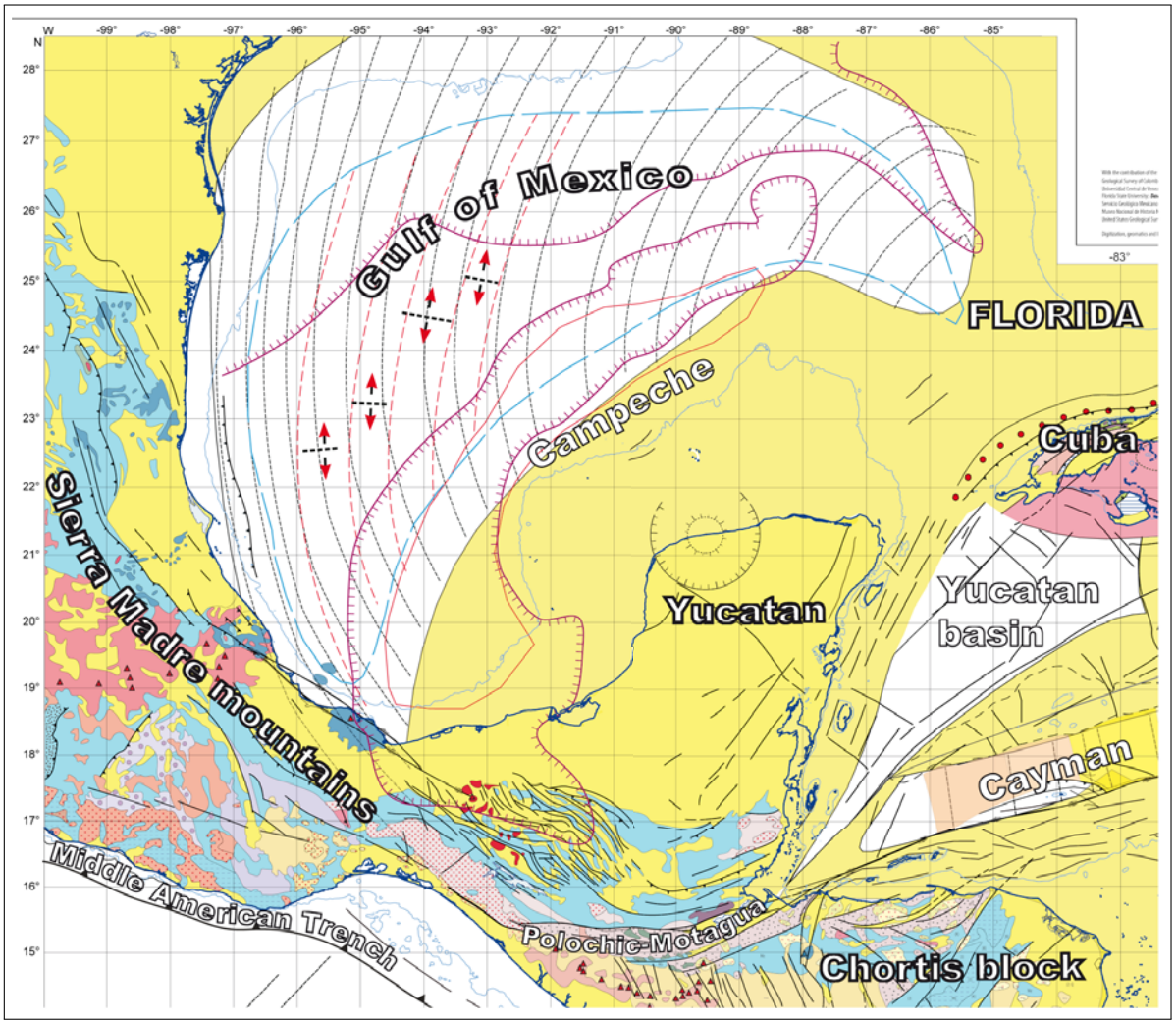

Figure 3.31 – Crustal terrains with our COB interpretation in the GoM (zoom in to the Structural Map of the Caribbean - see Appendix A)

3.9 Conclusion

We consider the amplitude of the magnetic anomalies, their shape and distribution and propose that the fan-like set of anomalies in the GoM reflects the opening of ocean floor that gave it birth. The magnetic anomalies in the flanks (outer conjugate anomalies) represent the oldest magnetic structures in the GoM. Our attempt to use the newly observed intermediate wavelengths magnetic anomalies also took advantage of the VGG signature of FZ and margin (COB).

The magnetic anomalies of the Yucatán Block show a distinct pattern compared to those observed in the interior of the GoM. Our model supports the counter clockwise rotation of the Yucatán Block during or after the Pangea break up with respect to the North American continent, and closely linked to the opening of the Central Atlantic and Equatorial Atlantic, implying a Late Triassic opening for the GoM. In our plate tectonic reconstruction for 200 Ma, with the Yucatán Block at its current position, we observe an overlap between the Yucatán Block and the Venezuelan Central and Eastern Ranges respectively. From this reconstruction, we envision that the Yucatán Block could be close to the Amazonian craton before the Pangea break up. The obtained total parameters for the rotation of the Yucatán Block with respect to the North American continent is a pole at 85.26°W, 23.85°N and an angle of 60.25°. We obtained this pole of rotation from the juxtaposition of the northern limit of the Yucatán Block, interpreted from the magnetic anomaly data, with the southern edge of the North American plate.

We carried out the isochrons identification based on three GPTS (Gradstein and Ogg, 1996; Kent and Gradstein, 1986; Tominaga and Sager, 2010). We identified the isochrons M17 and M24n. The identified isochrons significantly suggest a formation of the Gulf of Mexico that precedes the Kimmeridgian and suggests that the seafloor spreading in the Gulf of Mexico ceased during the Berriasian. Our plate reconstruction allows us to correlate a group of three prominent magnetic anomalies of the Yucatán Block with similar magnetic anomalies in the Florida Block. From this correlation we propose that Yucatán and Florida blocks formed a single magnetic domain, before the Pangea break-up. This block could have detached from the African continent due to the Pangea's rupture, as proposed by other authors (Thomas et al., 2006).

Also we calculated distinct stages of rotation using the orientation of the interpreted fracture zones. We interpreted the fracture zones from the vertical gradient of gravity and from the interpreted prominent magnetic anomalies. We conclude that the seafloor spreading of the Gulf of Mexico was asymmetrical. As a result of that asymmetry, in the western part of the GoM seafloor spreading was faster to the South of the ridge axis. On the contrary, in the Central and Eastern parts of the GoM, spreading was faster north of the ridge axis.

3.10 References

Amato, J. M., Lawton, T. F., Mauel, D. J., Leggett, W. J., González-León, C. M., Farmer, G. L., and Wooden, J. L. (2009). Testing the Mojave-Sonora megashear hypothesis: Evidence from Paleoproterozoic igneous rocks and deformed Mesozoic strata in Sonora, Mexico. *Geology*, 37(1):75–78.

Bartok, P. (1993). Prebreakup geology of the Gulf of Mexico-Caribbean: Its relation to Triassic and Jurassic rift systems of the region. *Tectonics*, 12(2):441–459.

Biari, Y., Klingelhoefer, F., Sahabi, M., Funck, T., Benabdellouahed, M., Schnabel, M., Reichert, C., Gutscher, M.-A., Bronner, A., and Austin, J. (2017). Opening of the central Atlantic Ocean: Implications for geometric rifting and asymmetric initial seafloor spreading after continental breakup. *Tectonics*.

Bird, D., Burke, K., et al. (2006). Pangea breakup: Mexico, Gulf of Mexico, and Central Atlantic Ocean. In *2006 SEG Annual Meeting*. Society of Exploration Geophysicists.

Bird, D. E., Burke, K., Hall, S. A., and Casey, J. F. (2005). Gulf of Mexico tectonic history: Hotspot tracks, crustal boundaries, and early salt distribution. *AAPG bulletin*, 89(3):311–328.

Bird, D. E., Burke, K., Hall, S. A., and Casey, J. F. (2011). Tectonic evolution of the Gulf of Mexico Basin. *Gulf of Mexico Origin, Waters, and Biota: Volume 3, Geology*, 3:1.

Blackburn, T. J., Olsen, P. E., Bowring, S. A., McLean, N. M., Kent, D. V., Puffer, J., McHone, G., Rasbury, E. T., and Et-Touhami, M. (2013). Zircon U-Pb geochronology links the end-Triassic extinction with the Central Atlantic Magmatic Province. *Science*, 340(6135):941–945.

Blum, M. D., Milliken, K. T., Pecha, M. A., Snedden, J. W., Frederick, B. C., and Galloway, W. E. (2017). Detrital-zircon records of Cenomanian, Paleocene, and Oligocene Gulf of Mexico drainage integration and sediment routing: Implications for scales of basin-floor fans. *Geosphere*, 13(6):2169–2205.

Bonvalot, S., Balmino, G., Briais, A., Kuhn, M., Peyrefitte, A., Vales, N., Biancale, R., Gabalda, G., Moreaux, G., Reinquin, F., et al. (2012). World Gravity Map, 1:50000000 map. Eds. BGI-CGMW-CNES-IRD.

Bouysse, P. (2009). Geological Map of the World. *Commission for the Geological Map of the World*.

Buffler, R. T. (1984). Early history and structure of the deep Gulf of Mexico basin. In *Characteristics of Gulf Basin Deep-water Sediments and their Exploration Potential, 5th Annual Gulf Coast Research Conference Proceedings, Soc. Econ. Paleontol. Mineral*, pages 31–34.

Buffler, R. T. and Sawyer, D. S. (1985). Distribution of crust and early history, Gulf of Mexico basin. *Gulf Coast Association of Geological Societies Transactions*, 35:333–344.

Bullard, E., Everett, J. E., and Smith, A. G. (1965). The fit of the continents around the Atlantic. *Phil. Trans. R. Soc. Lond. A*, 258(1088):41–51.

Carey, S. W. (1958). *Continental Drift, a Symposium: Being a Symposium on the Present Status of the Continental Drift Hypothesis, Held in the Geology Department of the University of Tasmania in March, 1956*, volume 2. Geology Department, University of Tasmania.

Carlson, R. and Herrick, C. (1990). Densities and porosities in the oceanic crust and their variations with depth and age. *Journal of Geophysical Research: Solid Earth*, 95(B6):9153–9170.

Centeno-García, E. (2017). Mesozoic tectono-magmatic evolution of Mexico: An overview. *Ore Geology Reviews*, 81:1035–1052.

Christensen, N. I. and Mooney, W. D. (1995). Seismic velocity structure and composition of the continental crust: A global view. *Journal of Geophysical Research: Solid Earth*, 100(B6):9761–9788.

Christeson, G., Van Avendonk, H., Norton, I., Snedden, J., Eddy, D., Karner, G., and Johnson, C. (2014). Deep crustal structure in the eastern Gulf of Mexico. *Journal of Geophysical Research: Solid Earth*, 119(9):6782–6801.

Christeson, G. L., Mann, P., Escalona, A., and Aitken, T. J. (2008). Crustal structure of the Caribbean–northeastern South America arc-continent collision zone. *Journal of Geophysical Research: Solid Earth*, 113(B8).

Clift, P. D., Heinrich, P., Dunn, D., Jacobus, A., and Blusztajn, J. (2018). The Sabine block, Gulf of Mexico: Promontory on the North American margin? *Geology*, 46(1):15–18.

Dallmeyer, R. (1989). Contrasting accreted terranes in the southern Appalachian Orogen, basement beneath the Atlantic and Gulf Coastal Plains, and West African orogens. *Precambrian Research*, 42(3-4):387–409.

Dickinson, W. R. (2009). The Gulf of Mexico and the southern margin of Laurentia. *Geology*, 37(5):479–480.

Dickinson, W. R. and Lawton, T. F. (2001). Carboniferous to Cretaceous assembly and fragmentation of Mexico. *Geological Society of America Bulletin*, 113(9):1142–1160.

Diegel, F. A., Karlo, J., Schuster, D., Shoup, R., and Tauvers, P. (1995). Cenozoic structural evolution and tectono-stratigraphic framework of the northern Gulf Coast continental margin.

Dyment, J., Lesur, V., Choi, Y., Hamoudi, M., Thébault, E., and Catalan, M. (2015). Release of the World Digital Magnetic Anomaly Map version 2 (WDMAM v2) scheduled. In *EGU General Assembly Conference Abstracts*, volume 17, page 15430.

Eagles, G., Pérez-Díaz, L., and Scarselli, N. (2015). Getting over continent ocean boundaries. *Earth-Science Reviews*, 151:244–265.

Eddy, D. R., Van Avendonk, H. J., Christeson, G. L., and Norton, I. O. (2018). Structure and origin of the rifted margin of the northern Gulf of Mexico. *Geosphere*.

Eddy, D. R., Van Avendonk, H. J., Christeson, G. L., Norton, I. O., Karner, G. D., Johnson, C. A., and Snedden, J. W. (2014). Deep crustal structure of the northeastern Gulf of Mexico: Implications for rift evolution and seafloor spreading. *Journal of Geophysical Research: Solid Earth*, 119(9):6802–6822.

Fort, X. and Brun, J.-P. (2012). Kinematics of regional salt flow in the northern Gulf of Mexico. *Geological Society, London, Special Publications*, 363(1):265–287.

Fort, X., Brun, J.-P., and Chauvel, F. (2004). Salt tectonics on the Angolan margin, synsedimentary deformation processes. *AAPG bulletin*, 88(11):1523–1544.

Galloway, W. E. (2008). Depositional evolution of the Gulf of Mexico sedimentary basin. *Sedimentary basins of the world*, 5:505–549.

Garcia-Reyes, A., Dyment, J., and Thebault, E. (2017). Insights on the Understanding of the Circum-Caribbean Region from Potential Field Data. In *AGU Fall Meeting Abstracts*.

Garza, R. S. M. (2005). Paleomagnetic reconstruction of Coahuila, Mexico: the Late Triassic Acatita intrusives. *Geofísica Internacional*, 44(2):197–210.

Gradstein, F. and Ogg, J. (1996). Geological time scale for the Phanerozoic. *Episodes*, 19(1–2):3–5.

Hall, D., Cavanaugh, T., Watkins, J., and McMillen, K. (1982). The rotational origin of the Gulf of Mexico based on regional gravity data. *Studies in continental margin geology: AAPG Memoir*, 34:115–126.

Hall, S. (2002). The role of autochthonous salt inflation and deflation in the northern Gulf of Mexico. *Marine and Petroleum Geology*, 19(6):649–682.

Hall, S. A. and Najmuddin, I. J. (1994). Constraints on the tectonic development of the eastern Gulf of Mexico provided by magnetic anomaly data. *Journal of Geophysical Research: Solid Earth*, 99(B4):7161–7175.

Heatherington, A. and Mueller, P. (2003). Mesozoic igneous activity in the Suwannee terrane, southeastern USA: petrogenesis and Gondwanan affinities. *Gondwana Research*, 6(2):296–311.

Hellinger, S. J. (1979). *The statistics of finite rotations in plate tectonics*. PhD thesis, Massachusetts Institute of Technology.

Hemant, K., Thébault, E., Mandea, M., Ravat, D., and Maus, S. (2007). Magnetic anomaly map of the world: merging satellite, airborne, marine and ground-based magnetic data sets. *Earth and Planetary Science Letters*, 260(1-2):56–71.

Hinze, W. J., Von Frese, R. R., and Saad, A. H. (2013). *Gravity and magnetic exploration: Principles, practices, and applications*. Cambridge University Press.

Hudec, M. R., Norton, I. O., Jackson, M. P., and Peel, F. J. (2013). Jurassic evolution of the Gulf of Mexico salt basinGulf of Mexico Jurassic Evolution. *AAPG bulletin*, 97(10):1683–1710.

Hunt, C. P., Moskowitz, B. M., and Banerjee, S. K. (1995). Magnetic properties of rocks and minerals. *Rock physics & phase relations: a handbook of physical constants*, pages 189–204.

Ibrahim, A., Carye, J., Latham, G., and Buffler, R. (1981). Crustal structure in Gulf of Mexico from OBS refraction and multichannel reflection data. *AAPG Bulletin*, 65(7):1207–1229.

Jones, N. W., McKee, J. W., Márquez D, B., Tovar, J., Long, L. E., and Laudon, T. S. (1984). The Mesozoic La Mula Island, Coahuila, Mexico. *Geological Society of America Bulletin*, 95(10):1226–1241.

Kent, D. V. and Gradstein, F. M. (1986). A Jurassic to recent chronology. *The Geology of North America*, 1000:45–50.

Keppie, D. F. and Keppie, J. D. (2012). An alternative Pangea reconstruction for Middle America with the Chortis Block in the Gulf of Mexico: tectonic implications. *International Geology Review*, 54(14):1685–1696.

Keppie, D. F. and Keppie, J. D. (2014). The Yucatan, a Laurentian or Gondwanan fragment? Geophysical and palinspastic constraints. *International Journal of Earth Sciences*, 103(5):1501–1512.

Keppie, F. (2013). The Rationale and Essential Elements for the New 'Pirate'Model of Caribbean Tectonics. *Geoscience Canada*, 40(1).

Kim, Y., Clayton, R. W., and Keppie, F. (2011). Evidence of a collision between the Yucatán Block and Mexico in the Miocene. *Geophysical Journal International*, 187(2):989–1000.

Kneller, E. A. and Johnson, C. A. (2011). Plate kinematics of the Gulf of Mexico based on integrated observations from the Central and South Atlantic.

Kring, D. A., Claeys, P., Gulick, S. P., Morgan, J. V., and Collins, G. S. (2017). Chicxulub and the exploration of large peak-ring impact craters through scientific drilling.

Lawton, T. F. and Amato, J. M. (2017). U-Pb ages of igneous xenoliths in a salt diapir, La Popa basin: Implications for salt age in onshore Mexico salt basins. *Lithosphere*, 9(5):745–758.

Lawton, T. F., Vega, F. J., Giles, K. A., and Rosales-Domnguez, C. (2001). AAPG Memoir 75, Chapter 9: Stratigraphy and Origin of the La Popa Basin, Nuevo Len and Coahuila, Mexico.

Legendre, A. M. (1852). *Elements of geometry and trigonometry*.

López-Martínez, R., Barragán, R., Bernal, J. P., Reháková, D., Gómez-Tuena, A., Martini, M., and Ortega, C. (2017). Integrated stratigraphy and isotopic ages at the Berriasian–Valanginian boundary at Tlatlauquitepec (Puebla, Mexico). *Journal of South American Earth Sciences*, 75:1–10.

Lundin, E. and Doré, A. (2017). The Gulf of Mexico and Canada Basin: Genetic Siblings on Either Side of North America. *GSA Today*, 27(1):4–11.

Martens, U., Weber, B., and Valencia, V. A. (2010). U/Pb geochronology of Devonian and older Paleozoic beds in the southeastern Maya block, Central America: Its affinity with peri-Gondwanan terranes. *Bulletin*, 122(5-6):815–829.

Marton, G. and Buffler, R. (2016). Jurassic-Cretaceous Tectonic Evolution of the Southeastern Gulf of Mexico, Constrains on the Style and Timing of Gulf of Mexico Rift-Drift Development. In *AAPG/SEG International Conference & Exhibition*.

Marton, G. and Buffler, R. T. (1994). Jurassic reconstruction of the Gulf of Mexico Basin. *International Geology Review*, 36(6):545–586.

Marzoli, A., Renne, P. R., Piccirillo, E. M., Ernesto, M., Bellieni, G., and De Min, A. (1999). Extensive 200-million-year-old continental flood basalts of the Central Atlantic Magmatic Province. *Science*, 284(5414):616–618.

Morgan, W. J. (1968). Rises, trenches, great faults, and crustal blocks. *Journal of Geophysical Research*, 73(6):1959–1982.

Moy, C. and Traverse, A. (1986). Palynostratigraphy of the subsurface eagle mills formation (Triassic) from a well in east-central texas, USA. *Palynology*, 10(1):225–234.

Mueller, P. A., Heatherington, A. L., Foster, D. A., Thomas, W. A., and Wooden, J. L. (2014). The Suwannee suture: Significance for Gondwana-Laurentia terrane transfer and formation of Pangaea. *Gondwana Research*, 26(1):365–373.

Müller, R. D., Royer, J.-Y., Cande, S. C., Roest, W. R., and Maschenkov, S. (1999). New constraints on the Late Cretaceous/Tertiary plate tectonic evolution of the Caribbean. In *Sedimentary basins of the world*, volume 4, pages 33–59. Elsevier.

Nguyen, L. and Mann, P. (2016). Quantitative restoration the Gulf of Mexico continental margins based on a newly-derived, basin-wide, crustal thickness map. In *AGU Fall Meeting Abstracts*.

Olsen, P., Schlische, R., and Fedosh, M. (1996). 580 ky duration of the Early Jurassic flood basalt event in eastern North America estimated using Milankovitch cyclostratigraphy. *The continental Jurassic: Museum of Northern Arizona Bulletin*, 60:11–22.

Olsen, P. E. (1997). Stratigraphic record of the early Mesozoic breakup of Pangea in the Laurasia-Gondwana rift system. *Annual Review of Earth and Planetary Sciences*, 25(1):337–401.

Peel, F., Travis, C., and Hossack, J. (1995). Genetic structural provinces and salt tectonics of the Cenozoic offshore US Gulf of Mexico: A preliminary analysis.

Pindell, J. and Dewey, J. F. (1982). Permo-Triassic reconstruction of western Pangea and the evolution of the Gulf of Mexico/Caribbean region. *Tectonics*, 1(2):179–211.

Pindell, J., Kennan, L., Maresch, W. V., Stanek, K.-P., Draper, G., and Higgs, R. (2005). Plate-kinematics and crustal dynamics of circum-Caribbean arc-continent interactions: Tectonic controls on basin development in Proto-Caribbean margins. *Geological Society of America Special Papers*, 394:7–52.

Pindell, J., Miranda, C., Ceron, A., and Hernandez, L. (2016). Aeromagnetic map constrains Jurassic–Early Cretaceous synrift, break up, and rotational seafloor spreading history in the Gulf of Mexico. In *Mesozoic of the Gulf Rim and Beyond: New Progress in Science and Exploration of the Gulf of Mexico Basin. 35th Annual Gulf Coast Section SEPM Foundation Perkins-Rosen Research Conference, GCSSEPM Foundation, Houston, TX, USA*, pages 123–153.

Pindell, J. L. (1985). Alleghenian reconstruction and subsequent evolution of the Gulf of Mexico, Bahamas, and proto-Caribbean. *Tectonics*, 4(1):1–39.

Pindell, J. L. (1994). Evolution of the Gulf of Mexico and the Caribbean. *Caribbean geology: an introduction*, pages 13–39.

Pindell, J. L. and Kennan, L. (2009). Tectonic evolution of the Gulf of Mexico, Caribbean and northern South America in the mantle reference frame: an update. *Geological Society, London, Special Publications*, 328(1):1–55.

Ross, M. I. and Scotese, C. R. (1988). A hierarchical tectonic model of the Gulf of Mexico and Caribbean region. *Tectonophysics*, 155(1-4):139–168.

Rowan, M. (2014). Passive-margin salt basins: hyperextension, evaporite deposition, and salt tectonics. *Basin Research*, 26(1):154–182.

Royer, J., Sclater, J., Sandwell, D., Cande, S., Schlich, R., Munschy, M., Dyment, J., Fisher, R., Müller, R., Coffin, M., et al. (1992). Indian Ocean plate reconstructions since the Late Jurassic. *Synthesis of Results From Scientific Drilling in the Indian Ocean, Geophys. Monogr. Ser*, 70:471–475.

Sahabi, M., Aslanian, D., and Olivet, J.-L. (2004). Un nouveau point de départ pour l'histoire de l'Atlantique central. *Comptes Rendus Geoscience*, 336(12):1041–1052.

Salvador, A. (1987). Late Triassic-Jurassic paleogeography and origin of Gulf of Mexico basin. *AAPG Bulletin*, 71(4):419–451.

Salvador, A. (1991). Origin and development of the Gulf of Mexico basin. *The gulf of Mexico basin*, pages 389–444.

Sandwell, D. T., Müller, R. D., Smith, W. H., Garcia, E., and Francis, R. (2014). New global marine gravity model from CryoSat-2 and Jason-1 reveals buried tectonic structure. *Science*, 346(6205):65–67.

Sawyer, D. S., Buffler, R. T., and Pilger Jr, R. H. (1991). The crust under the Gulf of Mexico Basin. *The Gulf of Mexico Basin: Geological Society of America, The Geology of North America, v. J*, pages 53–72.

Schnetzler, C. (1985). An estimation of continental crust magnetization and susceptibility from Magsat data for the conterminous United States. *Journal of Geophysical Research: Solid Earth*, 90(B3):2617–2620.

Schouten, H. and Klitgord, K. D. (1994). Mechanistic solutions to the opening of the Gulf of Mexico. *Geology*, 22(6):507–510.

Seton, M., Müller, R., Zahirovic, S., Gaina, C., Torsvik, T., Shephard, G., Talsma, A., Gurnis, M., Turner, M., Maus, S., et al. (2012). Global continental and ocean basin reconstructions since 200 Ma. *Earth-Science Reviews*, 113(3-4):212–270.

Seton, M., Whittaker, J. M., Wessel, P., Müller, R. D., DeMets, C., Merkouriev, S., Cande, S., Gaina, C., Eagles, G., Granot, R., et al. (2014). Community infrastructure and repository for marine magnetic identifications. *Geochemistry, Geophysics, Geosystems*, 15(4):1629–1641.

Steiner, M. B. and Anderson, T. (2005). Pangean reconstruction of the Yucatan Block: Its Permian, Triassic, and Jurassic geologic and tectonic history. *SPECIAL PAPERS-GEOLOGICAL SOCIETY OF AMERICA*, 393:457.

Stephens, B. P. (2009). Basement controls on subsurface geologic patterns and coastal geomorphology across the northern Gulf of Mexico: Implications for subsidence studies and coastal restoration. *Gulf Coast Association of Geological Societies Transactions*, 59(1):729–751.

Stern, R. J. and Dickinson, W. R. (2010). The Gulf of Mexico is a Jurassic backarc basin. *Geosphere*, 6(6):739–754.

Thomas, W. A. et al. (2006). Tectonic inheritance at a continental margin. *GSA today*, 16(2):4–11.

Tominaga, M. and Sager, W. W. (2010). Revised Pacific M-anomaly geomagnetic polarity timescale. *Geophysical Journal International*, 182(1):203–232.

Van Avendonk, H. J., Christeson, G. L., Norton, I. O., and Eddy, D. R. (2015). Continental rifting and sediment infill in the northwestern Gulf of Mexico. *Geology*, 43(7):631–634.

Vine, F. J. and Matthews, D. H. (1963). Magnetic anomalies over oceanic ridges. *Nature*, 199(4897):947–949.

Welsink, H., Dwyer, J., and Knight, R. (1989). Tectono-Stratigraphy of the Passive Margin Off Nova Scotia: Chapter 14: North American Margins.

Whalen, L., Gazel, E., Vidito, C., Puffer, J., Bizimis, M., Henika, W., and Caddick, M. J. (2015). Supercontinental inheritance and its influence on supercontinental breakup: The Central Atlantic Magmatic Province and the breakup of Pangea. *Geochemistry, Geophysics, Geosystems*, 16(10):3532–3554.

Withjack, M. O., Schlische, R. W., and Olsen, P. E. (1998). Diachronous rifting, drifting, and inversion on the passive margin of central eastern North America: an analog for other passive margins. *AAPG bulletin*, 82(5):817–835.

Worrall, D. and Snelson, S. (1989). Evolution of the northern Gulf of Mexico. *The geology of North America; an overview: Geological Society of America, v. A*, pages 97–138.

Worzel, J. L. and Watkins, J. S. (1973). Evolution of the Northern Gulf Coast Deduced from Geophysical Data (1).

Chapter 4

Magnetic anomalies in the Colombia and Venezuela Basins

Yesterday is gone and its tale told. Today new seeds are growing.

— RUMI

4.1 Introduction

Many authors extensively discussed the origin of the Caribbean plate (e.g. Giunta et al., 1997; Kerr et al., 1999; Meschede and Frisch, 1998; Pindell, 1991) but many questions remain open on its age and its origin. The Caribbean plate is associated with a Large Igneous Provinces (LIP). The LIP are globally mapped (Bouysse, 2009) (see Fig. 4.1) but the causes of the abundant magmatism at their origin is still a matter of question. Geochemical data suggest the Caribbean LIP (CLIP) formed in three magmatic pulses at 124-112 Ma, 92-88 Ma and 76-72 Ma (Kerr et al., 2000; Sinton et al., 1998) respectively, however its origin and extension continue to be debated (see Fig. 4.2).

Deciphering the magnetic pattern of either the crust of the Caribbean plate or the CLIP province is important to properly understand the origin and nature of the Caribbean plate. A proper magnetic interpretation depends on the proximity of the magnetic Equator at its creation, the direction of the spreading center, and the spreading rate, among other parameters. Magnetic anomalies of N-S elongated bodies (such as N-S trending seafloor spreading magnetic anomalies) display very low amplitude near the magnetic equator. Their pattern is hard to decipher at ridge jumps, at slow-spreading center with sharp topographical relief, and at any other tectonically complex areas (Sclater et al., 1971). The magnetic pattern may also be blurred in areas where the extensive layers of volcanic rocks of the LIPs overlay the oceanic crust, because of the superimposition of two possibly different (if not contemporaneous) magnetic signals of the oceanic crust and the overlying plateau. The confused pattern can be significant for LIPs formed over a preexisting oceanic crust, possibly

resulting in the removal of the magnetic lineations produced by seafloor spreading.

Some authors proposed the existence of magnetic isochrons in parts of the Caribbean region. Leroy et al. (2000) interpreted magnetic isochrons along the Cayman Ridge and Christofferson (1973) in the Colombia Basin. In the Venezuela Basin, some authors tentatively identified magnetic lineations inside the basin, although the anomalies are hardly discernible (see Fig. 4.3) (Donnelly, 1973; Ghosh et al., 1984). Uncertainties remain regarding the presence of lineated magnetic anomalies in most of the Caribbean plate, leading several authors to affirm it is impossible to identify magnetic anomalies there. The crust of the Colombia and Venezuela basins is presumably oceanic. Diebold et al. (1981) reported two types of crust in the Venezuela Basin: a fragment of crust resembling normal oceanic crust in its southern part, and anomalously thick oceanic plateau basalt (17-20 km) composed of extensive basaltic sills and flows and characterized by deeper mantle. The Beata Ridge NE-SW structural trend separates both types of crust (Diebold et al., 1981). The Venezuela Basin may be Early Cretaceous age (Boynton et al., 1979; Diebold et al., 1999; Fox and Heezen, 1975; Officer et al., 1957). From the interpretation of the marine magnetic maps (see Chapter 2), we associate the volcanic layers in the Caribbean plate with three distinct episodes of volcanism: First, an extensive volcanism of the Caribbean Large Igneous Province (CLIP) which covers part of the Venezuela Basin and the Colombia Basin; second, a volcanic episode posterior to the emplacement of the Caribbean plate and overlapping the first extensive volcanic layer; and third, a volcanic episode related to the Beata Ridge deformation which could be produced by faults rearrangement in a compressional regime.

This chapter aims to integrate previous results with an analysis of the magnetic anomalies observed in the Colombia and Venezuela Basins, in order to shed light on the structures in the Caribbean seafloor and therefore to contribute to the understanding of the origin and age of the Caribbean plate.

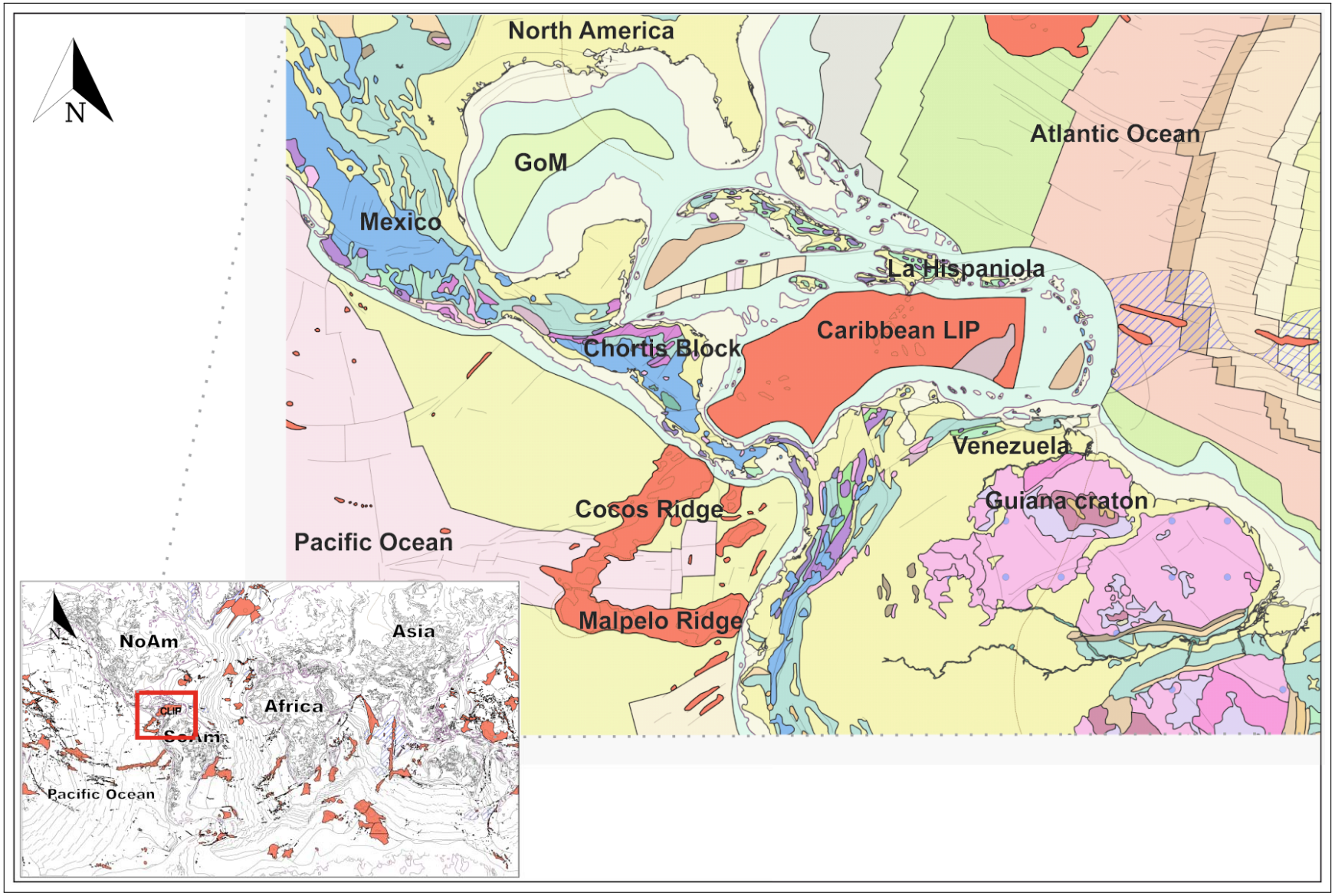

Figure 4.1 – Global distribution of large igneous provinces (Bouysse, 2009). Colors represent crustal ages and are according to the Commission for the Geological Map of the World, excepting orange color which represents oceanic plateaus

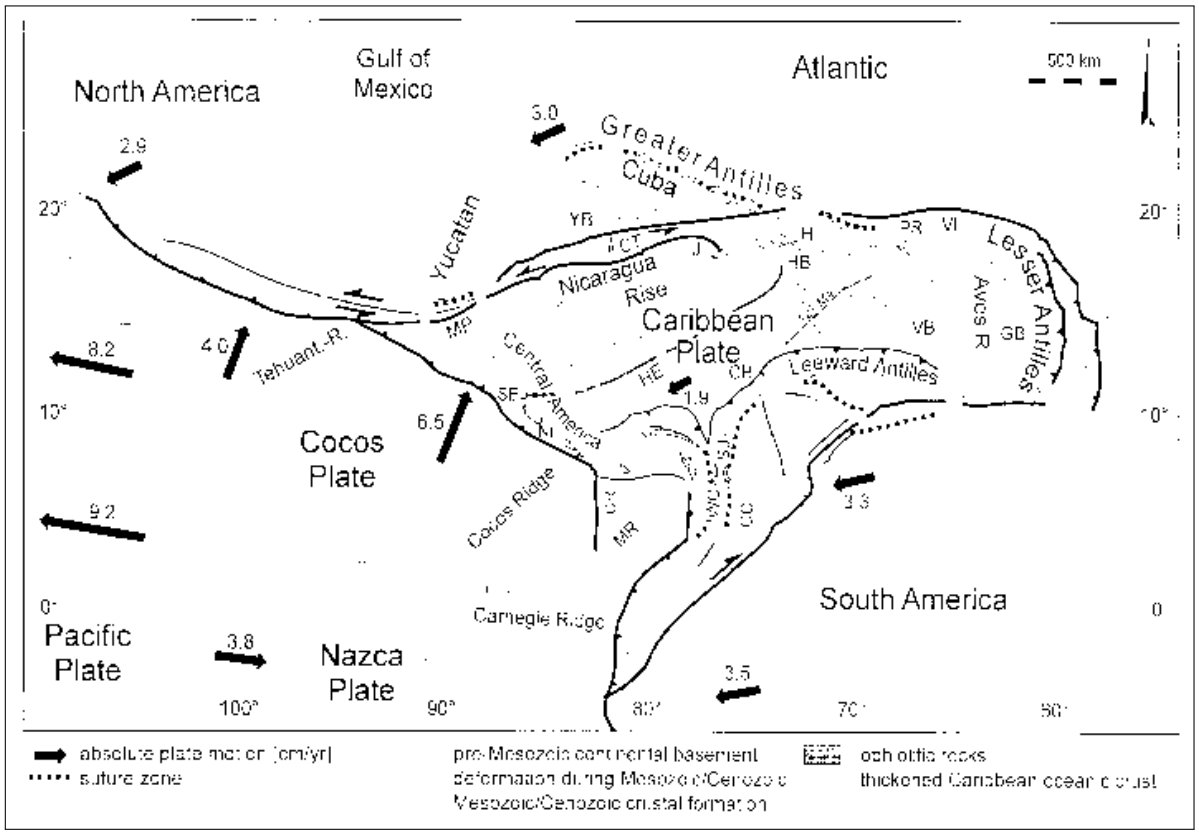

Figure 4.2 – Interpretation of thickened oceanic crust in the Caribbean domain from seismic data (Meschede and Frisch, 1998)

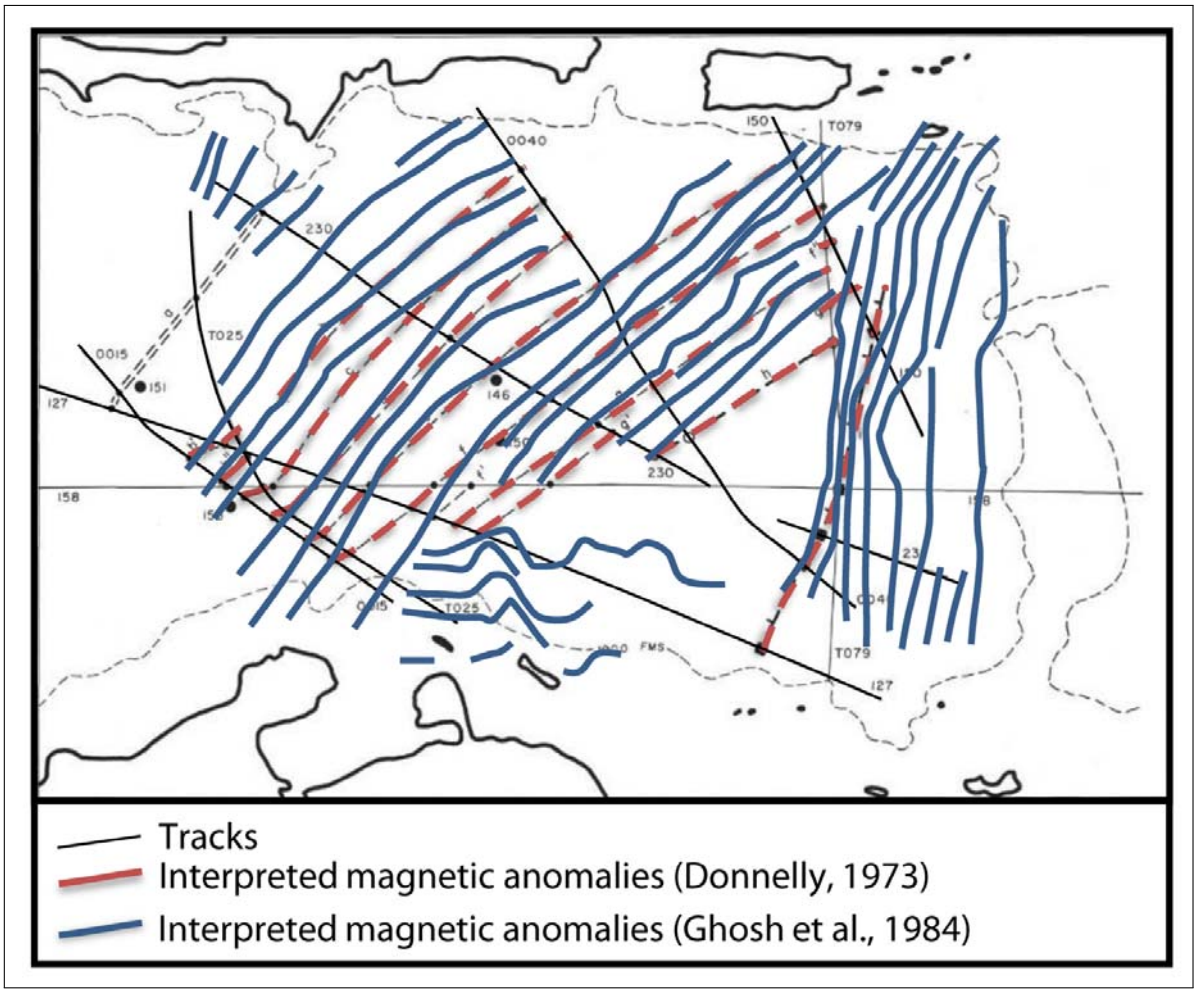

Figure 4.3 – Magnetic profiles previously interpreted over the Venezuela Basin, the Aves Ridge and the Grenada Basin (Donnelly, 1973; Ghosh et al., 1984)

4.2 Method and results

4.3 Magnetic anomalies in the Venezuela and Colombia basins

We describe the magnetic anomaly pattern in the Colombia and Venezuela basins and extract a set of representative profiles in order to characterize the magnetic signal observed in these basins (see Fig. 4.4 and Fig. 4.6).

4.3.1 The Colombia Basin

Recently acquired N-S trending magnetic profiles in the Colombia Basin were provided by Udo Barckausen (personal communication, 2016). These profiles are perpendicular to the observed parallel magnetic anomalies in the southern and central Colombia Basin (see 'a' in Fig. 4.5). The amplitude of these magnetic anomalies varies approximately between -200 to 200 nT, making them one of the strongest in the area. Further Northeast, there is no major boundary between the Colombia Basin sensu stricto (where the E-W magnetic anomalies are observed) and an elongated triangle (see 'c' in Fig. 4.5) located between the Hess Escarpment (see 'd' in Fig. 4.5) to the west and the Beata Ridge to the east, suggesting that both belongs to the same geological unit.

A complex magnetic pattern interrupts to the west the linear pattern of magnetic anomalies observed in the Colombia Basin (see 'b' in Fig. 4.5). We interpret this pattern as marking a volcanic area, most probably created during the second volcanic episode of the Caribbean, as suggested by Sinton et al. (2000). These complex anomalies extend west of the Hess Escarpment, on the Lower Nicaragua Rise, and partly overpass this escarpment in the Colombia Basin, obscuring the magnetic anomalies there.

We extracted a profile from the magnetic anomaly grid across the Colombia basin and the elongated triangle northward, running from the central Colombia Basin to south of the Hispaniola Island. This profile displays a smooth magnetic signal (see 'e' in Fig. 4.5). The Colombia Basin and its northern extension is therefore characterized by clear magnetic anomalies of high amplitude between 11°N and 15°N and a magnetically smooth area with anomalies of short wavelength and low amplitude northward.

This sequence of magnetic anomalies is eligible for identification by comparison with the Geomagnetic Polarity Time Scale. All anomalies reflect the age of the seafloor, i.e. the smooth area also is significant. We consider that this smooth pattern marks the beginning of the Cretaceous Normal Superchron (CNS, 84-120 Ma). The strong anomalies in the Colombia Basin would therefore be anomalies 33 and 33r (73-83 Ma). The Vertical Gradient of Gravity (VGG) reveals a linear structure parallel to the magnetic anomalies observed in the Colombia Basin (see 'a' in Fig. 4.4). This structure probably marks the location of an

extinct spreading center, suggesting the presence of duplicated anomalies 33 and 33r in the Colombia Basin.

4.3.2 The Venezuela Basin

The structure of the Venezuela Basin is dominated by a major N-S structure in the Vertical Gradient of the Gravity (see 'a' Fig. 4.6) that we interpret as a large fracture zone (FZ). This structure is also marked by an elongated magnetic low (see 'a' in Fig. 4.7). We extracted profiles from the grid in the N-S direction in order to evaluate the magnetic anomalies and the possible presence of isochrons.

In general magnetic anomalies display greater amplitudes in the Colombia Basin than in the Venezuela Basin. N-S trending short wavelengths magnetic anomalies in the center of the basin allow us to infer the position of secondary fracture zones, in agreement with the gravity

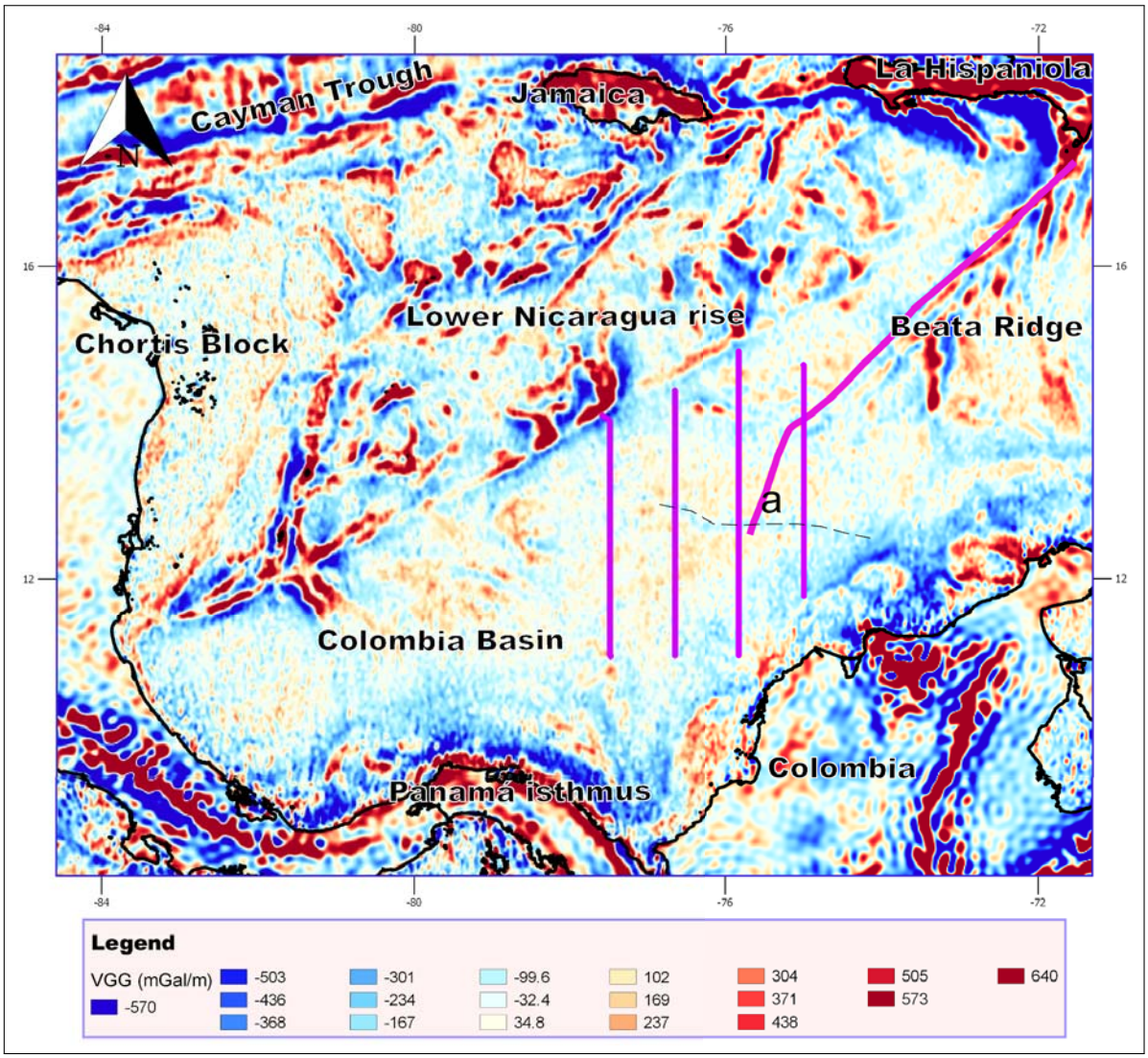

Figure 4.4 – N-S profiles used to evaluate the magnetic anomalies in the Colombia Basin. The grid of Vertical Gradient of Gravity is in the background. Color scale from blue to red, represents negative to positive VGG respectively. The Colombian Basin exhibits the minimum averaged VGG of this area

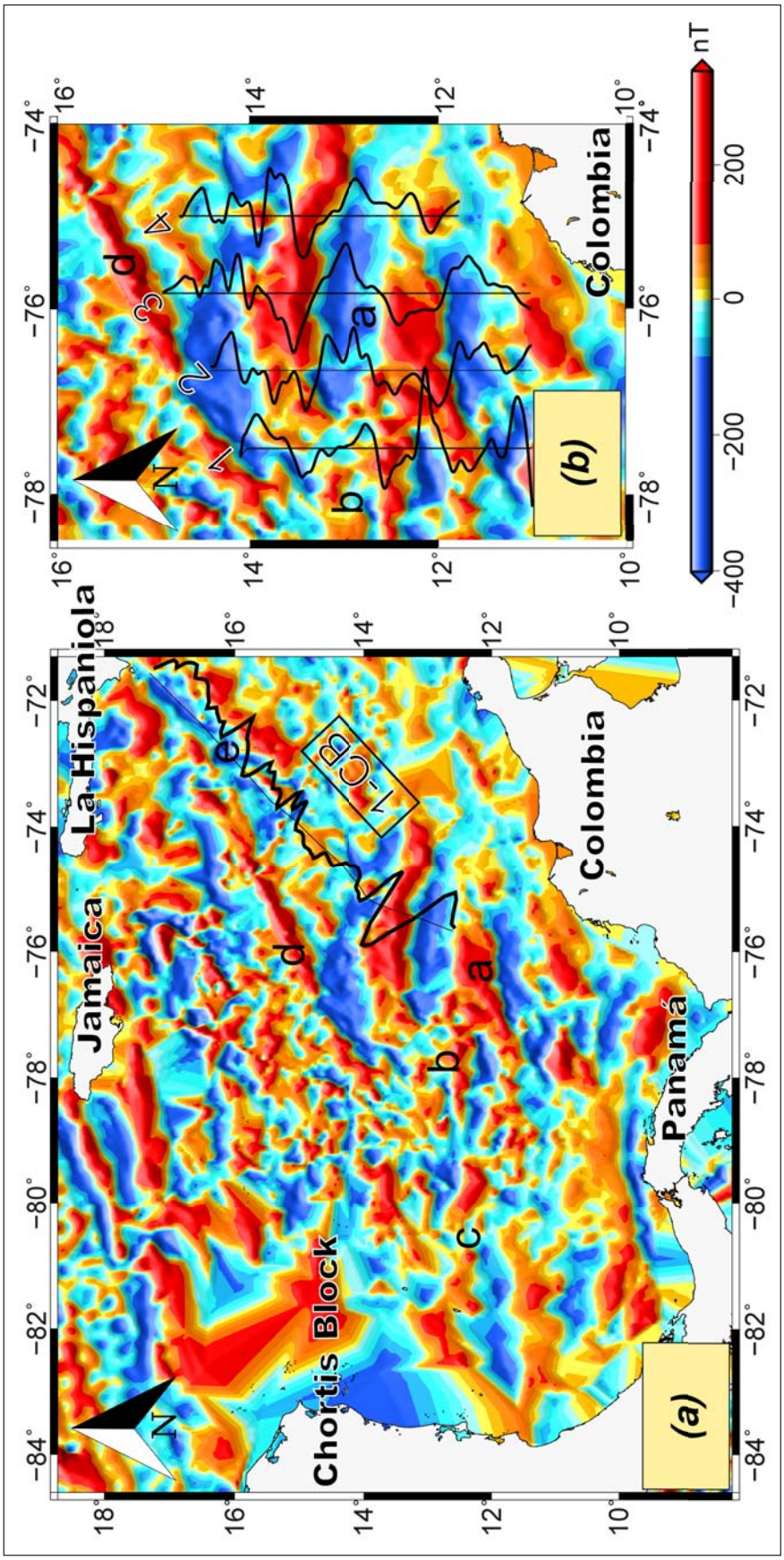

Figure 4.5 – Extracted magnetic anomaly from tracks in the Colombia Basin. Solid black lines: Profile 1-CB extracted from the northern segment of the basin (a) and profiles 1, 2, 3 and 4 extracted in NS direction from the southern segment of the basin (b)

data. The two extracted profiles show similarities that confirm that the observed anomalies record geomagnetic signal. However, they do not present the character of classical marine magnetic anomalies associated to polarity reversals as recorded by seafloor spreading. We suggest that they record geomagnetic intensity variations within the CNS. These anomalies are bounded to the south by a magnetically smooth zone similar to the one observed north of the Colombia Basin. This smooth zone may reflect the effect of the sediment load and associated demagnetization of layer 2A – the sediments are twice thicker in the southern Venezuela Basin than in the other parts of the basin (see Fig. 4.15), but it more likely corresponds to the younger part of the CNS, as in the northern Colombia Basin. Granot et al. (2012) have shown that three main periods, with different geomagnetic fluctuation patterns, can be distinguished within the CNS, separated by two ubiquitous anomalies named Q1 and Q2, tentatively dated ∼92 and ∼108 Ma. The older period, between Anomaly M0 (∼120 Ma) and Q2, displays moderate fluctuations; the intermediate period, between Q2 and Q1, shows strong and rapid variations; and the younger period, between Q1 and Anomaly 34 (84 Ma), is characterized by a very smooth field, almost devoid of short wavelength variations. We suggest that the smooth magnetic anomaly patterns observed north of the Colombia Basin and in the southern Venezuela Basin corresponds to the younger period of the CNS, whereas the rest of the Venezuela Basin would record the strong and rapid magnetic variations of the intermediate period. Anomaly Q1 may therefore tentatively be located in the southeastern part of the Venezuela Basin.

Our magnetic interpretation of the Venezuela Basin is confirmed by the scalar magnetic anomaly of the satellite magnetic model LCS-1 downward-continued at sea level ((Olsen et al., 2017); Fig. 4.9). Despite the difference of wavelengths apprehended by the marine (see Fig. 4.7) and the satellite data, we note a significant correlation between the two data sets. The interpretation derived from the marine magnetic anomalies is perfectly consistent with the satellite data (see Fig. 4.9).

4.3.3 Origin of the Caribbean plate

We use the World Digital Magnetic Anomaly Map (WDMAM; (Dyment et al., 2015)) in an attempt to find magnetic anomalies similar to the anomalies 33-34 identified in the Colombia Basin in World oceans. After visual inspection, we observe that anomalies 33-34 with similar width to that in the Colombia Basin are present in the Pacific Ocean (see green square in Fig. 4.10). We therefore test the hypothesis of a Pacific origin for the Caribbean Plate by further examining magnetic anomalies of the same age in the Pacific Ocean.

We extracted marine magnetic anomaly profiles parallel to the spreading direction in this part of the Pacific Ocean (see Fig. 4.11) from the NCEI (formerly known as National Geophysical Data Centre, NGDC) Marine Geology and Geophysics Trackline database. Many seamounts produce additional high amplitude anomalies that disturb the seafloor

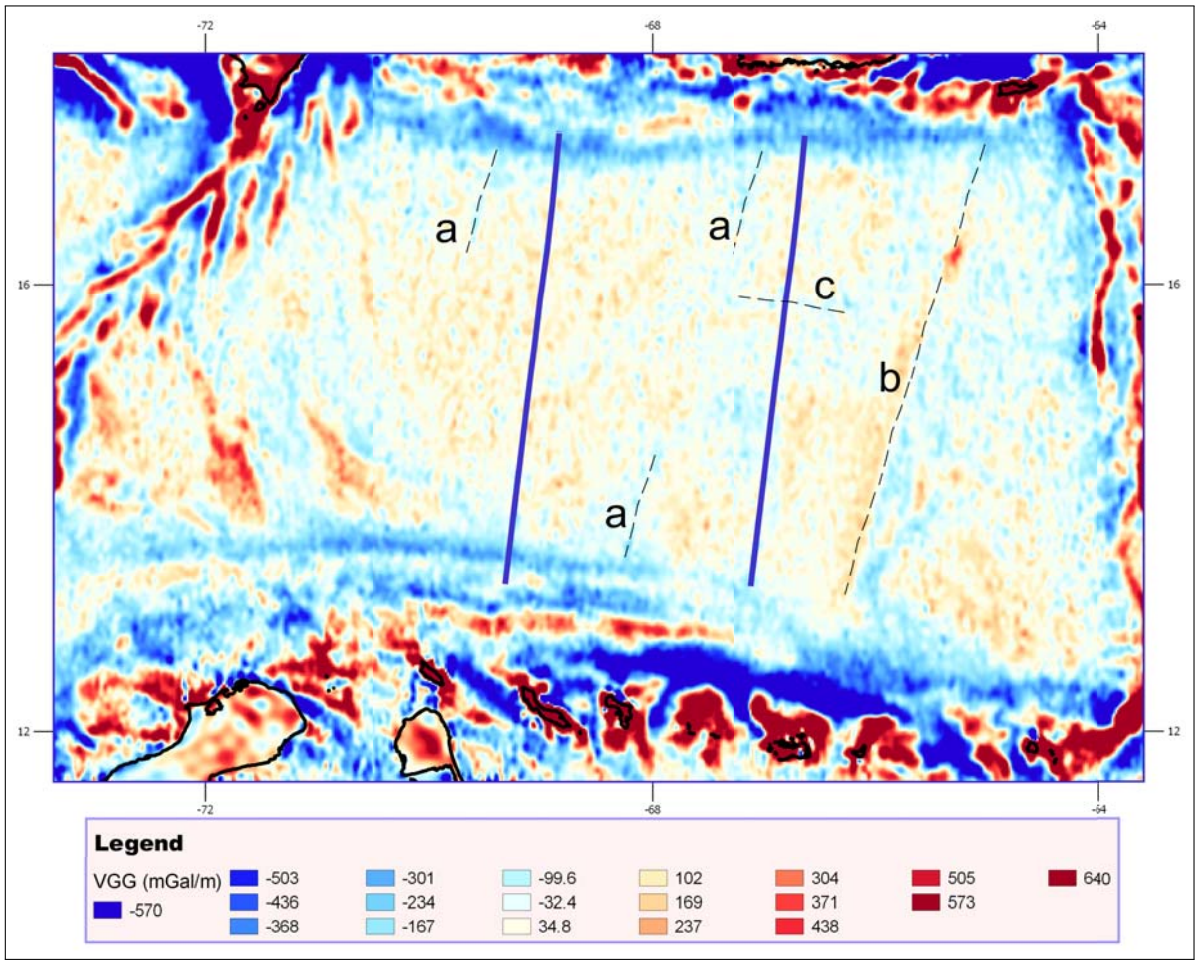

Figure 4.6 – Profiles used to evaluate the magnetic anomalies in the Venezuela Basin. The grid of Vertical Gradient of Gravity is in the background. Color scale from blue to red, represents negative to positive VGG respectively. Solid black lines represent the direction of the extracted profiles whereas dashed black lines represent our tentative fracture zones ('a' and 'b')

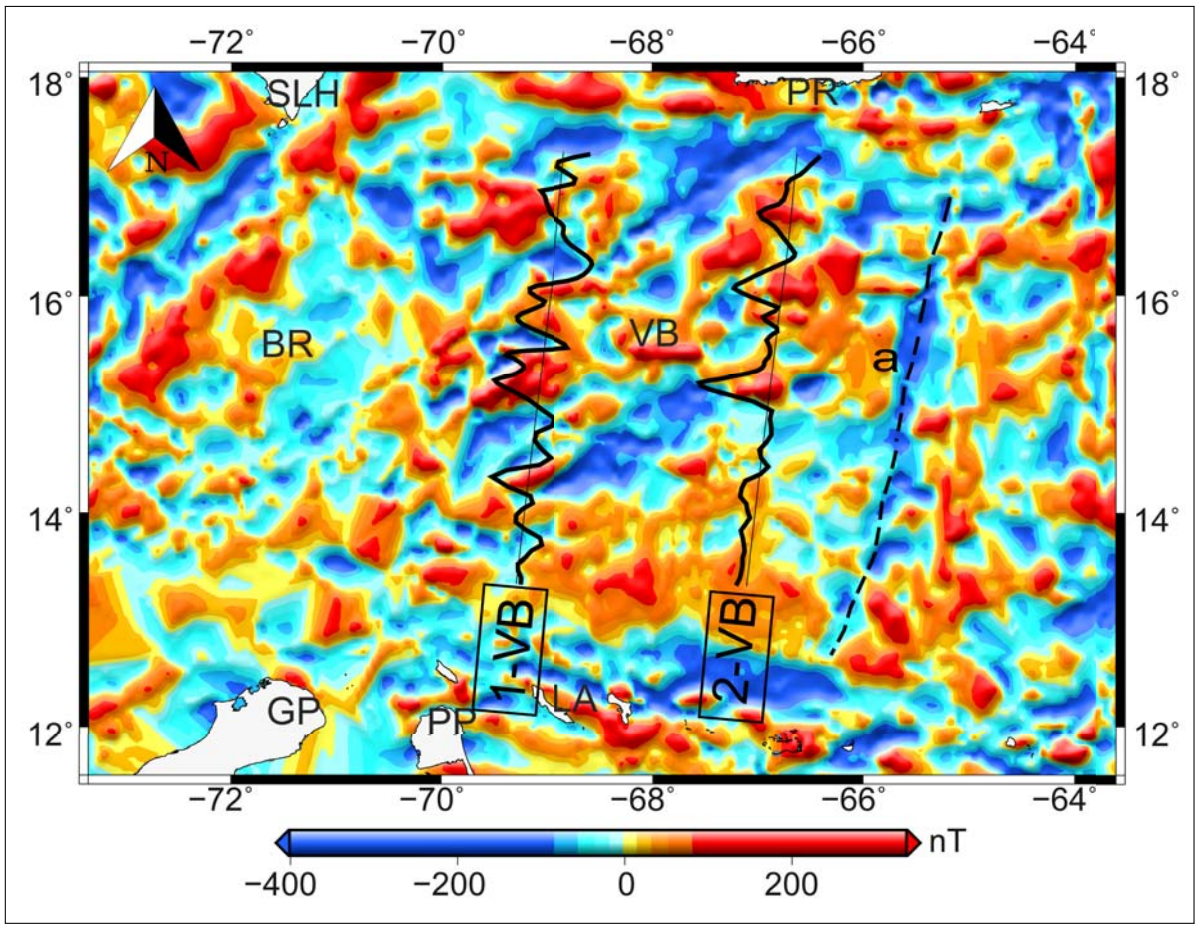

Figure 4.7 – Approximately N-S trending magnetic profiles selected in the Venezuela Basin

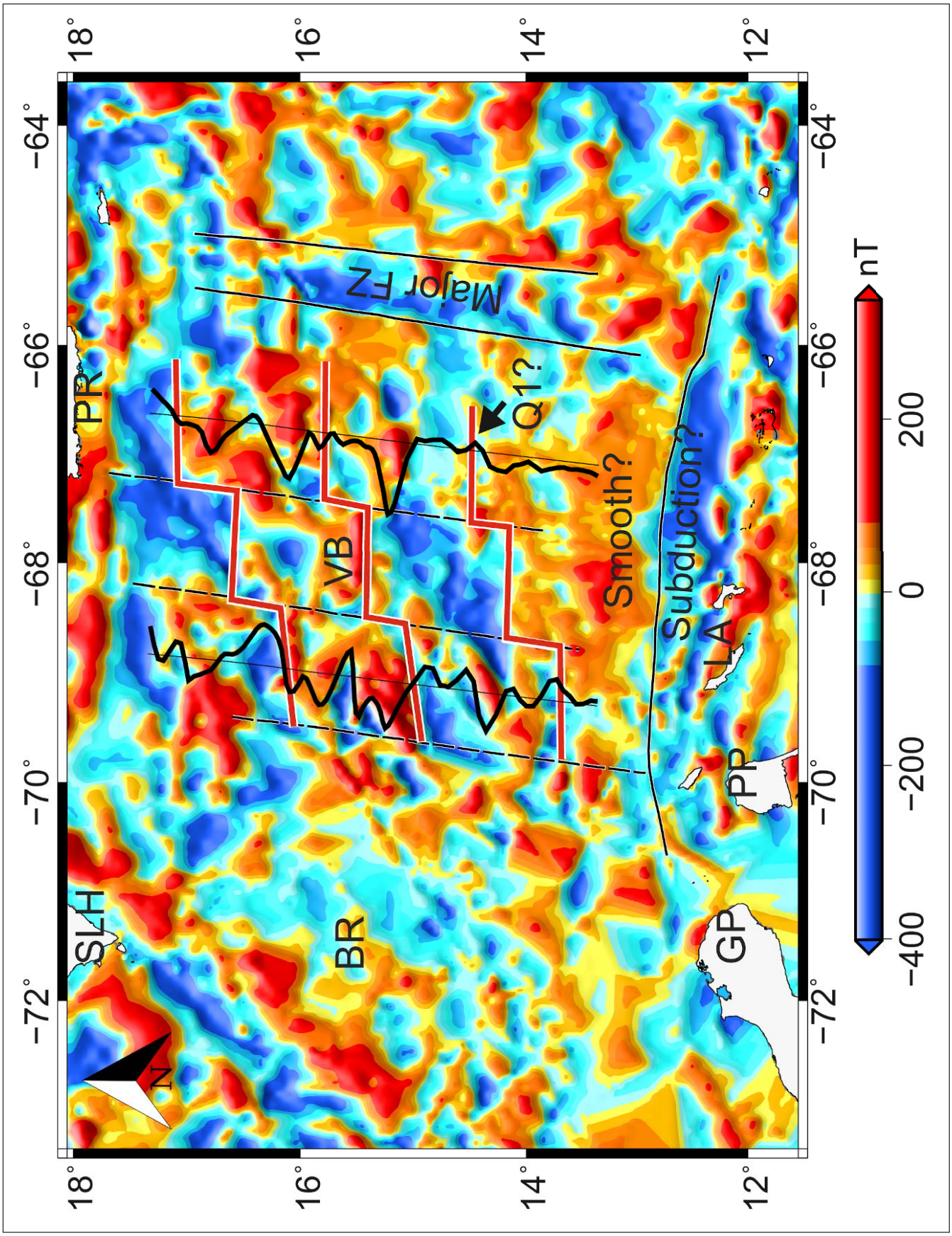

Figure 4.8 – Magnetic interpretation over the Venezuela Basin from marine data. Black dashed lines represent second order fracture zones, thick solid lines are the limit of a major fracture zone interpreted in the NS direction

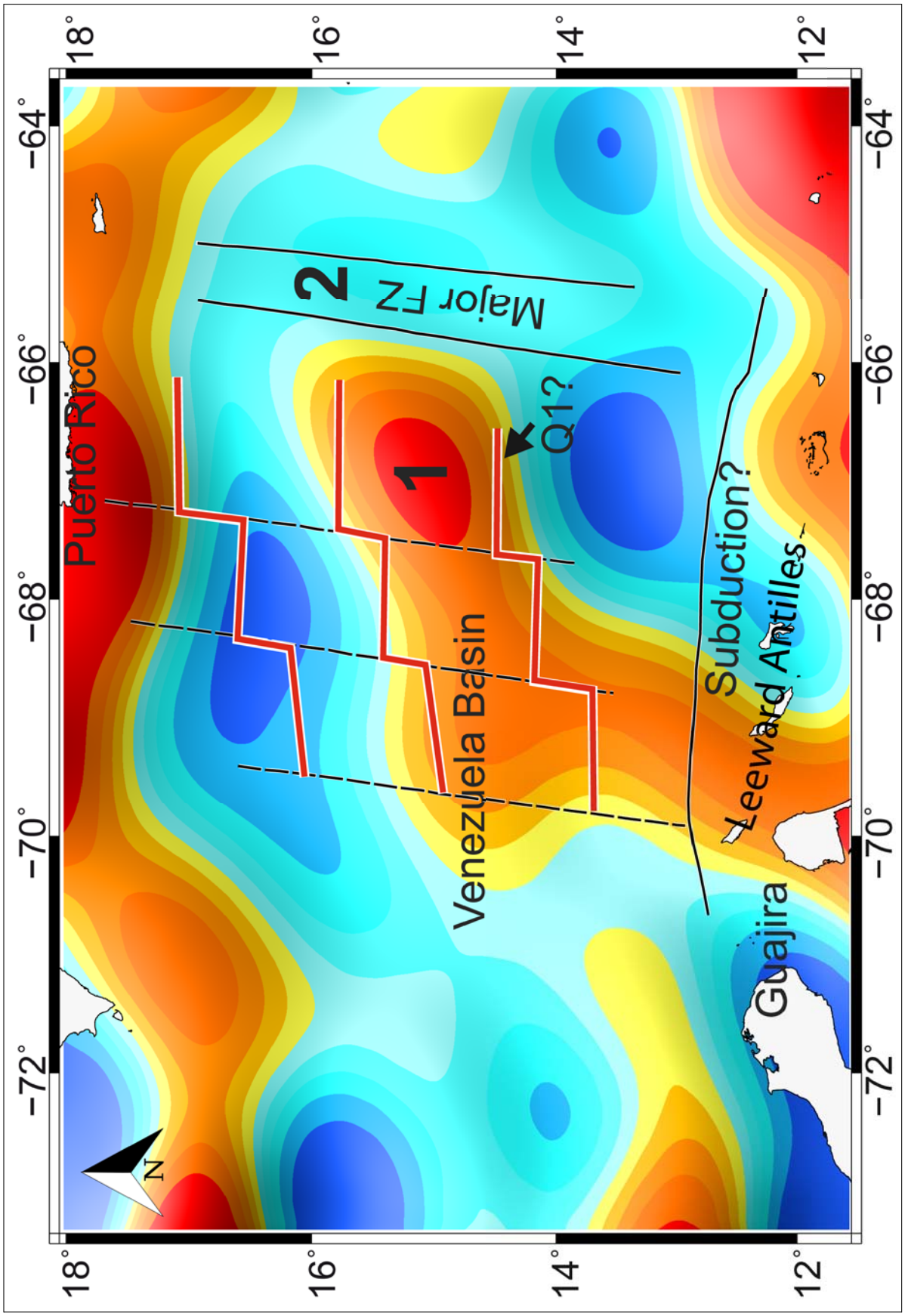

Figure 4.9 – Magnetic interpretation from marine data superimposed on satellite magnetic data (satellite magnetic data from (Olsen et al., 2017))

spreading anomalies. Data crossing the seamounts were discarded. The selected profiles are the 12 and 13, which lies near the Marquesas Islands (see Fig. 4.11 and Fig. 4.12).

We modelled magnetic anomalies formed by a spreading center (Vine and Matthews, 1963) using the Talwani (1964) method. Our goal was to compare profiles from the Pacific Ocean and the Colombia Basin, under the assumption that both crusts originated in the same latitude, and taking into account their current position. On profile PPTU03WT we identified the sequence of magnetic anomalies 34 to 23 (see 'a' in Fig. 4.13). Legendre (2003) reported a (half) spreading rate of 3.5 cm/yr to 3.6 cm/yr for Chrons 33-34. On Profile No. 2 of the Colombia Basin we identified Chrons 33, 33r and 34 (see 'b' in Fig. 4.13). We modelled the magnetic anomalies using the spreading rate obtained in the Pacific Ocean for the same period (Legendre, 2003). According to our results, the magnetic anomalies observed in the Colombia Basin could be explained if they were formed at a latitude of $\sim$10°S, with a seafloor spreading rate similar to that of anomalies 33-34 in the Pacific Ocean.

4.3.4 Discussion

We estimated the age of the Colombia Basin from its magnetic anomalies. We propose that the Caribbean plate formed at the Pacific-Farallón spreading center between approx. 70 Ma and approx. 108 Ma. Our observations suggest that magnetic anomalies in the Colombia Basin created at a paleo-latitude $\sim$10°S.

In the Colombia basin, the presence of CLIP volcanics does not prevent the observation of magnetic lineations, at least for the initial volcanic episode. This lead us to propose the initial CLIP may have formed at the same time as the plate did, i.e. at the spreading center. Our observations are consistent with the tectonic models that locate the origin of the Caribbean plate in the Pacific Ocean. The oceanic plateau migrated northeastward as the Farallón plate subducted. One hypothesis is the buoyancy of the oceanic plateau prevented its subduction, resulting in the inversion of the subduction, the continuous migration of the oceanic plateau northeastward, and finally the emplacement of the present Caribbean plate. The age of the Colombia basin is approximately 70-91 Ma (Cretaceous - Upper Campanian) and that of the Venezuela Basin 91-108 Ma.

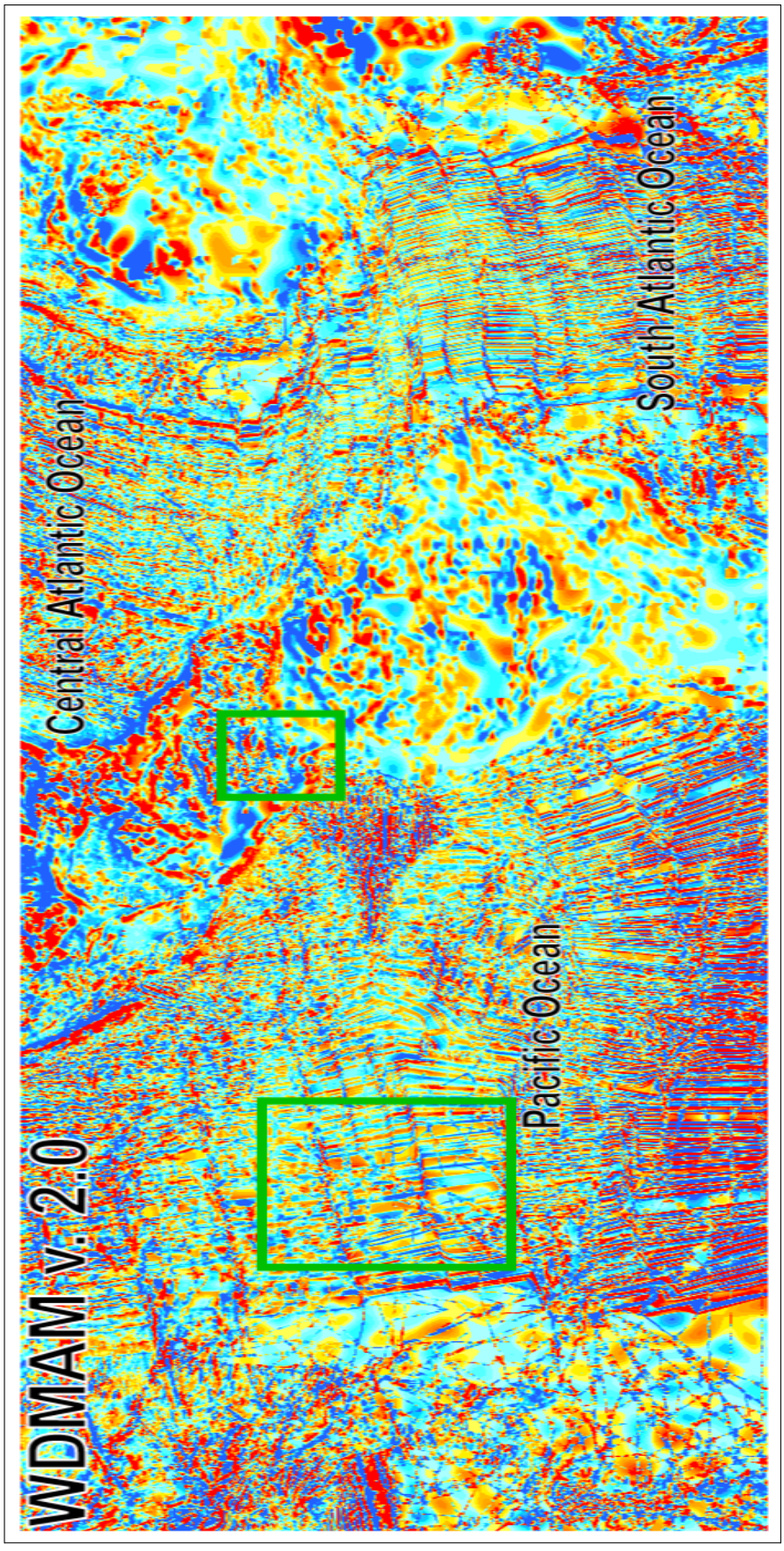

Figure 4.10 – Magnetic anomaly map (from (Dyment et al., 2015)) used to compare the wavelengths of magnetic anomalies obtained in the Colombia Basin with other marine magnetic wavelengths (In the Caribbean region, we replaced data with the database obtained in this study). Green boxes represent identified compatible areas in the Pacific Ocean and Colombia Basin respectively

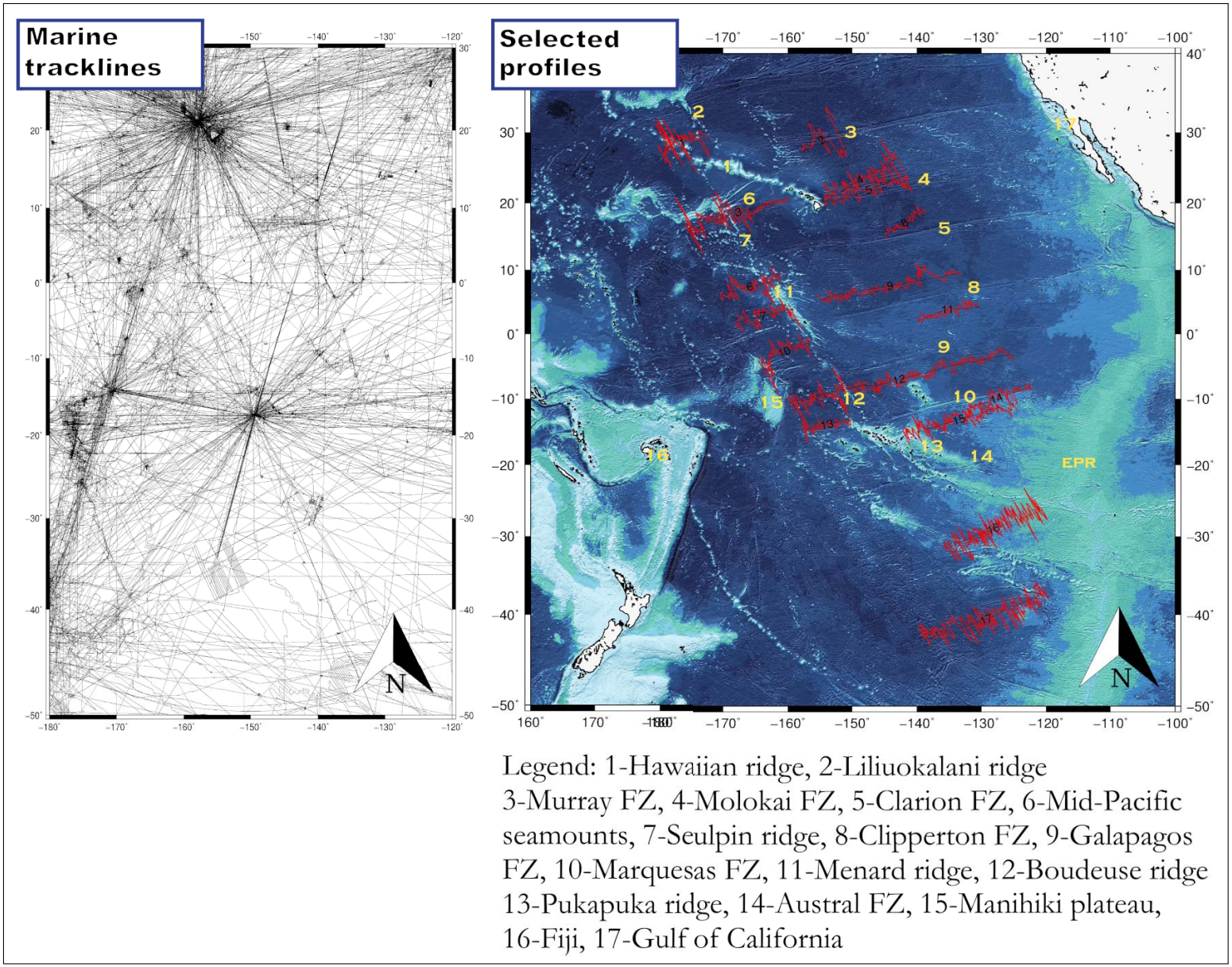

Figure 4.11 – Close up on the evaluated area in the Pacific Ocean. We selected magnetic data from available marine tracklines (a) and plotted the magnetic wiggles on those selected tracks (b)

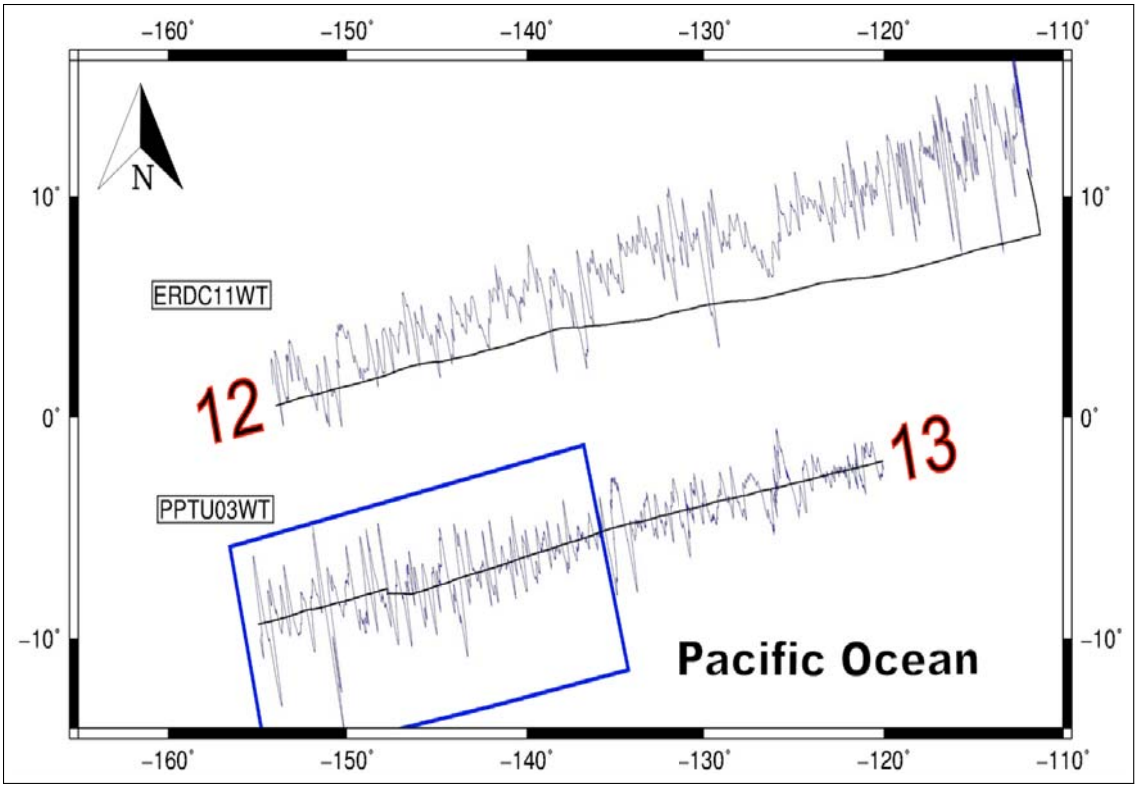

Figure 4.12 – Sub-group of magnetic profiles in the Pacific Ocean used for the magnetic modelling and comparison

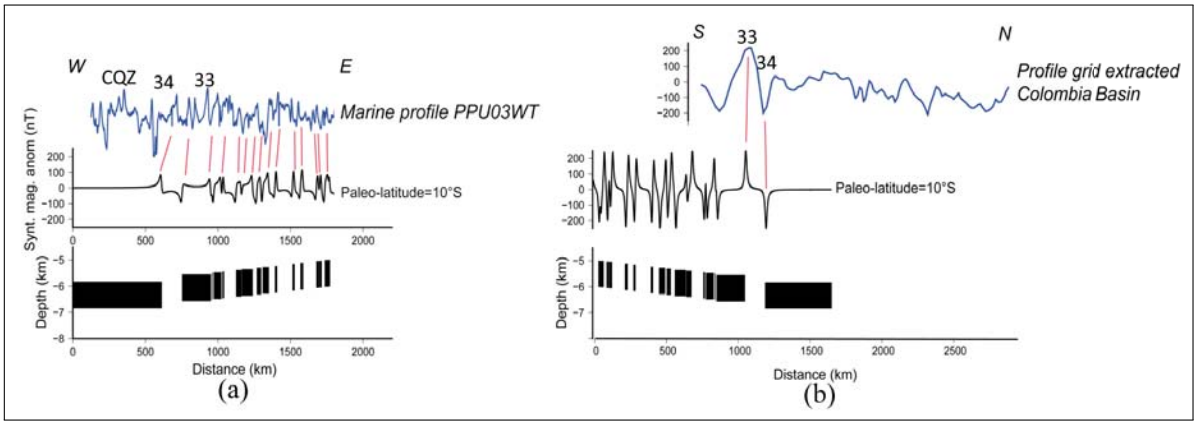

Figure 4.13 – Forward modelling of the selected Pacific Ocean and Colombia Basin magnetic anomalies

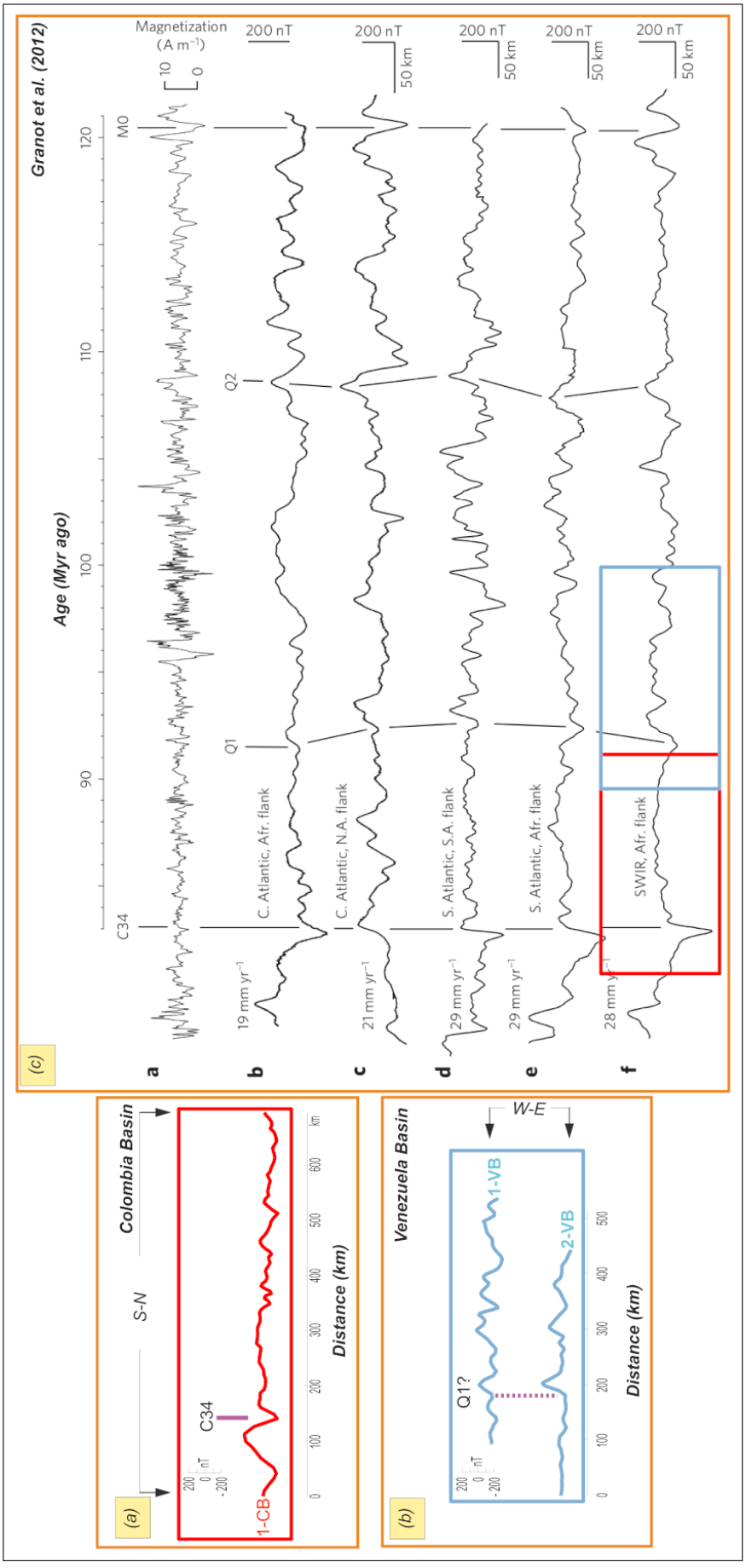

Figure 4.14 – Magnetic anomalies on the Cretaceous Normal Superchron (Granot et al., 2012)

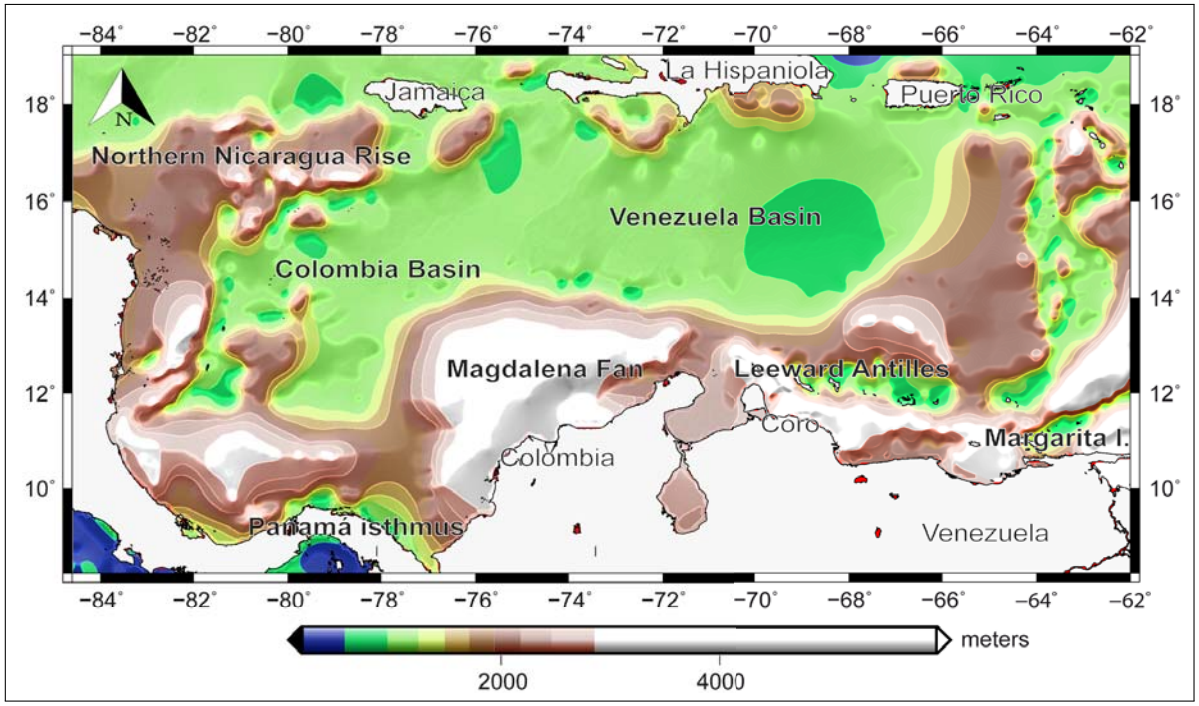

Figure 4.15 – Sediments thickness in the Caribbean region (from (Whittaker et al., 2013) database)

4.4 Conclusion

The origin and age of the Caribbean plate and the Caribbean Large Igneous Provinces (CLIP) that overlay it is a subject still under debate. The map build from our recent compilation of marine magnetic anomalies allows us to interpret magnetic anomalies in two large parts of the Caribbean plate, namely the Colombia and Venezuela basins, from which we propose a model for the origin and age of the Caribbean plate and the CLIP.

In the Colombia Basin we identify a sequence of strong magnetic anomalies in the South and a smooth magnetic zone extending to the North. We interpret the anomalies as Chrons 33 and 33r and the smooth magnetic zone as the youngest part of the Cretaceous Normal Superchron (CNS). The comparison of anomalies 33 and 33r in the Colombia Basin and Worldwide suggests that the crust in the Caribbean plate originated in the Pacific Ocean. Simple forward modeling of the shape of the anomalies supports a formation of the Colombia Basin at a paleo-latitude of $\sim$10°S and at a (half) spreading rate of $\sim$3.6 cm/yr.

In the Venezuela Basin we identify a major N-S fracture zone on both the gravity and magnetic data. A consistent pattern of anomalies in the Central part of the basin is interpreted as the intermediate part of the CNS, whereas a smooth area in the southern part of the basin may correspond to its younger part.

These observations therefore argue in favour of a Pacific origin of the Colombia Basin, formed 70-91 million years ago, and the basin of Venezuela formed 91-108 million years ago. The two basins would have formed at ridge axis separating the plates Pacific and Farallón. Our results suggest that the CLIP created at the same time as the Caribbean plate.

Hypothetically, the two basins separated during the "tightening" of the North and South American plates, the compressive zone of the Beata Ridge constituting the border, perhaps currently still active.

4.5 References

Bouysse, P. (2009). Geological Map of the World. *Commission for the Geological Map of the World*.

Boynton, C., Westbrook, G., Bott, M., and Long, R. (1979). A seismic refraction investigation of crustal structure beneath the Lesser Antilles island arc. *Geophysical Journal of the Royal Astronomical Society*, 58(2):371–393.

Christofferson, E. (1973). Linear magnetic anomalies in the Colombia Basin, central Caribbean Sea. *Geological Society of America Bulletin*, 84(10):3217–3230.

Diebold, J., Driscoll, N., et al. (1999). New insights on the formation of the Caribbean basalt province revealed by multichannel seismic images of volcanic structures in the Venezuelan Basin. *Sedimentary Basins of the World*, 4:561–589.

Diebold, J., Stoffa, P., Buhl, P., and Truchan, M. (1981). Venezuela Basin crustal structure. *Journal of Geophysical Research: Solid Earth*, 86:7901–7923.

Donnelly, T. W. (1973). Magnetic anomaly observations in the Eastern Caribbean sea. *Initial reports, Deep Sea Drilling Project*, 15(33).

Dyment, J., Lesur, V., Hamoudi, M., Choi, Y., Thebault, E., Catalan, M., the WDMAM Task Force*, the WDMAM Evaluators**, and the WDMAM Data Providers** (2015). World Digital Magnetic Anomaly Map version 2.0. `http://www.wdmam.org`.

Fox, P. J. and Heezen, B. C. (1975). Geology of the Caribbean crust. In *The Gulf of Mexico and the Caribbean*, pages 421–466. Springer.

Ghosh, N., Hall, S., and Casey, J. (1984). Seafloor spreading magnetic anomalies in the Venezuelan Basin. *Geological Society of America Memoirs*, 162:65–80.

Giunta, G., Beccaluva, L., Coltorti, M., Siena, F., and Vaccaro, C. (1997). Ophiolitic units of the southern margin of Caribbean plate in Venezuela: a reappraisal of their petrogenesis and original tectonic setting. In *Memorias del VIII Congreso Geologico Venezolano Porlamar*, volume 1, pages 331–337.

Granot, R., Dyment, J., and Gallet, Y. (2012). Geomagnetic field variability during the Cretaceous Normal Superchron. *Nature Geoscience*, 5(3):220–223.

Kerr, A. C., Iturralde-Vinent, M. A., Saunders, A. D., Babbs, T. L., and Tarney, J. (1999). A new plate tectonic model of the Caribbean: Implications from a geochemical reconnaissance of Cuban Mesozoic volcanic rocks. *Geological Society of America Bulletin*, 111(11):1581–1599.

Kerr, A. C., White, R. V., and Saunders, A. D. (2000). LIP reading: recognizing oceanic plateaux in the geological record. *Journal of Petrology*, 41(7):1041–1056.

Legendre, C. (2003). *Pétrogenèse de laves différenciées en contexte intraplaque océanique et hétérogénéité géochimique au niveau du point chaud des Marquises (Polynésie française): étude des îles de Ua Pou et de Nuku Hiva*. PhD thesis, Université de Bretagne occidentale-Brest.

Leroy, S., Mauffret, A., Patriat, P., and de Lépinay, B. M. (2000). An alternative interpretation of the Cayman trough evolution from a reidentification of magnetic anomalies. *Geophysical Journal International*, 141(3):539–557.

Meschede, M. and Frisch, W. (1998). A plate-tectonic model for the Mesozoic and Early Cenozoic history of the Caribbean plate. *Tectonophysics*, 296(3):269–291.

Officer, C., Ewing, J., Edwards, R., and Johnson, H. (1957). Geophysical investigations in the eastern Caribbean: Venezuelan basin, Antilles island arc, and Puerto Rico trench. *Geological Society of America Bulletin*, 68(3):359–378.

Olsen, N., Ravat, D., Finlay, C. C., and Kother, L. K. (2017). LCS-1: A high-resolution global model of the lithospheric magnetic field derived from CHAMP and Swarm satellite observations. *Geophysical Journal International*, 211(3):1461–1477.

Pindell, J. (1991). Geological arguments suggesting a Pacific origin for the Caribbean Plate. In *Transactions 12th Caribbean Geological Conference St Croix*.

Sclater, J. G., Anderson, R. N., and Bell, M. L. (1971). Elevation of ridges and evolution of the central eastern Pacific. *Journal of Geophysical Research*, 76(32):7888–7915.

Sinton, C. W., Duncan, R., Storey, M., Lewis, J., and Estrada, J. (1998). An oceanic flood basalt province within the Caribbean plate. *Earth and Planetary Science Letters*, 155(3):221–235.

Sinton, C. W., Sigurdsson, H., and Duncan, R. A. (2000). Major element oxides and 40Ar/39Ar plateau and isochron ages of ODP Hole 165-1001A. *Proceedings of the Ocean Drilling Program, Scientific Results, College Station, TX*, 165:1–4.

Talwani, M. (1964). Computation of magnetic anomalies caused by two-dimensional bodies of arbitrary shape. *Computers in the mineral industries*, 1:464–480.

Vine, F. J. and Matthews, D. H. (1963). Magnetic anomalies over oceanic ridges. *Nature*, 199(4897):947–949.

Whittaker, J. M., Goncharov, A., Williams, S. E., Müller, R. D., and Leitchenkov, G. (2013). Global sediment thickness data set updated for the Australian-Antarctic Southern Ocean. *Geochemistry, Geophysics, Geosystems*, 14(8):3297–3305.

Chapter 5

General conclusions and Perspectives

5.1 General conclusions

We undertook a review on the Caribbean region based on extensive literature. We assimilated information from regional publications and underlined the need to review marine magnetic anomalies in the Caribbean region in the light of a detailed compilation of the area. The Caribbean plate is a complex area, about which subsists a lively debate about its origin and the extension of the CLIP, with an abnormal and contrasting thickness. The step forward in the study of the oceanic structures in this area was the compilation of marine magnetic anomalies.

Our compilation of marine magnetic anomalies led to the development of a methodology for gathering data acquired at different times and updating the results with recent models of the internal magnetic field. We also examined the influence of the external magnetic field given the proximity of the electro-jet currents and the magnetic equator. As a result, we obtained a detailed magnetic map of the Caribbean and Gulf of Mexico region, highlighting the most prominent structural features of the region. From west to east, the characteristics of the magnetic map that stand out most are long-wavelength magnetic anomalies in the Gulf of Mexico; short wavelength magnetic anomalies in the Yucatán basin, possibly associated with the creation of oceanic crust of the basin; and strong positive anomalies associated with the Florida and Bahamas tectonic blocks which confirm the continental nature of these two blocks. We interpreted an area of more confused magnetic anomalies extending south of the Nicaragua Ridge and as far as the Colombia Basin as reflecting a volcanic episode posterior to the Caribbean crust emplacement. We associated a strong positive anomaly, trending obliquely with respect to the Colombia Basin anomalies, with the Hess Escarpment, which represents a major tectonic boundary. The linear anomalies of high amplitude observed in the southern part of the basin of Colombia confirm its oceanic nature. We also interpreted the dominant magnetic signature of Beata Ridge as reflecting an episode of late volcanism. The observed anomalies do not bear a clear signature associated with the Beata Ridge

and extend eastward, encompassing the western part of the Venezuela Basin. From the integration of aeromagnetic data with the marine magnetic data gathered on the Caribbean Plate, we describe the boundary zone between the Caribbean Plate and the northern end of the South American Plate as a band characterized by a strong magnetic gradient parallel to the Pilar fault that may represent the contact between continental and oceanic crust. A North-South trending low magnetic anomaly is also characteristic of the eastern part of the Venezuela Basin, parallel to the Aves Ridge and interpreted as an oceanic fracture zone. A discontinuous positive magnetic signature characterizes the Aves Ridge. The magnetic map obtained from the marine data, as well as the database, constitute the basis of the subsequent steps of our study of magnetic anomalies of the Caribbean plate.

We undertook the study of the Gulf of Mexico (GoM) based on magnetic anomalies and the vertical gradient of gravity. We interpreted the structures associated with the seafloor opening in the GoM. We interpreted long-wavelength magnetic anomalies as isochrons, allowing us to describe the GoM tectonic evolution. Using plate kinematic techniques also allowed rigorous calculation of the rotation poles for the distinct stages of evolution of the GoM, but also to pursue another approach of the interpretation of isochrons in the conjugate basins of the ocean ridges. The magnetic information we use is not strictly adequate — long wavelength anomalies as isochrons — but can be traced back to a reasonable description of the seafloor opening which would otherwise be difficult to unravel. Our results show that the Gulf of Mexico opened in at least two main stages and that one step is not enough to explain the orientation of the fracture zones (constrained by the vertical gradient of gravity) and the present position of the Yucatán block. The dating of the isochrons is tentative and based on the hypothesis of anomalies created near the equator following a sub meridian seafloor spreading direction, making it possible to compare the inverted magnetic profiles with smoothed versions of the scale of magnetic polarity reversals. We suggest that the Gulf of Mexico opened before the Kimmeridgian and seafloor spreading ceased in the Berriasian. The central magnetic anomaly, interpreted as the ridge axis, does not coincide perfectly with the segments of the fossil axis described by the vertical gradient of gravity, the latter probably marking ridge jumps anterior to seafloor spreading cessation and compatible with the observed spreading asymmetry.

We analyzed magnetic anomalies in the Caribbean plate, more specifically in the Colombia and Venezuela Basins. We interpreted the sequence of linear anomalies in the Colombia Basin as Chrons 33 and 33r. The remarkably smooth magnetic zone extending from the center of the Colombia Basin northward in a triangle pinched between Beata Rise and the Nicaragua Ridge would date from the youngest part of the CQZ. A comparison of the width of anomalies 33-34 of the Colombia Basin, the Atlantic and Pacific oceans suggests that the Colombia Basin is of Pacific origin. Our forward models suggest that anomalies observed in the Colombia Basin formed at a paleolatitude of $\sim$10°S at a spreading rate of $\sim$3.6 cm/yr. Conversely, the high frequency anomalies observed in the northern and central Venezuela

Basin are interpreted as the middle part of the CQZ, whereas the smooth anomalies depicted in the Southern Venezuela may be the younger part of the CQZ, the limit being the marker Q1 of (Granot et al., 2012). These observations argue for a Pacific origin of the Colombia Basin, formed 70-91 million years ago, and the Venezuela Basin formed 91-108 million years ago. The two basins would have separated during the "tightening" of the Caribbean plate between the North and South American plates, the compressive zone of the Beata Ridge constituting their border, perhaps currently still active. Our results suggest that the CLIP was formed at the same time as the Caribbean plate. Therefore, our model favors the hypothesis that the Caribbean plate is essentially of Pacific origin and could be a fragment of an oceanic plateau, possibly the one that included the Manihiki, Ontong Java and Hikurangi plateaus.

5.2 Perspectives

The map obtained from marine magnetic anomalies is an essential product for the interpretation of Caribbean oceanic structures. However, due to the limitation or the poor quality of some data, some of them should be completed by the acquisition of new ones in specific areas, for example in the Venezuelan Basin, the Yucatán Basin, the Grenada Basin and the Gulf of Mexico. The proposed orientation of the fracture zones provide relevant information to acquire new data and define with more precision the isochrons present in the area, contributing to feed the tectonic model. This step would represent not only a contribution to the magnetic map but also a contribution to the knowledge of magnetic anomalies in the global ocean, to the comprehensive kinematic description of present and past plate tectonics, to the study of the evolution of the Caribbean plate in a more regional context, and ultimately to the energy potential of ocean basins and margins. The acquisition of marine magnetic profiles in the basins of Yucatán and Venezuela, but also in the supposed conjugated areas of the Pacific Ocean, where existing data are old and poorly navigated, is high desirable.

It will be essential to include and integrate seismic and drill data in the Gulf of Mexico, specifically in the central and western Gulf, which in many cases are acquired and interpreted by the industry, to improve our tectonic model. One of the primary tasks to perform in order to better constrain our model is the plate tectonic reconstruction of the Gulf of Mexico taking into account the precise position of the North and South American continents at each epoch. This step, insufficiently thorough for lack of time in this thesis, will allow us to firmly establish the rotation poles obtained in this thesis by constraining the existing space between the North and South American continents during the breakup of the Pangea, allowing to the Caribbean plate to move eastward.

Regarding the Caribbean plate, the comparison of magnetic anomalies dated from the CQZ with those of other ocean basins could help refine our interpretation and more accurately date the observed anomalies. Acquiring high-resolution magnetic data close to the seafloor is an

option that should not be ruled out. Comparing data from the Lesser Antilles arc with basins with similar geometry, such as the Mariana back-arc basin, may help to better understand the basins adjacent to this arc and the Aves Ridge.

5.3 References

Granot, R., Dyment, J., and Gallet, Y. (2012). Geomagnetic field variability during the Cretaceous Normal Superchron. *Nature Geoscience*, 5(3):220–223.

Chapter 6

Conclusions générales et Perspectives

6.1 Conclusions générales

Une analyse bibliographique sur la région des Caraïbes a été entreprise, à partir d'une littérature abondante. Les informations de publications à caractère régional ont été assimilées et ont montré la nécessité de revoir les anomalies magnétiques marines dans la région des Caraïbes à la lumière d'une compilation détaillée de la zone. La plaque Caraïbe est une zone complexe, sur laquelle subsiste encore un débat animé sur son origine et l'extension du CLIP, avec une épaisseur anormale et contrastée. L'étape suivante pour l'étude des structures océaniques dans cette zone était la compilation des anomalies magnétiques marines.

La compilation des anomalies magnétiques marines a conduit au développement d'une méthodologie pour rassembler des campagnes acquises à des moments différents et mettre à jour les résultats avec des modèles récents du champ magnétique interne. Nous avons également vérifié si l'influence du champ magnétique externe est bien corrigée compte tenu de la proximité de la zone des courants d'électrojet et de l'équateur magnétique. Par conséquent, nous avons obtenu une compilation détaillée de la région des Caraïbes et du golfe du Mexique, ce qui a permis de mettre en évidence les caractéristiques structurales les plus importantes de la région. D'ouest en est, les caractéristiques de la carte magnétique qui se démarquent le plus sont, des anomalies magnétiques de grande longueur d'onde distribuées en éventail dans le golfe du Mexique; des anomalies magnétiques de courte longueur d'onde dans le bassin Yucatan reflétant peut-être la formation de croute océanique dans ce bassin; et des anomalies positives fortes associées aux blocs tectoniques de Floride et des Bahamas qui confirment la nature continentale des deux blocs. Une zone d'anomalies magnétiques plus confuses au Sud de la ride du Nicaragua s'étend jusqu'au bassin de Colombie et est interprétée comme la marque d'un niveau volcanique postérieur à l'emplacement de la croûte. Une anomalie positive forte, oblique par rapport au bassin de Colombie, est associée à l'escarpement de Hess et paraît constituer une limite tectonique majeure. Les anomalies linéaires de forte amplitude observées dans la partie méridionale du

bassin de Colombie confirment sa nature océanique. La signature magnétique prédominante de la ride de Beata est interprétée comme reflétant un épisode de volcanisme tardif; cette ride parait affectée de failles réactivées dans un domaine tectonique compressif. Les anomalies observées ne présentent pas de signature claire associée à la ride de Beata et s'étendent vers l'est, englobant la partie occidentale du bassin du Venezuela. La zone limitant la plaque Caraïbes et le nord de la plaque Sud-Américaine a pu être décrite grâce à l'intégration de données aéromagnétiques avec les données marines recueillies sur la plaque Caraïbes et correspond à une bande caractérisée par un fort gradient magnétique parallèle à la faille du Pilar, qui pourrait représenter le contact entre croûte continentale et océanique. Une anomalie magnétique d'orientation NS est également caractéristique de la partie orientale du bassin du Venezuela, parallèle à la ride d'Aves et interprétée comme une zone de fracture océanique. La ride d'Aves se caractérise par une signature magnétique positive discontinue. La carte magnétique obtenue à partir des données marines, ainsi que la base de données correspondante, est le socle des prochaines étapes de notre étude des anomalies magnétiques de la plaque Caraïbe.

Nous avons entrepris l'étude du golfe du Mexique sur la base des anomalies magnétiques et du gradient vertical de gravité. L'étude a permis d'interpréter les structures associées à l'expansion de la croute océanique dans le golfe du Mexique. Les anomalies en éventail décrites, interprétées comme des isochrones magnétiques, nous permettent de décrire l'évolution tectonique du golfe du Mexique au fil du temps. L'utilisation de ces données et des techniques de la cinématique des plaques m'a également permis de générer des outils permettant de calculer rigoureusement les pôles de rotation pour les différents stades d'évolution du golfe, mais aussi d'apprendre une autre approche pour l'interprétation des isochrons dans les bassins conjugués des dorsales océaniques. L'information magnétique que nous utilisons n'est pas à strictement parler adéquate - anomalies de grande longueur d'onde en lieu d'isochrones - mais permet de remonter à une description raisonnable de l'expansion du fond océanique qui serait sinon difficilement accessible. Nos résultats montrent que le golfe du Mexique s'est ouvert en au moins deux étapes principales et qu'une seule étape ne suffit pas à expliquer l'orientation des zones de fracture (contraintes par le gradient vertical de gravité) et la position présente du bloc du Yucatan. La datation des isochrones reste spéculative et repose sur l'hypothèse d'anomalies créées près de l'équateur suivant une direction d'expansion subméridienne, permettant de comparer les profils magnétiques inversés à des versions lissées de l'échelle des inversions de polarité magnétique. Nous suggérons que le golfe du Mexique s'est ouvert avant le Kimméridgien et que l'expansion océanique y a cessé au Berriasien. L'anomalie magnétique centrale, interprétée comme l'axe de la zone d'expansion, ne coïncide pas parfaitement avec les segments d'axe fossile décrit par le gradient vertical de gravité, ces derniers pouvant marquer des sauts de dorsale antérieurs à l'arrêt de la dorsale compatibles avec l'asymétrie d'expansion observée.

Nous avons aussi procédé à l'analyse d'anomalies magnétiques de la plaque Caraïbes, plus

spécifiquement dans les bassins de Colombie et du Venezuela. La séquence d'anomalies linéaires du bassin de Colombie est interprétée comme les Chrones 33 et 33r. La zone magnétique très lisse s'étendant du centre du bassin de Colombie vers le nord en formant un triangle daterait de la partie la plus jeune de la Période Magnétique Calme du Crétacé. Une comparaison de la largeur des anomalies 33-34 du bassin de Colombie et des océans Atlantique et Pacifique favorise l'hypothèse d'une croûte d'origine Pacifique. Nos modèles suggèrent que les anomalies observées dans le bassin de la Colombie se sont formées à une paléo latitude de $\sim$10°S à une vitesse d'expansion d'environ 3,6 cm/an. Par ailleurs, les anomalies de haute fréquence observées au Nord et au centre du bassin du Venezuela sont interprétées comme la partie moyenne de la Période Calme, alors que les anomalies très lisses du Sud de ce bassin pourraient marquée la partie la plus jeune de cette période, la limite étant le marqueur Q1 de (Granot et al., 2012). Ces observations plaident en faveur d'une origine Pacifique du bassin de Colombie, formé il y a 70-91 millions d'années, et du bassin du Venezuela, formé il y a 91-108 Ma. Les deux bassins se seraient formés à l'axe de la dorsale séparant les plaques Pacifique et Farallon. Nos résultats suggèrent en effet que le CLIP a été créé en même temps que la plaque Caraïbe. Les deux bassins se seraient séparés lors du "serrage" de la plaque Caraibe entre les plaques Nord et Sud-Américaines, la zone compressive de la ride de Beata en constituant la frontière, peut-être actuellement encore active. Notre modèle favorise donc l'hypothèse selon laquelle la plaque des Caraïbes est essentiellement d'origine Pacifique et pourrait être un fragment d'un plateau océanique, peut-être celui qui incluait les plateaux de Manihiki, d'Ontong Java et d'Hikurangi.

6.2 Perspectives

La carte obtenue à partir des anomalies magnétiques marines constitue un produit essentiel pour l'interprétation des structures océaniques des Caraïbes. Cependant, en raison de l'ancienneté de certains profils ou de leur mauvaise qualité, certains d'entre eux devraient être confirmés par l'acquisition de nouvelles données, par exemple dans le bassin du Venezuela, le bassin du Yucatan, le bassin de la Grenade et le golfe du Mexique. L'orientation probable des zones de fracture à la lumière des nouvelles données pourrait contribuer à alimenter le modèle tectonique et donner des informations pertinentes pour acquérir de nouvelles données et définir avec plus de précision les isochrones présentes dans la zone. Je crois que cette étape ne serait pas seulement une contribution à la carte magnétique, mais également une contribution à la connaissance globale des anomalies magnétiques dans l'océan mondial, à la description cinématique globale des plaques tectoniques présentes et passées, à l'étude de l'évolution de la plaque Caraïbe dans un contexte régional mieux défini, et in fine le potentiel énergétique des bassins océaniques et des marges. L'acquisition de profils magnétiques marins dans les bassins du Yucatan et du Venezuela, mais également dans les zones conjuguées supposées de l'océan Pacifique, où

les données existantes sont anciennes et mal naviguées, est fortement souhaitable.

En ce qui concerne le golfe du Mexique, l'intégration de données sismiques ou de forages acquises et, dans de nombreux cas, interprétées par l'industrie, plus spécifiquement au centre et à l'ouest du golfe, est essentielle pour améliorer notre modèle. Reconstruire l'évolution du golfe en tenant compte de la position à chaque période des continents Nord et Sud-américains sera une tâche primordiale pour mieux contraindre notre modèle. Cette étape, insuffisamment approfondie faute de temps dans cette thèse, nous permettra d'asseoir solidement les pôles de rotation obtenus dans cette thèse en contraignant l'espace existant entre les continents nord et sud-américain lors de l'éclatement de la Pangée, permettant à la plaque Caraïbe de s'insinuer vers l'est.

En ce qui concerne la plaque Caraïbe, la comparaison des anomalies magnétiques datée de la Période Magnétique Calme du Crétacé avec celles d'autres bassins océaniques pourrait permettre d'affiner notre interprétation et de dater plus finement les anomalies observées. L'acquisition de données magnétiques de haute résolution, à proximité du fond, est une option qu'il convient de ne pas exclure. La comparaison des données de l'arc des Petites Antilles avec des bassins ayant une géométrie similaire, comme le bassin d'arrière-arc des Mariannes, pourrait aider à une meilleure compréhension des bassins voisins de cet arc et de la ride d'Aves.

6.3 References

Granot, R., Dyment, J., and Gallet, Y. (2012). Geomagnetic field variability during the Cretaceous Normal Superchron. *Nature Geoscience*, 5(3):220–223.

Appendix A

Carte Structurale des Caraïbes

A.1 Le projet et ma contribution

Ce chapitre présente la carte structurelle des Caraïbes à l'échelle 1:4.000.000. Cette carte structurelle des Caraïbes fait partie des efforts remarquables déployés par Philippe Bouysse au sein de la Commission pour la Carte Géologique du Monde (CCGM) pour compiler les informations les plus récentes concernant les structures géologiques des Caraïbes. Un effort réalisé au fil de nombreuses années de recherche et de détail. Un effort qui, de mon point de vue, aurait été impossible à accomplir sans l'aide désintéressée et patiente de Clara Cárdenas, sans la faible sagesse et l'accompagnement de Philipe Rossi et l'énergie inépuisable de Manuel Pubellier. De même, ce travail n'aurait pas été possible sans l'aide précieuse que Total nous a apportée pour la numérisation de la carte. Ma contribution se limite à l'interprétation des structures dans les bassins des Caraïbes et la définition du type de croûte à partir de données géophysiques et il faut continuer à en discuter.

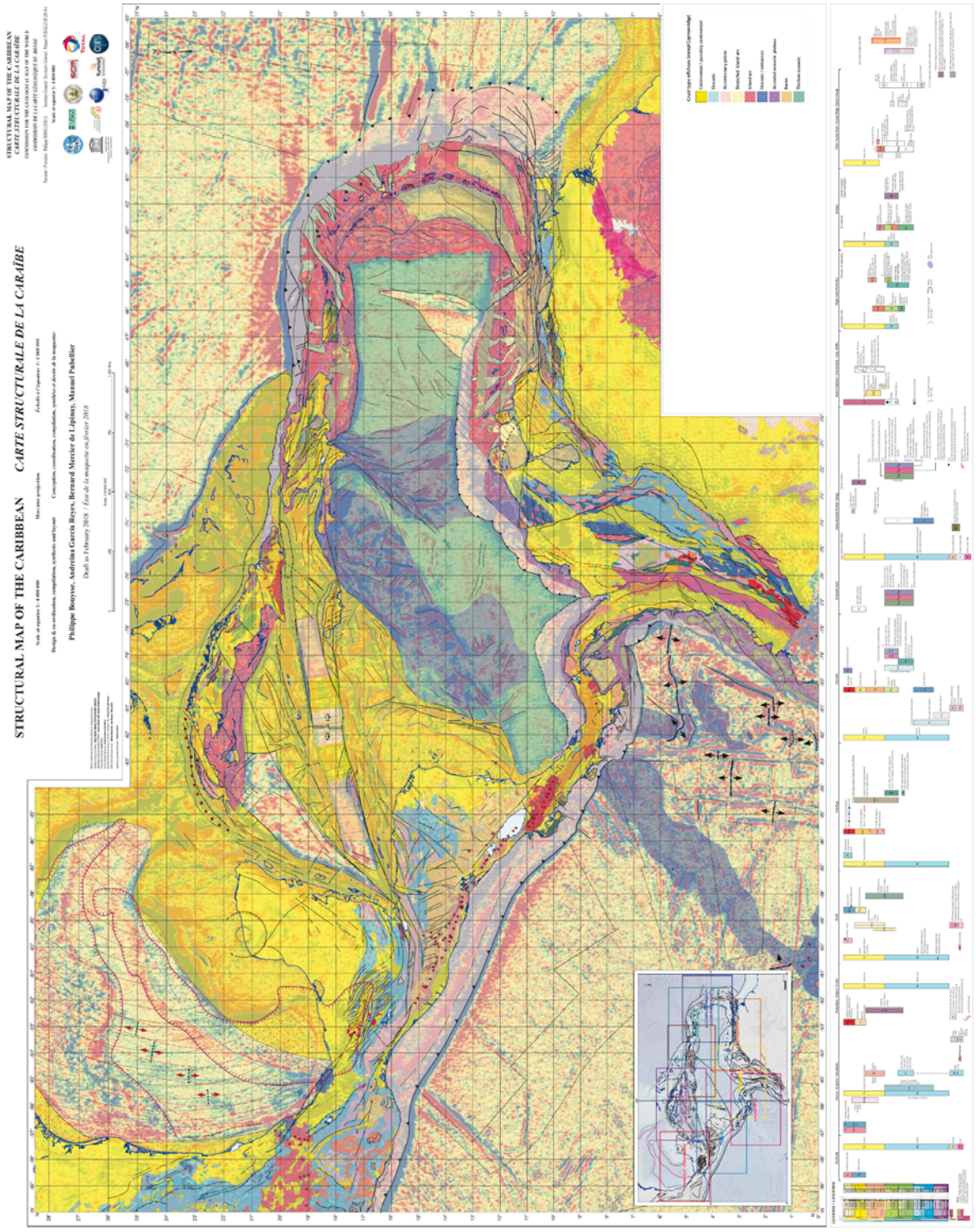
STRUCTURAL MAP OF THE CARIBBEAN
CARTE STRUCTURALE DE LA CARAÏBE
Philippe Bouysse, Andrémia Garcia Reyes, Bernard Mercier de Lépinay, Manuel Pubellier
Draft as February 2018 / État de la maquette en février 2018

Appendix B

References

B.1 References

Abdel-Kader, K., El-Kabbani, A., Yahya, A., Soliman, F., Ismail, A., and Abdel-Maksood, A. (2017). A New Electronic Technique for Real-Time Correction of Heading and DC-Shift Noises in Airborne Magnetic Data. *Journal of Multidisciplinary Engineering Science and Technology*, 4(6):7390–7396.

Acton, G. D., Galbrun, B., and King, J. W. (2000). 9. Paleolatitude of the Caribbean plate since the Late Cretaceous. *Atlantic*, 25:25.

Amato, J. M., Lawton, T. F., Mauel, D. J., Leggett, W. J., González-León, C. M., Farmer, G. L., and Wooden, J. L. (2009). Testing the Mojave-Sonora megashear hypothesis: Evidence from Paleoproterozoic igneous rocks and deformed Mesozoic strata in Sonora, Mexico. *Geology*, 37(1):75–78.

Anderson, T. H., Silver, L. T., Nourse, J., McKee, J., and Steiner, M. (2005). The Mojave-Sonora megashear-Field and analytical studies leading to the conception and evolution of the hypothesis. *SPECIAL PAPERS-GEOLOGICAL SOCIETY OF AMERICA*, 393:1.

Audemard, F. A. (2009). Key issues on the post-Mesozoic southern Caribbean plate boundary. *Geological Society, London, Special Publications*, 328(1):569–586.

Bankey, V., Cuevas, A., David, D., Finn, C. A., Hernandez, I., Hill, P., Kucks, R., Warner, M., Pilkington, M., Carter, R., Rystrom, W., Shearer, V., Snyder, S., Sweeney, R., Velez, J., J.D., P., Ravat, D., et al. (2002). Digital data grids for the magnetic anomaly map of North America. *U.S. Geological Survey Open-File Report 02-414 U.S. Geological Survey Denver Colorado USA*.

Baquero, M., Grande, S., Urbani, F., Cordani, U., Hall, C., and Armstrong, R. (2015). New Evidence for Putumayo Crust in the Basement of the Falcon Basin and Guajira Peninsula, Northwestern Venezuela. In *AAPG Special Volumes*.

Bartok, P. (1993). Prebreakup geology of the Gulf of Mexico-Caribbean: Its relation to Triassic and Jurassic rift systems of the region. *Tectonics*, 12(2):441–459.

Beamish, D. et al. (2015). Levelling aeromagnetic survey data without the need for tie-lines. *Geophysical Prospecting*, 63(2):451–460.

Beard, L., Goitom, B., and Reidar, J. (2000). Interpretation of Low Latitude magnetic anomalies. *NGU Report, Geological Survey of Norway*, 2000:31.

Benaissa, M., Berguig, M., Doumbia, V., and Bouraoui, S. (2017). The equatorial electrojet (EEJ) current deduced from CHAMP satellite and ground magnetic measurements in West Africa. *Arabian Journal of Geosciences*, 10(15):329.

Benford, B. (2012). *Faulting and strain partitioning in Jamaica from GPS and structural data: Implications for Gonave and Hispaniola microplate kinematics, northern Caribbean*. PhD thesis, The University of Wisconsin-Madison.

Biari, Y., Klingelhoefer, F., Sahabi, M., Funck, T., Benabdellouahed, M., Schnabel, M., Reichert, C., Gutscher, M.-A., Bronner, A., and Austin, J. (2017). Opening of the central Atlantic Ocean: Implications for geometric rifting and asymmetric initial seafloor spreading after continental breakup. *Tectonics*.

Bird, D., Burke, K., et al. (2006). Pangea breakup: Mexico, Gulf of Mexico, and Central Atlantic Ocean. In *2006 SEG Annual Meeting*. Society of Exploration Geophysicists.

Bird, D. E., Burke, K., Hall, S. A., and Casey, J. F. (2005). Gulf of Mexico tectonic history: Hotspot tracks, crustal boundaries, and early salt distribution. *AAPG bulletin*, 89(3):311–328.

Bird, D. E., Burke, K., Hall, S. A., and Casey, J. F. (2011). Tectonic evolution of the Gulf of Mexico Basin. *Gulf of Mexico Origin, Waters, and Biota: Volume 3, Geology*, 3:1.

Bird, D. E., Hall, S. A., Casey, J. F., and Millegan, P. S. (1993). Interpretation of magnetic anomalies over the Grenada Basin. *Tectonics*, 12(5):1267–1279.

Blackburn, T. J., Olsen, P. E., Bowring, S. A., McLean, N. M., Kent, D. V., Puffer, J., McHone, G., Rasbury, E. T., and Et-Touhami, M. (2013). Zircon U-Pb geochronology links the end-Triassic extinction with the Central Atlantic Magmatic Province. *Science*, 340(6135):941–945.

Blakely, R. J. (1983). Statistical averaging of marine magnetic anomalies and the aging of oceanic crust. *Journal of Geophysical Research: Solid Earth*, 88(B3):2289–2296.

Blakely, R. J. (1996). *Potential theory in gravity and magnetic applications*. Cambridge University Press.

Blum, M. D., Milliken, K. T., Pecha, M. A., Snedden, J. W., Frederick, B. C., and Galloway, W. E. (2017). Detrital-zircon records of Cenomanian, Paleocene, and Oligocene Gulf of Mexico drainage integration and sediment routing: Implications for scales of basin-floor fans. *Geosphere*, 13(6):2169–2205.

Bonvalot, S., Balmino, G., Briais, A., Kuhn, M., Peyrefitte, A., Vales, N., Biancale, R., Gabalda, G., Moreaux, G., Reinquin, F., et al. (2012). World Gravity Map, 1:50000000 map. Eds. BGI-CGMW-CNES-IRD.

Boschman, L. M., van Hinsbergen, D. J., Torsvik, T. H., Spakman, W., and Pindell, J. L. (2014). Kinematic reconstruction of the Caribbean region since the Early Jurassic. *Earth-Science Reviews*, 138:102–136.

Bouysse, P. (1984). The Lesser Antilles island-arc-structure and geodynamic evolution. *Initial Reports of the Deep Sea Drilling Project*, 78(AUG):83–103.

Bouysse, P. (1988). Opening of the Grenada back-arc basin and evolution of the Caribbean Plate during the Mesozoic and early Paleogene. *Tectonophysics*, 149(1-2):121–143.

Bouysse, P. (2009). Geological Map of the World. *Commission for the Geological Map of the World*.

Bouysse, P., Pubellier, M., and Garcia, A. (2016). Structural Map of the Caribbean. In *35th International Geological Congress, Cape Town, South Africa*, number 5243 in -.

Bouysse, P., Schmidt-Effing, R., and Westercamp, D. (1983). La Desirade Island (Lesser Antilles) revisited: Lower Cretaceous radiolarian cherts and arguments against an ophiolitic origin for the basal complex. *Geology*, 11(4):244–247.

Bowin, C. O. (1968). Geophysical study of the Cayman Trough. *Journal of Geophysical Research*, 73(16):5159–5173.

Bowland, C. L. (1993). Depositional history of the western Colombian Basin, Caribbean Sea, revealed by seismic stratigraphy. *Geological Society of America Bulletin*, 105(10):1321–1345.

Boynton, C., Westbrook, G., Bott, M., and Long, R. (1979). A seismic refraction investigation of crustal structure beneath the Lesser Antilles island arc. *Geophysical Journal of the Royal Astronomical Society*, 58(2):371–393.

Buffler, R. T. (1984). Early history and structure of the deep Gulf of Mexico basin. In *Characteristics of Gulf Basin Deep-water Sediments and their Exploration Potential, 5th Annual Gulf Coast Research Conference Proceedings, Soc. Econ. Paleontol. Mineral*, pages 31–34.

Buffler, R. T. and Sawyer, D. S. (1985). Distribution of crust and early history, Gulf of Mexico basin. *Gulf Coast Association of Geological Societies Transactions*, 35:333–344.

Bullard, E., Everett, J. E., and Smith, A. G. (1965). The fit of the continents around the Atlantic. *Phil. Trans. R. Soc. Lond. A*, 258(1088):41–51.

Bullard, E. and Mason, R. (1961). The magnetic field astern of a ship. *Deep Sea Research (1953)*, 8(1):20–27.

Burger, H. R., Sheehan, A. F., and Jones, C. H. (2006). *Introduction to applied geophysics: Exploring the shallow subsurface*. WW Norton.

Burke, K. (1988). Tectonic evolution of the Caribbean. *Annual Review of Earth and Planetary Sciences*, 16(1):201–230.

Burke, K., Cooper, C., Dewey, J. F., Mann, P., and Pindell, J. L. (1984). Caribbean tectonics and relative plate motions. *Geological Society of America Memoirs*, 162:31–64.

Calais, E., Stephan, J., Beck, C., Carfantan, J.-C., Tardy, M., Thery, J., Olivet, J., Bouysse, P., Mercier de Lepinay, B., Tournon, J., et al. (1989). Évolution paléogéographique et structurale du domaine caraıbe du lias al'actuel: 14 étapes pour 3 grandes périodes. *CR Acad. Sci. Paris*, 309:1437–1444.

Calais, É., Symithe, S., de Lépinay, B. M., and Prépetit, C. (2016). Plate boundary segmentation in the northeastern Caribbean from geodetic measurements and Neogene geological observations. *Comptes Rendus Geoscience*, 348(1):42–51.

Cande, S. C. and Kent, D. V. (1992). Ultrahigh resolution marine magnetic anomaly profiles: a record of continuous paleointensity variations? *Journal of Geophysical Research: Solid Earth*, 97(B11):15075–15083.

Carey, S. W. (1958). *Continental Drift, a Symposium: Being a Symposium on the Present Status of the Continental Drift Hypothesis, Held in the Geology Department of the University of Tasmania in March, 1956*, volume 2. Geology Department, University of Tasmania.

Carlson, R. and Herrick, C. (1990). Densities and porosities in the oceanic crust and their variations with depth and age. *Journal of Geophysical Research: Solid Earth*, 95(B6):9153–9170.

Cebull, S. and Shurbet, D. (1987). Mexican Volcanic Belt: an intraplate transform. *Geofísica International*, 26:1–14.

Centeno-García, E. (2017). Mesozoic tectono-magmatic evolution of Mexico: An overview. *Ore Geology Reviews*, 81:1035–1052.

Christensen, N. I. and Mooney, W. D. (1995). Seismic velocity structure and composition of the continental crust: A global view. *Journal of Geophysical Research: Solid Earth*, 100(B6):9761–9788.

Christeson, G., Van Avendonk, H., Norton, I., Snedden, J., Eddy, D., Karner, G., and Johnson, C. (2014). Deep crustal structure in the eastern Gulf of Mexico. *Journal of Geophysical Research: Solid Earth*, 119(9):6782–6801.

Christeson, G. L., Mann, P., Escalona, A., and Aitken, T. J. (2008). Crustal structure of the Caribbean–northeastern South America arc-continent collision zone. *Journal of Geophysical Research: Solid Earth*, 113(B8).

Christofferson, E. (1973). Linear magnetic anomalies in the Colombia Basin, central Caribbean Sea. *Geological Society of America Bulletin*, 84(10):3217–3230.

Clark, S. C., Frey, H., and Thomas, H. H. (1985). Satellite magnetic anomalies over subduction zones: the Aleutian Arc anomaly. *Geophysical Research Letters*, 12(1):41–44.

Clifford, G. (2005). Singular Value Decomposition and Independent Component Analysis. *J. Biomedical and Image Processing*.

Clift, P. D., Heinrich, P., Dunn, D., Jacobus, A., and Blusztajn, J. (2018). The Sabine block, Gulf of Mexico: Promontory on the North American margin? *Geology*, 46(1):15–18.

Corbeau, J., Rolandone, F., Leroy, S., de Lépinay, B. M., Meyer, B., Ellouz-Zimmermann, N., and Momplaisir, R. (2016). The northern Caribbean plate boundary in the Jamaica Passage: structure and seismic stratigraphy. *Tectonophysics*, 675:209–226.

Counil, J.-L., Achache, J., and Galdeano, A. (1989). Long-wavelength magnetic anomalies in the Caribbean: Plate boundaries and allochthonous continental blocks. *Journal of Geophysical Research: Solid Earth*, 94(B6):7419–7431.

Cunningham, A. (1998). Neogene evolution of the Pedro Channel carbonate system. *Northern Nicaragua Rise [Ph. D. thesis]: Houston, Texas, Rice University*.

Dallmeyer, R. (1989). Contrasting accreted terranes in the southern Appalachian Orogen, basement beneath the Atlantic and Gulf Coastal Plains, and West African orogens. *Precambrian Research*, 42(3-4):387–409.

DeMets, C., Jansma, P. E., Mattioli, G. S., Dixon, T. H., Farina, F., Bilham, R., Calais, E., and Mann, P. (2000). GPS geodetic constraints on Caribbean-North America plate motion. *Geophysical Research Letters*, 27(3):437–440.

Dickinson, W. R. (2009). The Gulf of Mexico and the southern margin of Laurentia. *Geology*, 37(5):479–480.

Dickinson, W. R. and Lawton, T. F. (2001). Carboniferous to Cretaceous assembly and fragmentation of Mexico. *Geological Society of America Bulletin*, 113(9):1142–1160.

Diebold, J. (2009). Submarine volcanic stratigraphy and the Caribbean LIP's formational environment. *Geological Society, London, Special Publications*, 328(1):799–808.

Diebold, J., Driscoll, N., et al. (1999). New insights on the formation of the Caribbean basalt province revealed by multichannel seismic images of volcanic structures in the Venezuelan Basin. *Sedimentary Basins of the World*, 4:561–589.

Diebold, J., Stoffa, P., Buhl, P., and Truchan, M. (1981). Venezuela Basin crustal structure. *Journal of Geophysical Research: Solid Earth*, 86:7901–7923.

Diegel, F. A., Karlo, J., Schuster, D., Shoup, R., and Tauvers, P. (1995). Cenozoic structural evolution and tectono-stratigraphic framework of the northern Gulf Coast continental margin.

Dillon, W. P., Vedder, J., and Graf, R. (1972). Structural profile of the northwestern Caribbean. *Earth and Planetary Science Letters*, 17(1):175–180.

Dillon, W. P. and Vedder, J. G. (1973). Structure and development of the continental margin of British Honduras. *Geological Society of America Bulletin*, 84(8):2713–2732.

Donnelly, T. W. (1973). Magnetic anomaly observations in the Eastern Caribbean sea. *Initial reports, Deep Sea Drilling Project*, 15(33).

Duncan, R. and Hargraves, R. (1984). Plate-tectonic evolution of the Caribbean region in the mantle reference frame. *The Caribbean-South American plate boundary and regional tectonics*.

Dyment, J. and Arkani-Hamed, J. (1995). Spreading-rate-dependent magnetization of the oceanic lithosphere inferred from the anomalous skewness of marine magnetic anomalies. *Geophysical Journal International*, 121(3):789–804.

Dyment, J., Lesur, V., Choi, Y., Hamoudi, M., Thébault, E., and Catalan, M. (2015a). Release of the World Digital Magnetic Anomaly Map version 2 (WDMAM v2) scheduled. In *EGU General Assembly Conference Abstracts*, volume 17, page 15430.

Dyment, J., Lesur, V., Hamoudi, M., Choi, Y., Thebault, E., Catalan, M., the WDMAM Task Force*, the WDMAM Evaluators**, and the WDMAM Data Providers** (2015b). World Digital Magnetic Anomaly Map version 2.0. `http://www.wdmam.org`.

Eagles, G., Pérez-Díaz, L., and Scarselli, N. (2015). Getting over continent ocean boundaries. *Earth-Science Reviews*, 151:244–265.

Eddy, D. R., Van Avendonk, H. J., Christeson, G. L., and Norton, I. O. (2018). Structure and origin of the rifted margin of the northern Gulf of Mexico. *Geosphere*.

Eddy, D. R., Van Avendonk, H. J., Christeson, G. L., Norton, I. O., Karner, G. D., Johnson, C. A., and Snedden, J. W. (2014). Deep crustal structure of the northeastern Gulf of Mexico: Implications for rift evolution and seafloor spreading. *Journal of Geophysical Research: Solid Earth*, 119(9):6802–6822.

Edgar, N. T. (1973). Site 148. *Initial Reports of the Deep Sea Drilling Project*, 15:217. Affiliation (analytic): Scripps Inst. Oceanogr., Deep Sea Drilling Project, La Jolla, CA.

Edgar, N. T., Ewing, J. I., and Hennion, J. (1971). Seismic refraction and reflection in Caribbean Sea. *AAPG Bulletin*, 55(6):833–870.

Escalona, A. and Mann, P. (2011). Tectonics, basin subsidence mechanisms, and paleogeography of the Caribbean-South American plate boundary zone. *Marine and Petroleum Geology*, 28(1):8–39.

Ewing, J., Antoine, J., and Ewing, M. (1960). Geophysical measurements in the western Caribbean Sea and in the Gulf of Mexico. *Journal of Geophysical Research*, 65(12):4087–4126.

Farnetani, C. G., Richards, M. A., and Ghiorso, M. S. (1996). Petrological models of magma evolution and deep crustal structure beneath hotspots and flood basalt provinces. *Earth and Planetary Science Letters*, 143(1-4):81–94.

Ferré, E. C., Friedman, S. A., Martín-Hernández, F., Feinberg, J. M., Till, J. L., Ionov, D. A., and Conder, J. A. (2014). Eight good reasons why the uppermost mantle could be magnetic. *Tectonophysics*, 624:3–14.

Feuillet, N., Manighetti, I., Tapponnier, P., and Jacques, E. (2002). Arc parallel extension and localization of volcanic complexes in Guadeloupe, Lesser Antilles. *Journal of Geophysical Research: Solid Earth*, 107(B12).

Finlay, C., Maus, S., Beggan, C., Bondar, T., Chambodut, A., Chernova, T., Chulliat, A., Golovkov, V., Hamilton, B., Hamoudi, M., et al. (2010). International geomagnetic reference field: the eleventh generation. *Geophysical Journal International*, 183(3):1216–1230.

Fort, X. and Brun, J.-P. (2012). Kinematics of regional salt flow in the northern Gulf of Mexico. *Geological Society, London, Special Publications*, 363(1):265–287.

Fort, X., Brun, J.-P., and Chauvel, F. (2004). Salt tectonics on the Angolan margin, synsedimentary deformation processes. *AAPG bulletin*, 88(11):1523–1544.

Fox, P. J. and Heezen, B. C. (1975). Geology of the Caribbean crust. In *The Gulf of Mexico and the Caribbean*, pages 421–466. Springer.

Friedman, S. A. (2015). *Investigation of the upper mantle as a source for contribution to magnetic anomalies*. Southern Illinois University at Carbondale.

Friis-Christensen, E., Lühr, H., and Hulot, G. (2006). Swarm: A constellation to study the Earth's magnetic field. *Earth, planets and space*, 58(4):351–358.

Fritsch, F. N. and Carlson, R. E. (1980). Monotone piecewise cubic interpolation. *SIAM Journal on Numerical Analysis*, 17(2):238–246.

Galloway, W. E. (2008). Depositional evolution of the Gulf of Mexico sedimentary basin. *Sedimentary basins of the world*, 5:505–549.

García-Reyes, A. (2009). Mapas de anomalías de gravedad y magnetismo de Venezuela generados a partir de datos satelitales. *Dissertation. Universidad Central de Venezuela, Caracas*, 175:191.

Garcia-Reyes, A., Dyment, J., and Thebault, E. (2017). Insights on the Understanding of the Circum-Caribbean Region from Potential Field Data. In *AGU Fall Meeting Abstracts*.

Garza, R. S. M. (2005). Paleomagnetic reconstruction of Coahuila, Mexico: the Late Triassic Acatita intrusives. *Geofísica Internacional*, 44(2):197–210.

Gee, J. S. and Kent, D. V. (2007). Source of oceanic magnetic anomalies and the geomagnetic polarity time scale. *Treatise on Geophysics, Vol. 5: Geomagnetism*, pages 455–507.

Ghosh, N., Hall, S., and Casey, J. (1984). Seafloor spreading magnetic anomalies in the Venezuelan Basin. *Geological Society of America Memoirs*, 162:65–80.

Giunta, G., Beccaluva, L., Coltorti, M., Siena, F., and Vaccaro, C. (1997). Ophiolitic units of the southern margin of Caribbean plate in Venezuela: a reappraisal of their petrogenesis and original tectonic setting. In *Memorias del VIII Congreso Geologico Venezolano Porlamar*, volume 1, pages 331–337.

Giunta, G. and Orioli, S. (2011). The Caribbean plate evolution: trying to resolve a very complicated tectonic puzzle. In *New Frontiers in Tectonic Research-General Problems, Sedimentary Basins and Island Arcs*. InTech.

Golynsky, A., Chiappini, M., Damaske, D., Ferraccioli, F., Ferris, J., Finn, C., Ghidella, M., Isihara, T., Johnson, A., Kim, H., et al. (2001). ADMAP–Magnetic Anomaly Map of the Antarctic, 1: 10 000 000 scale map. *BAS (Misc.)*, 10:1109–1112.

Gradstein, F. and Ogg, J. (1996). Geological time scale for the Phanerozoic. *Episodes*, 19(1–2):3–5.

Granja-Bruña, J., Carbó-Gorosabel, A., Estrada, P. L., Muñoz-Martín, A., Ten Brink, U., Ballesteros, M. G., Druet, M., and Pazos, A. (2014). Morphostructure at the junction between the Beata ridge and the Greater Antilles island arc (offshore Hispaniola southern slope). *Tectonophysics*, 618:138–163.

Granot, R., Dyment, J., and Gallet, Y. (2012). Geomagnetic field variability during the Cretaceous Normal Superchron. *Nature Geoscience*, 5(3):220–223.

Guevara, N. O., García, A., and Arnaiz, M. (2013). Magnetic anomalies in the Eastern Caribbean. *International Journal of Earth Sciences*, 102(3):591–604.

Hall, D., Cavanaugh, T., Watkins, J., and McMillen, K. (1982). The rotational origin of the Gulf of Mexico based on regional gravity data. *Studies in continental margin geology: AAPG Memoir*, 34:115–126.

Hall, S. (2002). The role of autochthonous salt inflation and deflation in the northern Gulf of Mexico. *Marine and Petroleum Geology*, 19(6):649–682.

Hall, S. A. and Najmuddin, I. J. (1994). Constraints on the tectonic development of the eastern Gulf of Mexico provided by magnetic anomaly data. *Journal of Geophysical Research: Solid Earth*, 99(B4):7161–7175.

Hamid, N., Liu, H., Uozumi, T., Yoshikawa, A., and Annadurai, N. (2017). Peak time of equatorial electrojet from different longitude sectors during fall solar minimum. In *Journal of Physics: Conference Series*, number 1 in 852. IOP Publishing.

Hamid, N. S. A., Liu, H., Uozumi, T., Yumoto, K., Veenadhari, B., Yoshikawa, A., and Sanchez, J. A. (2014). Relationship between the equatorial electrojet and global Sq currents at the dip equator region. *Earth, Planets and Space*, 66(1):146.

Hastie, A. R. (2007). *Tectonomagmatic evolution of the Caribbean plate: Insights from igneous rocks on Jamaica*. Cardiff University (United Kingdom).

Heatherington, A. and Mueller, P. (2003). Mesozoic igneous activity in the Suwannee terrane, southeastern USA: petrogenesis and Gondwanan affinities. *Gondwana Research*, 6(2):296–311.

Hellinger, S. J. (1979). *The statistics of finite rotations in plate tectonics*. PhD thesis, Massachusetts Institute of Technology.

Hemant, K., Thébault, E., Mandea, M., Ravat, D., and Maus, S. (2007). Magnetic anomaly map of the world: merging satellite, airborne, marine and ground-based magnetic data sets. *Earth and Planetary Science Letters*, 260(1-2):56–71.

Herrero O., E. and Navarro, J. (1989). Mapa de anomalías magnéticas de Venezuela. *Direccion de Geologia*.

Heubeck, C. and Mann, P. (1991). Geologic evaluation of plate kinematic models for the North American-Caribbean plate boundary zone. *Tectonophysics*, 191(1-2):1–26.

Hey, R. (1977). Tectonic evolution of the Cocos-Nazca spreading center. *Geological Society of America Bulletin*, 88(12):i–vi.

Hinze, W. J., Von Frese, R. R., and Saad, A. H. (2013). *Gravity and magnetic exploration: Principles, practices, and applications*. Cambridge University Press.

Holcombe, T. L., Ladd, J. W., Westbrook, G., Edgar, N. T., and Bowland, C. L. (1990). Caribbean marine geology; ridges and basins of the plate interior. *The Caribbean Region, The Geology of North America, vol. H, Geological Society of America*, pages 231–260.

Horner-Johnson, B. C. and Gordon, R. G. (2003). Equatorial Pacific magnetic anomalies identified from vector aeromagnetic data. *Geophysical Journal International*, 155(2):547–556.

Houtz, R. E. and Ludwig, W. J. (1977). Structure of Colombia Basin, Caribbean Sea, from profiler-sonobuoy measurements. *Journal of Geophysical Research*, 82(30):4861–4867.

Hudec, M. R., Norton, I. O., Jackson, M. P., and Peel, F. J. (2013). Jurassic evolution of the Gulf of Mexico salt basinGulf of Mexico Jurassic Evolution. *AAPG bulletin*, 97(10):1683–1710.

Hulot, G., Eymin, C., Langlais, B., Mandea, M., and Olsen, N. (2002). Small-scale structure of the geodynamo inferred from Oersted and Magsat satellite data. *Nature*, 416(6881):620–623.

Hunt, C. P., Moskowitz, B. M., and Banerjee, S. K. (1995). Magnetic properties of rocks and minerals. *Rock physics & phase relations: a handbook of physical constants*, pages 189–204.

Ibrahim, A., Carye, J., Latham, G., and Buffler, R. (1981). Crustal structure in Gulf of Mexico from OBS refraction and multichannel reflection data. *AAPG Bulletin*, 65(7):1207–1229.

Intermagnet (2017). International Real-time Magnetic Observatory Network. `http://intermagnet.org`. Accessed: January 23, 2017.

Ishihara, T. (2015). A new leveling method without the direct use of crossover data and its application in marine magnetic surveys: weighted spatial averaging and temporal filtering. *Earth, Planets and Space*, 67(1):1–14.

Iturralde-Vinent, M., García-Casco, A., Rojas-Agramonte, Y., Proenza, J., Murphy, J., and Stern, R. (2016). The geology of Cuba: A brief overview and synthesis. *GSA Today*, 26(10):4–10.

Jones, N. W., McKee, J. W., Márquez D, B., Tovar, J., Long, L. E., and Laudon, T. S. (1984). The Mesozoic La Mula Island, Coahuila, Mexico. *Geological Society of America Bulletin*, 95(10):1226–1241.

Kent, D. V. and Gradstein, F. M. (1986). A Jurassic to recent chronology. *The Geology of North America*, 1000:45–50.

Keppie, D. F. and Keppie, J. D. (2012). An alternative Pangea reconstruction for Middle America with the Chortis Block in the Gulf of Mexico: tectonic implications. *International Geology Review*, 54(14):1685–1696.

Keppie, D. F. and Keppie, J. D. (2014). The Yucatan, a Laurentian or Gondwanan fragment? Geophysical and palinspastic constraints. *International Journal of Earth Sciences*, 103(5):1501–1512.

Keppie, F. (2013). The Rationale and Essential Elements for the New 'Pirate'Model of Caribbean Tectonics. *Geoscience Canada*, 40(1).

Kerr, A. C., Iturralde-Vinent, M. A., Saunders, A. D., Babbs, T. L., and Tarney, J. (1999). A new plate tectonic model of the Caribbean: Implications from a geochemical reconnaissance of Cuban Mesozoic volcanic rocks. *Geological Society of America Bulletin*, 111(11):1581–1599.

Kerr, A. C., Marriner, G., Tarney, J., Nivia, A., Saunders, A., Thirlwall, M., and Sinton, C. (1997a). Cretaceous Basaltic Terranes in western Columbia: elemental, chronological and Sr–Nd isotopic constraints on petrogenesis. *Journal of petrology*, 38(6):677–702.

Kerr, A. C., Tarney, J., Marriner, G. F., Nivia, A., and Saunders, A. D. (1997b). The Caribbean-Colombian Cretaceous igneous province: the internal anatomy of an oceanic plateau. *Large igneous provinces: Continental, oceanic, and planetary flood volcanism*, pages 123–144.

Kerr, A. C., White, R. V., and Saunders, A. D. (2000). LIP reading: recognizing oceanic plateaux in the geological record. *Journal of Petrology*, 41(7):1041–1056.

Kim, Y., Clayton, R. W., and Keppie, F. (2011). Evidence of a collision between the Yucatán Block and Mexico in the Miocene. *Geophysical Journal International*, 187(2):989–1000.

Kneller, E. A. and Johnson, C. A. (2011). Plate kinematics of the Gulf of Mexico based on integrated observations from the Central and South Atlantic.

Krawl, K. A. (2014). *A petrogenetic model for the Caribbean Large Igneous Province*. PhD thesis, Oregon State University.

Kring, D. A., Claeys, P., Gulick, S. P., Morgan, J. V., and Collins, G. S. (2017). Chicxulub and the exploration of large peak-ring impact craters through scientific drilling.

Ladd, J. W. and Watkins, J. S. (1980). Seismic stratigraphy of the western Venezuela Basin. *Marine Geology*, 35(1-3):21–41.

Ladd, J. W., Westbrook, G. K., Buhl, P., and Bangs, N. (1990). Wide aperture seismic reflection profiles across Barbados ridge complex. *Proceedings of the Ocean Drilling program, Scientific resutls*, 110.

Lawton, T. F. and Amato, J. M. (2017). U-Pb ages of igneous xenoliths in a salt diapir, La Popa basin: Implications for salt age in onshore Mexico salt basins. *Lithosphere*, 9(5):745–758.

Lawton, T. F., Vega, F. J., Giles, K. A., and Rosales-Domnguez, C. (2001). AAPG Memoir 75, Chapter 9: Stratigraphy and Origin of the La Popa Basin, Nuevo Len and Coahuila, Mexico.

Legendre, A. M. (1852). *Elements of geometry and trigonometry*.

Legendre, C. (2003). *Pétrogenèse de laves différenciées en contexte intraplaque océanique et hétérogénéité géochimique au niveau du point chaud des Marquises (Polynésie française): étude des îles de Ua Pou et de Nuku Hiva*. PhD thesis, Université de Bretagne occidentale-Brest.

Leliak, P. (1961). Identification and evaluation of magnetic-field sources of magnetic airborne detector equipped aircraft. *IRE Transactions on Aerospace and Navigational Electronics*, 3(ANE-8):95–105.

Leroy, S. and Mauffret, A. (1996). Intraplate deformation in the Caribbean region. *Journal of Geodynamics*, 21(1):113–122.

Leroy, S., Mauffret, A., Patriat, P., and de Lépinay, B. M. (2000). An alternative interpretation of the Cayman trough evolution from a reidentification of magnetic anomalies. *Geophysical Journal International*, 141(3):539–557.

Lesur, V., Hamoudi, M., Choi, Y., Dyment, J., and Thébault, E. (2016). Building the second version of the World Digital Magnetic Anomaly Map (WDMAM). *Earth, Planets and Space*, 68(1):1–13.

Lesur, V., Rother, M., Vervelidou, F., Hamoudi, M., and Thébault, E. (2013). Post-processing scheme for modelling the lithospheric magnetic field. *Solid Earth*, 4(1):105.

López-Martínez, R., Barragán, R., Bernal, J. P., Reháková, D., Gómez-Tuena, A., Martini, M., and Ortega, C. (2017). Integrated stratigraphy and isotopic ages at the Berriasian–Valanginian boundary at Tlatlauquitepec (Puebla, Mexico). *Journal of South American Earth Sciences*, 75:1–10.

Lu, R. and McMillen, K. (1982). Multichannel seismic survey of the Colombia Basin and adjacent margins. In *Studies in Continental Margin Geology*, volume 34, pages 395–410. American Association of Petroleum Geologists Tulsa, Okla.

Lugo, J. and Mann, P. (1995). Jurassic-Eocene tectonic evolution of Maracaibo basin, Venezuela.

Lundin, E. and Doré, A. (2017). The Gulf of Mexico and Canada Basin: Genetic Siblings on Either Side of North America. *GSA Today*, 27(1):4–11.

Luyendyk, A. (1997). Processing of airborne magnetic data. *AGSO Journal of Australian Geology and Geophysics*, 17:31–38.

Mann, P., Escalona, A., and Castillo, M. V. (2006). Regional geologic and tectonic setting of the Maracaibo supergiant basin, western Venezuela. *AAPG bulletin*, 90(4):445–477.

Mann, P., Taylor, F., Edwards, R. L., and Ku, T.-L. (1995). Actively evolving microplate formation by oblique collision and sideways motion along strike-slip faults: An example from the northeastern Caribbean plate margin. *Tectonophysics*, 246(1):1–69.

Martens, U., Weber, B., and Valencia, V. A. (2010). U/Pb geochronology of Devonian and older Paleozoic beds in the southeastern Maya block, Central America: Its affinity with peri-Gondwanan terranes. *Bulletin*, 122(5-6):815–829.

Marton, G. and Buffler, R. (2016). Jurassic-Cretaceous Tectonic Evolution of the Southeastern Gulf of Mexico, Constrains on the Style and Timing of Gulf of Mexico Rift-Drift Development. In *AAPG/SEG International Conference & Exhibition*.

Marton, G. and Buffler, R. T. (1994). Jurassic reconstruction of the Gulf of Mexico Basin. *International Geology Review*, 36(6):545–586.

Marzoli, A., Renne, P. R., Piccirillo, E. M., Ernesto, M., Bellieni, G., and De Min, A. (1999). Extensive 200-million-year-old continental flood basalts of the Central Atlantic Magmatic Province. *Science*, 284(5414):616–618.

Mauffret, A. and Leroy, S. (1997). Seismic stratigraphy and structure of the Caribbean igneous province. *Tectonophysics*, 283(1):61–104.

Mauffret, A., Leroy, S., d'Acremont, E., Maillard, A., de Lepinay, B. M., Dos Reis, A. T., Miller, N., Nercessian, A., Perez-Vega, R., and Perez, D. (2001a). Une coupe de la province volcanique Caraibe: premiers resultats de la campagne sismique Casis 2. *Comptes Rendus de l'Academie des Sciences-Series IIA-Earth and Planetary Science*, 333(10):659–667.

Mauffret, A., Leroy, S., Vila, J.-M., Hallot, E., De Lépinay, B. M., and Duncan, R. A. (2001b). Prolonged magmatic and tectonic development of the Caribbean Igneous Province revealed by a diving submersible survey. *Marine Geophysical Researches*, 22(1):17–45.

Maus, S. (2008). The geomagnetic power spectrum. *Geophysical Journal International*, 174(1):135–142.

Maus, S. (2010). Magnetic field model MF7.

MENEVEN (1983). Aeromagnetic survey 1981-1982, Contract CAR-62. Technical Report 1, GEOTERREX LTD and CGG. 199pp.

Mercier de Lepinay, B., Mauffret, A., Jany, I., Bouysse, P., Mascle, A., Renard, V., Stéphan, J.-F., and Hernández, E. (1988). Une collision oblique sur la bordure nord-caraïbe à la jonction entre la ride de Beata et la fosse de Muertos. *Comptes rendus de l'Académie des sciences. Série 2, Mécanique, Physique, Chimie, Sciences de l'univers, Sciences de la Terre*, 307(10):1289–1296.

Meschede, M. and Frisch, W. (1998). A plate-tectonic model for the Mesozoic and Early Cenozoic history of the Caribbean plate. *Tectonophysics*, 296(3):269–291.

Morgan, W. J. (1968). Rises, trenches, great faults, and crustal blocks. *Journal of Geophysical Research*, 73(6):1959–1982.

Moy, C. and Traverse, A. (1986). Palynostratigraphy of the subsurface eagle mills formation (Triassic) from a well in east-central texas, USA. *Palynology*, 10(1):225–234.

Mueller, P. A., Heatherington, A. L., Foster, D. A., Thomas, W. A., and Wooden, J. L. (2014). The Suwannee suture: Significance for Gondwana-Laurentia terrane transfer and formation of Pangaea. *Gondwana Research*, 26(1):365–373.

Müller, R. D., Royer, J.-Y., Cande, S. C., Roest, W. R., and Maschenkov, S. (1999). New constraints on the Late Cretaceous/Tertiary plate tectonic evolution of the Caribbean. In *Sedimentary basins of the world*, volume 4, pages 33–59. Elsevier.

Neill, I., Kerr, A. C., Hastie, A. R., Stanek, K.-P., and Millar, I. L. (2011). Origin of the Aves Ridge and Dutch–Venezuelan Antilles: interaction of the Cretaceous 'Great Arc'and Caribbean–Colombian Oceanic Plateau? *Journal of the Geological Society*, 168(2):333–348.

Nerlich, R., Clark, S. R., and Bunge, H.-P. (2014). Reconstructing the link between the Galapagos hotspot and the Caribbean Plateau. *GeoResJ*, 1:1–7.

Nguyen, L. and Mann, P. (2016). Quantitative restoration the Gulf of Mexico continental margins based on a newly-derived, basin-wide, crustal thickness map. In *AGU Fall Meeting Abstracts*.

Núñez, D., Córdoba, D., Cotilla, M. O., and Pazos, A. (2016). Modeling the Crust and Upper Mantle in Northern Beata Ridge (CARIBE NORTE Project). *Pure and Applied Geophysics*, 173(5):1639–1661.

Officer, C., Ewing, J., Edwards, R., and Johnson, H. (1957). Geophysical investigations in the eastern Caribbean: Venezuelan basin, Antilles island arc, and Puerto Rico trench. *Geological Society of America Bulletin*, 68(3):359–378.

Olsen, N., Lühr, H., Sabaka, T. J., Mandea, M., Rother, M., Tøffner-Clausen, L., and Choi, S. (2006). CHAOS—a model of the Earth's magnetic field derived from CHAMP, Ørsted, and SAC-C magnetic satellite data. *Geophysical Journal International*, 166(1):67–75.

Olsen, N., Ravat, D., Finlay, C. C., and Kother, L. K. (2017). LCS-1: A high-resolution global model of the lithospheric magnetic field derived from CHAMP and Swarm satellite observations. *Geophysical Journal International*, 211(3):1461–1477.

Olsen, P., Schlische, R., and Fedosh, M. (1996). 580 ky duration of the Early Jurassic flood basalt event in eastern North America estimated using Milankovitch cyclostratigraphy. *The continental Jurassic: Museum of Northern Arizona Bulletin*, 60:11–22.

Olsen, P. E. (1997). Stratigraphic record of the early Mesozoic breakup of Pangea in the Laurasia-Gondwana rift system. *Annual Review of Earth and Planetary Sciences*, 25(1):337–401.

Orihuela Guevara, N., Tabare, T., et al. (2011). Mapas de gravedad y anomalía gravimétrica de venezuela derivados de datos satelitales. *Revista de la Facultad de Ingeniería Universidad Central de Venezuela*, 26(1):51–58.

Pearson, K. (1901). LIII. On lines and planes of closest fit to systems of points in space. *The London, Edinburgh, and Dublin Philosophical Magazine and Journal of Science*, 2(11):559–572.

Peel, F., Travis, C., and Hossack, J. (1995). Genetic structural provinces and salt tectonics of the Cenozoic offshore US Gulf of Mexico: A preliminary analysis.

Pérez-Díaz, L. and Eagles, G. (2014). Constraining South Atlantic growth with seafloor spreading data. *Tectonics*, 33(9):1848–1873.

Pérez-Díaz, L. and Eagles, G. (2017). South Atlantic paleobathymetry since early Cretaceous. *Scientific reports*, 7(1):11819.

Pindell, J. (1991). Geological arguments suggesting a Pacific origin for the Caribbean Plate. In *Transactions 12th Caribbean Geological Conference St Croix*.

Pindell, J. and Dewey, J. F. (1982). Permo-Triassic reconstruction of western Pangea and the evolution of the Gulf of Mexico/Caribbean region. *Tectonics*, 1(2):179–211.

Pindell, J., Kennan, L., Maresch, W. V., Stanek, K.-P., Draper, G., and Higgs, R. (2005). Plate-kinematics and crustal dynamics of circum-Caribbean arc-continent interactions: Tectonic controls on basin development in Proto-Caribbean margins. *Geological Society of America Special Papers*, 394:7–52.

Pindell, J., Miranda, C., Ceron, A., and Hernandez, L. (2016). Aeromagnetic map constrains Jurassic–Early Cretaceous synrift, break up, and rotational seafloor spreading history in the Gulf of Mexico. In *Mesozoic of the Gulf Rim and Beyond: New Progress in Science and Exploration of the Gulf of Mexico Basin. 35th Annual Gulf Coast Section SEPM Foundation Perkins-Rosen Research Conference, GCSSEPM Foundation, Houston, TX, USA*, pages 123–153.

Pindell, J. L. (1985). Alleghenian reconstruction and subsequent evolution of the Gulf of Mexico, Bahamas, and proto-Caribbean. *Tectonics*, 4(1):1–39.

Pindell, J. L. (1994). Evolution of the Gulf of Mexico and the Caribbean. *Caribbean geology: an introduction*, pages 13–39.

Pindell, J. L. and Barrett, S. F. (1990). Geological evolution of the Caribbean region: a plate tectonic perspective. *The Caribbean region: Boulder, Colorado, Geological Society of America, Geology of North America, v. H*, pages 405–432.

Pindell, J. L. and Kennan, L. (2009). Tectonic evolution of the Gulf of Mexico, Caribbean and northern South America in the mantle reference frame: an update. *Geological Society, London, Special Publications*, 328(1):1–55.

Pubellier, M., Mauffret, A., Leroy, S., Vila, J. M., and Amilcar, H. (2000). Plate boundary readjustment in oblique convergence: Example of the Neogene of Hispaniola, Greater Antilles. *Tectonics*, 19(4):630–648.

Purucker, M. and Whaler, K. (2007). Crustal magnetism. *Treatise on geophysics*, 5:195–237.

Purucker, M. E. and Dyment, J. (2000). Satellite magnetic anomalies related to seafloor spreading in the South Atlantic Ocean. *Geophysical research letters*, 27(17):2765–2768.

Quesnel, Y., Catalán, M., and Ishihara, T. (2009). A new global marine magnetic anomaly data set. *Journal of Geophysical Research: Solid Earth*, 114(B4).

Reeves, C. (2005). Aeromagnetic surveys: principles, practice and interpretation. *Published by Geosoft*, page 155.

Reigber, C., Schwintzer, P., and Lühr, H. (1999). The CHAMP geopotential mission. *Boll. Geof. Teor. Appl*, 40:285–289.

Révillon, S., Hallot, E., Arndt, N., Chauvel, C., and Duncan, R. (2000). A complex history for the Caribbean Plateau: petrology, geochemistry, and geochronology of the Beata Ridge, South Hispaniola. *The Journal of Geology*, 108(6):641–661.

Rodriguez Millan, I. (2014). *Gravity Anomalies, Geodynamic Modelling and the Eastern Venezuela Basin Evolution.* PhD thesis, Durham University.

Rosencrantz, E. (1990). Structure and tectonics of the Yucatan Basin, Caribbean Sea, as determined from seismic reflection studies. *Tectonics*, 9(5):1037–1059.

Rosencrantz, E. (1996). Basement structure and tectonics in the Yucatan basin. *Ofiolitas y Arcos Volcánicos de Cuba. Miami, USA, IGCP Project*, 364:36–47.

Rosencrantz, E., Ross, M. I., and Sclater, J. G. (1988). Age and spreading history of the Cayman Trough as determined from depth, heat flow, and magnetic anomalies. *Journal of Geophysical Research: Solid Earth*, 93(B3):2141–2157.

Ross, M. I. and Scotese, C. R. (1988). A hierarchical tectonic model of the Gulf of Mexico and Caribbean region. *Tectonophysics*, 155(1-4):139–168.

Roth, J. M., Droxler, A. W., Kameo, K., et al. (2000). The Caribbean carbonate crash at the middle to late Miocene transition: linkage to the establishment of the modern global ocean conveyor. In *Proceedings of the Ocean Drilling Program, Scientific Results*, volume 165, pages 249–273. Ocean Drilling Program College Station, TX.

Rowan, M. (2014). Passive-margin salt basins: hyperextension, evaporite deposition, and salt tectonics. *Basin Research*, 26(1):154–182.

Royer, J., Sclater, J., Sandwell, D., Cande, S., Schlich, R., Munschy, M., Dyment, J., Fisher, R., Müller, R., Coffin, M., et al. (1992). Indian Ocean plate reconstructions since the Late Jurassic. *Synthesis of Results From Scientific Drilling in the Indian Ocean, Geophys. Monogr. Ser*, 70:471–475.

Sabaka, T. J., Olsen, N., and Purucker, M. E. (2004). Extending comprehensive models of the Earth's magnetic field with Ørsted and CHAMP data. *Geophysical Journal International*, 159(2):521–547.

Sahabi, M., Aslanian, D., and Olivet, J.-L. (2004). Un nouveau point de départ pour l'histoire de l'Atlantique central. *Comptes Rendus Geoscience*, 336(12):1041–1052.

Salvador, A. (1987). Late Triassic-Jurassic paleogeography and origin of Gulf of Mexico basin. *AAPG Bulletin*, 71(4):419–451.

Salvador, A. (1991). Origin and development of the Gulf of Mexico basin. *The gulf of Mexico basin*, pages 389–444.

Sandwell, D. T., Müller, R. D., Smith, W. H., Garcia, E., and Francis, R. (2014). New global marine gravity model from CryoSat-2 and Jason-1 reveals buried tectonic structure. *Science*, 346(6205):65–67.

Sawyer, D. S., Buffler, R. T., and Pilger Jr, R. H. (1991). The crust under the Gulf of Mexico Basin. *The Gulf of Mexico Basin: Geological Society of America, The Geology of North America, v. J*, pages 53–72.

Schlaphorst, D., Kendall, J.-M., Baptie, B., Latchman, J. L., and Tait, S. (2017). Gaps, tears and seismic anisotropy around the subducting slabs of the Antilles. *Tectonophysics*, 698:65–78.

Schnetzler, C. (1985). An estimation of continental crust magnetization and susceptibility from Magsat data for the conterminous United States. *Journal of Geophysical Research: Solid Earth*, 90(B3):2617–2620.

Schouten, H. and Klitgord, K. D. (1994). Mechanistic solutions to the opening of the Gulf of Mexico. *Geology*, 22(6):507–510.

Schwindrofska, A., Hoernle, K., van den Bogaard, P., Hauff, F., and Werner, R. (2016). Submarine structures of the Caribbean Large Igneous Province: Age and Geochemistry of the Beata Ridge and Hess Escarpment. In *2nd European Minerogical Conference, Rimini, Italy*.

Sclater, J. G., Anderson, R. N., and Bell, M. L. (1971). Elevation of ridges and evolution of the central eastern Pacific. *Journal of Geophysical Research*, 76(32):7888–7915.

Seton, M., Müller, R., Zahirovic, S., Gaina, C., Torsvik, T., Shephard, G., Talsma, A., Gurnis, M., Turner, M., Maus, S., et al. (2012). Global continental and ocean basin reconstructions since 200 Ma. *Earth-Science Reviews*, 113(3-4):212–270.

Seton, M., Whittaker, J. M., Wessel, P., Müller, R. D., DeMets, C., Merkouriev, S., Cande, S., Gaina, C., Eagles, G., Granot, R., et al. (2014). Community infrastructure and repository for marine magnetic identifications. *Geochemistry, Geophysics, Geosystems*, 15(4):1629–1641.

Sigurdsson, H., Leckie, R., Acton, G., and et al (1997). *Proceedings of the Ocean Drilling Program. A.: Initial Reports: Vol. 165*. Ocean Drilling Program, Texas A&M University.

Sinton, C. W., Duncan, R., Storey, M., Lewis, J., and Estrada, J. (1998). An oceanic flood basalt province within the Caribbean plate. *Earth and Planetary Science Letters*, 155(3):221–235.

Sinton, C. W., Sigurdsson, H., and Duncan, R. A. (2000). Major element oxides and 40Ar/39Ar plateau and isochron ages of ODP Hole 165-1001A. *Proceedings of the Ocean Drilling Program, Scientific Results, College Station, TX*, 165:1–4.

Steiner, M. B. and Anderson, T. (2005). Pangean reconstruction of the Yucatan Block: Its Permian, Triassic, and Jurassic geologic and tectonic history. *SPECIAL PAPERS-GEOLOGICAL SOCIETY OF AMERICA*, 393:457.

Stéphan, J., Mercier de Lepinay, B., Calais, E., Tardy, M., Beck, C., Carfantan, J.-C., Olivet, J., Vila, J., Bouysse, P., Mauffret, A., et al. (1990). Paleogeodynamic maps of the Caribbean: 14 steps from Lias to Present. *Bull. Soc. Géol. Fr.*, 6(8):6–919.

Stephens, B. P. (2009). Basement controls on subsurface geologic patterns and coastal geomorphology across the northern Gulf of Mexico: Implications for subsidence studies

and coastal restoration. *Gulf Coast Association of Geological Societies Transactions*, 59(1):729–751.

Stern, R. J. and Dickinson, W. R. (2010). The Gulf of Mexico is a Jurassic backarc basin. *Geosphere*, 6(6):739–754.

Symithe, S., Calais, E., Chabalier, J., Robertson, R., and Higgins, M. (2015). Current block motions and strain accumulation on active faults in the Caribbean. *Journal of Geophysical Research: Solid Earth*, 120(5):3748–3774.

Tabare, T. and Orihuela Guevara, N. (2013). Estudio geofísico integrado del macizo ígneo-metamórfico de El Baúl, región central de Venezuela. *Revista Venezolana de Ciencias de La Tierra GEOS*, 45(1):171. ISSN: 0435-5601.

Talwani, M. (1964). Computation of magnetic anomalies caused by two-dimensional bodies of arbitrary shape. *Computers in the mineral industries*, 1:464–480.

ten Brink, U. S., Coleman, D. F., and Dillon, W. P. (2002). The nature of the crust under Cayman Trough from gravity. *Marine and Petroleum Geology*, 19(8):971–987.

Thébault, E., Lesur, V., Kauristie, K., and Shore, R. (2017). Magnetic field data correction in space for modelling the lithospheric magnetic field. *Space Science Reviews*, 206(1-4):191–223.

Thébault, E., Purucker, M., Whaler, K. A., Langlais, B., and Sabaka, T. J. (2010). The magnetic field of the Earth's lithosphere. *Space Science Reviews*, 155(1-4):95–127.

Thébault, E., Vigneron, P., Langlais, B., and Hulot, G. (2016). A Swarm lithospheric magnetic field model to SH degree 80. *Earth, Planets and Space*, 68(1):126.

Thomas, W. A. et al. (2006). Tectonic inheritance at a continental margin. *GSA today*, 16(2):4–11.

Tominaga, M. and Sager, W. W. (2010). Revised Pacific M-anomaly geomagnetic polarity timescale. *Geophysical Journal International*, 182(1):203–232.

Umino, S., Nonaka, M., and Kauahikaua, J. (2006). Emplacement of subaerial pahoehoe lava sheet flows into water: 1990 Kūpaianaha flow of Kilauea volcano at Kaimū Bay, Hawaii. *Bulletin of Volcanology*, 69(2):125–139.

Urbani, F., Grande, S., Baquero, M., Mendi, D., Fournier, H., Alemán, A., Camposano, L., and Baritto, I. (2013). Los diques de basalto de la quebrada Yaracuyabare, Municipio Silva, Estado Falcón, Venezuela. *Revista Venezolana de Ciencias de La Tierra*.

Urquhart, T. (1988). Decorrugation of enhanced magnetic field maps. In *SEG Technical Program Expanded Abstracts 1988*, pages 371–372. Society of Exploration Geophysicists.

Van Avendonk, H. J., Christeson, G. L., Norton, I. O., and Eddy, D. R. (2015). Continental rifting and sediment infill in the northwestern Gulf of Mexico. *Geology*, 43(7):631–634.

Vasicek, J. M., Frey, H. V., and Thomas, H. H. (1988). Satellite magnetic anomalies and the Middle America Trench. *Tectonophysics*, 154(1-2):19–24.

Villeneuve, M. and Marcaillou, B. (2013). Pre-Mesozoic origin and paleogeography of blocks in the Caribbean, South Appalachian and West African domains and their impact on the post "variscan" evolution. *Bulletin de la Société Géologique de France*, 184(1-2):5–20.

Vine, F. J. and Matthews, D. H. (1963). Magnetic anomalies over oceanic ridges. *Nature*, 199(4897):947–949.

Viscarret, P. and Urbani, F. a. (2005). Algunos aspectos de la geología de la región de El Baúl, estado Cojedes. *Revista Venezolana de Ciencias de la Tierra GEOS*, 38:49–51. ISSN: 0435-5601.

Voorhies, C. (1998). *Elementary theoretical forms for the spatial power spectrum of Earth's crustal magnetic field*. Number 1. 36pp.

Welsink, H., Dwyer, J., and Knight, R. (1989). Tectono-Stratigraphy of the Passive Margin Off Nova Scotia: Chapter 14: North American Margins.

Wessel, P. (2010). Tools for analyzing intersecting tracks: The x2sys package. *Computers & Geosciences*, 36(3):348–354.

Wessel, P. and Watts, A. B. (1988). On the accuracy of marine gravity measurements. *Journal of Geophysical Research: Solid Earth*, 93(B1):393–413.

Whalen, L., Gazel, E., Vidito, C., Puffer, J., Bizimis, M., Henika, W., and Caddick, M. J. (2015). Supercontinental inheritance and its influence on supercontinental breakup: The Central Atlantic Magmatic Province and the breakup of Pangea. *Geochemistry, Geophysics, Geosystems*, 16(10):3532–3554.

Whittaker, J. M., Goncharov, A., Williams, S. E., Müller, R. D., and Leitchenkov, G. (2013). Global sediment thickness data set updated for the Australian-Antarctic Southern Ocean. *Geochemistry, Geophysics, Geosystems*, 14(8):3297–3305.

Withjack, M. O., Schlische, R. W., and Olsen, P. E. (1998). Diachronous rifting, drifting, and inversion on the passive margin of central eastern North America: an analog for other passive margins. *AAPG bulletin*, 82(5):817–835.

Wold, S., Esbensen, K., and Geladi, P. (1987). Principal component analysis. *Chemometrics and intelligent laboratory systems*, 2(1-3):37–52.

Woodring, W. P. (1928). *Miocene Mollusks from Bowden, Jamaica: Pelecypods and Scaphopods*. The Carnegie Institution of Washington.

Worrall, D. and Snelson, S. (1989). Evolution of the northern Gulf of Mexico. *The geology of North America; an overview: Geological Society of America, v. A*, pages 97–138.

Worzel, J. L. and Watkins, J. S. (1973). Evolution of the Northern Gulf Coast Deduced from Geophysical Data (1).

Zmuda, A. (1969). International Geomagnetic Reference Field. *Transactions-American Geophysical Union*, 50(4):134.